Cancer Metabolic Pathways Regulated by Hypoxia



Thesis submitted by

Elena Favaro

St Hugh's College

For the degree of

Doctor of Philosophy

Supervisor: Professor Adrian L. Harris

CANCER METABOLIC PATHWAYS REGULATED BY HYPOXIA

Elena Favaro
St Hugh's College
University of Oxford

D.Phil
Hilary Term
January 2013

Metabolic reprogramming in cancer cells provides energy and important metabolites required to sustain tumour proliferation. Hypoxia represents a hostile environment that can encourage these transformations and other adaptive responses that contribute to poor prognosis and resistance to radiation and chemotherapy. Hypoxic signatures associated with worse prognosis were previously derived in different cancer types, and led to the selection of two candidates with potential metabolic implications, namely the mir210-putuative target iron-sulfur scaffold protein ISCU and glycogen phosphorylase (PYGL). Firstly, it was verified that the hypoxia-induced miR-210 targets ISCU. Iron-sulfur clusters represent cofactors for key enzymes involved in Krebs cycle and electron transport chain. Downregulation of ISCU was associated with the induction of reactive oxygen species (ROS) and reduced mitochondrial complex I and aconitase activity, caused a shift to glycolysis in normoxia and enhanced cell survival. This indicates that the induction of a single microRNA, miR-210, can mediate a new mechanism of adaptation to hypoxia, by regulating mitochondrial function via iron-sulfur cluster metabolism and free radical generation. Secondly, it was found that changes in PYGL expression reflect a characteristic upregulation of glycogen metabolism in hypoxia in both tumour xenografts and in cancer cell lines. More specifically, hypoxia stimulates glycogen accumulation and its utilisation, as well as the concurrent upregulation of several glycogen-metabolizing enzymes such as glycogen synthase (GYS1) and PYGL. PYGL depletion led to glycogen accumulation in hypoxic cells, increased intracellular levels of ROS, and a reduction in proliferation due to a p53-dependent induction of senescence. Furthermore, depletion of PYGL was associated with markedly impaired tumorigenesis *in vivo*. Finally, metabolic analyses indicated that glycogen degradation by PYGL is important for the optimal functioning of the pentose phosphate pathway. Collectively, this study shows the contribution of two important pathways to the metabolic adaptations induced by hypoxia.

ACKNOWLEDGEMENTS

I am deeply grateful to Professor Adrian Harris for allowing me to undertake this journey. His passion and enthusiasm for science have been inspirational during the years spent in his laboratory.

All the members of the Harris' laboratory, past and present, have been extremely helpful and a pleasure to work with. In particular, Ulrike Harjes, Jon Williams, Alan McIntyre, Karim Bensaad, Dean Singleton, Chris Blick, Andrew Lomas, Harriet Gee, Simon Wigfield, Simon Lord and Helen Sheldon: You have all been great companions.

Thanks also to Helen Turley, for her indispensable assistance with immunohistochemistry and great company during the long staining sessions, and Francesca Buffa, for her expert guidance with bioinformatics and for sparing some of her precious time for some proper Italian chats. I would like to reserve a special thank to Ana Ramachandran, Manu Milani and Io Ledaki. Your friendship is very dear to me.

I thank GSK and Richard Wooster in particular, for their financial support and insightful scientific discussions.

I also greatly benefited from collaborations with members of Dr Jiannis Ragoussis' group, especially Christine Blancher and Carme Camps; with Professor Francisco Iborra and Dr Ricardo Pires da Neves, doing science with them was such a great fun; with Professor David Ferguson, for his knowledgeable guidance in the field of electron microscopy; with Dr Daniel Tennant and Mei Chong for their precious help and strenuous work during the glycogen project.

Finally, a special thank to Hocine, for his support, patience and love.

This thesis is dedicated to my family, who always encourage and support me. My brother, who always wants the best for his sister. My father, because he is so proud of his kids, even if we did not become engineers as he hoped. My mother, because she has dedicated all of her life to make her childrens' dreams come true.

ABBREVIATIONS

Abbreviations	Meaning
%	Per cent
Acetyl-CoA	Acetyl coenzyme A
ACL	ATP-citrate lyase
ACVR1B	Activin receptor 1B
AGO	Argonaute protein
AldoA	Aldolase A
AMP	Adenosine monophosphate
AMPK	AMP-activated protein kinase
6-AN	6-aminonicotinamide
ATP	Adenosine triphosphate
Bcl-2	B-cell lymphoma 2
BDNF	Brain-derived neurotrophic factor
BNIP3	BCL2/adenovirus E1B 19kDa interacting protein 3
BOLD MRI	Blood oxygen level-dependent magnetic resonance
CA9	Carbonic anhydrase IX
CASP8P	Caspase8-associated protein 2
ChREBP	Carbohydrate responsive element binding protein
CoQ	Coenzyme Q
COX	Cytochrome c oxidase
COX10	Cytochrome c oxidase assembly homolog 10
CXCR4	C-X-C chemokine receptor type 4
DBE	Debranching enzyme
DCA	Dichloroacetic acid
DCIS	Ductal carcinoma *in situ*
DEPC	Diethylpyrocarbonate
DGCR8	DiGeorge syndrome critical region gene 8
2-DG	2-deoxyglucose
DHEA	Dehydroepiandrosterone
DNA	Deoxyribonucleic acid
dNTP	Deoxyribonucleotide triphosphate
EF5	2-(2-nitro-1H-imidazol-1-yl)-N-(2,2,3,3,3-pentafluoropropyl)-acetamide
E2F3	E2F transcription factor 3
EFNA3	Ephrin-A3
e.g.	Exempli gratia
ENO1	Enolase 1
ER	Endoplasmic reticulum
$FADH_2$	Flavin adenine dinucleotide (reduced)
FancJ	Fanconi anemia complementation group J
FDA	Food and drug administration
FGFRL1	Fibroblast growth factor-like 1

FH	Fumarate hydratase
^{18}F-MISO	[^{18}F]Fluoromisonidazole
g	Gram
GENX-3414	Genethonin-1
GLUT	Glucose transporter
Glucose-1-P	Glucose-1-phosphate
Glucose-6-P	Glucose-6-phosphate
GAA	α-acid glycosidase
GABARAPL1	γ-aminobutyric acid type A receptor-associated protein-like 1
GBE	Glycogen branching enzyme
GC/MS	Gas chromatography/mass spectrometry
GP	Glycogen phosphorylase
GPD	Glycerol-3-phosphate dehydrogenase
GPD1L	Glycerol-3-phosphate dehydrogenase 1-like
GS	Glycogen synthase
GSH	Glutathione (reduced)
GSK3	Glycogen synthase kinase 3
GSSG	Glutathione (oxidized)
GW182	Glycine-tryptophan repeat-containing protein
GYG	Glycogenin
GYS	Glycogen synthase
HCV	Hepatitis C virus
H&E	Hematoxylin and eosin
2HG	2-hydroxyglutarate
HIF	Hypoxia inducible factor
HKII	Hexokinase II
HLRCC	Hereditary leiomyomatosis and renal cell cancer
HNSCC	Head and neck squamous cell carcinoma
HOXA1	Homeobox A1
HRE	Hypoxic response elements
IC_{50}	Half maximal inhibitory concentration
IDH	Isocitrate dehydrogenase
i.e.	Id est
IND	Investigational new drug
IRP1	Iron regulatory protein 1
ISCU	Iron-sulfur cluster scaffold homolog
JMJD3	Jumonji domain-containing 3
l	Litre
LC/MS/MS	Liquid chromatography-tandem mass spectrometry
LDHA	Lactate dehydrogenase A
LNA	Locked nucleic acid
M	Molar
MCT4	Monocarboxylate transporter 4
MINK	Misshapen-like kinase
MnTMPyP	Manganese (III) tetrakis (1-methyl-4-pyridyl) porphyrin

MNT	MAX-binding protein
mRNA	Messenger RNA
mTORC1	Mammalian target of Rapamycin 1
NAD+	Nicotinamide adenine dinucleotide (oxidised)
NADH	Nicotinamide adenine dinucleotide (reduced)
NADP+	Nicotinamide adenine dinucleotide phosphate (oxidised)
NADPH	Nicotinamide adenine dinucleotide phosphate (reduced)
NAMPT	Nicotinamide phosphoribosyltransferase
NF-kB	Nuclear factor κB
NMR	Nuclear magnetic resonance
NPTX1	Neuronal Pentraxin-1
OCT4	Octamer-binding transcription factor 4
OXPHOS	Oxidative phosphorylation
PARP	Poly (ADP-ribose) polymerase
PAS	Periodic Acid-Schiff
PDH	Pyruvate dehydrogenase
PDK1	Pyruvate dehydrogenase kinase 1
PET	Positron emission tomography
PFK1	Phosphofructokinase 1
PGM	Phosphoglycerate mutase / phosphoglucomutase
PHD	Prolyl hydroxylase
PHDGH	Phosphoglycerate dehydrogenase
P4HB	Protein disulphide isomerase
PI3K	Phosphatidylinositol 3-kinase
PKA/B	Protein kinase A/B
PKM	Pyruvate kinase M
pO_2	Partial pressure of oxygen
PP1	Protein phosphatase 1
PPP	Pentose phosphate pathway
PPP1R3A/B/C	Protein phosphatase 1 regulatory subunit 3A/B/C
Pre-miRNA	Precursor-miRNA
Pri-miRNA	Primary-miRNA
PTEN	Phosphatase and tensin homolog
PTPN1	Tyrosine-protein phosphatase non-receptor type 1
PYGB/L/M	Glycogen phosphorylase brain/liver/muscle
RISC	RNA-induced silencing complex
RNA	Ribonucleic acid
RNAi	RNA interference
ROS	Reactive oxygen species
RT-qPCR	Real-time quantitative polymerase chain reaction
SA β-gal	Senescence-associated β-galactosidase
SCO2	Synthesis of cytochrome c oxidase 2
SDH	Succinate dehydrogenase
SDS	Sodium dodecyl sulfate
SHIP	SH2 domain-containing inositol-5'-phosphatase 1
Stbd1	Starch-binding domain-containing protein 1

TcF7l2	Transcription factor 7-like 2
TEM	Transmission electron microscopy
TIGAR	TP53-induced glycolysis and apoptosis regulator
TMA	Tissue microarray
UDP	Uridine diphosphate
UTP	Uridine triphosphate
UTR	Untranslated region
VEGF	Vascular endothelial growth factor
VHL	Von Hippel-Lindau
VMP1	Vacuole membrane protein 1
XPD	Xeroderma pigmentosum group D

TABLE OF CONTENTS

ABSTRACT ..... **ii**

ACKNOWLEDGEMENTS ..... **iii**

ABBREVIATIONS ..... **iv**

TABLE OF CONTENTS ..... **viii**

LIST OF FIGURES ..... **xi**

1 CHAPTER ONE - Introduction and aims of the study **1**

1.1 Cancer metabolism as a hallmark of cancer **2**

1.1.1 Main features of tumour metabolic adaptation 2

a Aerobic glycolysis (Warburg effect) 3

b Glutamine metabolism 5

1.1.2 Mechanisms of metabolic reprogramming 7

a Metabolic effects of oncogenes and tumour suppressors 7

b Genomic alteration of metabolic enzymes in cancer cells 9

1.2 Hypoxia and HIFs **11**

1.2.1 Tumour hypoxia 11

1.2.2 HIF and the hypoxia response 13

a Regulation 13

b Functions and target genes 15

c Methods for detecting hypoxia 16

1.2.3 Hypoxic regulation of miRNA expression 19

a Biogenesis and function 19

b MiRNAs and cancer 21

c Strategies for miRNA modulation in vivo 23

d MiR-210 and the hypoxia-regulated miRNAs 25

1.2.4 Glycogen metabolism 31

a Glycogen synthesis and degradation 31

b Glycogen synthase and phosphorylase, structure and regulation 34

c Role of glycogen in cancer 36

2 CHAPTER TWO - Materials and methods **39**

2.1 Cell culture **40**

2.1.1 Cell lines and growth conditions 40

2.1.2 Cell counting 40

2.1.3 Transient transfection with oligonucleotides 40

2.1.4 Transient transfection with plasmid DNA constructs 43

2.1.5 Transduction protocol 43

2.2 RNA extraction and RT-qPCR **44**

2.2.1 RNA extraction 44

2.2.2 Reverse transcription and Real-time PCR 45

2.2.3 Reverse transcription and Real-time PCR for miRNA 47

2.3 Protein extraction and analysis **48**

2.4 Enzymatic assays **51**

2.4.1 Aconitase activity 51

2.4.2 Complex I activity 51

2.4.3 Lactate, pyruvate, and glucose measurements 52

2.4.4 Glycogen measurement 53

2.4.5 Glucose-6-P measurement 54
2.4.6 NADP+/NADPH measurement 55
2.5 Spheroids generation 55
2.6 *In vivo* study 56
2.7 Immuhistochemistry and other staining techniques 56
2.7.1 Histology 56
2.7.2 Immunohistochemical staining of paraffin-embedded sections 57
2.7.3 Senescence-associated b-galactosidase (SA-b-gal) staining 58
2.7.4 Periodic Acid Schiff staining (PAS) 59
2.7.5 Superoxide levels detection 59
2.7.6 Fluorescent glycogen detection 60
2.7.7 Lysosomes detection 61
2.7.8 Annexin V flow cytometry 61
2.7.9 Cell Cycle Analysis using Propidium iodide DNA staining 62
2.7.10 Clonogenic assay 62
2.8 Oncomine analysis 63
2.9 Statistical analysis 63

3 CHAPTER THREE - Metabolic implications of ISCU regulation by miR-210 64
3.1 INTRODUCTION 65
3.2 RESULTS 67
3.2.1 Selection of ISCU as a potential miR-210 target 67
3.2.2 MiR-210 and ISCU mRNA undergo reciprocal regulation in hypoxia 68
3.2.3 MiR-210 controls the hypoxic regulation of ISCU 71
3.2.4 Effects of ISCU downregulation on Fe-S proteins 76
3.2.5 Effects of miR-210 on glycolysis 80
3.2.6 Effects of ISCU downregulation on free radical production 81
3.2.7 Effects of miR-210 on cell viability 82
3.2.8 *In vivo* regulation of ISCU expression by hypoxia 85
3.3 DISCUSSION 87

4 CHAPTER FOUR - Glycogen metabolism is upregulated in hypoxia 95
4.1 INTRODUCTION 96
4.2 RESULTS 98
4.2.1 *In vivo* regulation of glycogen metabolism by hypoxia 98
4.2.2 Hypoxia regulates GYS1 and PYGL expression and modulates glycogen accumulation *in vitro* 102
4.2.3 Physiological significance of hypoxic upregulation of glycogen metabolism 108
4.2.4 Role of HIF in the hypoxic regulation of glycogen metabolism 109
4.2.5 GYS1 sustains glycogen synthesis in hypoxia 111
4.2.6 Effects of GYS1 depletion in human cancer cell lines. 113
4.2.7 Clinical significance of GYS1 and PYGL induction 116
4.3 DISCUSSION 121

5 CHAPTER FIVE - PYGL sustains cancer cell proliferation 126
5.1 INTRODUCTION 127
5.2 RESULTS 128
5.2.1 PYGL depletion induces glycogen accumulation in hypoxia 128
5.2.2 PYGL knockdown induces premature senescence 137
5.2.3 ROS contribute to cell growth arrest in PYGL-depleted cells 142
5.2.4 Metabolic consequences of glycogen breakdown inhibition 145
5.2.5 PYGL depletion inhibits growth of spheroids 153
5.2.6 PYGL depletion impairs tumour growth *in vivo* 156

5.3 Discussion 159
6 CHAPTER SIX - Concluding remarks 166
6.1 Clinical perspectives on miR-210 regulation in cancer 167
6.2 Final considerations and open questions on glycogen metabolism in cancer 171
7 LIST OF PUBLICATIONS 175
8 REFERENCES 176

LIST OF FIGURES

CHAPTER 1

Figure 1.1 Main pathways involved in metabolic reprogramming of cancer cells. 4

Figure 1.2 HIF1α regulation in normoxic and hypoxic conditions and selection of genes directly regulated grouped by biological function. 14

Figure 1.3 MiRNA biogenesis. 20

Figure 1.4 Cellular processes regulated by miR-210-validated targets. 28

Figure 1.5 The mitochondrial ISCU assembly machinery. 30

Figure 1.6 Schematic representation of glycogen synthesis and breakdown. 33

CHAPTER 3

Figure 3.1 MiR-210 and ISCU expressions are reciprocally regulated in MCF-7 cells in hypoxia. 69

Figure 3.2 MiR-210 and ISCU regulation in hypoxia is HIF1α-dependent. 70

Figure 3.3 ISCU expression is modulated by miR-210 in MCF-7 cells. 72

Figure 3.4 ISCU is modulated by lower concentrations of anti-210 and mimic-210. 73

Figure 3.5 Validation of siRNA sequences targeting ISCU..... 75

Figure 3.6 Role of the 3' UTR in the regulation of ISCU by miR-210. 76

Figure 3.7 Modulation of aconitase activity in MCF-7 cells. 77

Figure 3.8 MiR210 modulates aconitase activity in MCF-7 cells..... 78

Figure 3.9 MiR-210 negatively regulates complex I activity in MCF-7 cells. 79

Figure 3.10 MiR-210 sustains glycolysis. 80

Figure 3.11 MiR-210 increases the levels of ROS. 82

Figure 3.12 MiR-210 and ISCU affects cell survival..... 84

Figure 3.13 *In vivo* regulation of ISCU after anti-angiogenic treatment with bevacizumab. 85

Figure 3.14 Working model: hypoxia regulates ISCU via HIF1α induction of miR-210. 93

CHAPTER 4

Figure 4.1 Glycogen metabolism is upregulated *in vivo* after bevacizumab treatment. 100
Figure 4.2 Hypoxia is associated with upregulation of glycogen metabolism..... 102
Figure 4.3 Pattern of GYS1 and PYGL induction in hypoxia. 104
Figure 4.4 Glycogen accumulation in hypoxia. 105
Figure 4.5 Hypoxic regulation of GYS1 activity. 107
Figure 4.6 Hypoxic induction of glycogen metabolising enzymes and regulatory proteins. 108
Figure 4.7 Glycogen metabolism is activated by hypoxia at physiological glucose concentrations (5 mM). 109
Figure 4.8 Role of HIF in the hypoxic regulation of GYS1 and PYGL. 111
Figure 4.9 Glycogen synthesis in hypoxia is impaired after GYS1 depletion 112
Figure 4.10 Effects of GYS1 knockdown on cell viability. 114
Figure 4.11 Effects of GYS1 knockdown on colony formation. 115
Figure 4.12 Consequences of GYS1 knockdown on spheroid growth. 116
Figure 4.13 Expression of GYS1 and PYGL in tumours versus normal tissues..... 117
Figure 4.14 Expression of glycogen metabolising enzymes in TMA of breast origin. 118
Figure 4.15 Staining of breast TMA for GYS1..... 119
Figure 4.16 Staining of breast TMA for PYGL. 120

CHAPTER 5

Figure 5.1 Efficiency of PYGL knockdown by RNAi..... 129
Figure 5.2 PYGL depletion results in increased glycogen accumulation. 131
Figure 5.3 GYS1 levels are unaffected by PYGL depletion. 132
Figure 5.4 PYGL sustains proliferation in cancer cells. 133
Figure 5.5 Consequences of PYGL knockdown in normoxic and hypoxic cells.... 134
Figure 5.6 PYGL knockdown induces glycogen accumulation and cell growth inhibition at physiological glucose concentrations. 134
Figure 5.7 PYGL depletion does not induce apoptosis. 135
Figure 5.8 PYGL knockdown induces a p53-dependent cell cycle arrest in hypoxia. 137

Figure 5.9 PYGL knockdown is associated with increased cell senescence. 139
Figure 5.10 PYGL knockdown cells have increased lysosome content. 141
Figure 5.11 PYGL depletion is associated with increased DEC1 levels. 142
Figure 5.12 PYGL depletion is associated with elevated ROS. 144
Figure 5.13 GYS1 knockdown prevents glycogen accumulation and premature senescence in PYGL-depleted cells. 146
Figure 5.14 PYGL knockdown leads to decreased availability of glucose-6-P. 147
Figure 5.15 Metabolite alterations induced by PYGL knockdown in MCF-7 cells. 150
Figure 5.16 NADPH levels are reduced in PYGL-depleted cells. 150
Figure 5.17 PYGL depletion reduces the activity of the oxidative pentose phosphate pathway. 152
Figure 5.18 Induction of senescence after pharmacological inhibition of the PPP. 153
Figure 5.19 PYGL knockdown impairs spheroid growth. 155
Figure 5.20 PYGL knockdown impairs tumour xenograft growth. 157
Figure 5.21 PYGL knockdown is associated with increased senescence *in vivo*. .. 158
Figure 5.22 Working model. 164

LIST OF TABLES

CHAPTER 2

Table 2.1 Transfection conditions 41

Table 2.2 Oligonucleotide sequences 42

Table 2.3 Primer sequences used for RT-qPCR 46

Table 2.4 Acrylamide gel components 49

Table 2.5 Primary antibody specifications 50

Table 2.6 Antibody specifications 58

CHAPTER 3

Table 3.1 List of the top four predicted miR-210 targets using algorithms and tumour data (courtesy of Dr Francesca Buffa). 68

CHAPTER 4

Table 4.1 Expression of glycogen-related enzymes is increased after bevacizumab treatment. 99

1 CHAPTER ONE

Introduction and aims of the study

1.1 Cancer metabolism as a hallmark of cancer

Cancer is a genetic disease that generates from a multistep process involving somatic, and in some instances, germ-line mutations of tumour oncogenes and suppressor genes. The puzzling complexity of mutations defining the neoplastic transformation has been organised 13 years ago (and recently revisited) into the 'hallmarks of cancer', described as distinctive and complementary capabilities that dictate tumour growth and metastatic dissemination (Hanahan and Weinberg, 2000, 2011). They include the ability to undergo uncontrolled proliferation, evade cell death, and induce angiogenesis.

Recently, reprogramming of cancer metabolism has been designated as an emerging hallmark of cancer, although its functional independence from the core hallmarks is still debated (Hanahan and Weinberg, 2011). The traditional cancer model describes metabolic reprogramming as a secondary response to cell cycle and proliferative signalling activated in cancer cells. In this model, the main role of metabolism is to provide energy (ATP) in order to sustain increased transcription and translation demands. New and strong evidences now support an alternative model, in which altered metabolism constitutes a primary response to growth factor signalling, mostly independent of ATP requirements, and primarily finalised to the generation of anabolic precursors for the synthesis of macromolecules required for proliferation (e.g. nucleotides, proteins, lipids) (Ward and Thompson, 2012).

1.1.1 Main features of tumour metabolic adaptation

The two most widely documented metabolic activities characterising tumour metabolic reprogramming are the Warburg effect and glutamine metabolism.

a Aerobic glycolysis (Warburg effect)

Aerobic glycolysis, also termed the Warburg effect, was first described in the 1920s by Otto Warburg, who observed that cancer cells consumed higher amounts of glucose compared to normal cells, and produced high levels of lactate even in normal oxygen conditions (Warburg, 1956). This peculiarity of cancer cells has since been observed across a variety of tumour types and has been largely exploited in the clinics to image cancer through the use of ^{18}Fluor-deoxyglucose positron emission tomography (Groves et al., 2007). This pathway consists in the uptake of glucose through specific transporters (GLUTs), its trapping in the cells by phosphorylation to glucose-6-phosphate (glucose-6-P) catalysed by hexokinase II (HKII), followed by a chain of reactions culminating in the formation of pyruvate (Figure 1.1). Pyruvate is then mainly converted into lactate by the enzyme lactate dehydrogenase A (LDHA), enabling the recycling of nicotinamide adenine dinucleotide (NAD+), which is required for continued flux through glycolysis. However, pyruvate can also enter the mitochondria, be metabolised through the Krebs cycle and either lead to the production of ATP through oxidative phosphorylation (OXPHOS) or the synthesis of precursors for anabolic pathways (e.g. lipid synthesis, amino acids) (Lunt and Vander Heiden, 2011).

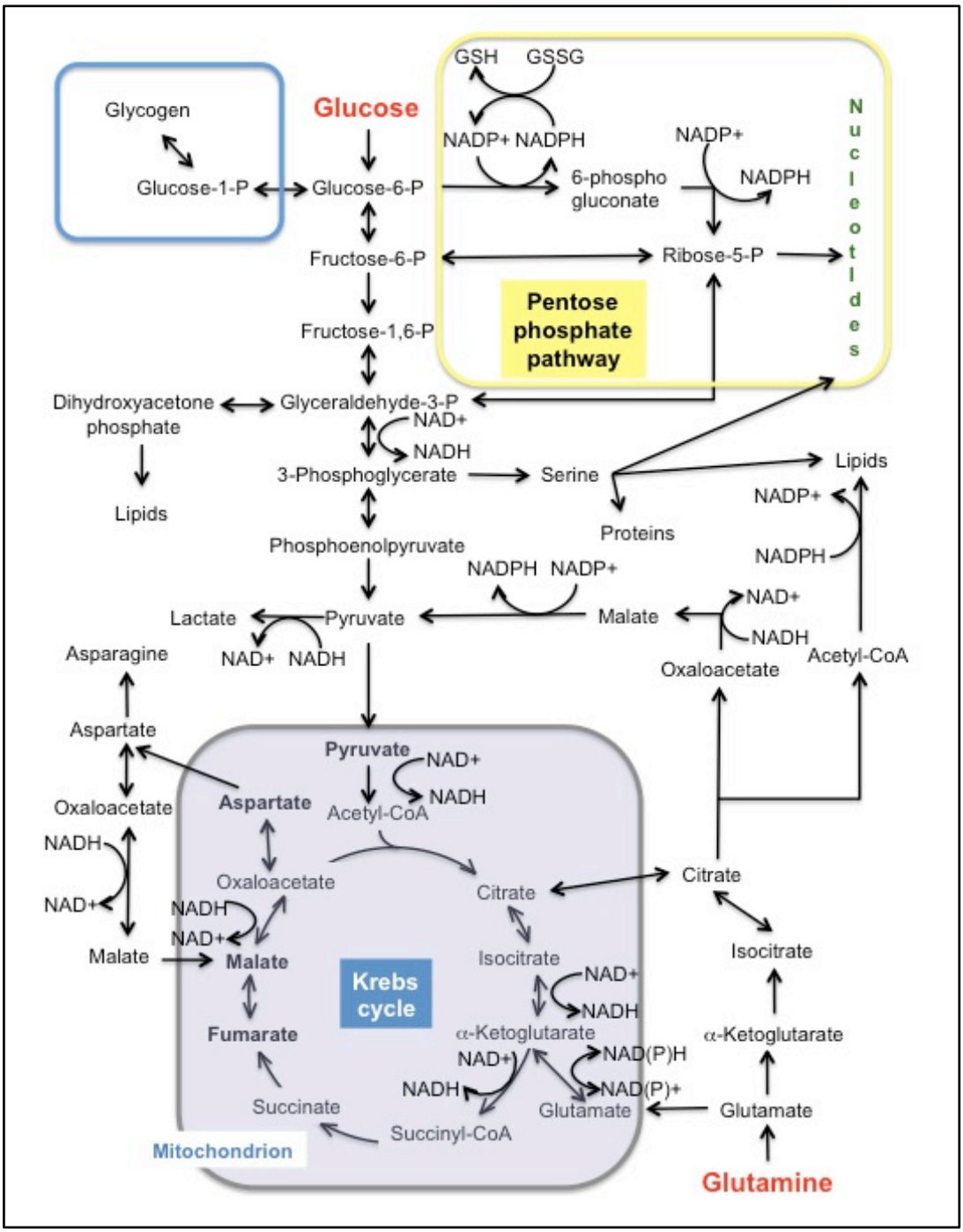


Figure 1.1 Main pathways involved in metabolic reprogramming of cancer cells. Metabolism of glucose and glutamine provides important substrates for the synthesis of macromolecules (nucleotides, lipids, amino acids) and energy, required for cancer cell proliferation.

Glycolysis is a relatively inefficient way to generate ATP (2 ATPs per glucose) as compared to OXPHOS (36 ATPs per glucose), and it contributes to only 17% of the

total ATP production in cancer cells (Zu and Guppy, 2004), suggesting other critical roles for aerobic glycolysis. Indeed, many observations have proposed a role for glycolysis in providing precursors for anabolic pathways (e.g. lipids, nucleotides and amino acids), as well as cofactors (e.g. reduced nicotinamide adenine dinucleotide [NADH] and reduced nicotinamide adenine dinucleotide phosphate [NADPH]), which are required for cancer cell proliferation (Ward and Thompson, 2012). There are a number of other reasons for glycolysis to constitute an advantage for tumour growth: i) a metabolism based on aerobic glycolysis can favour the survival of cancer cells exposed to fluctuating oxygen tension, a situation frequently encountered in tumours as a consequence of altered hemodynamics of tumour blood vessels; ii) channelling of glycolytic intermediates through the pentose phosphate pathway (PPP) and glutaminolysis can generate NADPH, which is not only required for macromolecule synthesis (lipids, nucleotides, amino acids) but also for anti-oxidant defences; iii) export of high amounts of the glycolytic end-product lactate can favour tumour invasion and the suppression of anticancer immune responses, and can be recycled by stromal cells and used to assist the growth of tumour cells (Kroemer and Pouyssegur, 2008).

b Glutamine metabolism

Glutamine is the most abundant amino acid in plasma and it constitutes another important source of energy, carbon, and nitrogen in the cells (DeBerardinis and Cheng, 2010). Some of the recognised roles of glutamine in cancer metabolic reprogramming include: i) synthesis of nonessential amino acids and proteins; ii) partial oxidation to lactate (glutaminolysis) through the malic enzyme, that provides

the cells with NADPH; iii) major contribution to anaplerosis through the conversion to α-ketoglutarate (i.e. the generation of intermediates of the Krebs cycle, to replace metabolites used for cataplerosis, which in turn, consists on efflux of Krebs cycle intermediates for biosynthetic reactions); iv) ATP generation through the Krebs cycle and OXPHOS; v) synthesis of lipids through the mitochondrial or cytosolic conversion into citrate (Figure 1.1) (DeBerardinis, 2008; Lunt and Vander Heiden, 2011).

Importantly, gene expression analysis performed on a set of 24 cancers representing more than 70% of human cancer histotypes demonstrated that several glycolytic genes were ubiquitously overexpressed, as compared to normal tissues (Altenberg and Greulich, 2004). Similarly, glutamine transporter and glutaminase expression has also been found to be upregulated in cancer versus normal tissues (Fuchs and Bode, 2005; Gao et al., 2009). Numerous studies have now shed light into the mechanisms of regulation of metabolic enzymes that contribute to the metabolic reprogramming of cancer cells. These studies provide evidence that most if not all oncogenes and tumour suppressors can also regulate metabolism, and that mutations in genes encoding metabolic enzymes can drive tumour growth.

1.1.2 Mechanisms of metabolic reprogramming

a Metabolic effects of oncogenes and tumour suppressors

Alterations in classic oncogenes and tumour suppressors with direct involvement in metabolic reprogramming of cancer cells include, for example, phosphatidylinositol 3-kinase (PI3K), Myc, p53, and von Hippel-Lindau protein (VHL) (DeBerardinis, 2008; Ivan et al., 2001; Kaelin, 2002; Ward and Thompson, 2012).

Activating mutations of the PI3K signalling pathway are common in cancer, where they influence cell metabolism through the downstream effectors Akt (also known as protein kinase B [PKB]) and mammalian target of Rapamycin (mTORC1). More specifically, Akt can promote glycolysis through the regulation of membrane translocation of glucose transporters and the activation of the glycolytic enzymes HKII and phosphofructokinase. Akt can also stimulate fatty acid synthesis by phosphorylating (activating) the enzyme ATP-citrate lyase (ACL), which converts citrate into acetyl coenzyme A (acetyl-CoA). Activation of mTORC1 is associated with increased protein synthesis, but it can also influence many aspects of mitochondrial biology, including mitochondrial biogenesis (Cunningham et al., 2007; Ramanathan and Schreiber, 2009; Schieke et al., 2006).

The oncogene *MYC* is involved in the genesis of most human cancers and contributes to the regulation of several aspects of tumour cell metabolism. MYC can promote glucose metabolism through the glycolytic pathway by enhancing the expression of glucose transporters and glycolytic enzymes. Among the glycolytic genes controlled by MYC are GLUT1, HKII, phosphofructokinase 1 (PFK1), enolase 1 (ENO1), LDHA, and pyruvate dehydrogenase kinase 1 (PDK1) (Dang et al., 2009a). On the other hand, MYC can also influence mitochondrial metabolism, and glutamine

utilisation in the mitochondria through the regulation of glutamine transporters, and the enzyme glutaminase. The importance of this pathway is underscored by the induction of apoptosis observed upon depletion of glutamine in MYC-transformed cells (Wise et al., 2008; Yuneva et al., 2007). Finally, MYC can regulate other aspects of metabolic reprogramming, such as lipid synthesis and serine/glycine metabolism (Cantor and Sabatini, 2012).

The tumour suppressor gene *TP53* is mutated in approximately 50% of cancers. The role of activated p53 in tumour surveillance is well established, and it is mediated by a number of mechanisms, including cell cycle arrest, DNA repair, and apoptosis (Vousden and Ryan, 2009). Increasing evidences demonstrate that p53 can also regulate cell metabolism at different levels: i) by direct inhibition of GLUT1 and GLUT4 expression; ii) by indirect inhibition of GLUT3 and phosphoglycerate mutase (PGM); iii) by inactivation of PFK1 enzyme mediated by the TP53-induced glycolysis and apoptosis regulator protein TIGAR, which concomitantly increases the flux of glucose-6-P through the PPP, and contributes to reactive oxygen species (ROS) removal (Bensaad et al., 2006). Additionally, p53 has been shown to play a role in OXPHOS, through the regulation of synthesis of cytochrome c oxidase 2 (SCO2), subunit I of cytochrome c oxidase amongst others (Matoba et al., 2006).

Loss of VHL is frequently encountered in renal cell carcinoma and it is associated with the normoxic stabilisation of hypoxia inducible factor (HIF), therefore resulting in a pseudohypoxic state characterised by HIF signalling (Ivan et al., 2001; Kaelin, 2002). The metabolic consequences of the activation of this pathway will be discussed in more detail later in this chapter.

The stronger evidence that metabolic reprogramming is selected for by cancer cells and is not just a bystander effect of transformation comes from the identification of mutations in metabolic enzymes.

b Genomic alteration of metabolic enzymes in cancer cells

In some situations, metabolic enzymes can function themselves as tumour suppressors or oncogenes. For example, succinate dehydrogenase (SDH) is a Krebs cycle enzyme and constitutes Complex II in the mitochondrial respiratory chain. SDH catalyses the conversion of succinate into fumarate, and the production of reduced flavin adenine dinucleotide ($FADH_2$) as a source of electrons for the respiratory chain. Mutations of genes encoding SDH subunits have been associated with hereditary and sporadic paragangliomas, pheochromocytomas, and renal cell cancers (Astuti et al., 2001; Baysal et al., 2000; Niemann and Muller, 2000; van Nederveen et al., 2007). Fumarate hydratase (FH) converts fumarate into malate in the next step of the Krebs cycle. Similarly to SDH, mutations of FH are associated with the development of neoplastic growth, i.e. benign leiomyomas of the skin and uterus, and renal cancer, collectively termed hereditary leiomyomatosis and renal cell cancer (HLRCC) (Launonen et al., 2001; Tomlinson et al., 2002). Accumulation of succinate and fumarate have been linked to the inhibition of α-ketoglutarate-dependent HIF prolyl hydroxylases (PHDs), resulting in the normoxic stabilisation and increased expression of HIF target genes (including glycolytic genes) (Isaacs et al., 2005; Selak et al., 2005). However, HIF hyperactivation has been excluded as the oncogenic driver of renal cyst formation in a murine model of FH deficiency (Adam et al., 2011). Importantly, recent evidences suggest that many other mechanisms

could contribute to tumour growth/development. For example, succinate-dependent inhibition of other prolyl hydroxylases has been described, including the histone demethylase jumonji domain-containing 3 (JMJD3) that affects the pattern of histone methylation and can potentially alter gene expression (Cervera et al., 2009). Activation of the reductive carboxylation of glutamine has also been demonstrated in cells with defective mitochondria (for example due to FH deficiency), as an alternative pathway adopted by cancer cells to generate precursors for the synthesis of lipids required for cell growth (Mullen et al., 2012). Notably, induction of heme biosynthesis and degradation has been proposed as a mechanism to dispose of the accumulating Krebs cycle intermediates and the production of reducing equivalents (NADH) required for mitochondrial respiration but also for the activation of transcription factors that control gene expression (Frezza et al., 2011; Lunt and Vander Heiden, 2011). Mutation of these genes (SDH and FH) follows the typical inheritance pattern of tumour suppressor genes. Conversely, mutations occurring in the active site of the enzymes isocitrate dehydrogenase 1 and 2 (IDH1 and IDH2) are associated with the acquisition of a neomorphic enzyme activity that enables to convert α-ketoglutarate into R(-)-2-hydroxyglutarate (2HG) instead of the canonical isocitrate-to-α-ketoglutarate reaction (Dang et al., 2009b). Mutations of IDH1 and IDH2 have been observed in patients with secondary glioblastoma multiforme, acute myeloid leukemia, and chondrosarcoma (Amary et al., 2011; Green and Beer, 2010; Parsons et al., 2008; Yan et al., 2009). Accumulation of 2HG can inhibit the activity of α-ketoglutarate-dependent enzymes, with effects on histone and DNA methylation and modulation of HIF activity (Xu et al., 2011). Amplification of metabolic enzymes, such as phosphoglycerate dehydrogenase (PHDGH) has been observed in

breast cancer and melanoma and can contribute to fuel macromolecule biosynthetic pathways through the associated increased flux through the serine biosynthetic pathway (Locasale et al., 2011; Possemato et al., 2011). Finally, preferential expression of specific enzyme isoforms has also been demonstrated to contribute to the metabolic reprogramming of cancer cells. One of the most representative examples is the preferential expression of the M2 isoform of pyruvate kinase M (PKM2), which catalyses the conversion of phosphoenolpyruvate into pyruvate in the glycolytic pathway. Compared to PKM1, the predominant isoform expressed in adult differentiated tissues, PKM2 presents a lower enzymatic activity that can therefore favour the accumulation of upstream glycolytic intermediates required for anabolic pathways (Mazurek, 2011).

1.2 Hypoxia and HIFs

Other important contributors to metabolic reprogramming of cancer cells are represented by HIFs and the development of hypoxia in tumours, where limited availability of oxygen and therefore ATP generation through the mitochondrial respiratory chain, maximises the reliance of tumour cells on glycolysis.

1.2.1 Tumour hypoxia

Hypoxia, defined as the presence of low levels of oxygen in cells, characterises most solid tumours. Specifically, up to 60% of locally advanced solid tumours exhibit hypoxic (1% or less oxygen, compared to 2%-9% oxygen in the adjacent tissue) and/or anoxic areas (less then 0.01% oxygen) (Vaupel and Mayer, 2007). Multiple

factors can contribute to the development of hypoxia: inadequate vascularization (tumour angiogenesis is often characterized by aberrant vessels, with altered perfusion), increase in diffusion distances associated with tumour expansion (increased distance that oxygen has to cover to oxygenate tumour cells due to uncontrolled cell growth), tumour or therapy-related anemia (caused by reduced oxygen transport capacity of the blood due to inadequate vascularization of the tumour or therapy), and increased oxygen consumption by the rapidly proliferating cells (Vaupel and Mayer, 2007).

Hypoxia contributes to malignant progression, by promoting survival, invasion, metastasis, angiogenesis, and metabolic adaptations. It also severely affects treatment outcome since hypoxic tumours are usually resistant to radiotherapy and chemotherapy (for examples see (Fyles et al., 2002; Hockel et al., 1996; Jubb et al., 2010; Nordsmark et al., 2005)). Mechanisms of resistance include lack of oxidation of DNA free radicals by oxygen (resistance to ionizing radiation and DNA breaks-inducing antibiotics), cell cycle arrest (drug-resistance), compromised drug exposure due to distance from vasculature (drug-resistance), and extracellular acidification (drug-resistance) (for a review see (Wilson and Hay, 2011)).

The adaptation of cancer cells to a hostile, low-oxygen environment is governed by many factors, including the selection of death-resistant mutated genotypes, and the induction of transcriptional and post-transcriptional changes in gene expression. For example, it has been shown that mutation of the tumour suppressor gene p53, or its downstream targets Apaf-1 and Caspase 9, and over-expression of the apoptosis-inhibitor Bcl-2 are associated with resistance to hypoxia-induced cell apoptosis in transformed cells (Graeber et al., 1996; Soengas et al., 1999). Selection of

unfavourable genotypes in hypoxia is also suggested by p53-null cells overtaking p53-wild type cells in co-cultures (Graeber et al., 1996).

The most extensively investigated hypoxia response is represented by the transcriptional changes in gene expression. In this respect, up to 1.5% of the human genome is estimated to be transcriptionally responsive to hypoxia (Denko et al., 2003). The master regulators of the hypoxia-induced transcriptional response are represented by the family of HIFs.

1.2.2 HIF and the hypoxia response

a Regulation

HIFs are heterodimers formed by an oxygen- and growth-factor-sensitive subunit α and a constitutively expressed subunit β (Ratcliffe et al., 1998; Semenza, 1998). In normoxic cells, the α subunit is hydroxylated by oxygen-dependent PHDs, is recognized by and forms a complex with VHL, which mediates its ubiquitination and degradation by the proteasome. In hypoxic cells, the α subunit is stabilized, it translocates to the nucleus where it forms a dimer with the β subunit and activates transcription of target genes by binding to the hypoxic response elements (HREs) present in their promoter region (Ratcliffe et al., 1998; Semenza, 1998) (Figure 1.2).

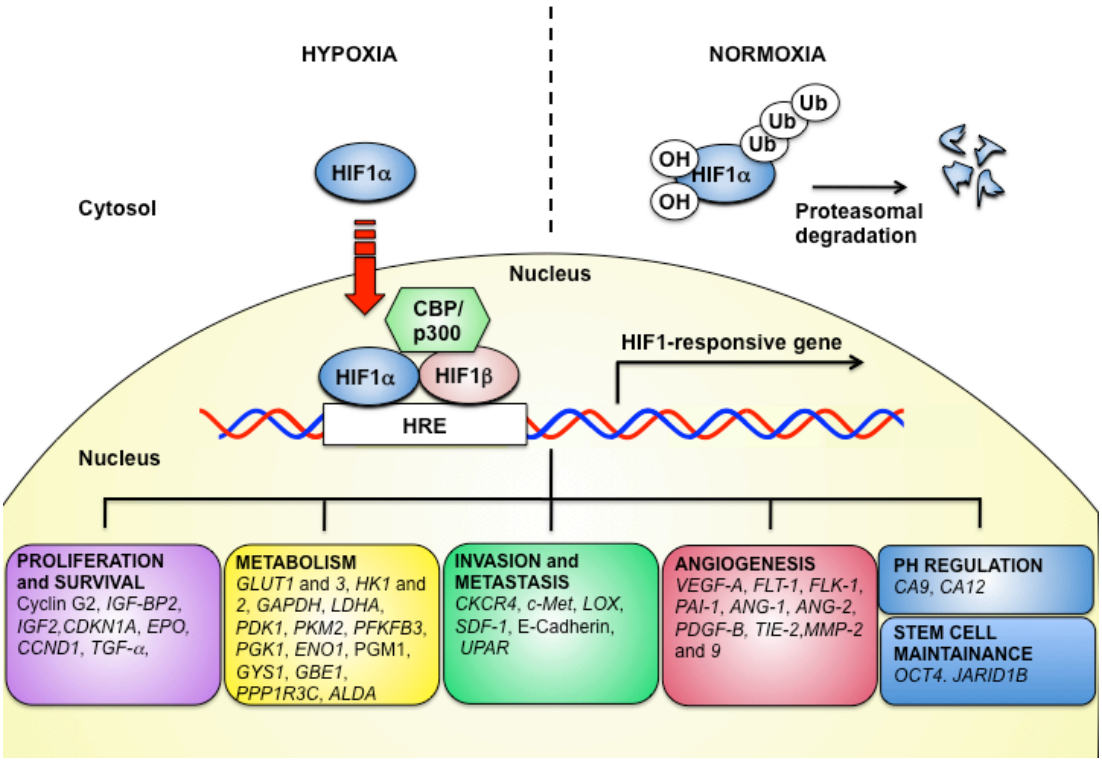


Figure 1.2 HIF1α regulation in normoxic and hypoxic conditions and selection of genes directly regulated grouped by biological function.
In normoxia, the subunit HIF1α is hydroxylated and rapidly degraded through ubiquitin-proteasome degradation. In hypoxia, HIF1α is stabilized, it translocates to the nucleus where it binds to the subunit HIF1β and the co-activator p300 and activates the transcription of target genes involved in several cellular processes, including proliferation, survival, metabolism, angiogenesis, invasion and metastasis, pH regulation and stem cell maintenance. Examples are given. Abbreviations: CBP= CREB binding protein, IGF2= insulin growth factor 2, IGF-BP2= IGF-binding protein 2, CDKN1A= cyclin-dependent kinase inhibitor 1A, CCND1= cyclin D1, TGF-α= transforming growth factor α, EPO= erythropoietin, GLUT1 and 3= glucose transporter 1 and 3, HK1 and 2= hexokinase 1 and 2, GAPDH= glyceraldehyde 3-phosphate dehydrogenase, LDHA= lactate dehydrogenase A, PDK1= pyruvate dehydrogenase kinase 1, PKM2= pyruvate kinase M2, PFKFB3= 6-phosphofructo-2-kinase/fructose-2,6-biphosphatase 3, PGK1= phosphoglycerate kinase 1, ENO1= enolase 1, PGM1= phosphoglucomutase 1, GYS1= glycogen synthase 1, GBE1= glycogen branching enzyme 1, ALDA= aldolase A, CKCR4= C-X-C chemokine receptor type 4, c-Met= hepatocyte growth factor receptor, LOX= lysyl oxidase, SDF-1= stromal-derived factor 1, UPAR= urokinase plasminogen activator receptor, VEGF-A= vascular endothelial growth factor A, FLT-1= fms-like tyrosine kinase-1, FLK-1= fetal liver kinase-1, PAI-1= plasminogen activator inhibitor-1, ANG-1 and 2= angiopoietin-1 and 2, PDGF-B= platelet-derived growth factor-B, TIE-2= tie-like receptor tyrosine kinase 2, MMP-2 and 9= matrix metalloproteinase 2 and 9, CA9 and 12= carbonic anhydrase 9 and 12, OCT4=

octamer-binding transcription factor 4, JARID1B= jumonji AT-rich interactive domain 1B.

Oxygen-independent regulation of HIF has also been documented; for example, HIF can accumulate after the activation of oncogenes, such as Ras, *SRC*, and PI3K, or loss of tumour suppressors such as *VHL* or phosphatase and tensin homolog (*PTEN),* even in normoxic conditions (Denko, 2008). Moreover, HIF can be stabilised by increased levels of metabolites such as succinate and fumarate or free radicals (Denko, 2008).

There are three isoforms of the α subunit, HIF1α, HIF2α and HIF3α and one β subunit, HIF1β. While HIF1α is the most ubiquitously expressed in cells, HIF2α and HIF3α expression is tissue-specific, with HIF2α being mainly found in endothelium, liver, lung and kidney where it acts similarly to HIF1α on target genes, and HIF3α being highly expressed in thymus, cerebellum and cornea, where it acts in a dominant-negative fashion to inhibit HIF1α and HIF2α (for a review see (Bertout et al., 2008)).

b Functions and target genes

HIF1 regulates key aspects of cancer biology, including cell proliferation and survival (for example through p21 and BCL2/adenovirus E1B 19kDa interacting protein 3 [BNIP3] regulation), pH regulation (carbonic anhydrase IX [CA9], monocarboxylate transporter 4 [MCT4]), invasion and metastasis (for example through C-X-C chemokine receptor type 4 [CXCR4] and c-Met), angiogenesis (vascular endothelial growth factor A [VEGF-A]), stem cell maintenance (octamer-

binding transcription factor 4 [OCT4]), and metabolism (GLUT1 and 3, HKII, LDHA, glycogen synthase 1 [GYS1], PDK1) (Figure 1.2) (Semenza, 2010). HIF1 can therefore promote both glucose uptake and its metabolism through the glycolytic pathway through the induction of transporters and glycolytic enzymes (Semenza et al., 1996). Excessive intracellular acidification due to the glycolytic switch and the consequent increased generation of lactate through LDHA is prevented by the HIF-dependent induction of multiple acid-regulatory systems. Amongst these, CA9 is a carbonic anhydrase located on the plasma membrane that converts carbon dioxide into bicarbonate with the release of protons in the extracellular space (Swietach et al., 2010; Wykoff et al., 2000). The monocarboxylate transporter MCT4 also contributes to the regulation of intracellular pH by cotransporting protons and lactate molecules across the plasma membrane (Ullah et al., 2006). HIF-dependent regulation of PDK1 blocks the conversion of pyruvate into acetyl-coenzyme by the enzyme pyruvate dehydrogenase (PDH), and therefore limits the metabolism of pyruvate through the Krebs cycle (Kim et al., 2006). The secretion of VEGF and other angiogenic factors by the hypoxic cells stimulates endothelial cell proliferation and leads to the formation of new vessels from pre-existing ones (angiogenesis) in order to provide cancer cells with oxygen, nutrients, and factors, required for survival and proliferation (Pugh and Ratcliffe, 2003).

c Methods for detecting hypoxia

Given its role in tumour progression, assessment of the level of hypoxia is of great importance for the selection and the optimisation of treatment. Various methods are currently used to detect hypoxia in solid tumours. Oxygen measurement with

polarographic oxygen needle electrode represents the most direct method, but presents some limitations like invasiveness, non-representativeness of the whole tumour, and the potential generation of false positives due to oxygen consumption by the electrodes (Vaupel et al., 2007). Assessment of hypoxia in the clinic is moving towards the evaluation of endogenous and exogenous markers. HIF1α and some of its targets like GLUT1, CA9 and VEGF, are examples of the endogenous markers that can be detected by immunohistochemistry on tumour biopsies. One limitation associated with these markers is their potential regulation also by non-hypoxia related factors, like pH, metabolite concentrations (e.g. glucose and glutamine), and oncogenic signalling. Moreover, the predictive and prognostic role of these markers is sometimes not unanimous among different studies (for a review see (Vaupel and Mayer, 2007)). Exogenous markers are represented by 2-nitroimidazole derivatives (*e.g.* pimonidazole, and 2-(2-nitro-1H-imidazol-1-yl)-N-(2,2,3,3,3-pentafluoropropyl)-acetamide [EF5]), that need to be systemically administered to patients and generate stable adducts with SH-containing molecules in hypoxic conditions; these are then detected by specific antibodies on tumour biopsies. The main limitations of these methods are invasiveness, non-representativeness of the sampling (the tumour can be very heterogeneous and biopsies can be non-representative of the whole tumour), and inability to perform multiple evaluations to follow changes in tumour oxygenation after treatment (Tatum et al., 2006). A more recently developed technique to image hypoxic tumours that is now being implemented in the clinic is the use of 2-nitroimidazole molecules in combination with positron emission tomography (PET). There are several derivatives of 2-nitroimidazole under study in order to identify the best tracer with high uptake and

low toxicity (Postema et al., 2009; van Loon et al., 2010). Among these, [^{18}F]Fluoromisonidazole (^{18}F-MISO) is the most extensively studied and it has investigational new drug (IND) authorization from the Food and Drug Administration (FDA) as an investigational product for use in humans (http://imaging.cancer.gov/programsandresources/Cancer-Tracer-Synthesis-Resources). Although this technique is non-invasive and allows serial imaging of hypoxia, accumulation of ^{18}F-MISO in hypoxic tumours is relatively low, resulting in a low signal-to-noise ratio hence a low contrast between hypoxic tumours and surrounding normal tissues (for a detailed review refer to (Chitneni et al., 2011)). Imaging tumour hypoxia by blood oxygen level-dependent magnetic resonance (BOLD MRI) is also being investigated and relies on the detection of paramagnetic deoxyhemoglobin within red blood cells, with no need to administer exogenous tracers. The main limitations of this technique are the fact that it does not measure tissue oxygen partial pressure (pO_2) directly and the possible confounding influence of blood flow, tumour perfusion and other vascular parameters.

In addition to these difficulties, it is becoming clear that assessing one single factor such as HIF1 does not reflect the complexity of tumour response to hypoxia, and hence is unlikely to be a reliable marker *per se*. Therefore, more comprehensive approaches to detect and select hypoxic tumours for therapy are needed and are currently under investigation. In particular, the identification of gene and microRNA (miRNA) expression signatures that are responsive to hypoxia is now being explored (Favaro et al., 2011; Toustrup et al., 2012). These signatures have the potential to reflect the complexity of the tumour hypoxia response.

1.2.3 Hypoxic regulation of miRNA expression

Altered microRNA expression is also part of the global changes induced by hypoxia in cancer cells, and several reports indicate their potential role in cancer metabolic reprogramming.

a Biogenesis and function

MiRNAs are small non-coding RNAs (approximately 22 nucleotides) that post-transcriptionally regulate protein synthesis by regulating mRNA translation and stability (Bartel, 2009; Filipowicz et al., 2008). They are generally transcribed by RNA polymerase II into long primary transcripts (pri-miRNA) (Figure 1.3). These primary constructs contain a stem-loop structure that is recognised and cleaved by the ribonuclease Drosha and its partner protein DiGeorge syndrome critical region gene 8 (DGCR8) into the precursor miRNA (pre-miRNA). Pre-miRNAs are exported to the cytoplasm by Exportin 5, where they are further processed by the ribonuclease Dicer1 into a 19-24 nucleotide long double stranded miRNA. One strand of the duplex (the mature miRNA or guide strand) is then incorporated into a complex of proteins called RNA-induced silencing complex (RISC complex) that contains a miRNA-loaded Argonaute protein (AGO) and a glycine-tryptophan repeat-containing protein (GW182), whereas the other strand (passenger strand) is generally degraded (Lee et al., 2004b; Rodriguez et al., 2004). The miRNA sequence is important for loading into the RISC complex and for specific mRNA-target recognition, which is determined by base complementarity between positions 2 to 8 in the miRNA (seed region) and (usually) the 3' untranslated region (UTR) in the target mRNA sequence. The RISC complex is responsible for inhibition of cap-

dependent translation and/or decapping and decay of target mRNA (Fabian and Sonenberg, 2012).

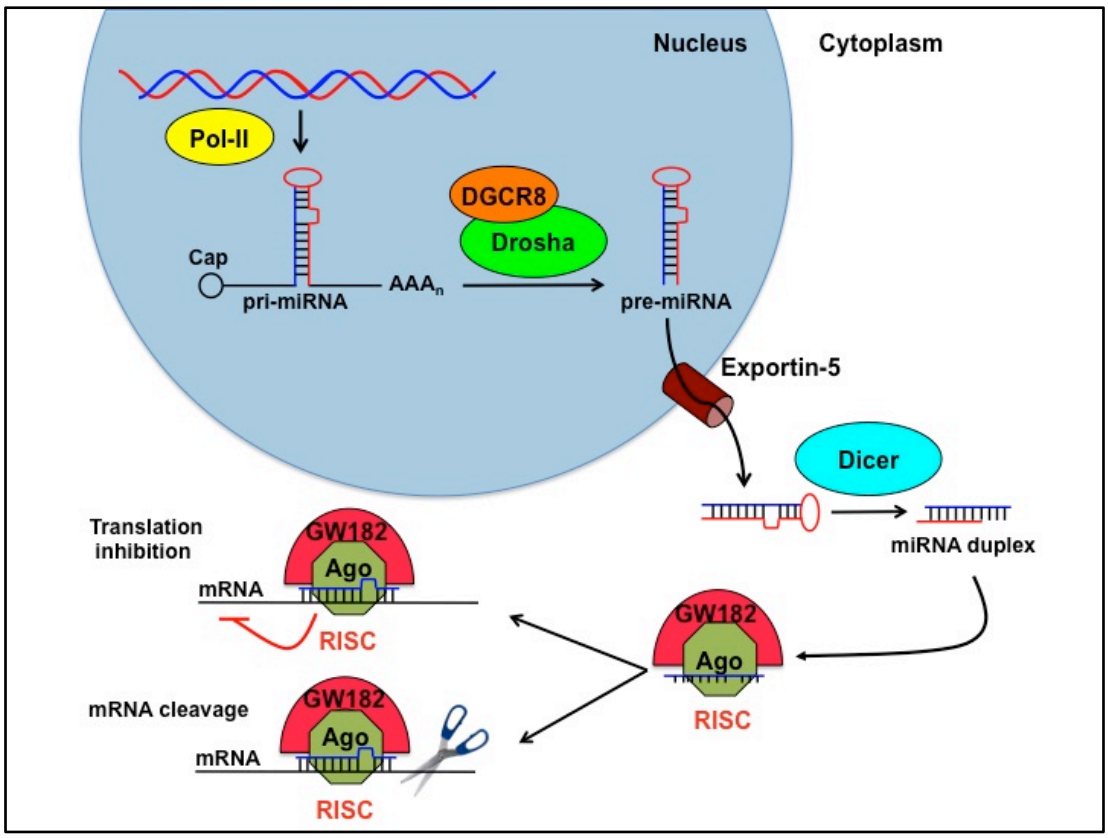


Figure 1.3 MiRNA biogenesis.
MiRNAs are transcribed by RNA polymerase II (Pol-II) into primary miRNAs (pri-miRNAs). Pri-miRNAs are then processed in the nucleus into precursor miRNAs (pre-miRNAs) by the ribonuclease Drosha, and exported in the cytosol where they are further processed into miRNA duplexes by the ribonuclease Dicer. The mature miRNAs are then loaded into the RISC complex to induce posttranscriptional repression, by mRNA cleavage or translation inhibition.

Many target prediction algorithms are based around this model of base complementarity, although it is now recognised that binding to the 3'-UTR is not always required for target recognition. Other strategies have been developed in order to implement the *in silico* approaches for target identification, mostly based on

modulation of miRNA expression (upregulation or downregulation) followed by gene expression or proteomic analysis, or immunoprecipitation of the RISC complex followed by microarray or deep sequencing analysis (Thomson et al., 2011). In particular, the ability of miRNAs to affect the stability of mRNA, which accounts for ≥84% of the decreased protein synthesis (Guo et al., 2010), endorses the use of transcriptomic approaches for the identification of putative miRNA targets.

MiRNAs are responsible for the regulation of genes involved in several normal processes, including development and differentiation, and changes in their expression have been observed in several pathological processes, including cancer (Lujambio and Lowe, 2012).

b MiRNAs and cancer

Aberrant expression of miRNAs has been extensively documented in cancer, in which they can act either as oncogenes or tumour suppressors, depending on the role of the target mRNAs in tumour biology (for an extensive review see (Lujambio and Lowe, 2012)). Multiple mechanisms can be responsible for altered miRNA expression in cancer: 1) genomic alterations, including deletions, insertions, point mutations, translocations, and amplifications (first evidence of miRNA deletion in (Calin et al., 2002)); 2) epigenetic regulation, including promoter DNA methylation and loss of histone acetylation of the miRNA encoding genes (the first evidence of miRNA downregulation following promoter hypermethylation was reported in (Saito et al., 2006)); 3) altered transcription of miRNA genes due to abnormal transcription factor signalling (for example the MYC-dependent repression of several miRNAs (Chang et al., 2008), or increased miR-210 expression following HIF stabilisation

(Camps et al., 2008; Kulshreshtha et al., 2007)); 4) altered function of the miRNA processing machinery (for example, depletion of Dicer1 or Drosha and the consequent repression of miRNA processing can promote cellular transformation and tumorigenesis *in vivo* (Kumar et al., 2007)).

Aberrant miRNA expression profiles can represent useful and accurate tools for cancer diagnosis and prognosis because of their close correlation with tumour of origin and tumour stage, and because of the ability to easily detect them in both tissue specimens and body fluids (Calin et al., 2005; Lu et al., 2005; Shen et al., 2012; Yanaihara et al., 2006).

The ability of miRNAs to influence potentially all cancer traits, including proliferation, apoptosis and metabolism, makes them noteworthy candidates for cancer therapy (Ambros, 2004; Ventura and Jacks, 2009). In particular, recent studies have demonstrated that miRNAs can play an important role in cancer cell metabolism, through either the direct modulation of metabolic enzymes and transporters, or the regulation of metabolism-associated oncogenic signalling pathways. For example, miR-195 is a downregulated miRNA in bladder cancer (Han et al., 2011) that has been demonstrated to target the glucose transporter GLUT3 (Fei et al., 2012). Several studies have demonstrated a miRNA-dependent regulation of HKII, which is the first enzyme in the glycolytic cascade, responsible for the phosphorylation of glucose to glucose-6-P. MiR-143 is also a frequently downregulated miRNA in cancer, and its direct regulation of HKII has been validated in lung, head and neck, and colon cancer cell lines (Fang et al., 2012; Gregersen et al., 2012; Peschiaroli et al., 2012). Aldolase A (AldoA) is a glycolytic enzyme that catalyses the conversion of fructose-1,6-bisphosphate into

glyceraldehyde-3-phosphate and dihydroxyacetone phosphate. Its regulation by the liver-specific microRNA miR-122 has been recently reported (Tsai et al., 2009). Moreover, the influence of miR-122 on lipid metabolism in physiological and pathological conditions, including cancer, has been abundantly documented in the recent years (Hu et al., 2012). Liver-selective depletion of miR-122 in mice is associated with altered cholesterol and triglyceride metabolism, and the development of tumours resembling hepatocellular carcinomas (Hsu et al., 2012). The influence of miR-210 on cell metabolism is discussed below.

The impact of miRNAs on metabolism could also be predicted by their documented influence on master regulators of tumour cell metabolism like p53, c-Myc, and HIF. Several cancer-deregulated miRNAs can target p53, including miR-125b, miR-30, and miR-504 (Hu et al., 2010; Le et al., 2009; Li et al., 2010). Notably, MYC is post-transcriptionally regulated by the miRNAs miR-Let-7, miR-34, and miR-145. In turn, MYC-dependent regulation of gene expression is in part mediated through the suppression of miRNAs, including miR-Let-7, miR-23, and miR-34a (Dang, 2012). Several miRNAs have been demonstrated to regulate HIF expression in cancer cell lines, including the miR-17-92 cluster in lung cancer cells (Taguchi et al., 2008), miR-20b in hepatocarcinoma and breast cancer cells (Cascio et al., 2010; Lei et al., 2009), miR-107 in colon cancer cells (Yamakuchi et al., 2010), and miR-155 in colorectal cancer cells (Bruning et al., 2011).

c Strategies for miRNA modulation in vivo

Several strategies are under development to target miRNAs *in vivo*. To block the expression of a miRNA, the available tools are represented by antagomirs, locked

nucleic acid constructs (LNA), miRNA sponges, and miRNA masks (Garzon et al., 2010). Antagomirs consist of a single-stranded RNA sequence with a hairpin structure that anneals to the target mature miRNA guide strand and induce its degradation or the formation of an inactive duplex. These inhibitors present chemical modifications that improve their stability, their binding affinity, and specificity. LNA molecules consist of nucleotides with a methylene bridge that 'locks' the ribose ring allowing improved affinity towards the targeted miRNA, and solubility in water. MiRNA sponges consist of a long transcript containing multiple tandem binding sites for the target miRNA, whereas miR masks consist of chemically-modified antisense nucleotides complementary to the miRNA-binding sequence in the target mRNA. To restore the expression of a downmodulated miRNA, miRNA mimics or miRNA-encoding viral vectors are under consideration (Garzon et al., 2010). The main challenges for the *in vivo* modulation of miRNAs are represented by tissue-specific delivery and sufficient uptake by the targeted tissue in order to obtain an efficient and sustained inhibition/induction of the target miRNA. Moreover, the risk of off-target effects (due to the miRNA intrinsic property of multiple targeting, or to displacement of endogenous miRNAs form the miRNA-processing machinery) has to be carefully considered when designing a drug for potential *in vivo* applications.

The only miRNA-targeted drug tested in clinical trials to date is represented by 'miravirsen', a LNA construct targeting miR-122 in patients with chronic Hepatitis C virus (HCV) infection. It has been demonstrated that miR-122 can bind to the HCV genome and induce upregulation of viral RNA in infected liver cells (Jopling et al., 2005). Phases I and II studies have shown that subcutaneous administration of miravirsen is well tolerated, and provides a robust, dose-dependent anti-viral activity,

which persists for more than 4 weeks after the last injection (htpp://www.santaris.com).

d MiR-210 and the hypoxia-regulated miRNAs

Several hypoxia-inducible miRNAs have been identified and they are referred to as 'hypoxamiRs' (Chan et al., 2012). A first list of hypoxia-upregulated miRNAs was generated from a panel of breast and colon cancer cell lines exposed to hypoxia and included miR-23, -24, -26, -27, -103, -107, -181, -210, and -213 (Kulshreshtha et al., 2007). Moreover, several miRNAs included in this signature were also found to be overexpressed in breast cancer and other solid tumours, providing evidence that hypoxia could represent a key contributor for miRNA modulation in cancer (Kulshreshtha et al., 2007). Other studies went to confirm the presence of hypoxia miRNA signatures, although the lists generated differed substantially, probably due to the different cell lines, experimental conditions, and detection techniques used (Camps et al., 2008; Guimbellot et al., 2009; Hebert et al., 2007; Pulkkinen et al., 2008). However, miR-210 appeared to be the most robustly and consistently upregulated across different studies, in both normal and cancer cells exposed to hypoxia (Devlin et al., 2011).

The stem-loop of miR-210 is located in an intron of a noncoding RNA, which is transcribed from the gene AK123483 on chromosome 11p15.5 (Huang et al., 2010). It has been validated both as a HIF1α (Camps et al., 2008; Crosby et al., 2009; Huang et al., 2009; Kim et al., 2009; Kulshreshtha et al., 2007) and a HIF2α target (Zhang et al., 2009), and its expression levels significantly correlate with a hypoxia gene expression signature in breast and head and neck cancers, suggesting regulation

by hypoxia also *in vivo* (Gee et al., 2010). Furthermore, miR-210 expression was found to be prognostic in several tumour types. In breast cancer, a study on 210 early invasive breast cancers demonstrated that miR-210 expression correlates with poor outcome (determined by both disease-free and overall survival) (Camps et al., 2008). Another study reported that triple-negative (oestrogen receptor, progesterone receptor, and Her2 negative) breast cancer patients with low miR-210 levels experienced better disease-free and overall survival than patients with high miR-210 levels (Toyama et al., 2012). A meta-analysis on 511 cases of breast cancer also confirmed that high expression of miR-210 was associated with poor survival (Hong et al., 2012). A recent study demonstrated that miR-210 was not only associated with prognosis but also with the invasive transition in breast cancer progression (Volinia et al., 2012). In head and neck cancer patients, high levels of miR-210 were associated with locoregional disease recurrence and short overall survival (Gee et al., 2010).

Finally, the ability to non-invasively detect altered miR-210 expression further supports the clinical potential of miR-210 as a diagnostic and prognostic tool. For example, elevated circulating levels of miR-210 can be used as a marker for the detection of renal cell cancer (Zhao et al., 2012), diffuse large B-cell lymphoma (Lawrie et al., 2008), pancreatic ductal carcinoma (Ho et al., 2010; Wang et al., 2009), malignant solitary pulmonary nodules (Shen et al., 2011). In breast cancer patients, prior to the administration of neoadjuvant chemotherapy in combination with trastuzumab, the detection of elevated miR-210 levels in plasma was able to distinguish patients with residual disease from patients with a complete pathological response. Moreover, miR-210 levels were found to be significantly higher in

preoperative plasma samples and in patients with lymph node metastases (Jung et al., 2012). Detection of miR-210 in stool samples of pancreatic cancer patients has also proved a valuable prognostic indicator (Ren et al., 2012).

Great effort is now directed to unveil targets contributing to tumour aggressiveness. Several miR-210 targets have been validated so far, showing roles of miR-210 in cell cycle regulation (E2F transcription factor 3 [E2F3], MAX-binding protein [MNT]), apoptosis (Caspase8-associated protein 2 [CASP8P], SH2 domain-containing inositol-5'-phosphatase 1 [SHIP], Bcl-2), iron accumulation (iron-sulfur cluster scaffold homolog [ISCU]), ROS production and cell metabolism (subunit D of SDH [SDHD], cytochrome c oxidase assembly homolog 10 [COX10], ISCU, glycerol-3-phosphate dehydrogenase 1-like [GPD1L], DNA repair (RAD52, ISCU), tumour initiation (homeobox A1 [HOXA1], Fibroblast growth factor-like 1 **[**FGFRL1]), metastasis (vacuole membrane protein 1 [VMP1]), endothelial cell survival, migration and differentiation (ephrin-A3 **[**EFNA3], brain-derived neurotrophic factor [BDNF], tyrosine-protein phosphatase non-receptor type 1 **[**PTPN1], protein disulphide isomerase [P4HB]), and osteoblast and adipocyte differentiation (activin receptor 1B [ACVR1B], transcription factor 7-like 2 **[**TcF7l2]) (Chan et al., 2009; Chen et al., 2010; Chio et al., 2012; Crosby et al., 2009; Fasanaro et al., 2008; Fasanaro et al., 2009; Favaro et al., 2010; Giannakakis et al., 2008; Huang et al., 2009; Kim et al., 2009; Lee et al., 2012; Mizuno et al., 2009; Puissegur et al., 2011; Pulkkinen et al., 2008; Qin et al., 2010; Tsuchiya et al., 2011; Ying et al., 2011; Yoshioka et al., 2012; Zhang et al., 2009) (Figure 1.4).

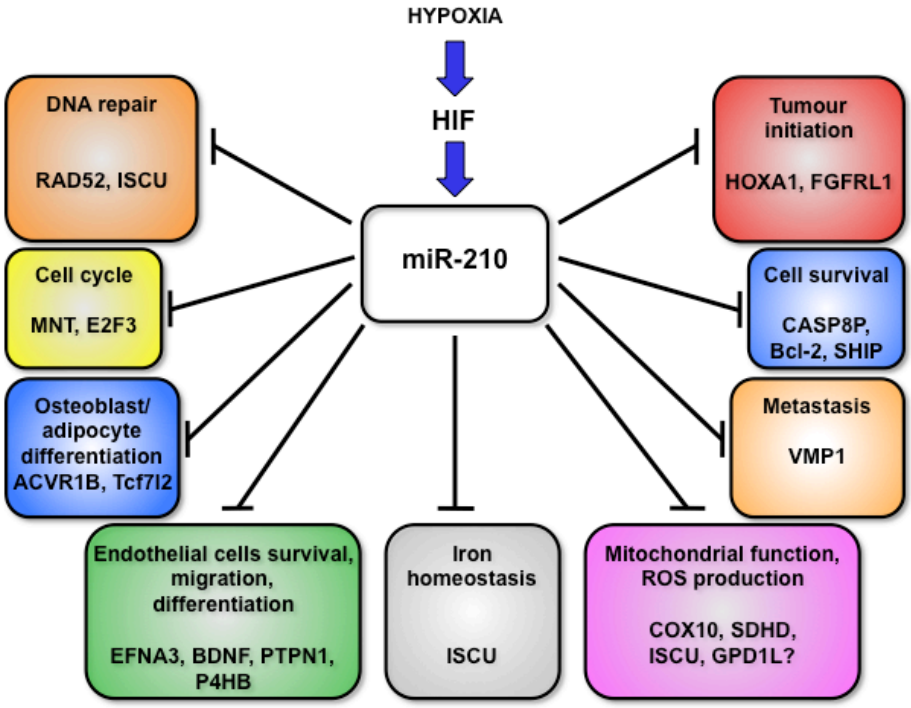


Figure 1.4 Cellular processes regulated by miR-210-validated targets.
Abbreviations: RAD52= Rad52 Homolog, ISCU Iron-sulfur cluster scaffold homolog, MNT= MAX-binding protein, E2F3= E2F transcription factor 3, ACVR1B= Activin receptor 1B, Tcf7l2= Transcription factor 7-like 2, EFNA3= Ephrin-A3, BDNF= Brain-derived neurotrophic factor, PTPN1= Tyrosine-protein phosphatase non-receptor type 1, P4HB= Protein disulphide isomerase, COX10= Cytochrome c oxidase assembly homolog 10, SDHD= Succinate dehydrogenase complex subunit D, GPD1L= Glycerol-3-phosphatase dehydrogenase 1-like, VMP1= vacuole membrane protein 1, CASP8P= Caspase8-associated protein 2, Bcl-2= B-cell lymphoma 2, SHIP= SH2 domain-containing inositol-5'-phosphatase 1, HOXA1= Homeobox A1, FGFRL1= Fibroblast growth factor-like 1.

In particular, increasing evidence indicates that miR-210 can regulate mitochondrial metabolism by repressing the expression or the activity of several enzymes operating in this pathway. MiR-210 overexpression in lung cancer cells has been associated with alterations of mitochondrial morphology (enlarged mitochondria and modified organisation of cristae) and mitochondrial membrane potential, which are both considered indicators of mitochondrial dysfunction. This phenotype could be

recapitulated by depletion of the miR-210 target SDHD, which is a subunit of complex II in the electron transport chain (Puissegur et al., 2011). Another study performed on colon cancer cell lines, showed that miR-210 can trigger the metabolic switch from aerobic respiration to glycolysis (as indicated by reduced oxygen consumption and concomitant increase in lactate production), and induces the generation of ROS, indicating COX10 and ISCU as miR-210 targets related to mitochondrial metabolism. COX10 is important for the biosynthesis of heme-α, which is an essential component of cytochrome c oxydase, complex IV (COX) in the respiratory chain (Puissegur et al., 2011). While the present manuscript was in preparation, ISCU has been validated as a miR-210 target in normal pulmonary endothelial cells, where it contributes to the Pasteur effect (switch to glycolysis in hypoxia) and controls the level of ROS production in hypoxia, suggesting its potential adaptive role to hypoxia in the context of pulmonary endothelium (Chan et al., 2009). Iron-sulfur clusters [Fe-S] are present in the active sites of many enzymes and proteins, critical for their activity and capable of conferring regulation by redox status (Rouault and Tong, 2008). These clusters are assembled in mitochondria (Muhlenhoff and Lill, 2000) by a complex series of chaperones and enzymes including ISCU, then exported to the cytoplasm, where they are assembled into the relevant protein (Tong and Rouault, 2000). Amongst the Fe-S cluster proteins involved are several that comprise key components of complex I, II and III in the mitochondria, and components of the Krebs cycle such as SDH and aconitase (Figure1.5).

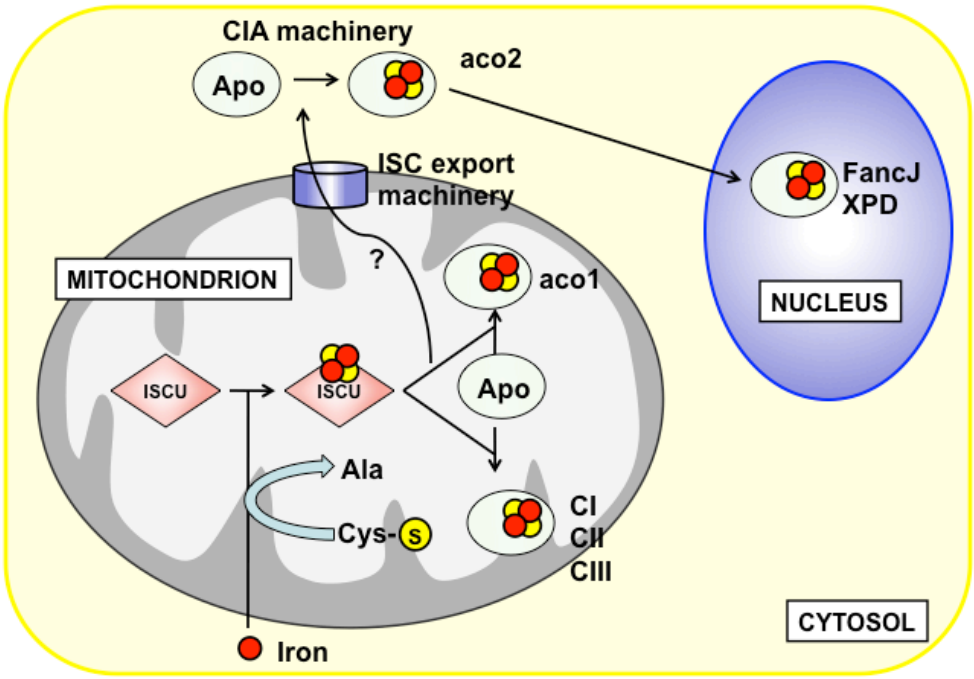


Figure 1.5 The mitochondrial ISCU assembly machinery.
Iron is imported into the mitochondria through specific transporters, whereas sulfur is released from cysteine (cys) by a cysteine desulfurase. These are assembled into clusters in the scaffold protein ISCU and then transferred to the recipient apoproteins in the mitochondrion. Alternatively, the clusters can be exported in the cytosol through a ISC export machinery (still undefined) and transferred to the relevant proteins in the cytosol or in the nucleus. Abbreviations: ala= alanine, C I/II/II= Complex I/II/III, Apo= apoprotein, Aco1/2= aconitase 1/2, ISC= iron-sulfur clusters, CIA= cytosolic iron-sulfur assembly, FancJ= Fanconi anemia complementation group J, XPD= xeroderma pigmentosum group D.

Another interesting target, which may be involved in the regulation mitochondrial metabolism, is GPD1L, as suggested by the high homology with glycerol-3-phosphate dehydrogenase (GPD). GPD oxidizes glycerol-3-phosphate to dihydroxyacetone phosphate with concurrent reduction of flavin adenine dinucleotide and transfers electrons to coenzyme Q (CoQ) in the electron transport chain (Mracek et al., 2012). However, further investigations are required to demonstrate its role on mitochondrial function.

Although most of the studies focused their attention on miR-210, other miRNAs could contribute to the hypoxic response. For example, experimental evidence suggests that miR-26 and miR-107 may play a role in cell survival in a low-oxygen environment (Kulshreshtha et al., 2007). A recent study has shown that miR-495 is robustly upregulated in a subset of breast cancer stem cell population, both in stabilized cancer cell lines and in primary cells (Hwang-Verslues et al., 2011) where it promotes colony formation and tumourigenesis. Moreover, it is involved in cancer stem cell phenotype maintenance, invasion by suppression of E-cadherin, and hypoxia resistance through modulation of the REDD1-mTOR pathway.

1.2.4 Glycogen metabolism

Glycogen metabolism has recently been proposed as an important pathway of metabolic reprogramming in cancer cells exposed to hypoxia (Brahimi-Horn et al., 2010; Pelletier et al., 2012; Pescador et al., 2010; Shen et al., 2010).

a Glycogen synthesis and degradation

Glycogen comprises a store of glucose, which is mainly present in liver and muscles. The structure consists of long polymeric chains of glucose units linked by alpha (α)-1,4 glycosidic bonds with occasional α-1,6 glycosidic bonds that generate branching points and increase solubility (Berg et al., 2002). Synthesis and breakdown of glycogen involves the activity of several enzymes and regulatory proteins. The main precursor for glycogen synthesis is represented by glucose transported into the cells through glucose transporters localised in the plasma

membrane (direct pathway). Alternatively, gluconeogenic precursors such as lactate and alanine can be utilised through an indirect pathway, also termed 'glyconeogenesis' (Roach et al., 2012). The first reaction of glycogen biosynthesis is the ATP-dependent phosphorylation of glucose to glucose-6-P by the enzyme HK or glucokinase in the liver. Glucose-6-P is converted into glucose-1-phosphate (glucose-1-P) by phosphoglucomutase (PGM), and activated to uridine diphospho-glucose (UDP-glucose) by UDP-glucose pyrophosphorylase at the expense of converting uridine triphosphate (UTP) into UDP. A glucosyl unit is first added to a tyrosine residue of glycogenin (GYG) with a concomitant release of UDP, and GYG then catalyses the formation of α-1,4 glycosidic linkages until a short oligosaccharide primer is built up. Glycogen synthase elongates the glycogen chains initiated by GYG, by formation of α-1,4 glycosidic bridges, whereas a branching enzyme (GBE) transfers a segment from the end of a glycogen chain to generate a branch with a α-1,6 glycosidic linkage. Conversely, glycogen breakdown is mostly catalysed by glycogen phosphorylase, which cleaves α-1,4 glycosidic linkages by the addition of orthophosphate to yield glucose-1-P. Glucose-1-P can be utilised by the cell through the glycolytic pathway or the pentose phosphate pathway, by conversion into glucose-6-P (PGM). When glycogen phosphorylase reaches the fourth unit from a branching point, a debranching enzyme (DBE) transfers three units to the end of another glycogen chain and catalyses the hydrolysis of the α-1,6 glycosidic linkage, yielding free glucose (Figure 1.6) (Berg et al., 2002; Roach et al., 2012).

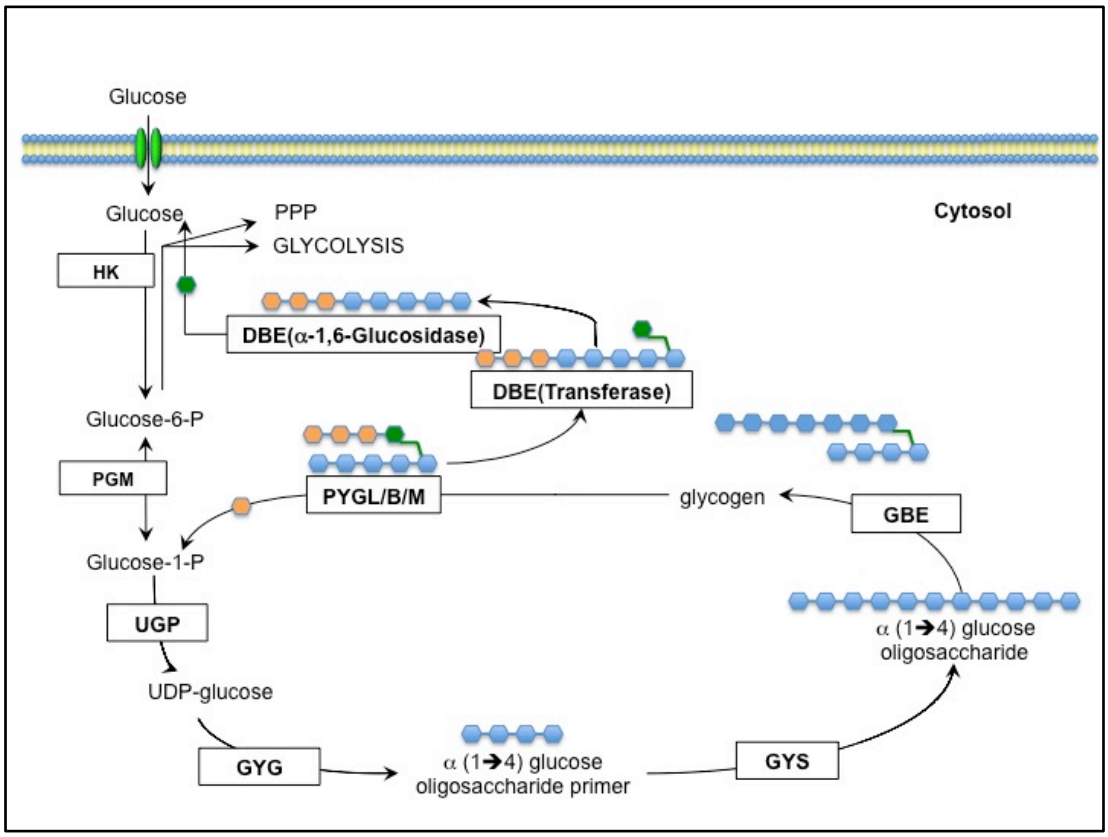


Figure 1.6 Schematic representation of glycogen synthesis and breakdown.
Abbreviations: HK= hexokinase, glucose-6/1-p= glucose-6/1-phosphate, PGM= phosphoglucomutase, UGP= UDP-glucose pyrophosphatase, UDP-glucose= uridine diphospho-glucose, GYG= glycogenin, GYS= glycogen synthase, GBE= glycogen branching enzyme, PYGL/B/M= glycogen phosphorylase, liver/brain/muscle, DBE= debranching enzyme, PPP= pentose phosphate pathway.

Although glycogen degradation occurs primarily through glycogen phosphorylase and debranching enzyme in the cytosol, glycogen can also be transferred to the lysosomes and be hydrolysed by the enzyme α-acid glycosidase (GAA) in a process named 'glycogen autophagy' (Singh and Cuervo, 2011). Under physiological conditions, only 10% of glycogen is confined to the lysosomal compartment in the liver, but the importance of this pathway is indicated by the severe consequences that can be associated with GAA deficiency in the infantile onset of the Pompe disease (hypotonia, idiopathic hypertrophy of the heart, death (www.omim.org)). The exact

mechanism by which glycogen accumulates in lysosomes is still unclear, however, recent evidence suggests that glycogen engulfment into lysosomes could be mediated by anchoring to cell membranes through the Starch Binding Domain-containing Protein 1 (Stbd1)/Genethonin 1 and interaction with the autophagy protein γ-aminobutyric acid type A receptor-associated protein-like 1 (GABARAPL1) (Jiang et al., 2010).

b Glycogen synthase and phosphorylase, structure and regulation

Amongst the multiple enzymes involved in glycogen metabolism, glycogen synthase (GS) and glycogen phosphorylase (GP) represent the rate-limiting enzymes of glycogen synthesis and degradation, respectively (Berg et al., 2002).

GS has two isoforms: GYS1 (muscle), expressed in skeletal muscle and most other cells capable of glycogen synthesis, and GYS2 (liver), which appears to be restricted to liver (Roach et al., 2012). The two isoforms are approximately 70% identical in their amino acid sequence, and the highest degree of identity is present in the central region, which contains the catalytic sites, whereas the amino- and carboxyl-terminal regions present the lower degree of identity and contain multiple phosphorylation sites (Ferrer et al., 2003). The activity of GS is modulated by the allosteric activator glucose-6-P and by phosphorylation. GS contains nine known phosphorylation sites, which are targets of multiple protein kinases, including protein kinase A (PKA), glycogen synthase kinase 3 (GSK3), and adenosine monophosphate (AMP)-activated protein kinase (AMPK) (Roach et al., 2012). Phosphorylation induces the conversion

of the active form *a* into the inactive form *b*, that requires high levels of glucose-6-P for activity.

GP has three isoforms: PYGM (muscle), liver (PYGL) and brain (PYGB) (Newgard et al., 1989), that are predominantly expressed in muscle, liver, and brain/fetal tissues, respectively. The enzyme consists of two identical subunits, with a glycogen-binding site localised in the amino-terminal domain, and a catalytic site formed by residues of both the amino- and the carboxyl-terminal domains, including a binding site for the cofactor pyridoxal phosphate (Berg et al., 2002). Although PYGM and PYGL share 90% amino acid sequence homology, they differ substantially in their regulation. The brain isoform shares 83% sequence homology with PYGM and 80% with PYGL, and it is more similar to the muscle isoform with regard to allosteric regulation (Brown, 2004). Similarly to GS, the activity of GP is regulated by allosteric effectors and reversible phosphorylation (Berg et al., 2002). In particular, phosphorylation dictates the conversion from a dephosphorylated form *b* to a phosphorylated form *a*. In the muscle, PYGM *a* is generally present in a relaxed (R)/active state, whereas *b* is generally present in a tense (T)/inactive state with the catalytic site partially blocked. This inactive state of the enzyme can be reversed to the R state only in the presence of high concentrations of the allosteric activator AMP, whereas ATP and glucose-6-P act as negative allosteric effectors by favouring the T state of the molecule. In the liver, PYGL is insensitive to regulation by AMP and the *a* form is the most sensitive to allosteric regulation mediated by free glucose, which favours the R-to-T transition, inactivating the enzyme. Phosphorylation of serine 14 of GP is mediated by phosphorylase kinase that requires activation by

PKA. In turn, PKA activation is triggered by epinephrine (muscle)- and glucagon (liver)-dependent increase in cytosolic cyclic AMP levels. Allosteric effectors and hormonal-induced phosphorylation of GS and GP (which has inhibitory and activating effects on GS and GP, respectively), ensure a tight and reciprocal regulation of glycogen synthesis and degradation, and the prevention of futile cycles. Importantly, this phenomenon is also controlled by the activity of protein phosphatase 1 (PP1), that mediate dephosphorylation of both GS and GP. PP1 is negatively regulated by PKA and positively regulated by insulin, and consists of three components: i) a catalytic subunit P1, ii) a glycogen-binding subunit R_{G1}, and iii) a small regulatory subunit inhibitor 1. To date, seven glycogen-binding subunits have been described, including the more extensively studied R_{GL} (product of the gene protein phosphatase 1 regulatory subunit 3A [*PPP1R3A*]), G_L (product of the gene *PPP1R3B*), and R5 (product of the gene *PPP1R3C*) (Roach et al., 2012).

c Role of glycogen in cancer

A number of observations have suggested that the turnover of glycogen is altered in tumour cells. The levels of glycogen were demonstrated to be particularly high in breast, kidney, uterus, bladder, ovary, skin and brain cancer cell lines. Glycogen content in these cells was inversely correlated with proliferation rate (Rousset et al., 1981). Glycogen accumulation under hypoxic conditions has also been observed in several non-cancer and cancer cell lines (Mamedova et al., 2003; Pelletier et al., 2012; Pescador et al., 2010; Shen et al., 2010; Vigoda et al., 2003). Consistent with these observations, GYS1 and other proteins involved in glycogen synthesis are induced in hypoxia in a HIF1α-dependent manner (Mole et al., 2009; Pelletier et al., 2012; Pescador et al., 2010; Shen et al., 2010). PYGL was included in a list of 99

genes defining the hypoxia 'metagene', a signature defined *in vivo* in head and neck squamous cell carcinomas (HNSCC) by clustering genes with similar expression patterns to that of well-characterised hypoxia-regulated genes (Winter et al., 2007). This signature proved to be prognostic in independent HNSCC and breast cancer series.

Recent studies have suggested a critical role of glycogen in promoting the survival of cancer cells. In particular, it has been demonstrated that a small molecule inhibitor of glycogen breakdown could induce apoptosis in pancreatic tumour cells (Lee et al., 2004a). Furthermore, it has been shown by two independent studies that glycogen accumulation in cancer cells improves survival in response to low oxygen concentration and glucose deprivation (Pelletier et al., 2012; Pescador et al., 2010). Taken together, these observations suggested a role for glycogen in promoting tumour growth in hypoxic environments.

Aims of the study

The focus of this project was the identification of factors modulated by hypoxia, with a specific role in the metabolic adaptation of cancer cells. Two different approaches were adopted. The first one developed from the study of the most widely expresses and upregulated HIF1α-dependent miRNA, miR-210 and investigated the possible metabolic functions of its target ISCU; the second one looked directly at metabolism-related genes that were differentially expressed in hypoxic tumours.

Therefore, the aims of this project were as follows:

1. To verify the regulation of the miR-210-ISCU pathway in cancer cells in hypoxia and evaluate the contribution of ISCU to metabolic reprogramming through the regulation on Fe-S-dependent metabolic enzymes;

2. To characterise the regulation of glycogen metabolism in cancer cells exposed to hypoxia and investigate the consequences of glycogen breakdown inhibition in tumour growth *in vitro* and *in vivo*.

2 CHAPTER TWO

Materials and Methods

2.1 Cell culture

2.1.1 Cell lines and growth conditions

The breast cancer MCF-7, glioblastoma U87, and colon cancer HCT116 cell lines were provided by Cancer Research UK Cell Services (Clare Hall, UK) and were grown in high glucose (25 mM) Dulbecco's modified Eagle's medium (DMEM) supplemented with 10% fetal calf serum Gibco-BRL). In a set of experiments, U87 cells were cultivated in low glucose (5 mM) DMEM (Gibco-BRL). All cells were maintained in a tissue culture incubator at 5% carbon dioxide (CO_2), 21% oxygen (O_2), and 37°C, unless otherwise specified. Cells were used only until passage 20.

Cell exposure to hypoxia (1% or 0.1% O_2) was undertaken in a hypoxia incubator (1% O_2) (MiniGalaxy A, RS Biotech), or an *in vivo*$_2$ 400 hypoxic workstation (0.1% O_2) (Ruskinn Technologies).

2.1.2 Cell counting

Cell counting was performed with the Z2 Coulter Particle Counter (Beckman Coulter) according to manufacturer's instructions. Briefly, a volume of 19.6 ml of ISOTON® II Diluent (Beckman Coulter) was added to 400 μl of cell suspension and counts were determined on particles in the range of 9-27 μm.

2.1.3 Transient transfection with oligonucleotides

Transfections of siRNA duplexes targeting HIF1α, HIF-2α, ISCU (siISCU1, 2, 3, and 4), GYS1, PYGL, p53 or a scramble control (scr) at a final concentration of 20

nM, were performed in Optimem (Invitrogen), using Oligofectamine reagent (Invitrogen). Oligofectamine was diluted in Optimem and after 5 minutes at room temperature (RT), the mix was added to 20 nM siRNA in Optimem, and complexes were allowed to form for 20 minutes at RT. Finally, complexes were added to cell suspensions in antibiotic-free media, and plated in cell culture dishes. The next day, media was removed from the cells and replaced with normal growth media.

For most of the experiments, transfection was performed in 6 cm dishes. For TEM sample preparation and nicotinamide adenine dinucleotide phosphate (oxidised) ($NADP^+$)/ NADPH quantification, transfection was performed in 10 cm dishes, for glucose-6-P quantification, and sample preparation for Metabolon 15 cm dishes were used. Volumes of reagents used in each format are specified in the following table.

Dish size	**20 µM siRNA (µl)/Optimem (µl)**	**Oligofectamine (µl)/Optimem (µl)**	**Cells (number)/ DMEM (µl)**	**Final volume (µl)**
6 cm	2/368	6/24	$3.5*10^5$/1600	2000
10 cm	8/1472	24/96	$1*10^6$/6400	8000
15 cm	18/3312	54/216	$5.5*10^6$/14400	18000

Table 2.1 Transfection conditions

Knockdown of GYS1, PYGL, and p53, was performed with a pool of 4 siRNA sequences (ON-TARGETplus SMARTpool, Thermo Scientific). To knockdown PYGL a pool of the following 4 sequences of siRNA was used: 1) 5'-TTACATGGGCCGAACATTA-3'; 2) 5'-TAAGATTGAAGCAGGAATA-3'; 3) 5'-GAACAATGACCCTATGGTT-3' and 4) 5'-CGTGGAACCTTCAGATCTA-3'. A pool of non-targeting sequences was used as a control (ON-TARGETplus Non-

targeting Pool, Thermo Scientific). Knockdown of HIF1α, HIF-2α, and ISCU (1, 2, 3, and 4) was performed with single siRNA sequences, and a single non-targeting sequence was used as a control (Eurogentec). Details of the oligonucleotides are summerised in Table 2.2.

Target	**Oligonucleotide sequences**
HIF1α	Antisense: 5'-CUGAUGACCAGCAACUUGAdTdT-3' Sense: 5'-UCAAGUUGCUGGUCAUCAGdTdT-3'
HIF2α	Antisense: 5'-UUCAAUCUUCAGGUCGUUAdTdT-3' Sense: 5'-UAACGACCUGAAGAUUGAAdTdT-3'
ISCU	1) Antisense: 5'-UUUCCUUUCACCCAUUCAGdTdT-3' Sense 5'-CUGAAUGGGUGAAAGGAAAdTdT-3' 2) Antisense: 5'-UUCUUCUCUGCCUCUCCUUdTdT-3' Sense 5'-AAGGAGAGGCAGAGAAGAAdTdT-3' 3) Antisense: 5'-AAUUUCAUUACGUCACCACdTdT-3' Sense: 5'-GUGGUGACGUAAUGAAAUUdTdT-3' 4) Antisense: 5'-UCAGCCAGGGCGGCCUUGAdTdT-3' Sense 5'-UCAAGGCCGCCCUGGCUGAdTdT-3'
Scr	Antisense 5'-ACGACACGCAGGUCGUCAUdTdT-3' Sense: 5'-AUGACGACCUGCGUGUCGUdTdT-3'

Table 2.2 Oligonucleotide sequences

For miR-210 depletion or over-expression, miRIDIAN anti-210, miR-210 mimic, or control oligos (Thermo Scientific), were used at a final concentration of 20 nM, using the same protocol as above. In a set of experiments, 1 nM anti-miRNA or 100 pM mimic-RNA were used. MiRIDIAN mimics consist of chemically modified double-stranded RNA molecules that 'mimic' a specific miRNA. MiRIDIAN miRNA inhibitors consist of chemically modified RNA molecules with a hairpin structure that inhibit a specific miRNA.

2.1.4 Transient transfection with plasmid DNA constructs

The day before transfection, cells were seeded at 50-80% confluence in a 6-well plate. The following day, 6.5 μl of Lipofectamine 2000 (Invitrogen) was added to 250 μl of Optimem and left for 5 minutes at RT. 250 μl of Optimem with 1 μg plasmid overexpressing a C-terminal Myc-DKK tagged ISCU2 (pCMV6-ISCU2, OriGene Technologies), and 20 nM siRNA or mimic-RNA/anti-miR were then added, and complexes were allowed to form for 20 minutes at RT. Adherent cells were washed in Optimem and incubated with 500 μl of complexes for 4-6 hours at 37°C. Media was then removed and replaced with normal growth media. For the ROS rescue experiments, cells were co-transfected with 1 μg pcDNA3-GFP for co-localisation.

2.1.5 Transduction protocol

The lentiviral transduction particles containing GYS1 or PYGL shRNA expression cassette or a non-targeting shRNA sequence were purchased from Sigma-Aldrich. The sequence targeting PYGL was the following: 5'-CCGGTACCAGCTTGGATTGGATATACTCGAGTATATCCAATCCAAGCTGGTATTTTTG-3'. All particles contained a puromycin resistance cassette for cell selection. Cells were seeded at a density of 4 x 10^4 per well in a 48-well plate. The following day, when cells were at 50-80% confluence, they were transduced with the appropriate amount of viral particles at a multiplicity of infection (MOI) of 3, in the presence of 6 μg/ml Polybrene (Sigma), in a 100 μl of media per well, according to manufacturer's instructions. A titration curve was performed to determine the

appropriate concentration of puromycin to use (Invitrogen). Briefly, 4 x 10^4 cells were seeded in a 48-well plate, and a range of 0.5-10 μg/ml of puromycin was added to the wells. Viability was examined after 3 days, and the minimum concentration of puromycin that caused complete cell death was used to select for cells expressing the shRNA (1 μg/ml in U87 cells).

2.2 RNA extraction and RT-qPCR

2.2.1 RNA extraction

RNA extraction and processing was performed with diethyl pyrocarbonate (DEPC)-treated water (DNase and RNase free water) (Ambion). DNase, RNase and pyrogen-free pipette tips, and sterile microcentrifuge tubes were used (Axygen Scientific).

Cells were lysed directly on the culture dish with 1 ml of TRI Reagent (Sigma-Aldrich). Cells were then scraped and the lysate was collected in a sterile tube, and allowed to stand for 5 minutes at RT. For phase separation (RNA from DNA and proteins), 0.2 ml of chloroform was added (Fisher Scientific), the tubes were shaken vigorously for 15 seconds, and allowed to stand for 2 minutes at RT. The resulting mixture was then centrifuged at 12000 x *g* for 15 minutes at 4°C. The aqueous phase containing RNA was transferred to a new tube, and RNA was precipitated with 0.5 ml of 2-propanol (Fisher Scientific). The sample was allowed to stand for 10 minutes at RT, then it was centrifuged at 12000 x *g* for 10 minutes at 4°C. The supernatant was removed and the RNA pellet was washed with 1 ml of 75% ethanol (Fisher Scientific) in DEPC-water. The samples were centrifuges at 7500 x *g* for 5 minutes

at 4°C and air-dried before being resuspended in DEPC-water. RNA samples were stored at -80°C until further processing.

For tumour samples, frozen tissues were homogenised with the Mikro-Dismembrator U (Sartorius) before processing with TRI Reagent.

RNA quantification was performed on 2 µl of sample with the NAnoDrop ND-1000 spectrophotometer (Thermo Scientific). Absorbance at 260 nm (A260) was used to calculate RNA yield with the following formula:

$$\text{RNA concentration (µg/ml)} = \text{A260} \times 40$$

Absorbance is multiplied by a factor of 40 µg/ml corresponds to an A260 of 1. The ratio of the absorbance at 260 and 280 nm was used to assess the purity of RNA, where pure RNA has a ratio of 2.1.

2.2.2 Reverse transcription and Real-time PCR

Reverse transcription of RNA into cDNA was performed with the High Capacity cDNA kit (Applied Biosystems), as per manufacturer's instructions. Briefly, 1 µg of RNA in 10 µl of DEPC-water was added to 10 µl of Master Mix (2 µl of 10x RT buffer, 0.8 µl of 25x dNTPs mix, 2 µl of 10x random primers, 1 µl of reverse transcriptase, and 4.2 µl of DEPC-water). A 2-step reaction (10 minutes at 25°C followed by 2 hours at 37°C) was run in the Q-cycler Thermocycler (Quanta Biotech). cDNA was diluted to 1 ng/µl and stored at -20°C until further use.

Real-time PCR (RT-qPCR) was performed with the SensiMix SYBR No-ROX kit (Bioline), using 5 µl of cDNA and 15 µl of a mix (12.5 µl of 2x SensiMix SYBR No-ROX, 1 µl of 10 µM Forward Primer, 1 µl of 10 µM Reverse Primer, and 5.5 µl of DEPC-water) containing specific primers for the product of interest. RT-qPCR

reaction was run in the 72-well Rotor-Gene RG-3000 Thermocycler (Corbett Research) using the following thermal cycling conditions:

- 10 minutes at 95°C
- 40 cycles of 95°C for 15 seconds and 60°C for 1 minute

Each PCR reaction was done in triplicate. To normalize for total RNA, *HPRT1* or β-actin was amplified in the same reaction with commercially available primers sets. The $2^{(-DDCt)}$ method (Vandesompele et al., 2002) was used for normalization. Primer sequences used are listed in Table 2.3.

Gene	**Primer sequence**
β-actin	Forward: ATTGGCAATGAGCGGTTC Reverse: GGATGCCACAGGACTCCAT
HPRT1	Forward: CCAGTCAACAGGGGACATAAA Reverse: CACAATCAAGACATTCTTTCCAGT
ISCU	Forward: AATGGGTGAAAGGAAAGACG Reverse: GCTCCTTGGCGATATCTGTG
CA9	Forward: CTTGGAAGAAATCGCTGAGG Reverse: TGGAAGTAGCGGCTGAAGTC
GYS1	Forward: CCGCTATGAGTTCTCCAACAAGG Reverse: AGAAGGCAACCACTGTCTGCTC
PYGL	Forward: CACTTCAGTGGCAGATGTGGTG Reverse: GCAGTGGAAATCTGCTCTGACAG
GAA	Forward: TCTACAGCGTGGAGTTCTCCGA Reverse: GCTGAAGGAACTGGTCCGCAAA
GBE	Forward: TGGGCAAAGTATGTGGTTCG Reverse: AGACTCCGTGGCTTCTTTGG
PPP1R3B	Forward: TTGACGACAGCAGAGAGCGAGA Reverse: GGTTCTGAACCTTCACAGTGCC
PPP1R3C	Forward: CCTCTGCCTTAAAACACCACGAG Reverse: CAACGAGCAGTTCTCCAGACAG

Table 2.3 Primer sequences used for RT-qPCR

2.2.3 Reverse transcription and Real-time PCR for miRNA

MiRNA expression was quantified by RT-qPCR using the TaqMan MicroRNA Assay (Applied Biosystems). cDNA was synthesized with the TaqMan MicroRNA Reverse Transcription Kit (Applied Biosystems) from 100 ng of RNA using TaqMan miR-210 specific primers (sequence: CUGUGCGUGUGACAGCGGCUGA), or the small nucleolar RNA 48 (snoRNA) specific primers (sequence: GAUGACCCCAGGUAACUCUGAGUGUGUCGCUGAUGCCAUCACCGCAGC GCUCUGACC) (Applied Biosystems). These primers have a stem-loop hairpin structure in order to bind specifically to the mature miRNA, and not to the precursor molecule (Chen et al., 2005). Briefly, 5 µl of RNA was added to 1 µl of 50U/µl MultiScribe Reverse Transcriptase, 1.5 µl of 10x Reverse Transcription buffer, 0.19 µl of 20 U/µl RNAse inhibitor, 4.16 µl of DEPC-water, and 3 µl of miRNA or snoRNA specific primer. The reaction was run in the Q-cycler Thermocycler using the following conditions:

- 30 minutes at 16°C
- 30 minutes at 42°C
- 5 minutes at 85°C

Samples were diluted 1:10 and stored at -20°C until further use.

RT-qPCR was performed in triplicate, from 1.33 µl of cDNA, using 10 µl of the Universal PCR master mix NO AmpErase UNG, 1 µl of primers and probe mix of the TaqMan MicroRNA Assay (both from Applied Biosystems), and 7.67 µl of DEPC-water. The reaction was run in the Rotor-Gene 3000. MiRNA expression was determined with the $2^{(-DDCt)}$ method (Vandesompele et al., 2002).

2.3 Protein extraction and analysis

For Western blotting analyses, cells were washed twice with ice cold PBS, and lysed in 300-500 µl of urea lysis buffer (5 ml of glycerol, 0.5 ml of 1 M Tris-HCl pH 6.8, 250 µl of 1 M dithiothreitol, 5 ml of 10% sodium dodecyl sulphate (SDS), protease inhibitor cocktail Complete (Roche), phosphatase inhibitor PhoSTOP (Roche), made up to 50 ml with 8 M urea) while plates were kept on ice to prevent protein degradation. Lysates were harvested with a Costar cell scraper (Corning Inc.) and passed through a 1 ml syringe with a 25-gauge needle (Terumo).

Protein quantification was performed with the BioRad protein assay. A standard curve was generated with serial dilutions of bovine serum albumin (Sigma-Aldrich). Samples were diluted 1:6 in water, and 5 µl of each sample or standard were added in triplicate to a 96-well plate. 25 µl of a mix containing 50 parts of Reagent A and 1 part of Reagent S were added to each well. 200 µl of Reagent B was then added to each well, and the plate was incubated for 30 minutes at RT. Colour change was measured with the µQuant microplate spectrophotometer (BioTeK Instruments Inc.). Protein concentration of each sample was calculated by applying the readings to the standard curve.

30 µg of samples were mixed with 4x NuPage LDS Sample Buffer (Invitrogen) containing 2-mercaptoethanol, and then heated at 95°C for 5 minutes. Samples were loaded into the wells of an acrylamide gel, together with 10 µl of Rainbow Marker (GE Healthcare) to determine the molecular weight of proteins.

Various percentage acrylamide gels were made in gel casters (Bio-Rad). Volumes of reagents used for a 10% gel are specified in Table 2.4.

Solution	**Resolving gel**	**Stacking gel**
30% acrylamide (National Diagnostics)	3.33 ml	830 µl
1.5 M Tris-HCl, 0.4% SDS pH 8.8 (National Diagnostics)	2.5 ml	_
0.5 M Tris-HCl, 0.4% SDS pH 6.8 (National Diagnostics)	_	1.25 ml
Distilled water	4.064 ml	2.865 ml
10% ammonium persulfate (Sigma-Aldrich)	100 µl	50 µl
Temed (Sigma-Aldrich)	6 µl	5 µl

Table 2.4 Acrylamide gel components

Samples were electrophoresed in the gel in the presence of running buffer (made from a 5x stock solution of 125 mM Tris Base, 1.25 M Glycine, 0.5% SDS, made up to 1 L with distilled water) at a voltage of 150V until the appropriate separation had been reached. Samples were then transferred to an Immobilon-P PVDF membrane (Millipore) with a semi-dry transfer, using the semi-dry multi-blotter (W.E.P Company), at 0.13 Amperes for 60 minutes. For semi-dry transfer, the membrane was rehydrated in methanol, washed in distilled water, and soaked in transfer buffer (made with 80% running buffer, 20% methanol).

Following transfer, the membrane was blocked in 5% skimmed milk (Marvel, Premier Brands) in TBST (100 ml of 10x Tris-Buffered saline, 900 ml of distilled water, and 1 ml of Tween 20), for 1 hour at RT. The membrane was then washed 3 times in TBST, 5 minutes each time, and incubated overnight at 4°C with primary antibodies. Details of the primary antibodies used are specified in Table 2.5.

Antigen	**Producer**	**Specie**	**Dilution**
ISCU	Novus Biologicals	Mouse	1:500
Actin	Sigma-Aldrich	Mouse	1:1000
HIF1α	BD Transduction Laboratories	Mouse	1:1000
HIF2 α	Novus Biologicals	Rabbit	1:1000
Aconitase 1	Abcam	Mouse	1:500
Aconitase 2	Abcam	Rabbit	1:1000
Complex I		Mouse	1:2000
GYS1	Abcam	Rabbit	1:5000
Phospho-GYS1	Cell Signalling	Rabbit	1:1000
PYGL	Sigma-Aldrich	Rabbit	1:1000
GLUT1	Abcam	Rabbit	1:500
HX II	Cell Signalling	Mouse	1:1000
PARP	Cell Signalling	Rabbit	1:1000
P21	Cell Signalling	Mouse	1:1000
P53	Calbiochem	Mouse	1:5000

Table 2.5 Primary antibody specifications

The next day, the membrane was washed 3 times in TBST, and incubated with secondary antibodies conjugated with horseradish peroxidase (DAKO), for 1 hour at RT. After 3 washes with TBST, signal was developed with the ECL or ECL plus chemiluminescent kit and exposed onto Hyperfilm (GE Healthcare). Alternatively, signal was detected with the ImageQuant LAS 4000 mini luminescent image

analyser (GE Healthcare). If required, the membrane was stripped with the Restore Plus Stripping Buffer (Thermo Scientific).

2.4 Enzymatic assays

2.4.1 Aconitase activity

Aconitase activity was measured with the BIOXYTECH Aconitase-340 kit (OxisResearch), according to manufacturer's instructions. The procedure utilizes the enzyme isocitrate dehydrogenase which catalyses the conversion of isocitrate produced from aconitase and NADP+ to α-ketoglutarate and NADPH. The generation of NADPH is monitored by the increase in the absorbance at 340 nm, and is proportional to aconitase activity. Briefly 200 μl with 200 μg of cell lysates were added to a cuvette, together with 200 μl of substrate, 200 μl of enzyme, and 200 μl of NADP+. The reaction was incubated at 37°C for 15 minutes, and absorbance change was monitored at 340 nm for 5 minutes at 37°C with the DU640 spectrophotometer (Beckman). Data are presented as % of activity compared to controls.

2.4.2 Complex I activity

Complex I activity was measured with the Microplate Assay for Human Complex I Activity (MitoSciences), as per manufacturer's instructions. The enzyme is immunocaptured within the wells of the microplate and activity is determined by following the oxidation of NADH to NAD+ and the simultaneous reduction of a dye, which leads to increased absorbance at 450 nm. Briefly, 200 μl with 200 μg of cell

lysates were applied to a 96-well plate provided with the kit, and incubated for 3 hours at RT, during which Complex I enzyme is immunocaptured at the bottom of the wells. The wells were washed twice with buffer, then 200 µl of assay solution were added to each well, and absorbance was measured every minute for 30 minutes at RT with the µQuant microplate spectrophotometer. Data are presented as % of activity compared to controls.

2.4.3 Lactate, pyruvate, and glucose measurements

Lactate, pyruvate, and glucose concentrations in the media were quantified with enzymatic kits, according to manufacturer's instructions (Instruchemie).

For lactate measurement, the procedure utilizes the enzyme lactate dehydrogenase which catalyses the conversion of lactate and NAD+ to pyruvate and NADH. In the presence of excess NAD+ and hydrazine, most of lactate is converted to pyruvate, and the increase of absorbance at 340 nm due to reduction of NAD+ to NADH is a measure of the amount of lactate present in the sample. Absorbance was measured with the µQuant microplate spectrophotometer.

For pyruvate measurement, the same procedure was utilised, but in this case, the reaction was run in the presence of excess NADH, inducing the conversion of pyruvate into lactate. The reduction of absorbance at 340 nm due to oxidation of NADH to NAD+ was used as a measure of the amount of pyruvate originally present.

For glucose measurement, a 2-step reaction was used. The procedure utilises the enzyme hexokinase that converts glucose and ATP into glucose-6-P and ADP. A second enzyme, glucose-6-P dehydrogenase, then converts glucose-6-P into 6-

phosphogluconate, NADH, and H+. The rate of NADH formation is monitored by the increase in absorbance at 340 nm, and it is proportional to the concentration of glucose in the sample. Values were normalised by cell number.

2.4.4 Glycogen measurement

Glycogen levels were quantified using the Glycogen Assay Kit (BioVision) following manufacturer's instructions. The procedure utilizes the enzyme glucoamylase, which hydrolyses glycogen to glucose. This is then specifically oxidized to a product that reacts with the OxyRed probe to generate fluorescence. Briefly, cells were washed with ice-cold PBS and scraped in 1 ml of PBS on ice. Cells were collected in a microcentrifuge tube and tubes were centrifuged at 2000 rounds per minute (rpm) for 5 minutes at 4°C. Supernatants were removed, cell pellets were rapidly transferred on dry ice, and then stored at -80°C until further use. Cells were homogenized with 200 ml of dH_2O on ice and then boiled for 5 minutes. Homogenates were spun at 13000 rpm for 5 minutes and supernatants were assayed for glycogen content. 1 μl of each sample were added in duplicate in a 96-well plate, and volume was adjusted to 50 μl/well with hydrolysis buffer. A standard curve was generated by adding serial dilutions of the glycogen standard to a series of wells. 1 μl of hydrolysis enzyme mix was added to standards and one well of samples, and the plate was incubated for 30 minutes at RT. Finally, 50 μl of development mix (48.7 μl of development buffer, 1 μl of development enzyme mix, and 0.3 μl of OxiRed probe) was added to each well and after 30 minute incubation at RT in the dark, fluorescence generation in each well was measured with the SpectraMax M2e Multi-

Mode Microplate reader (Molecular Devices). Glucose background, due to free glucose present in the cell, was represented by the fluorescence generated in wells where no hydrolysis enzyme was added, and was subtracted from glycogen readings. Sample readings were applied to the standard curve to get the amount of glycogen in the sample wells. Results were normalized by protein content or cell number.

2.4.5 Glucose-6-P measurement

Glucose-6-P levels were quantified with the Glucose-6-phosphate assay kit (BioVision). In the assay, glucose-6-P is oxidized with the generation of a product that converts a nearly colourless probe to an intensely coloured product. Briefly, cell pellets were generated as described for glycogen quantification. Samples were homogenised in 2-3 volume of ice cold PBS with a dounce homogenizer and filtered with centrifugal filter units (Millipore) as per manufacturer's instructions. 50 µl of each sample were added into duplicate wells of a 96-well plate. A standard curve was generated by adding serial dilutions of the glycogen standard to a series of wells. 50 µl of reaction mix (46 µl of assay buffer, 2 µl of enzyme mix, and 2 µl of substrate mix) was added to samples and standards. In order to quantify the possible background generated by NADH or NADPH, a background mix without enzyme mix was added in a set of wells. After 30-minute incubation at RT, the colorimetric reaction was quantified with the µQuant microplate spectrophotometer. For the analysis, the background readings were subtracted from the sample readings and values were applied to the standard curve to quantify the amount of glucose-6-P present in each well. Values were normalised by cell number.

2.4.6 NADP+/NADPH measurement

NADP+/NADPH levels were quantified with the NADP+/NADPH quantification kit (BioVision). The enzymes in the kit specifically recognize NADP+/NADPH. Briefly, cell pellets were prepared as described for glycogen quantification, and the cells were extracted with Extraction buffer by 2 freeze/thaw cycles (20 minutes in dry ice followed by 10 minutes at RT). The extraction was then vortexed for 10 seconds, spun at 14000 rpm for 5 minutes at 4°C, and then transferred to new microcentrifuge tubes. 50 µl of each sample were directly transferred in duplicate to a 96-well plate to detect total NADP+ and NADPH, whereas 150 µl were first heated for 30 minutes at 60°C, in order to decompose NADP+ and detect NADPH only. A standard curve was generated by adding serial dilutions of the NADPH standard to a series of wells. 100 µl of Cycling mix (98 µl of Cycling buffer mix and 2 µl of Cycling enzyme mix) were added to each well, and the plate was incubated for 5 minutes at RT to convert NADP+ to NADPH. Finally, 10 µl of developer were added to each well, and after 1 to 4 hours, the colour intensity generated in each sample was quantified with the µQuant microplate spectrophotometer. For the analysis, sample readings were applied to the standard curve, and values were normalized by cell number.

2.5 Spheroids generation

Spheroids were generated according to (Ivascu and Kubbies, 2007). Briefly, 200 µl of a $2.5x10^4$/ml cell suspension was added to each well of a 96-well plate with round bottom (Nunc). For MCF-7 cells, Matrigel (BD Bioscience) was added at a final

concentration of 2.5%. Plates were centrifuged at 1000x g for 10 minutes and then incubated under standard cell culture conditions. Pictures were taken with Images were acquired with a Zeiss Axiovert 135 microscope, and volumes were measured at day 1, 3, 5 and 7.

2.6 *In vivo* study

All protocols were carried out under Home Office regulations (Li et al., 2007). Six to eight-week old female BALB/c NuNu mice (Harlan Sprague Dawley, Inc.) were injected subcutaneously in the lower flank with 100 μl of Matrigel (BD Bioscience) and $1x10^7$ cells suspended in 100 μl of serum-free medium. Tumour growth was monitored and measured three times per week using calipers. Tumour volume was calculated from the formula $V = L \times W \times H \times \pi/6$ (L=length, W=width and H=height). When tumours reached 1.44 cm^3, mice were sacrificed by cervical dislocation. Ninety minutes prior to sacrifice, mice were injected intraperitoneally with 100 mg/kg of pimonidazole (Hypoxyprobe-1; Chemicon International). The excised tumours were appropriately store until further processing.

2.7 Immuhistochemistry and other staining techniques

2.7.1 Histology

A standard Haematoxylin & Eosin (H&E) protocol was followed to assess the morphology of HCT116 spheroids and U87 xenografts. Briefly, paraffin-embedded

sections were dewaxed by heating them at 60°C for 10 minutes, rehydrated in graded Industrial Methylated Spirit solutions, and rinsed in tap water. Sections were immersed in haematoxylin for 1 minutes, rinsed in tap water, immersed in 0.3% acid alcohol for 5 seconds, washed in tap water, immersed in Scott's water for 10 seconds, washed in tap water, immersed in eosin for 90 seconds, and rinsed in tap water again, before gradual dehydration in increasing concentrations of Industrial Methylated Spirit solutions. Finally, sections were immersed in xylene and coverslips were mounted with DPX mountant for histology (all from Sigma-Aldrich).

2.7.2 Immunohistochemical staining of paraffin-embedded sections

Sections of formalin-fixed, paraffin-embedded cell pellets, spheroids, xenografts, and human tissues were stained using a common procedure. Sections were dewaxed and rehydrated as described for histological analysis. Antigen retrieval was performed in a decloaking chamber (Biocare Medical) set at 125°C for 2 minutes, in buffers as indicated in Table 2.6. After cooling, sections were immersed in PBS, and blocked for non-specific antibody binding with 10% normal horse serum (Vector Laboratories) for 30 minutes at RT. For Pimonidazole detection, blocking was anticipated by peroxidase block (0.03% hydrogen peroxide, DAKO) for 5 minutes at RT. Primary antibodies were applied according to dilutions indicated in Table 2.6, for 1 hour (40 minutes for Pimonidazole detection) at RT. All primary antibodies were diluted in PBS with 0.2% 9w/v) sodium azide and 10% bovine serum (Sigma-Aldrich). Sections were then washed in PBS and incubated with anti-rabbit/anti-mouse secondary antibody (DAKO REAL EnVision kit) for 30 minutes at RT.

Sections were washed in PBS, and staining was visualised by application of 3, 3'-diaminobenzidine (DAKO), for 8 minutes at RT. After washing in PBS, sections were counterstained by immersion in haematoxylin and coverslips were mounted with Aquamount (VWR).

In a set of experiments, combined CA9 and Periodic Acid Schiff (PAS) staining in xenograft sections was obtained by routine immunohistochemical staining for CA9 followed by PAS staining as described below.

Slides were scored by two researchers blinded to grouping or analysed quantitatively by image analysis in imageJ using colour deconvolution as described previously (Ruifrok and Johnston, 2001).

Antigen	**Dilution**	**Antigen retrieval**	**Source**
Pimonidazole (mouse)	1:200	EDTA buffer pH 8	Chemicon International
GYS1 (rabbit)	1:500	Sodium citrate buffer pH 6	Abcam
PYGL (rabbit)	1:400	Sodium citrate buffer pH 6	Sigma-Aldrich
CA9 (mouse)	1:500	Sodium citrate buffer pH 6	Abcam
DEC1 (rabbit)	1:5000	Sodium citrate buffer pH 6	Clone CW27
p21 (mouse)	1:200	Tris-EDTA pH 9	DAKO

Table 2.6 Antibody specifications

2.7.3 Senescence-associated β-galactosidase (SA-β-gal) staining

In order to detect senescent cells, a Senescence Detection Kit (Calbiochem) was used and staining was performed according to manufacturer's instructions. Briefly, culture media was removed and cells were washed with PBS. Cells were fixed with fixative

solution for 15 minutes at RT, and then washed twice with PBS. A staining solution mix (470 μl of staining solution, 5 μl of staining supplement, and 25 μl of 20 mg/ml X-gal in N-N-dimethylformamide) was added to each well for overnight incubation. Images were acquired with a Zeiss Axiovert 135 microscope.

In a set of experiments, 100 μM 6-aminonicotinamide (6-AN) and dehydroepiandrosterone (DHEA) (Sigma-Aldrich) were added to U87 cells for 24 hours prior to SA-β-gal staining.

2.7.4 Periodic Acid Schiff staining (PAS)

Glycogen was detected in cells, spheroids and tumour sections following a standardized PAS staining technique**.** Briefly, cells were fixed with 4% paraformaldehyde for 15 minutes and washed with PBS. Cells were then incubated in 1% Periodic Acid (Sigma-Aldrich) for 5 minutes, rinsed in water and placed in Schiff's reagent (Sigma-Aldrich) for 10 minutes. Finally, cells were washed with water. Amylase (Sigma-Aldrich) was used in a set of experiments to verify that staining was specific for glycogen. Images were obtained using a Zeiss Axiovert 135 microscope.

2.7.5 Superoxide levels detection

ROS levels were measured using MitoSOX Red (Molecular Probes), as an indicator of mitochondrial superoxide. MitoSOX Red is a cell permeant fluorogenic dye, which selectively accumulates in the mitochondria. In the mitochondria, MitoSOX Red is oxidised by superoxide and exhibits red fluorescence. The oxidised product is

particularly fluorescent when bound to nucleic acids. Cells were treated as appropriate and subsequently loaded with 5 μM MitoSOX Red for 16 hours (miR-210 experiments) or 45 minutes (PYGL experiments). For miR-210 experiments, Dr Ricardo Pires De Neves and Dr Francisco Iborra performed the analysis. For PYGL experiments, for microscopic analysis, cells were washed with PBS and mounted with VectaShield (Vector Laboratories) with DAPI. Images were acquired with a Zeiss Axioskop 2 plus microscope. For flow cytometry analysis, cells were washed and scraped in PBS and immediately analysed in a FACS analyzer Cyan ADP. In a set of experiments, cells were cultivated in the presence of 25 μM manganese (III) tetrakis (1-methyl-4-pyridyl) porphyrin (MnTMPyP) (Calbiochem).

2.7.6 Fluorescent glycogen detection

To detect glycogen particles, $1*10^5$ U87 cells were seeded in glass bottom microwell dishes (MatTek corporation). After 48 hours in hypoxia or normoxia, cells were washes with buffer solution (138 mM NaCl, 5.5 mM D-glucose, 5 mM KCl, 1 mM $MgCl_2$, 1.5 mM $CaCl_2$ and 10 mM Hepes, pH 7.4) and then incubated in buffer solution with 500 mM fluorescent 2-NBDG (Molecular Probes) at 37°C. After 3 hours, the dye was removed and cells were incubated for another 3 hours under standard cell culture conditions. Nuclei were stained with DAPI (Vector Laboratories). Images were acquired with a Zeiss Axioskop 2 plus microscope.

2.7.7 Lysosomes detection

$1*10^5$ U87 cells were seeded in glass bottom microwell dishes, and incubated for 48 hours in hypoxic or normoxic conditions. To visualize lysosomes, cells were incubated with 100 nM LysoTracker-Red (Molecular Probes) for 30 minutes at 37°C. To identify nuclei, cells were then incubated with DAPI for 20 minutes in the dark. Pictures were acquired with a Zeiss Axioskop 2 plus microscope.

2.7.8 Annexin V flow cytometry

To measure viability, cells were stained with Annexin V and Propidium iodide (PI) (Molecular Probes). Annexin V binds to the phospholipid phosphatidylserine, which is located in the cytoplasmic surface of the plasma membrane in viable cells or necrotic cells, whereas it translocates to the outer leaflet of the plasma membrane in apoptotic cells. To discriminate between dead and apoptotic cells, the membrane impermeable PI was added simultaneously (van Engeland et al., 1998). Cells were harvested with trypsin after the incubation period and washed in cold phosphate-buffer saline (PBS). Cells were then resuspended in 100 μl of annexin-binding buffer (10 mM Hepes, 140 mM NaCl, and 2.5 mM $CaCl_2$, pH 7.4), 5 μl of Annexin V Alexa Fluor 647 conjugate and 5μl of PI, and incubated at RT for 15 minutes. Subsequently, 400 μl of annexin-binding buffer were added, and samples were kept on ice until analysis. Analysis was performed in a FACS analyzer Cyan ADP (Dako).

2.7.9 Cell Cycle Analysis using Propidium iodide DNA staining

PI is a fluorescent dye that binds to the DNA stoichiometrically, which means that there is a direct correlation between the amount of DNA and the quantity of DNA-bound dye. Therefore, this enables to identify the proportion of cells present in each phase of the cell cycle. To evaluate cell cycle distribution, 3-5 x 10^5 cells were washed with ice-cold PBS, re-suspended in 1 ml of PBS and fixed by the drop-wise addition of 3 ml of 100% ethanol for 20 minutes at 4°C. Subsequently, cells were washed twice with ice-cold PBS and re-suspended in 500 µl of a PI solution (100 µg/ml) containing DNase-free RNase (12 µg/ml) (Sigma). After 15 minutes incubation at RT, cells were analysed in a FACS analyser Cyan ADP. For the analysis, firstly, the single cell population was gated using pulse width versus pulse area, and secondly, this gate was applied to the PI histogram plot. The percentage of cells in each cell cycle phase was quantified using markers set within the analysis program.

2.7.10 Clonogenic assay

Transfected cells were trypsinised and reseeded at a density of 1000 cells per 6 cm dish. Cells were exposed to hypoxia or normoxia for 48 hours and then grown in normoxia for 12 days. At the end of the experiment, the media was aspirated and 5 ml of fixing/staining solution was added to the plate. The fixing/staining solution contained 50% ethanol, 49.8% distilled water, and 0.2% methylene blue (Sigma Aldrich). After 30 minutes, plates were washed with tap water and air-dried. The number of colonies was counted using an automated scanner (ColCount, Oxford Optronics).

2.8 Oncomine analysis

The Oncomine website (Oncomine.org) was searched for microarrays containing the gene GYS1 or PYGL. Normalised relative expression from representative studies was downloaded and graphed.

2.9 Statistical analysis

Statistical analysis and graphs were performed using GraphPad Prism® v4.0b software (GraphPad). Statistics were carried out using Student's t-tests and linear regression of log transformed growth data. Correlation of GYS1 and PYGL expression with tumour stage of development was assessed using the non-parametric Kruskal-Wallis test for categorical variables. Significance is represented by: *, $p<0.05$, **, $p<0.01$, and ***, $p<0.001$.

3 CHAPTER THREE

Metabolic implications of ISCU regulation by miR-210

3.1 INTRODUCTION

Previous reports have demonstrated that miR-210 is the most consistently and robustly upregulated microRNA in hypoxia (Devlin et al., 2011). One of the miR-210 targets, ISCU was therefore analysed, because of its predicted influence on a number of metabolic processes. ISCU is involved in the assembling of Fe-S clusters, which are cofactors of many enzymes.

Validation if ISCU as a miR-210 target and evaluation of the role of this pathway in cancer metabolism were performed in the breast cancer cell line MCF-7. This cell line was chosen because of the role of miR-210 as a negative prognostic factor in breast carcinomas (Camps et al., 2008), and because of the previously demonstrated ability of MCF-7 cells to upregulate miR-210 in hypoxia (Camps et al., 2008; Kulshreshtha et al., 2007). Moreover, this cell line was previously used for the analysis of hypoxia microRNA signatures (Kulshreshtha et al., 2007). Key findings presented here were also reproduced in the colon cancer cell line HCT116 (Dr Anassuya Ramachandran) (Favaro et al., 2010).

Fe-S clusters are motifs that are present in the active sites of many enzymes and proteins, and are critical for their activity and regulation by modification of redox status (Rouault and Tong, 2008). These clusters are assembled in the mitochondria (Muhlenhoff and Lill, 2000) by a complex series of chaperones and enzymes including ISCU, and then exported to the cytoplasm, where they are assembled into the recipient proteins (Tong and Rouault, 2000). ISCU has two main alternatively spliced isoforms. ISCU1 has an alternative N-terminal sequence and is localised to the cytosol, while ISCU2 is associated with the mitochondria. Amongst the Fe-S

cluster proteins, are several enzymes that comprise key components of complex I, II and III in the mitochondria, as well as components of the Krebs cycle such as SDH and aconitase. Therefore, the consequences of miR-210 and ISCU modulation on the activity of aconitase and complex I were investigated. Aconitase exists in two isoforms: aconitase 1 (cytosolic), and aconitase 2 (mitochondrial). Both enzymes catalyse the conversion of citrate into isocitrate, which is an intermediate of the Krebs cycle in the mitochondria (Tong and Rouault, 2007). Complex I is the first enzyme in the mitochondrial electron transport chain, where it transfers electrons from reduced NADH to coenzyme Q10 (Fassone and Rahman, 2012). Finally, the metabolic consequences of aconitase inhibition and the effect of complex I impairment on ROS generation were interrogated.

3.2 RESULTS

3.2.1 Selection of ISCU as a potential miR-210 target

The identification of miR-210 targets was performed by Dr Francesca Buffa, an expert in bioinformatic analysis. Briefly, this method involved combining the list of genes obtained by four different approaches: 1) genes generated by five *in silico* target prediction algorithms (TargetScan, Pictar, miRanda, microT, and miRDB) that were directly interrogated for miR-210; 2) miR-210-clustered genes downregulated in breast cancer samples; 3) miR-210-clustered genes downregulated in head and neck cancer samples 4) downregulated genes in the hypoxia 'metagene' (Winter et al., 2007) (Table 3.1). For each transcript, a mean score was determined (overall rank score), and was used to rank the transcripts from highest (very likely to be a target; maximum score = 1) to lowest score (very unlikely to be a target; minimum score = 0). The analysis revealed that ISCU was the top predicted target, and two known miR-210-targets (ephrin-A3 [EFNA3] and neuronal Pentraxin-1 [NPTX1]) (Fasanaro et al., 2008; Pulkkinen et al., 2008) were also listed in highly ranked positions, supporting the validity of the adopted approach. Because of its potential regulation of many different metabolic processes in cancer cells, ISCU was selected among the top predicted targets for further investigation.

Symbol	Name	Overall Rank Score
ISCU	Iron-sulfur cluster scaffold homolog	0.52
EFNA3	Ephrin-A3	0.41
ENPP2	Ectonucleotide pyrophosphatase/phosphodiesterase 2	0.38
NPTX1	Neuronal Pentraxin-1	0.35

Table 3.1 List of the top four predicted miR-210 targets using algorithms and tumour data (courtesy of Dr Francesca Buffa).

3.2.2 MiR-210 and ISCU mRNA undergo reciprocal regulation in hypoxia

As a first step in the validation process, ISCU regulation by hypoxia was analysed in the breast cancer cell line, MCF-7. In order to characterise acute responses to hypoxia, cells were exposed to hypoxia (1% or 0.1% oxygen [O_2]) for 24 or 48 hours. In agreement with published data (Camps et al., 2008; Chan et al., 2009; Chen et al., 2010; Crosby et al., 2009; Kulshreshtha et al., 2007), miR-210 was robustly induced in MCF-7 cells by hypoxia (1% or 0.1% O_2) at 24 and 48 hours, with maximal induction observed after 48 hours at 0.1% O_2 (Figure 3.1A). Conversely, ISCU mRNA levels decreased in hypoxia (Figure 3.1B). Based on these observations, all of the subsequent analyses were performed in cells after 48 hours incubation at 0.1% O_2.

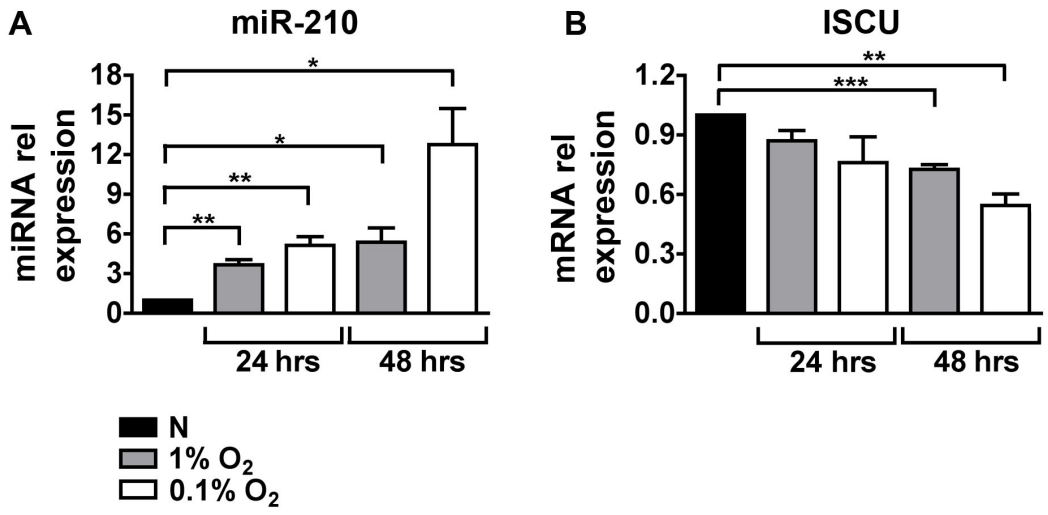


Figure 3.1 MiR-210 and ISCU expressions are reciprocally regulated in MCF-7 cells in hypoxia.
A, miR-210 increases under hypoxia, with the most robust induction seen after 48 hours at 0.1% O_2. **B**, under the same conditions, the strongest downregulation of ISCU mRNA is observed after 48 hours at 0.1% O_2. The expression levels of miR-210 and ISCU mRNA in hypoxia are relative to their normoxic expression levels at 24 hours (N). Mean ± SEM of three independent experiments is shown (* $p<0.05$, ** $p<0.01$, *** $p<0.001$).

Specific siRNA sequences directed against HIF1α or HIF2α were used to determine the role of HIF on the hypoxic regulation of ISCU (Figure 3.2A). ISCU downregulation in hypoxia was prevented by transfection of cells with siHIF1α, but not siHIF2α. In agreement with previous reports (Camps et al., 2008; Chan et al., 2009), the miR-210 upregulation observed in hypoxia was HIF1α-dependent, but unaffected by depletion of HIF2α. Therefore, reciprocal changes in mir210 and ISCU mRNA levels in MCF-7 cells in response to hypoxia are dependent on HIF1α (Figures 3.2B and 3.2C).

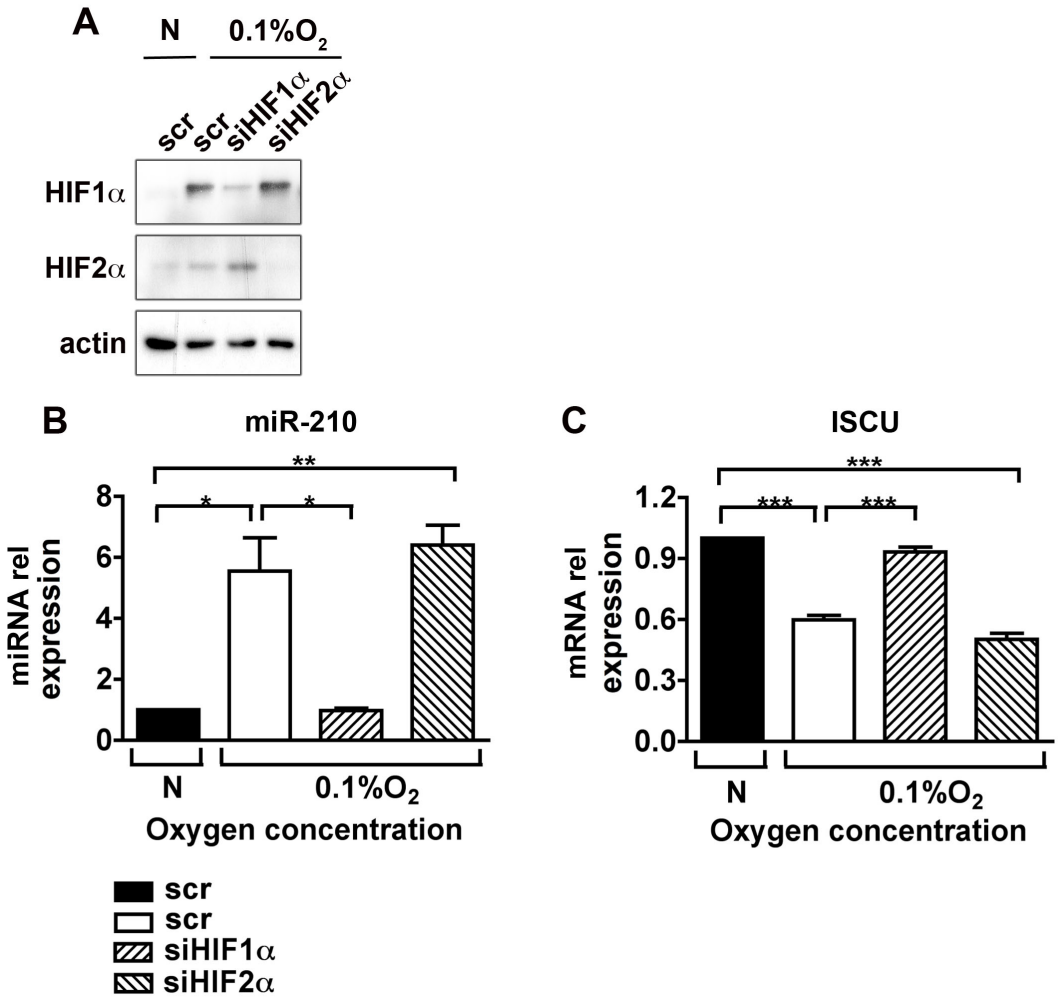


Figure 3.2 MiR-210 and ISCU regulation in hypoxia is HIF1α-dependent.
A, siRNA mediated knockdown of HIF1α and HIF2α was assessed by immunoblotting using specific antibodies against HIF1α or HIF2α. Lysates were obtained from MCF-7 cells cultivated in normoxia (N) or hypoxia (0.1% O_2) for 48 hours after transfection. Actin levels are shown as a loading control. **B**, siRNA-mediated knockdown of HIF1α but not HIF2α prevented the induction of miR-210 in hypoxia after 48 hours. Expression of miR-210 is relative to scr in normoxia (N). Mean ± SEM of three independent experiments is shown (* $p<0.05$, ** $p<0.01$). **C**, knockdown of HIF1α but not HIF2α reverses the hypoxic suppression of ISCU mRNA at 48 hours. Expression of ISCU mRNA is relative to scr in normoxia (N). Mean ± SEM of three independent experiments is shown (*** $p<0.001$).

3.2.3 MiR-210 controls the hypoxic regulation of ISCU

To determine if ISCU expression in hypoxia is regulated by miR-210, MCF-7 cells were transfected with commercially available RNA sequences, specifically designed to modulate miR-210 levels (see Materials and Methods). In particular, 'mimic-210' is a double-stranded miRNA-like RNA that was used to increase miR-210 levels in normoxia, and 'anti-210' is a single-stranded RNA sequence with a hairpin structure that was used to suppress its hypoxic induction. When cells were transfected with mimic-210 in normoxia, there was a 370-fold increase in miR-210 levels, and this was associated with a concomitant 70% decrease in ISCU mRNA levels (Figures 3.3A and 3.3B). Conversely, when cells were transfected with anti-210 in hypoxia, a 97% decrease in endogenous miR-210 levels was associated with increased ISCU mRNA levels (from 49% to 78% of the normoxic levels) although this was not complete (Figures 3.3A and 3.3B). Modulation of ISCU levels by mimic-210 and anti-210 transfection was also confirmed at the protein level by immunoblotting (Figure 3.3C).

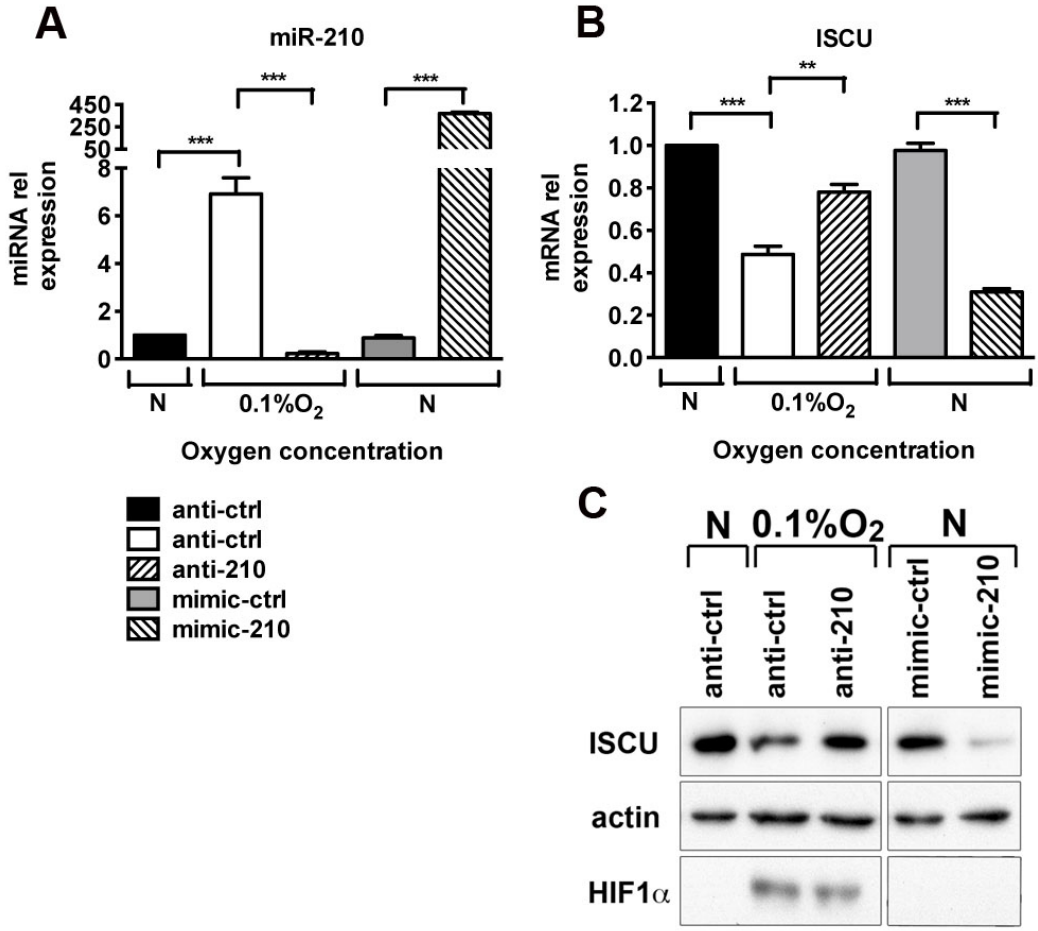


Figure 3.3 ISCU expression is modulated by miR-210 in MCF-7 cells.
A, miR-210 induction in hypoxia can be prevented by transfection with anti-210. MiR-210 levels were analysed after 48 hours from transfection with 20 nM of each construct, as indicated. Expression of miR-210 is relative to anti-ctrl in normoxia (N) Mean ± SEM of three independent experiments is shown (*** $p<0.001$). **B**, transfection of MCF-7 cells with anti-210 partially rescues the hypoxic suppression of ISCU mRNA and mimic-210 overexpression decreases ISCU mRNA in normoxia after 48 hours from transfection. Expression of ISCU mRNA is relative to anti-ctrl in normoxia (N). Mean ± SEM of three independent experiments is shown (** $p<0.01$, *** $p<0.001$). **C**, representative immunoblot showing downregulation of ISCU protein level in MCF-7 cells after 48 hours at 0.1% O_2 compared to normoxia (N). This decrease is partially rescued when cells are transfected with anti-210. Under normoxic conditions, mimic-210 suppresses ISCU protein levels compared to mimic-ctrl transfected cells. HIF1α levels are shown as a control for hypoxia. Actin levels are shown as a loading control.

For these experiments, mimic-210 and anti-210 sequences were transfected in MCF-7 cells at a final concentration of 20 nM, as reported for previous studies (Fasanaro et al., 2009; Kulshreshtha et al., 2007). These concentrations had pronounced effects on miR-210 levels. This was particularly evident with the transfection of mimic-210 in normoxia, in which an approximate 370-fold induction of miR-210 was observed, as opposed to a 7-fold induction physiologically induced by hypoxia (Figure 3.3A). Importantly, a similar effects on ISCU mRNA expression levels were observed when MCF-7 cells were transfected with lower concentrations of anti-210 (1 nM) and mimic-210 (100 pM), excluding the possibility that ISCU modulation could be an artefact of the high concentrations used (Figure 3.4).

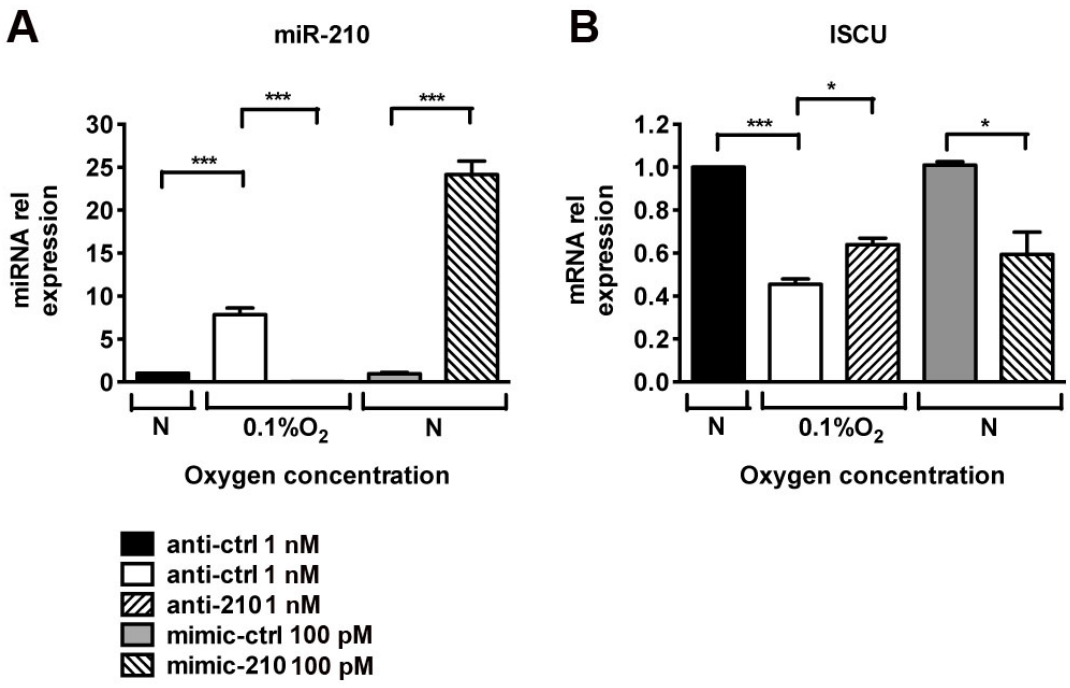


Figure 3.4 ISCU is modulated by lower concentrations of anti-210 and mimic-210.
MiR210 (**A**) and ISCU mRNA (**B**) levels were analysed in MCF-7 cells transfected with 1 nM anti-210 and 100 pM mimic-210, respectively, and cells were thereafter treated as in figure 3.3. Expression of miR-210 and ISCU is relative to anti-ctrl in

normoxia (N). Mean ± SEM of three independent experiments is shown (* $p<0.05$, *** $p<0.001$).

In most cases, miRNAs regulate their mRNA targets by binding to the 3' untranslated region (3'UTR) of the transcripts (Garzon et al., 2010). To test whether miR-210 downregulates ISCU mRNA and protein levels by targeting the 3'UTR, two different approaches were adopted. Firstly, MCF-7 cells were transfected with a plasmid encoding Myc-tagged ISCU lacking the 3'UTR. The presence of the Myc-tag confers a higher molecular weight, and allows the distinction of Myc-ISCU and endogenous ISCU by immunoblotting. Cells were simultaneously transfected with a siRNA sequence targeting the ISCU transcript open reading frame, or mimic-210. Four different ISCU siRNA sequences (siISCU1-4) were tested. All four ISCU siRNAs caused a similar, and pronounced reduction in ISCU mRNA and protein levels (Figure 3.5). The two isoforms of ISCU (cytosolic and mitochondrial) could not be distinguished by Western blotting of whole cell lysates because of the minor difference in molecular weight (15kD and 14kD, respectively). All sequences were associated with toxicity upon transfection; siISCU3 was selected for the following experiments because of its milder effects on MCF-7 cells.

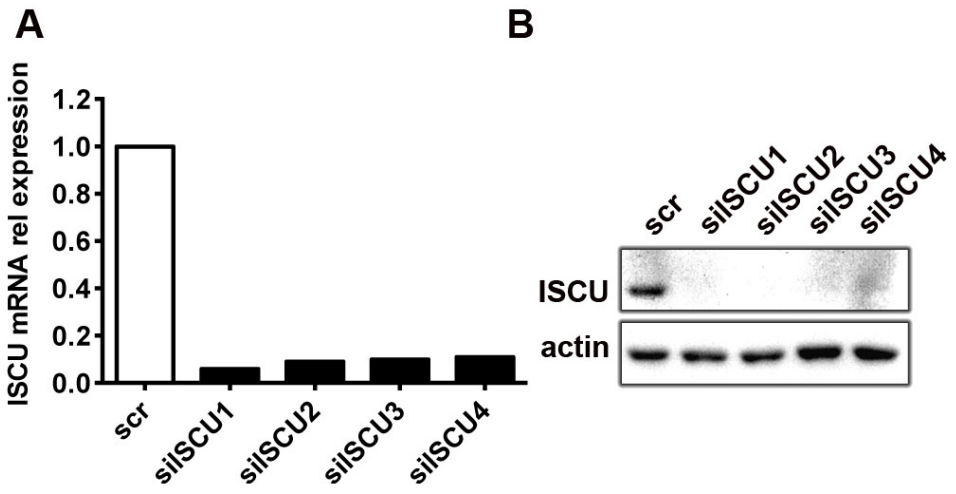


Figure 3.5 Validation of siRNA sequences targeting ISCU.
MCF-7 cells were transfected with 4 different siRNA sequences that target ISCU. 48 hours after transfection, ISCU knockdown was analysed at the mRNA level by RT-qPCR (**A**), or at the protein level by immunoblotting (**B**). ISCU mRNA levels are relative to scr.

Whereas siISCU3 led to a depletion of both endogenous ISCU and Myc-ISCU, mimic-210 lead to a reduction in endogenous ISCU protein, but not myc-ISCU (Figure 3.6A). This suggests that miR-210 downregulates ISCU mRNA and protein levels by targeting the 3'UTR of ISCU.

For the second approach, a collaborator, Dr Christine Blancher, utilised a luciferase reporter construct containing the full length 3′-UTR of ISCU (ISCU-3'-UTR) with the putative miR-210 target site, or a random sequence as a control (Ctrl-3′-UTR). Luciferase activity was strongly suppressed in hypoxic MCF-7 cells transfected with the ISCU-3'-UTR construct, and this suppression could be partially rescued by transient transfection with anti-210. In addition, in normoxia, mimic-210 substantially suppressed the luciferase activity as compared to mimic-ctrl (Figure 3.6B, courtesy of Dr Christine Blancher). These results confirm the role of the 3'UTR in ISCU regulation by miR-210.

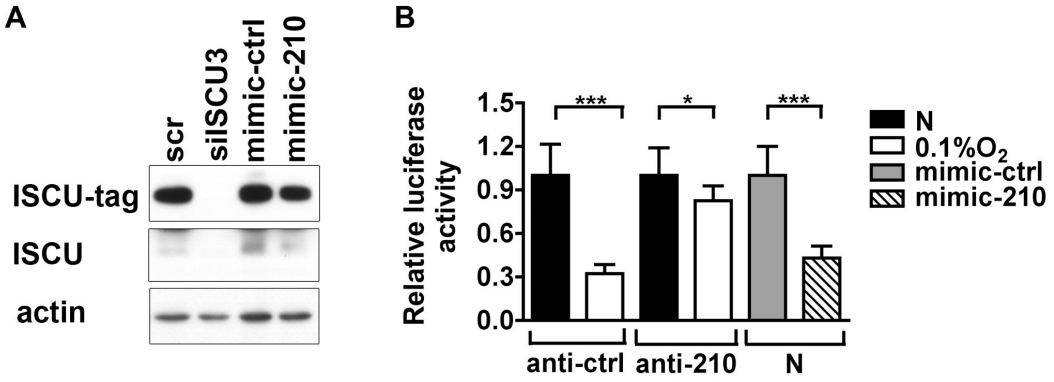


Figure 3.6 Role of the 3' UTR in the regulation of ISCU by miR-210.
A, MCF-7 cells were transfected with an expression plasmid for a Myc-DKK tagged ISCU lacking the 3'UTR. Subsequent transfection of siISCU3 reduced the protein levels of both endogenous and exogenous ISCU. Mimic-210 only affected the endogenous ISCU protein level. Actin levels are shown as a loading control. **B**, MCF-7 cells were transfected with a Firefly luciferase reporter construct containing the ISCU-3′-UTR or the ctrl-3′-UTR. Cells were then cotransfected with anti-210 or mimic-210 or their corresponding controls. Luciferase activity was measured after 48 hours in normoxia (N) or hypoxia, as indicated. Cotransfection with a vector expressing Renilla luciferase was used to normalize for transfection efficiency. Luciferase activity is expressed as a ratio of ISCU-3′-UTR to ctrl-3′-UTR, relative to expression in normoxia. Mean ± SD of 9 independent experiments is shown (* $p<0.05$, *** $p<0.001$) (courtesy of Dr Christine Blancher).

3.2.4 Effects of ISCU downregulation on Fe-S proteins

An expected effect of ISCU downregulation would be a reduction of Fe-S cluster delivery to recipient proteins. The levels of Fe-S clusters were not measured directly, but the impact of ISCU repression was evaluated on two important metabolic enzymes that require Fe-S clusters: aconitase and mitochondrial complex I. Transfection of MCF-7 cells with siISCU3 significantly reduced aconitase activity, as compared to control cells in normoxia, and a similar effect was observed following transfection of mimic-210 (Figure 3.7A). Moreover, hypoxia induced a similar decrease in aconitase activity to that induced by ISCU depletion or mimic-

210 (Figure 3.7B). Finally, transfection of anti-210 was able to significantly increase aconitase activity in hypoxia (Figure 3.7C).

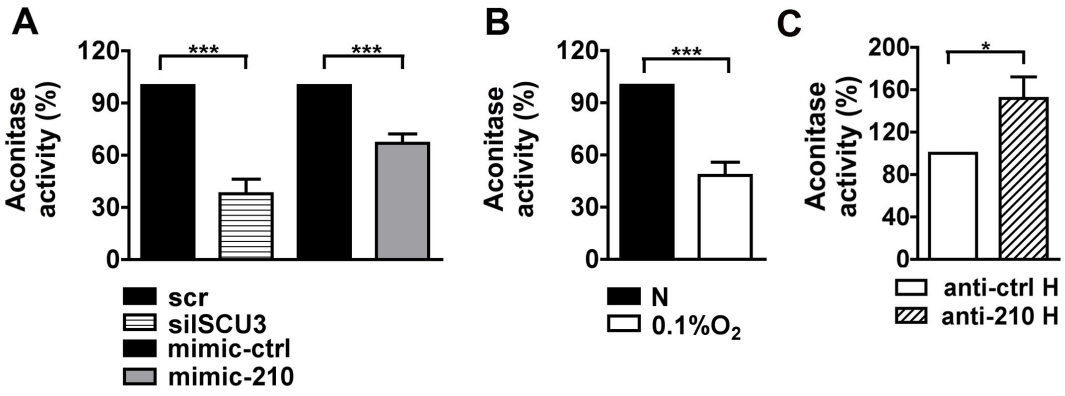


Figure 3.7 Modulation of aconitase activity in MCF-7 cells.
A, MCF-7 cells transfected with siRNA against ISCU or with mimic-210 showed a significant decrease in the activity of the Fe-S protein aconitase, as measured by enzymatic assay. Activity was measured at 48 hours from transfection and is expressed relative to scr for siISCU3 or to mimic-ctrl for mimic-210. Mean ± SEM of three independent experiments is shown (*** $p<0.001$). **B**, Aconitase activity was measured in MCF-7 cells after 48 hours exposure to hypoxia, and is relative to the level measured in normoxia (N). Mean ± SEM of three independent experiments is shown (*** $p<0.001$). **C**, transfection of MCF-7 cells with anti-210 in hypoxia, increases the level of aconitase activity, compared to anti-ctrl. Activity was measured at 48 hours from transfection and is expressed relative to anti-ctrl in hypoxia. Mean ± SEM of three independent experiments is shown (* $p<0.05$).

Immunoblot analysis of MCF-7 cells transfected with anti-210 in hypoxia or mimic-210 in normoxia, revealed that aconitase protein levels were unchanged throughout the different conditions (Figure 3.8). This excluded the possibility that a decrease in aconitase levels could be responsible for the observed decrease in activity.

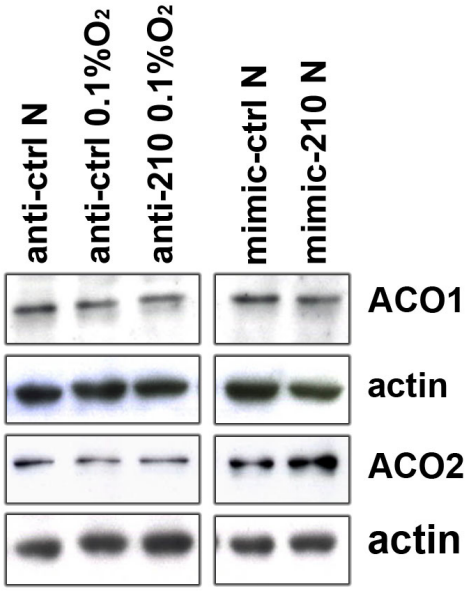


Figure 3.8 MiR210 modulates aconitase activity in MCF-7 cells.
Aconitase protein levels remain unchanged after transfection with either mimic-210 in normoxia or anti-210 in hypoxia, as compared to controls (ACO1= aconitase 1 mitochondrial, ACO2= aconitase 2, cytosolic). Actin levels are shown as a loading control.

Similar to what was observed for aconitase, complex I activity was significantly decreased in MCF-7 cells transfected with either siISCU3, or with mimic-210, as compared to their respective control sequences in normoxia (Figure 3.9A). A similar decrease in complex I activity was measured in cells after 48 hours incubation in hypoxia (Figure 3.9B). Immunoblot analysis also revealed that miR-210 modulation did not affect complex I protein levels (Figure 3.9C), supporting the hypothesis the miR-210 affects complex I activity through the regulation of ISCU.

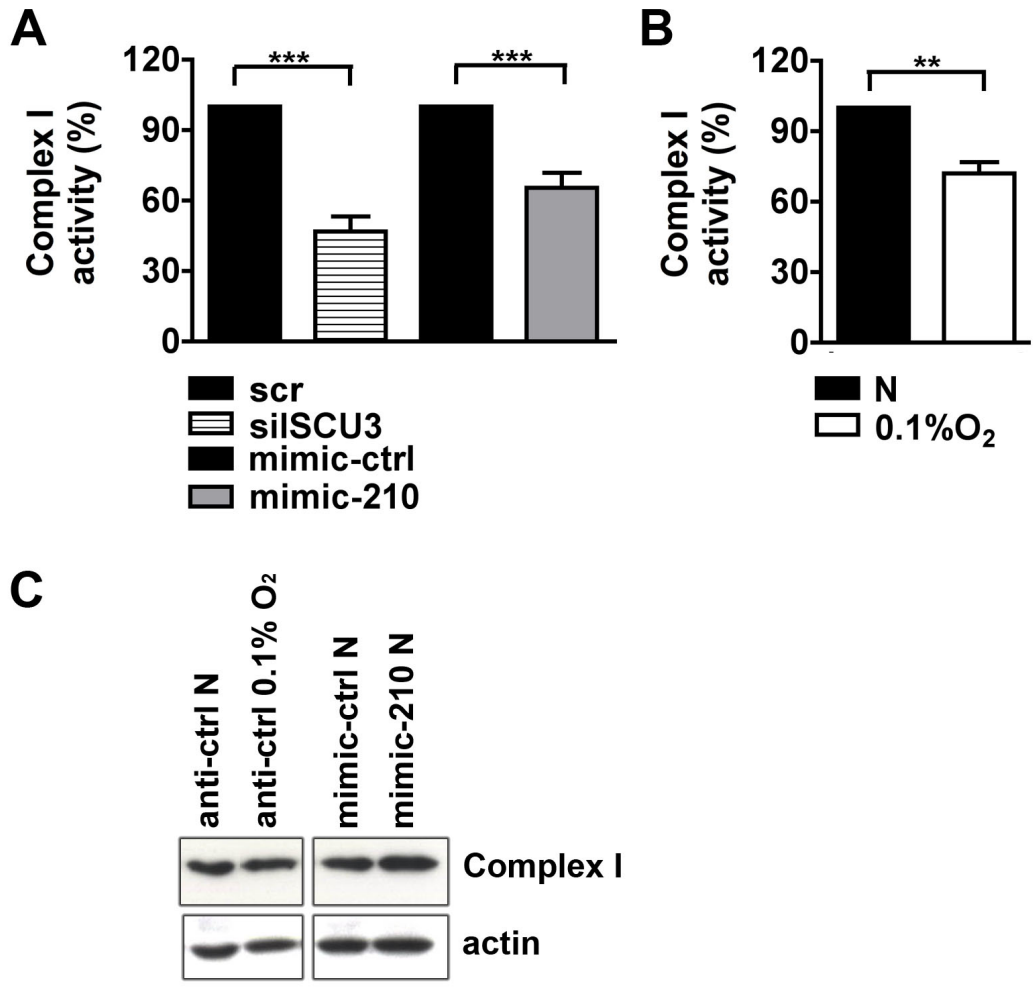


Figure 3.9 MiR-210 negatively regulates complex I activity in MCF-7 cells.
A, complex I activity was measured in MCF-7 cells after 48 hours from transfection with siISCU3, scr control, mimic-210 or mimic-ctrl. Activity is relative to the corresponding control sample. Mean ± SEM of three independent experiments is shown (*** $p<0.001$). **B**, complex I activity decreases in MCF-7 cells exposed to hypoxia for 48 hours. Activity in hypoxia is relative to the level in normoxia (N). Mean ± SEM of three independent experiments is shown (** $p<0.01$). **C**, immunoblot analysis of complex I protein levels in MCF-7 cells transfected with anti-ctrl or mimic-210 or relative controls. Samples were collected after 48 hours exposure to normoxia (N) or hypoxia, as indicated.

3.2.5 Effects of miR-210 on glycolysis

Because a decrease in aconitase and complex I activity would predict a decreased activity of the Krebs cycle and mitochondrial function with a compensatory increase in glycolytic metabolism and lactate generation from pyruvate, the presence of a shift to glycolysis and lactate production was investigated. Enzymatic determinations in cell culture media revealed a highly significant increase in lactate levels (Figure 3.10A), and a reduction of pyruvate levels (Figure 3.10B) in normoxia after transfection with mimic-210. As expected, lactate production was increased in hypoxia (Pasteur effect), and this could be prevented by transfection with anti-210 (Figure 3.10C).

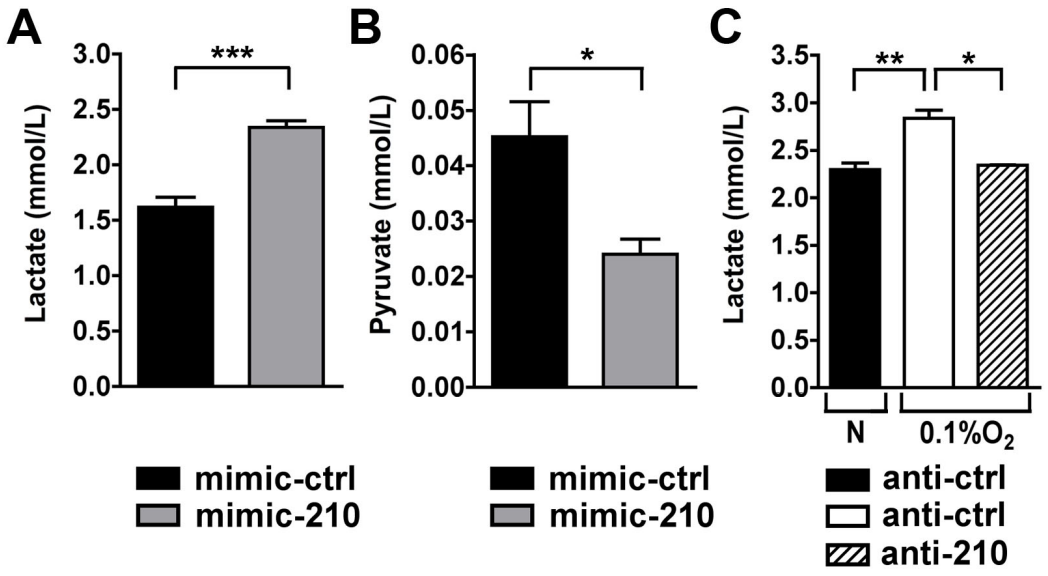


Figure 3.10 MiR-210 sustains glycolysis.
MCF-7 cells transfected with mimic-210 in normoxia revealed increased levels of lactate (**A)**, decreased levels of pyruvate (**B**). **C**, anti-210 prevents the hypoxic increase in lactate production. Metabolites were measured in culture media collected 48 hours after transfection. Values were normalized by cell number. Mean ± SEM of three biological replicates is shown (* $p<0.05$, ** $p<0.01$, *** $p<0.001$).

3.2.6 Effects of ISCU downregulation on free radical production

The loss of Fe-S from complex I is likely to affect the transport of electrons in the electron transport chain and impact on free radical production. Superoxide represents the proximal mitochondrial reactive oxygen specie generated in the presence of defective electron respiratory chain (Murphy, 2009); therefore the levels of mitochondrial superoxide were measured in MCF-7 cells. Detection of superoxide was performed using MitoSOX Red, a fluorogenic dye that selectively enters the mitochondria and fluoresces following oxidation by superoxide. Fluorescence was detected and quantified using a confocal microscope by a collaborator, Dr Ricardo Pires das Neves. In normoxia, there was a marked increase in free radical levels upon transfection of mimic-210, as compared to mimic-control (Figure 3.11A). In hypoxia, there was a highly significant increase in superoxide production, which was strongly attenuated by transfection with anti-210 (Figure 3.11B). Additionally, transfection with an ISCU construct lacking the 3'UTR strongly reduced the levels of free radicals induced by mimic-210 in normoxic conditions, suggesting that the miR-210-dependent effect on free radical levels is caused by suppression of ISCU (Figure 3.11C).

Taken together, these results demonstrate a new major mechanism for regulation of ROS in hypoxia, which is actively controlled by the miR-210-ISCU axis.

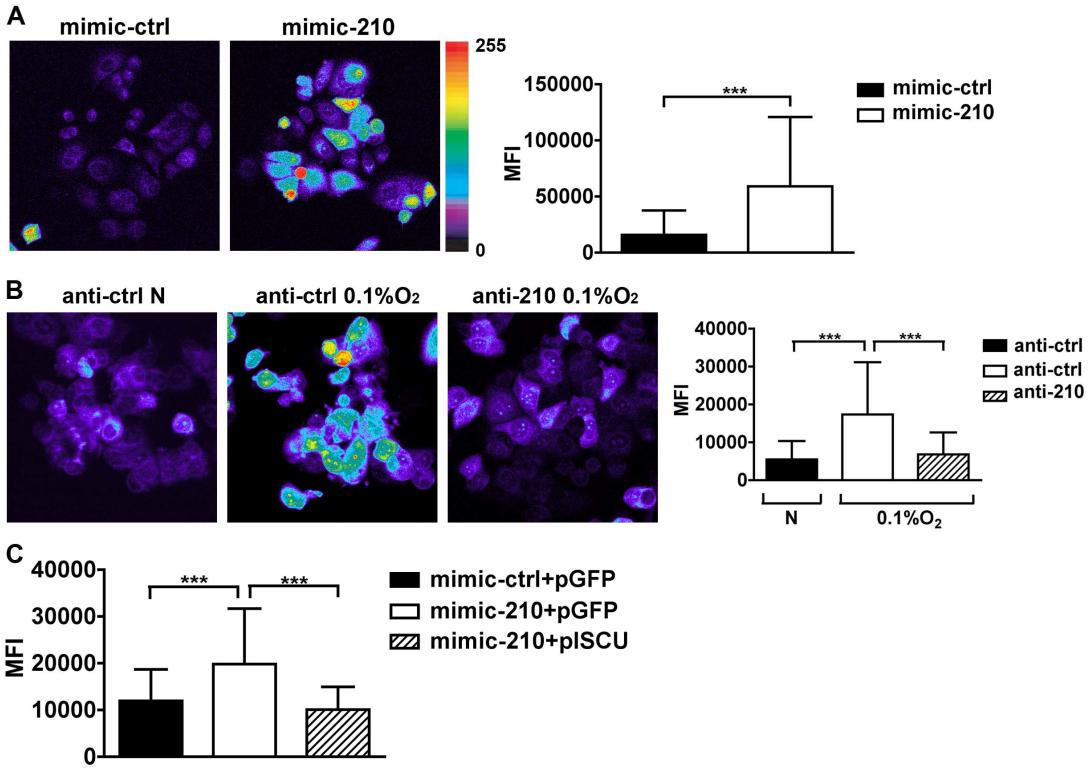


Figure 3.11 MiR-210 increases the levels of ROS.
A, in normoxia, transfection of mimic-210 significantly increases superoxide levels at 48 hours as measured by MitoSox staining. Representative images from mimic-210 transfected cells are shown on the left panels and the mean ± SD of approximately 300 cells is shown on the right panel (*** $p<0.001$). **B**, exposure of cells to hypoxia for 48 hours enhances the production of superoxide; this effect is attenuated by transfection with anti-210. Representative images are shown on the left panels and the mean ± SD of approximately 300 cells is shown on the right panel (*** $p<0.001$). **C**, ROS production induced by mimic-210 is inhibited by co-transfection with the ISCU expressing plasmid. Mean ± SD of approximately 300 cells is shown (*** $p<0.001$).

3.2.7 Effects of miR-210 on cell viability

Previous studies in yeast have demonstrated the lethal consequences of deleting ISCU homologs (Isu1 and Isu2) (Tong and Rouault, 2000). The effects of ISCU depletion and miR-210 modulation on apoptosis were therefore examined in normoxia and hypoxia. There was a striking difference in the effects of mir-210 transfection in these opposing conditions. In normoxia, mimic-210 substantially

increased apoptosis. A similar effect has been previously reported in different cell lines (Chen et al., 2010; Tong and Rouault, 2000; Tsuchiya et al., 2011). A similar decrease in cell viability was observed in MCF-7 cells following ISCU knockdown in normoxia (Figure 3.12), suggesting that mimic-210 may induce apoptosis in normoxia by reducing ISCU levels. Conversely, in hypoxia, depletion of miR-210 following anti-210 transfection was associated with increased apoptosis (Figure 3.12). Decreased survival after miR-210 depletion in hypoxia has also been reported by other studies in cancer cell lines (Kim et al., 2009; Kulshreshtha et al., 2007; Yang et al., 2012).

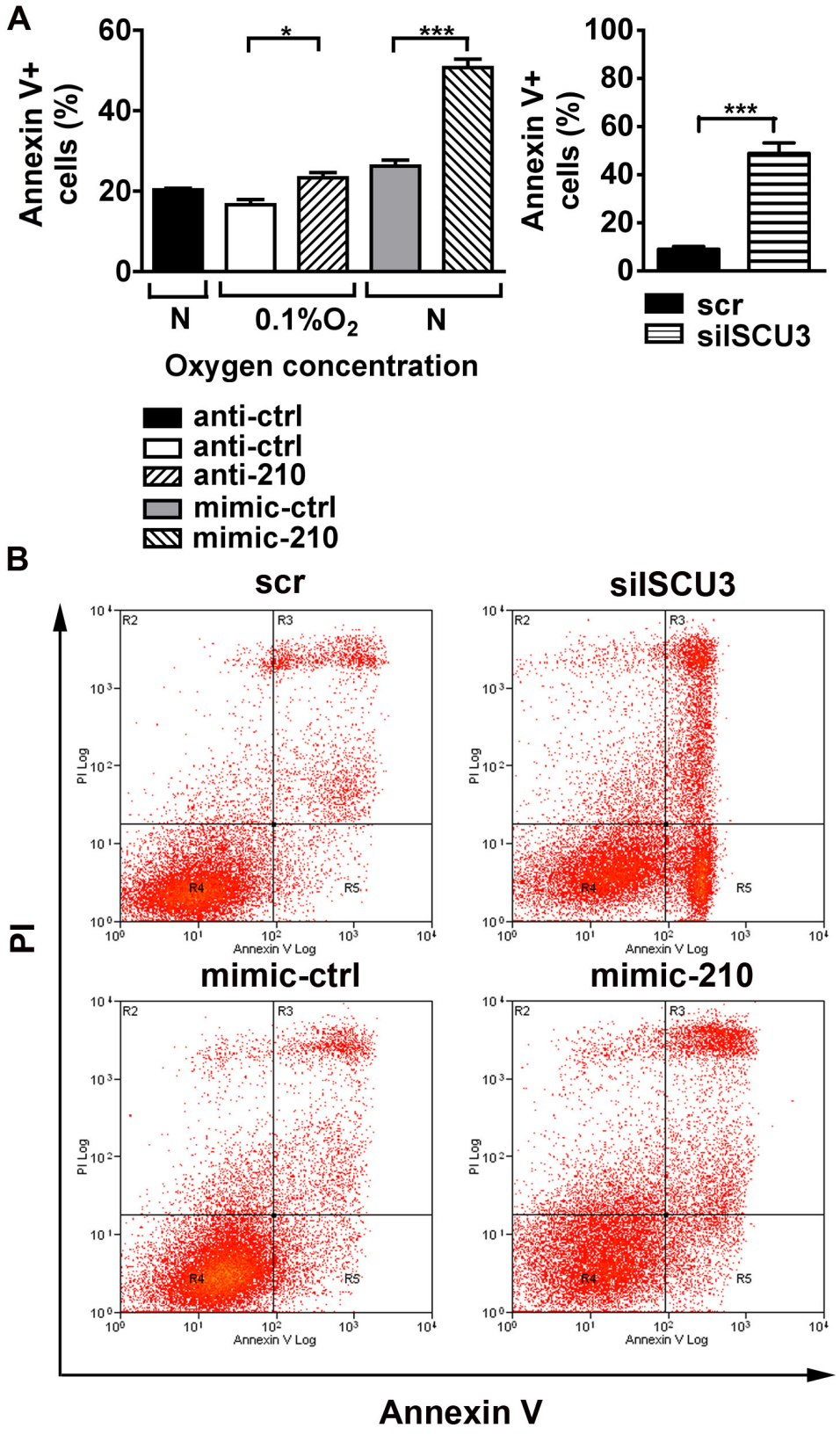


Figure 3.12 MiR-210 and ISCU affects cell survival.

Apoptosis (AnnexinV + cells) was measured in MCF-7 cells treated with anti-210, siISCU3, mimic-210, or corresponding controls after 48 hours exposure to 0.1% oxygen or normoxia. Cells were stained with Annexin V and Propidium iodide (PI) and analysed in a FACS analyser. Mean ± SEM is representative of 3 independent experiments is shown in **A** (* $p<0.05$, *** $p<0.001$), representative charts of cells transfected with siISCU3 or mimic-210 is shown in **B**.

3.2.8 *In vivo* regulation of ISCU expression by hypoxia

To test whether ISCU is modulated by hypoxia *in vivo*, RT-qPCR analysis for ISCU mRNA was performed in tumour samples derived form an *in vivo* model previously developed in our laboratory. In this model, xenografts of the glioblastoma cell line U87 were treated with the VEGF inhibitor, bevacizumab. These tumours were characterized by increased levels of hypoxia, as compared to untreated control tumours (described in more detailed in Chapter 4). As a consequence of increased levels of hypoxia in bevacizumab-treated tumours, there was a marked increase in miR-210 levels, as measured by RT-qPCR. This was associated with a significant decrease in ISCU expression (Figure 3.13).

In conclusion, these data verify the *in vitro* findings reported here for MCF-7 cells.

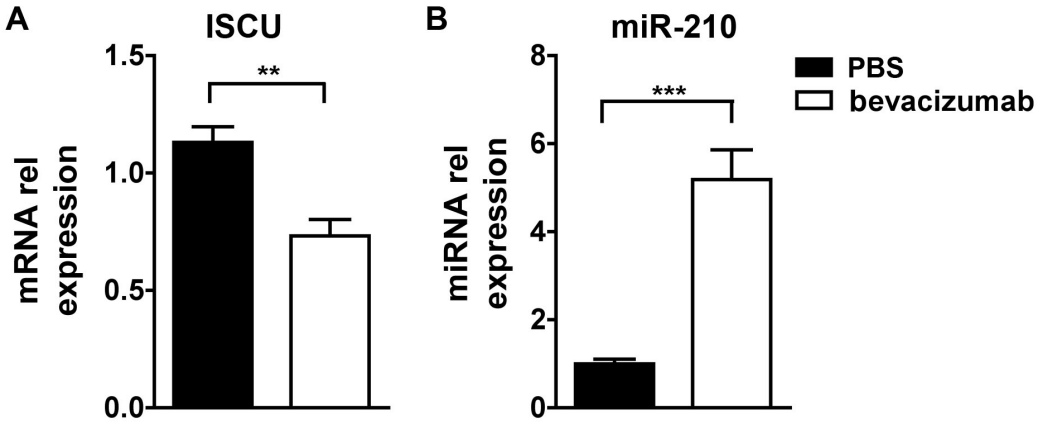


Figure 3.13 *In vivo* regulation of ISCU after anti-angiogenic treatment with bevacizumab.

RT-qPCR for ISCU (A) and miR-210 (B) in U87 xenografts treated with anti-angiogenic therapy (bevacizumab). Expression levels were normalised to those in untreated tumours. Mean ± SEM in 4 animals/group is shown (** $p<0.01$, ***$p<0.001$).

3.3 DISCUSSION

The data presented in this chapter provide evidence that a hypoxia-induced miRNA, miR-210, can modify cancer cell metabolism through regulation of its target, ISCU. ISCU was initially selected for analysis based on an integrative bioinformatic method that analysed for enrichment for hypoxia-regulated target genes that are downregulated in cancer samples. A number of other studies have confirmed ISCU as a miR-210 target, in both cancerous and non-cancerous cell lines (Chan et al., 2009; Chen et al., 2010; Lee et al., 2004a). Here, miR-210 regulation of ISCU mRNA and protein levels was demonstrated by experimentally increasing, or reducing, mir210 levels using the 'mimic-210' or 'anti-210' sequences, respectively. Interestingly, the reduction of ISCU mRNA and protein levels observed in hypoxia could be partially prevented by transfection with anti-210. Confirmation of transfection efficiency suggested that other mechanisms could contribute to ISCU downregulation in hypoxia. Among these, it is well recognised that RNA translation is reduced by hypoxia via the unfolded protein response (Wouters and Koritzinsky, 2008). This consists in a signalling program that occurs as a consequence of endoplasmic reticulum (ER) stress (induced by hypoxia) and the associated protein unfolding or misfolding. The program culminates with the inhibition of RNA translation in order to prevent further accumulation of altered proteins in the ER.

A decrease in ISCU levels is predicted to impair the ability of cells to generate Fe-S clusters, and therefore subsequently impact on the activity of Fe-S enzymes. It would be of great interest to directly measure Fe-S clusters with electron paramagnetic resonance spectroscopy in future studies. Interestingly, in the study by Chen et al,

decreased Fe-S clusters were measured in several tissues of VHL knockout mice, as compared to wild type mice (Chan et al., 2009). VHL knockout mice represent an established model of HIF protein stabilization in normoxic conditions. These results therefore support the hypothesis of a VHL-dependent regulation, possibly through the HIF-miR-210-ISCU axis, of Fe-S clusters synthesis *in vivo*.

Consistent with a reduction in ISCU levels in hypoxia affecting Fe-S proteins, the activity of two important Fe-S enzymes, aconitase and complex I, was reduced when miR210 was upregulated experimentally, or induced by hypoxia. Aconitase converts citrate into isocitrate, and exists in two isoforms: cytosolic aconitase 1, and mitochondrial aconitase 2. In the absence of Fe-S clusters, aconitase 1 functions as iron regulatory protein 1 (IRP1) and promote the uptake of iron, which is important for tumour growth (Tong and Rouault, 2007). As predicted, a member of our laboratory, Dr Christopher Blick, was able to detect increased intracellular levels of iron in cancer cells transfected with either mimic-210 or siISCU (personal communication) (Favaro et al., 2010). Mutations in ISCU give rise to lactic acidosis in individuals following moderate exercise, suggesting that ISCU is required for efficient Krebs cycle activity (Mochel et al., 2008; Olsson et al., 2008). An associated effect arising from decreased ISCU levels and a subsequent decrease in the Krebs cycle activity was a switch to glycolysis and increased lactate production. A similar switch to glycolyisis was induced in normoxia by mimic-210, suggesting that this may be relevant in situations where miR-210 upregulation occurs in normoxia. For example, this has been documented in renal cancer cell lines with mutations in the VHL protein (Camps et al., 2008; Neal et al., 2010; Redova et al., 2012). Conversely, in hypoxia, anti-210 reduced lactate production, reversing the

Pasteur effect. Although other studies confirmed the role of miR-210 in sustaining glycolysis and repressing mitochondrial metabolism in endothelial, colon cancer, and lung adenocarcinoma cell lines (Chan et al., 2009; Chen et al., 2010; Puissegur et al., 2011), a more extensive approach should be adopted for the correct characterisation of miR-210-dependent effects on glycolytic metabolism in MCF-7 cells, and it will be the focus of future analyses. Indeed, the simple measurement of increased lactate levels paired with reduced extracellular pyruvate concentrations in miR-210-overexpressing cells could potentially be the result of augmented metabolic requirements rather then a switch to aerobic glycolysis. For this purpose, measurements of glucose uptake and O_2 consumption would be useful to complement the previous analyses.

Fe-S clusters are integral for efficient activity of the mitochondrial electron transport chain. Complex I activity was decreased in hypoxia, and upon transfection of mimic-210 or siISCU in normoxia. In addition to Complex I, Complexes II and III also contain Fe-S clusters and the activities of all three complexes could potentially also be decreased in a miR-210-dependent manner and would be interesting to investigate. Recently, the Complex II subunit, SDHD, has also been validated as a direct miR-210 target, confirming the role of miR-210 as a major regulator of the electron transport chain (Puissegur et al., 2011).

Although similar effects were observed following either miR-210 or ISCU modulation, a direct demonstration that these cellular functions are controlled by miR-210 through the repression of ISCU has not been provided here. To demonstrate this, cotrasfection with a miR-210 resistant ISCU would be required, similar to what has been described by Chan et al in endothelial cells, where constitutive expression

of miR-210 resistant ISCU constructs was able to prevent the effects of miR-210 in aconitase and Complex I activity (Chan et al., 2009).

An impaired electron transport chain could lead to an increase in free radical production as a consequence of electron leakage. In particular, complex III is a major contributor to the generation of ROS in hypoxia (Guzy et al., 2005) but Complexes I and II represent two other major sites of superoxide production in the mitochondria (Poyton et al., 2009; Quinlan et al., 2012). In agreement with published data (Chan et al., 2009; Chen et al., 2010), transfection of mimic-210 led to increased free radical production in normoxic conditions. Furthermore, the normoxic ROS production observed with mimic-210 was attenuated by expressing a miR-210 resistant ISCU construct. This confirms that ROS arise due to miR210-dependent downregulation of ISCU, rather than due to downregulation of another putative miR210 target. Conversely, in hypoxia, the induction of miR-210 was associated with an increase in ROS that was prevented by anti-210 transfection. ROS accumulation can itself disrupt the activity of Fe-S enzymes by causing the release of iron from the clusters, suggesting that miR-210-dependent ROS induction could trigger an amplification of Fe-S protein disruption (Srinivasan et al., 2000). In contrast to the hypoxic induction of ROS and its alleviation with anti-210 observed here, Chan et al. did not observe any significant change in ROS production after exposure of endothelial cells to hypoxia, and documented an increase in ROS when miR-210 was depleted (Chan et al., 2009). The reason for this discrepancy is unclear but may potentially reflect an underlying difference between cancer and normal cells.

The contrasting effects on cells survival in normoxia, where miR-210 induction caused apoptosis, and hypoxia, where miR-210 induction was protective, are of

interest and suggest that miR210 upregulation is required to prevent apoptosis during the adaptation to hypoxia. Although ROS are commonly considered toxic by-products of metabolism, they have been demonstrated to activate HIF (Guzy et al., 2005), mediate tumour growth *in vivo* via a HIF dependent mechanism (Gao et al., 2007), extend lifespan of cells (Bell et al., 2007), and activate survival pathways including the KEAP1–NRF2 (Murphy, 2009) and Akt pathways (Clerkin et al., 2008). The toxicity observed in normoxia could be induced by several factors: i) a greater production of ROS with ISCU inhibition, compared to hypoxia, ii) reduced ROS-scavenging potential in normoxic cells, or iii) heightened sensitivity to ROS in normoxia. Notably, many mechanisms are induced in hypoxia to protect cells from mitochondrial changes induced by ROS (Semenza, 2007). It is important to clarify that in addition to ROS, many other factors could affect cell viability in response to miR-210 modulation, including the validated targets CASP8P and B-cell lymphoma 2 (Bcl-2) (Chio et al., 2012; Kim et al., 2009).

Importantly, ISCU represents only one of a few targets through which miR-210 exerts its metabolic and mitochondrial effects. For example, miR-210 upregulation has been demonstrated to induce mitochondrial dysfunction (altered morphology and mitochondrial membrane potential) through its target succinate dehydrogenase, subunit D (Pulkkinen et al., 2008). Another contributor to ROS generation is likely represented by the validated target COX10, which can regulate the functions of Complexes I and IV of the electron transport chain (Chen et al., 2010).

Taken together, the results presented here describe a novel important pathway contributing to metabolic adaptation of cancer cells to hypoxia, co-ordinated by miR-210 suppression of ISCU, and the subsequent decreased activity of Fe-S proteins

(Figure 3.14). In addition to aconitase and complex I described here, many other metabolic enzymes require Fe-S clusters for their activity (e.g. SDH and FH) suggesting that downregulation of ISCU could have far reaching consequences on cell metabolism.

In addition to metabolic enzymes, the activity of several important DNA repair enzymes with Fe-S clusters are also potentially regulated by the miR-210-ISCU axis, including the helicases xeroderma pigmentosum group D (XPD) and Fanconi anemia complementation group J (FancJ), involved in the nucleotide excision repair and Fanconi anemia repair pathways, respectively (Rudolf et al., 2006). Recently, mutations in the nucleotide excision repair protein homolog MMS19 have been associated with increased genomic instability (Stehling et al., 2012). MMS19 functions as part of the cytosolic iron-sulfur protein assembly (CIA) machinery, and specifically interacts with and facilitates iron-sulfur cluster insertion into apoproteins involved in methionine biosynthesis, DNA replication, DNA repair, and telomere maintenance. This suggests that ISCU downregulation by miR-210 could similarly contribute to genomic instability in tumours.

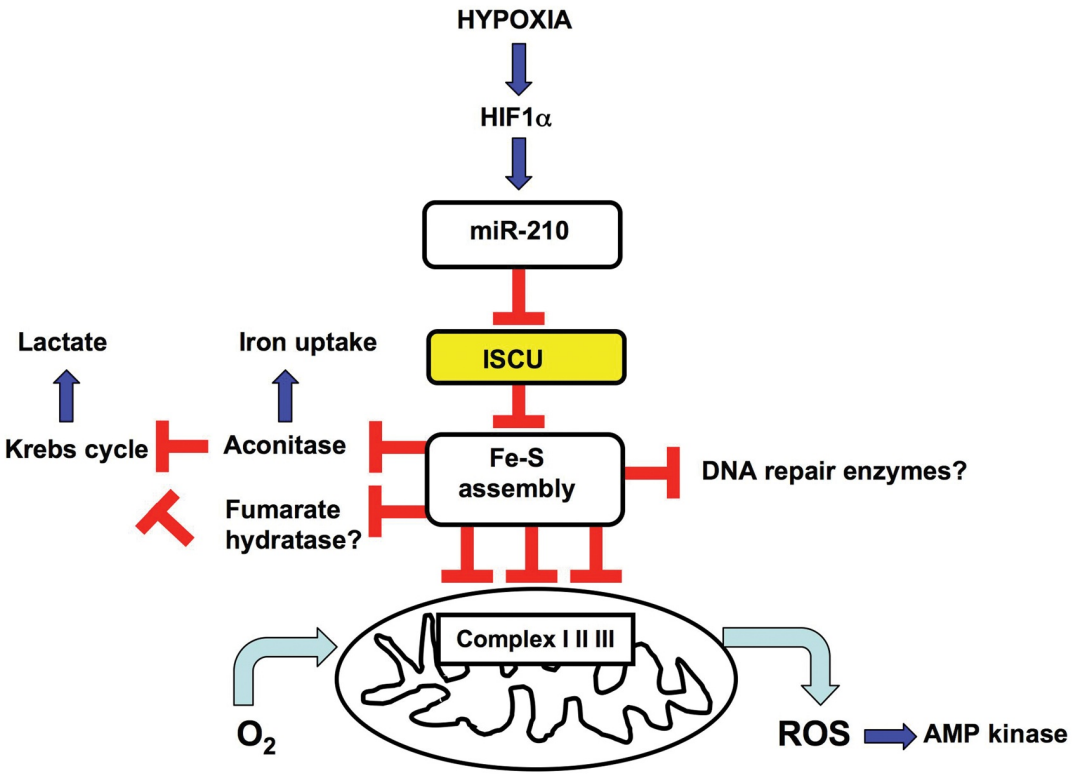


Figure 3.14 Working model: hypoxia regulates ISCU via HIF1α induction of miR-210.
MiR-210 targeting of ISCU 3'UTR reduces ISCU expression. Reduced Fe-S assembly and incorporation in the mitochondrial electron transport chain (Complex I, II, and II) impairs the normal transfer of electrons. This is a key mechanism for generating ROS, which have both positive and negative effects in hypoxia. Reduction of aconitase activity inhibits the Krebs cycle, resulting in an increase in glycolysis and lactate production. Aconitase 1 (cytosolic aconitase), when depleted of Fe-S becomes an iron regulatory protein, irp1, which enhances iron uptake through induction of transferrin receptor. Other Fe-S proteins are potential targets.

Circulating miR-210 can be detected at elevated levels in cancer patients and it has been proposed as a novel, non-invasive biomarker for diagnosis, other than prognosis in specific subsets of cancer patients (Jung et al., 2012; Lawrie et al., 2008; Zhao et al., 2012). It would be of interest to investigate whether miR-210 levels reflect the metabolic state of their primary cancer and hence could be used in future therapy selection. Notably, miR-210 levels will be evaluated in a clinical trial as a tool for pretherapeutic selection of head and neck cancer patients with more hypoxic

tumours, who therefore will benefit the most from the combination of radiotherapy and hypoxic radiosensitiser agents (oxygen mimic), as compared to radiotherapy alone (personal communication to Prof Adrian Harris from Overgaard's group [Danish Center for Interventional Research in Radiation Oncology]).

Finally, the clinical significance of ISCU regulation in primary tumours and the association with hypoxia were investigated by a colleague in the laboratory, Dr Francesca Buffa, who analysed ISCU expression in over 800 breast cancer patients in published series, where low ISCU expression was associated with poor outcome. Moreover, she found a striking inverse correlation of miR-210 with ISCU in both head and neck cancer and breast cancer (data not shown) (Favaro et al., 2010).

4 CHAPTER FOUR

Glycogen metabolism is upregulated in hypoxia

4.1 INTRODUCTION

Glycogen accumulation under hypoxic conditions has been observed in several non-cancer and cancer cell lines, and may therefore be an important general cellular response to hypoxia. Examples of non-cancer cell lines that have been demonstrated to accumulate glycogen deposits in hypoxia include skeletal and heart muscle cells, myoblasts, fibroblasts, and hepatocytes (Mamedova et al., 2003; Pelletier et al., 2012; Pescador et al., 2010; Vigoda et al., 2003). The proposed physiological basis for this is the generation of a source of fuel that can be readily used for cell survival under conditions of nutrient deprivation.

The presence of intracellular glycogen deposits has also been observed in several cancer cell lines (Rousset et al., 1984; Rousset et al., 1981), and glycogen turnover has been proposed to be an important metabolic pathway in cancer (Brahimi-Horn et al., 2010; Mamedova et al., 2003; Pelletier et al., 2012; Pescador et al., 2010; Shen et al., 2010; Vigoda et al., 2003). Indeed, the kinetics of glycogen accumulation as a function of cell growth were investigated in some of these cancer cell lines (colon cancer cells HT29 and SW-480, malignant melanoma cells MeWo, urinary bladder cancer cells RT-4, kidney cancer cells SW-839, ovary cancer cells SKOV-3, and lung cancer cells SW-900) and in human colorectal cancer tissues, and glycogen content was found to be inversely correlated with proliferation rate, suggesting that glycogen is consumed to sustain cancer cell growth (Rousset et al., 1984; Rousset et al., 1981; Takahashi et al., 1999). A need for a more extensive characterisation of the roles of glycogen metabolism in hypoxic tumours therefore constituted the basis for the following investigation.

In this chapter, the consequences of hypoxia on glycogen metabolism were explored *in vivo* and *in vitro*. Glycogen accumulation, and the upregulation of several glycogen metabolising enzymes, was observed *in vivo*, using bevacizumab-treated xenografts as a model for hypoxic tumours. The clinical significance of glycogen metabolism in tumours was also interrogated in different tumour types, based on published gene array data sets available from Oncomine.org, and in a small set of tissue microarrays of breast cancers at different stages of development. Finally, the roles of glycogen metabolising enzymes were analysed in cancer cell lines cultivated in hypoxic conditions *in vitro*, with a specific focus on GYS1 and PYGL, the two key enzymes involved in glycogen synthesis and breakdown, respectively.

4.2 RESULTS

4.2.1 *In vivo* regulation of glycogen metabolism by hypoxia

To address the effects of the hypoxic microenvironment on metabolic pathways, gene expression analysis was performed on an *in vivo* model for hypoxic tumours, where xenografts of U87 glioblastoma cells outgrew treatment with the anti-angiogenic drug bevacizumab (Paez-Ribes et al., 2009) (courtesy of Drs Francesca Buffa and Ji-Liang Li). More specifically, bevacizumab treatment was started once xenografts had reached 150 mm^3 in size, and was administered three times per week until sacrifice (i.e. when tumour size reached 1.44 cm^3). Gene expression analysis at the end of the experiment, revealed upregulation of several HIF1α targets, including *CA9* (Wykoff et al., 2000), indicating that bevacizumab-treated tumours were more hypoxic as compared to control tumours (Table 4.1). Several metabolic pathways were found to be deregulated, including a number of genes involved in glycogen metabolism that could potentially contribute to cancer cell survival in hypoxia (Table 4.1). These include: *GYS1*, *GAA*, *PYGL*, *GBE1*, *PGM1*, protein phosphatase 1, *PPP1R3B* and *PPP1R3C*, and Genethonin-1 (*GENX-3414)*. Further analyses focused on GYS1 and PYGL, because of their central roles in glycogen synthesis and breakdown, respectively.

Symbol	Description	Accession	Unigene	Fold Change	Q value (%)
CA9	Carbonic anhydrase IX	NM_001216	Hs.63287	11.2	0
PPP1R3B	Protein phosphatase 1, regulatory subunit 3B	NM_024607	Hs.458513	4.2	0
GYS1	Glycogen synthase 1	NM_002103	Hs.386225	4.1	0.2
GAA	Acid α-glucosidase	NM_000152	Hs.1437	4.1	0.4
PPP1R3C	Protein phosphatase 1, regulatory subunit 3C	N26005	Hs.303090	3.7	0
PYGL	phosphorylase, glycogen, liver	AU157823	Hs.282417	2.6	2.1
GBE1	Glycogen branching enzyme	NM_024607	Hs.436062	2.1	0
GENX-3414	Genethonin-1	NM_003943	Hs.109590	1.9	0.1
PGM1	phosphoglucomutase 1	NM_002633	Hs.1869	1.3	1.2

Table 4.1 Expression of glycogen-related enzymes is increased after bevacizumab treatment.
List of genes involved in glycogen metabolism that were found to be upregulated in U87 xenografts after treatment with bevacizumab. Gene expression was analyzed by Affimetrix gene arrays. CA9 is shown as a HIF1 control. Data shown are courtesy of Dr Francesca Buffa and Dr Ji-Liang Li.

Increased expression of *CA9*, *GYS1*, and *PYGL* in bevacizumab-treated tumours was confirmed at the mRNA levels by RT-qPCR (Figure 4.1A). Immunostaining of tumour sections for the hypoxic marker pimonidazole, also confirmed an increase in hypoxia following bevacizumab treatment (Figure 4.1B). Analysis of serial sections for glycogen-related parameters also revealed increased expression of GYS1 (27.8±1.4% of viable cells versus 14.3±3.7% in the control group), PYGL (69.9±7.0% versus 37.7±7.2%), and increased glycogen levels as determined by Periodic Acid-Schiff (PAS) staining (5.3±2.0% versus 0.4±0.2%) (Figure 4.1B).

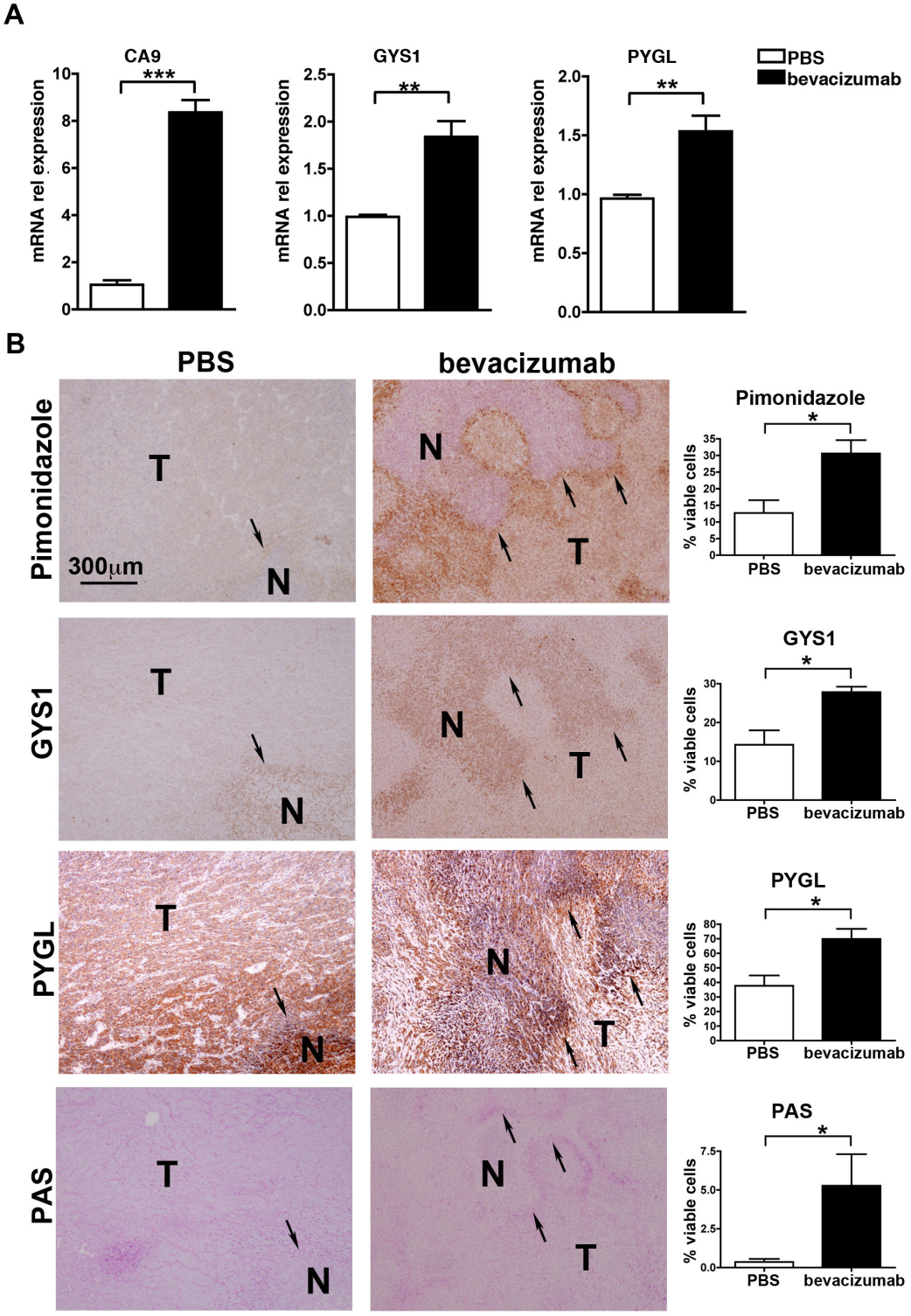


Figure 4.1 Glycogen metabolism is upregulated *in vivo* after bevacizumab treatment.

A, RT-qPCR for *CA9*, *GYS1* and *PYGL* in U87 xenografts treated with bevacizumab or PBS (control). Expression of *GYS1* and *PYGL* is relative to control tumours, and normalised to β-actin. Mean values ± SEM in 4 animals/group is shown (** p <0.01,

***p<0.001). **B**, serial sections derived from U87 xenografts treated with PBS (control) or bevacizumab were stained for pimonidazole, GYS1, PYGL or PAS. Representative images are shown on the left, quantification is shown on the right. N=necrosis, T=viable tumour, arrows indicate examples of positively stained areas. Mean values ± SEM in 4 animals/group is shown (* p <0.05).

The apparent overlapping distribution of glycogen-related markers and hypoxia was further investigated using two methods. First, a section from a bevacizumab-treated tumour was co-stained for CA9 and glycogen, revealing colocalization of hypoxia and glycogen in the perinecrotic areas (Figure 4.2A). Second, the expression of *GYS1* and *PYGL* was measured in spheroids derived from the colon cancer cell line, HCT116. These spheroids represent a 3-dimensional model of tumour growth that develops a central hypoxic/necrotic core when outgrowing the oxygen diffusion limit. Immunohistochemistry performed on HCT116 spheroids revealed that the expression of both enzymes was increased in cells surrounding the central necrotic core that were also positive for pimonidazole staining (Figure 4.2B).

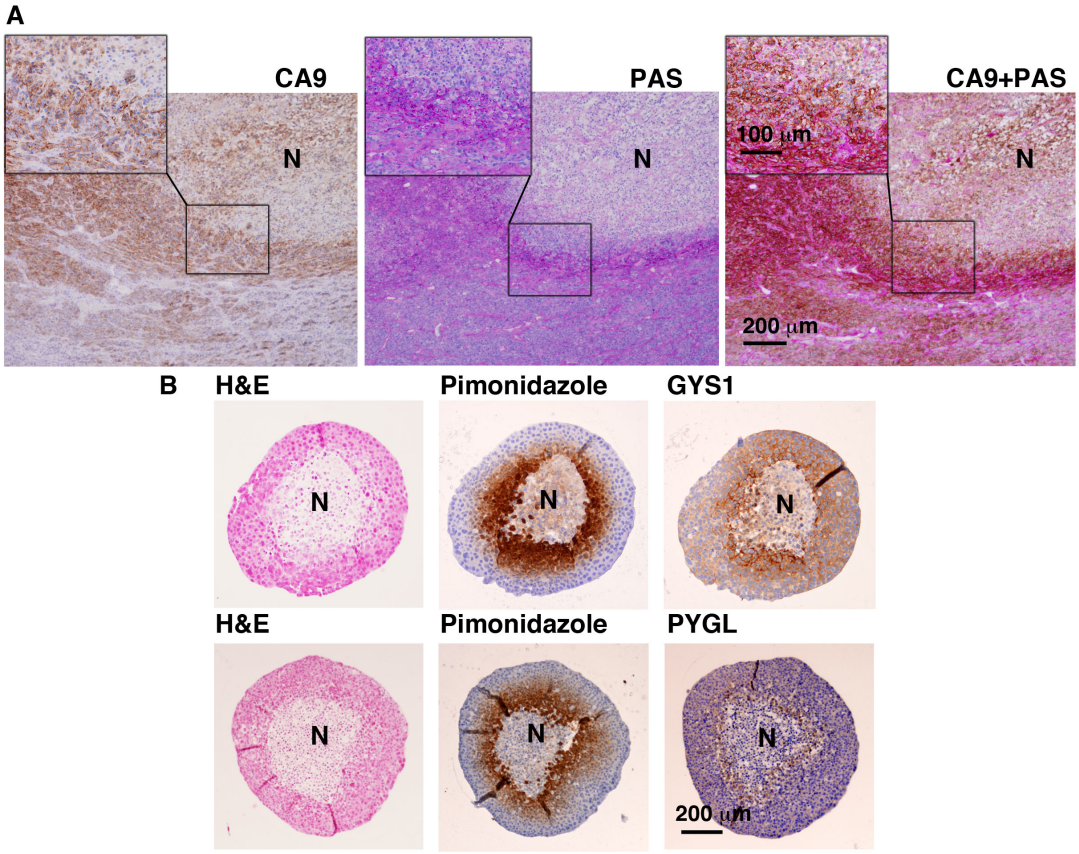


Figure 4.2 Hypoxia is associated with upregulation of glycogen metabolism. **A,** serial sections from a bevacizumab-treated tumour were stained for CA9 and PAS, alone (left and middle panel) or in combination (right panel). N=necrosis. **B**, Haematoxylin and Eosin (H&E) staining (left panels) and immunohistochemical staining of spheroid sections for pimonidazole (middle panels), GYS1 (top right panel), or PYGL (bottom right panel). N=necrosis.

4.2.2 Hypoxia regulates GYS1 and PYGL expression and modulates glycogen accumulation *in vitro*

To further investigate the roles of GYS1 and PYGL in the adaptation to hypoxia, the kinetics of their upregulation was measured *in vitro* in cancer cell lines exposed to hypoxia (0.1% O_2). These analyses were performed on a glioblastoma (U87), a breast (MCF-7), and/or a colon (HCT116) cancer cell line, as previous studies have measured elevated levels of glycogen in these tumour types (Rousset et al., 1981).

Furthermore, U87-derived xenografts were used for the initial gene expression analysis performed in our laboratory by Dr Francesca Buffa and Dr Ji-Liang Li. Analysis of *GYS1* and *PYGL* expression, at both the mRNA and protein levels, revealed a distinct pattern of induction in hypoxia. Specifically, GYS1 levels increased rapidly (12 hours), and then started to decline at the later time points (48/72 hours), whereas PYGL increased gradually and reached maximal levels at 72 hours (Figure 4.3).

Glycogen quantification in U87 and MCF-7 cells, revealed a rapid increase in glycogen levels, which peaked by 24 hours, and then gradually declined by 72 hours (Figure 4.4A). Glycogen accumulation in U87 cells after 48 hours in hypoxia, was also confirmed by PAS staining, and Transmission Electron Microscopy (TEM) (performed by Professor David Ferguson at the Nuffield Department of Clinical Medicine, University of Oxford) (Figures 4.4B and 4.4C). PAS staining revealed increased cytoplasmic staining in hypoxic cells. Specificity of the staining for glycogen granules was confirmed by pre-treatment with the glycogen depolymerizing enzyme, amylase. TEM revealed the presence of lucent pools of glycogen in the cytoplasm of hypoxic cells.

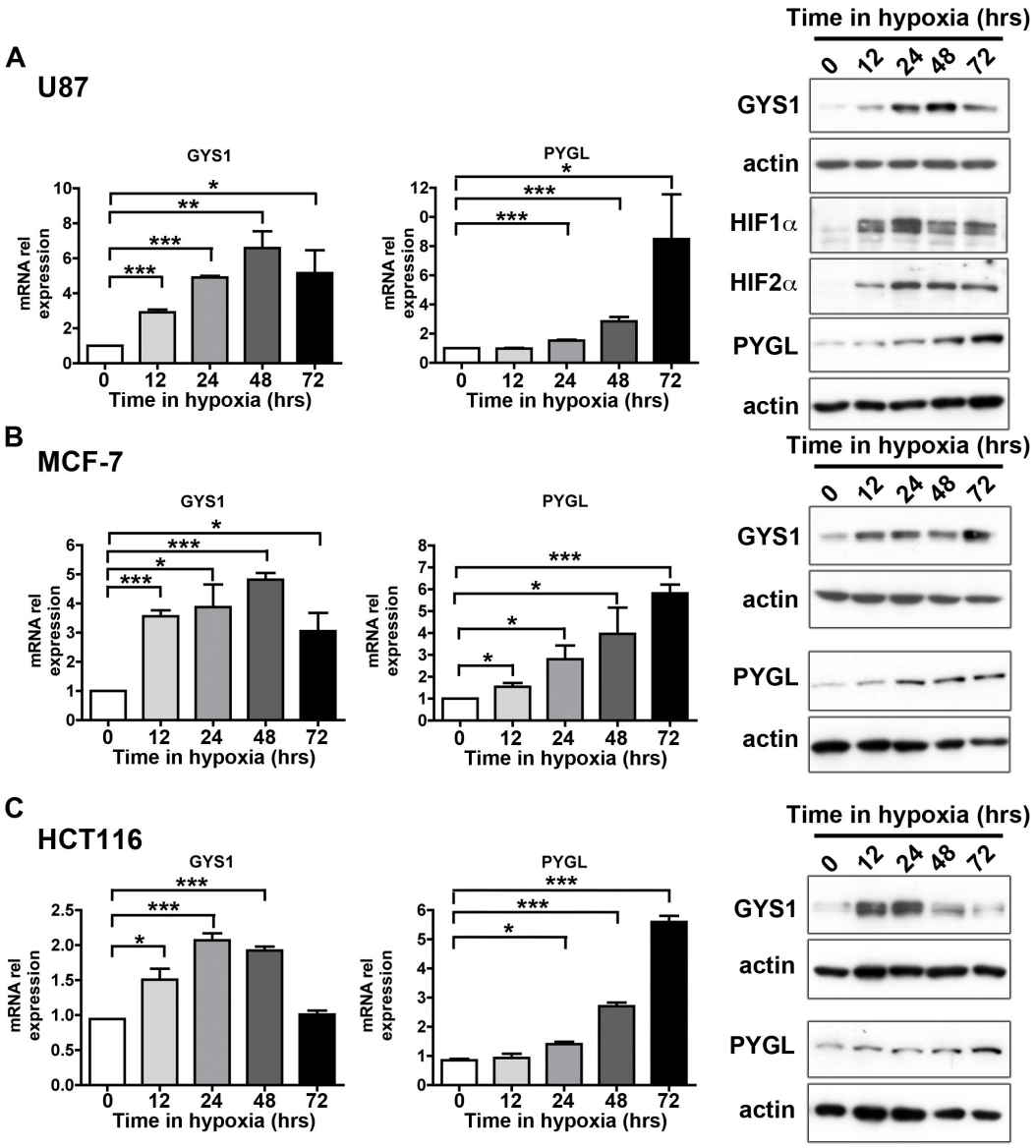


Figure 4.3 Pattern of GYS1 and PYGL induction in hypoxia.
U87 (**A**), MCF-7 (**B**), and HCT116 (**C**) cells were exposed to hypoxia (0.1% O_2) for 0, 12, 24, 48, and 72 hours. GYS1 and PYGL expression was analysed by RT-qPCR (left panels) and Western blotting (right panels). Levels of GYS1 and PYGL mRNA are relative to their levels at 0 hours in hypoxia. Mean ± SEM of three independent experiments is shown (* $p<0.05$, ** $p<0.01$, *** $p<0.001$).

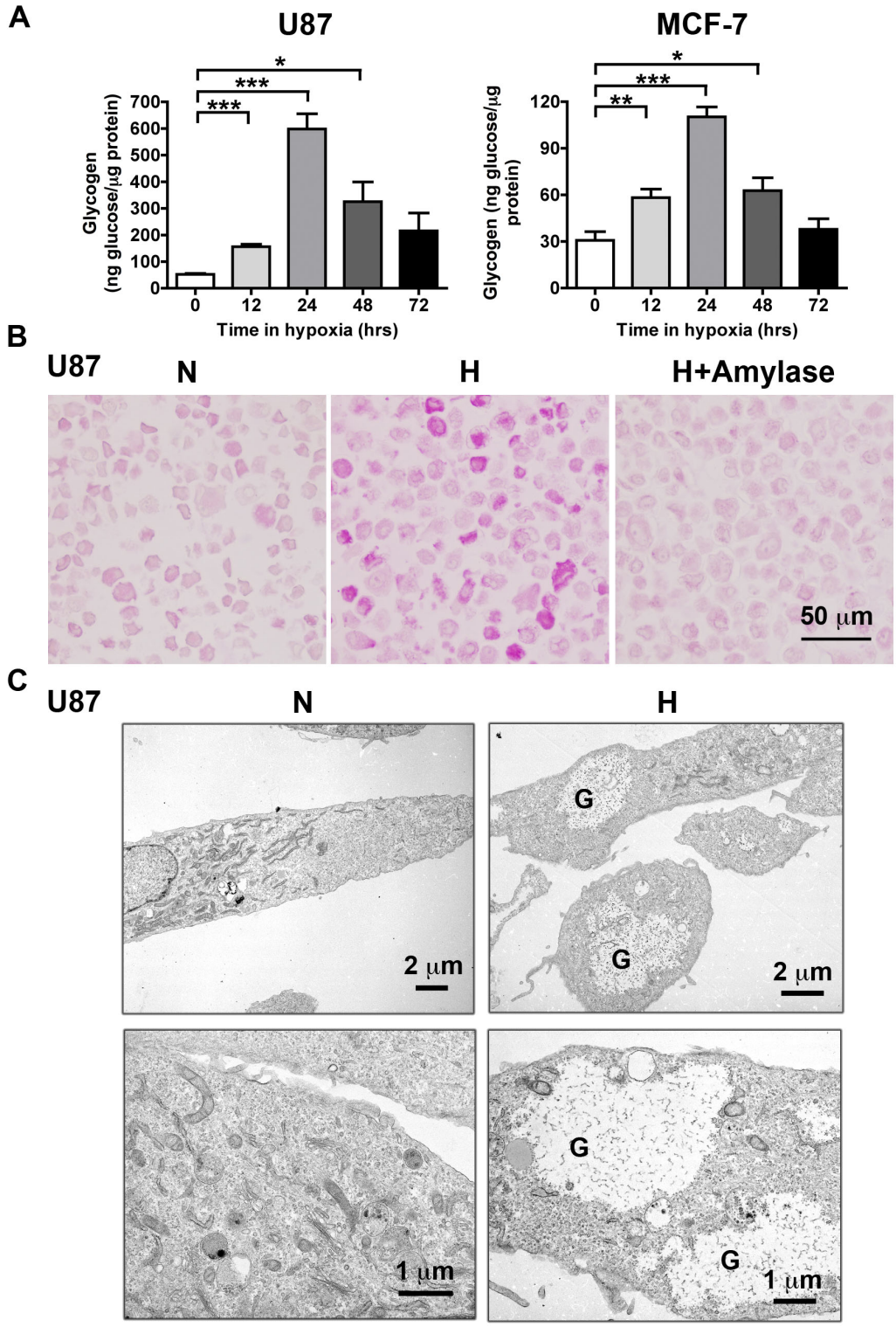


Figure 4.4 Glycogen accumulation in hypoxia.
A, glycogen accumulation in hypoxia was measured in U87 and MCF-7 cells exposed to hypoxia in a time course experiment. Glycogen levels were normalized by protein content. Mean ± SEM of three independent experiments is shown (*

$p<0.05$, *** $p<0.001$). Glycogen accumulation after 48 hours in hypoxia was detected in sections of U87 cell pellets by PAS staining (**B**) and TEM (**C**). The intensity of PAS staining (pink colour) correlates with glycogen content of the cells. Amylase treatment was used in conjunction with PAS staining as a negative control for glycogen staining. G=glycogen.

The activity of GYS1, and the consequent synthesis of glycogen, can be regulated at a number of different levels: i) by protein levels, ii) by allosteric activators such as glucose-6-P, and iii) by post-translational modifications (e.g. phosphorylation at one or more of the nine known phosphorylation sites, which inactivates GYS1 (Johnson, 1992)). As expected, U87 cells exposed to hypoxia, demonstrated induction of the HIF1-targets GLUT1 and HKII (Semenza, 2002), which are important for the transport of glucose into cells, and its subsequent phosphorylation into glucose-6-P, respectively (Figure 4.5). The analysis of the phosphorylation status of GYS1 revealed an initial decrease of phospho-GYS1 at 12 hours in hypoxia, followed by an increase at 24 hours that remained unchanged at later time points. When compared to the total GYS1 levels at the corresponding time points, this manifests as a decrease in the proportion of phospho (inactive)-GYS1 at 12 and 24 hours in hypoxia, followed by a gradual increase at 48 and 72 hours (Figure 4.5). Taken together, these data demonstrate that GYS1 activity increases as part of the acute response of cancer cells to hypoxia.

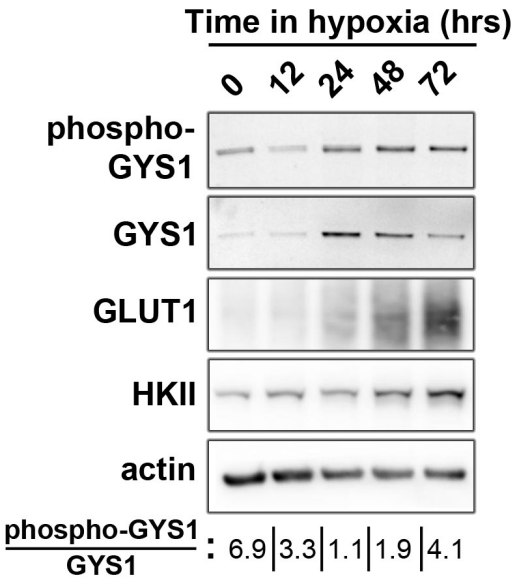


Figure 4.5 Hypoxic regulation of GYS1 activity.
Western blotting of U87 cell extracts revealed an initial decrease of phospho-GYS1 at 12 hours in hypoxia, followed by an increase in phospho-GYS1 at later time points. Hypoxia induces a progressive induction of GLUT1 and HKII.

The hypoxic regulation of other glycogen-metabolising enzymes that were induced by bevacizumab treatment was also evaluated in U87 cells by RT-qPCR. In particular, GAA, the lysosomal enzyme responsible for glycogen hydrolysis, increased gradually and peaked at 72 hours, similar to what was observed for PYGL. Conversely, the regulatory proteins PPP1R3B and PPP1R3C increased rapidly and started to decline at 72 hours, similar to what was observed for GYS1 (Figure 4.6). The branching enzyme GBE was also confirmed to be induced in hypoxia, revealing a rapid induction that was maintained until 72 hours (Figure 4.6).

Taken together, these data suggest that glycogen metabolising enzymes exhibit characteristic patterns of induction in response to hypoxia. It will be of interest to further determine the regulatory mechanisms for this induction in future studies.

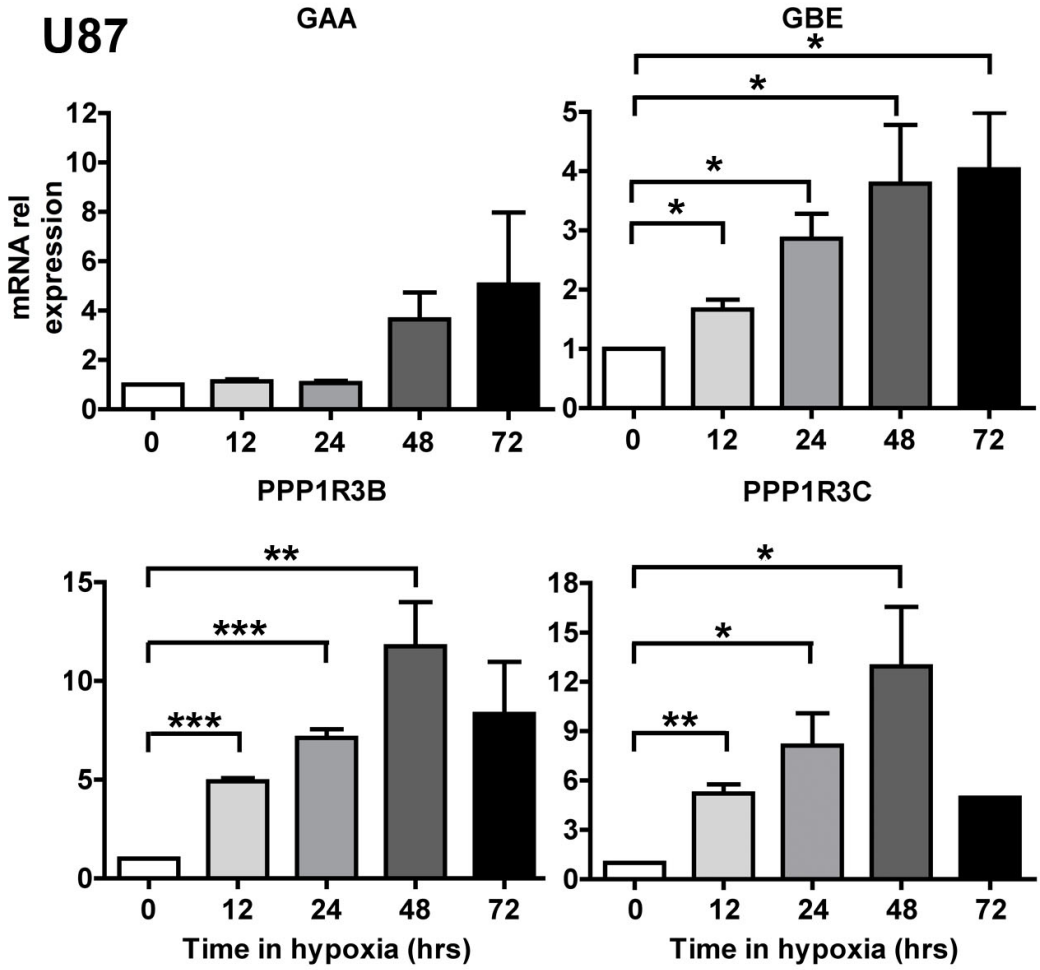


Figure 4.6 Hypoxic induction of glycogen metabolising enzymes and regulatory proteins.
Hypoxic induction of GAA, GBE, PPP1R3B, and PPP1R3C mRNA was evaluated in U87 cells in a time course experiment. mRNA levels are relative to their levels at 0 hours in hypoxia. Mean ± SEM of three independent experiments is shown (* $p<0.05$, ** $p<0.01$, *** $p<0.001$).

4.2.3 Physiological significance of hypoxic upregulation of glycogen metabolism

To exclude the possibility that glycogen accumulation in hypoxia could arise as a consequence of high glucose concentrations (25 mM) present in standard culture media, GYS1, PYGL and glycogen levels were measured in hypoxia at physiological

glucose concentrations (5 mM). Immunoblotting for GYS1 and PYGL in U87 cell extracts revealed a similar pattern of induction in hypoxia to that observed using 25 mM glucose medium (Figure 4.7). More specifically, this was characterized by early induction of GYS1 (24 hours), followed by decreased levels at 72 hours, and late induction of PYGL (72 hours) (Figure 4.7, left panel). Concordantly, glycogen levels increased rapidly, peaked at 48 hours, and started to decrease at 72 hours in hypoxia (Figure 4.7, right panel). This suggests that the findings reported here are not artefacts caused by high levels of extracellular glucose.

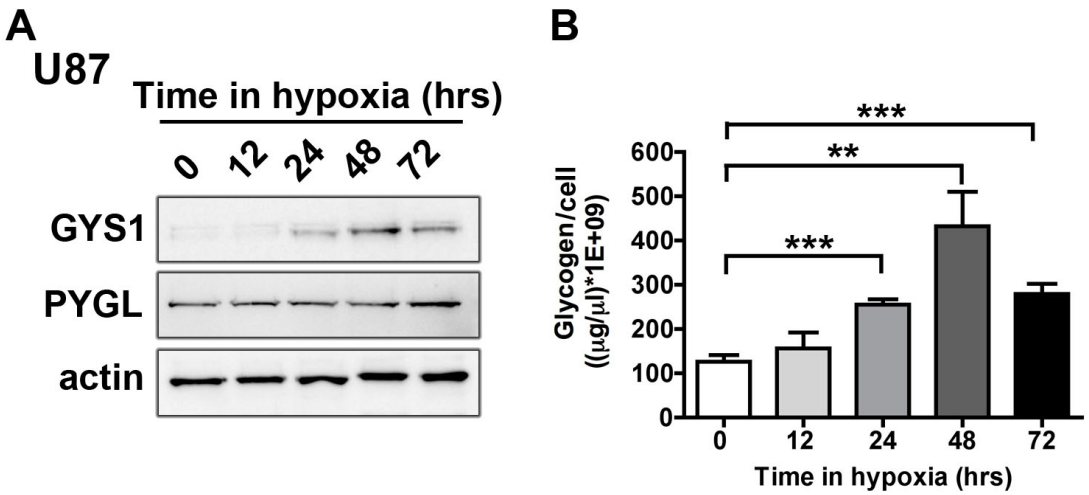


Figure 4.7 Glycogen metabolism is activated by hypoxia at physiological glucose concentrations (5 mM).
A, immunoblot analysis of GYS1 and PYGL expression in U87 cells in a time course experiment in hypoxia. **B**, glycogen levels were also measured at the indicated time points. Glycogen levels were normalized by cell number. Mean ± SEM of three independent experiments is shown (** $p<0.01$, *** $p<0.001$).

4.2.4 Role of HIF in the hypoxic regulation of glycogen metabolism

The observation that GYS1 and PYGL expression was regulated in hypoxia, led to investigate the contribution of HIF1α. In order to investigate the role of HIF, U87

and MCF-7 cells were transiently transfected with siRNA specific for HIF1α or HIF2α, and exposed to hypoxia for 48 or 72 hours, at the peak of induction for GYS1 and PYGL, respectively (Figure 4.3). The efficiency of HIF knockdown in hypoxia was verified by immublotting with specific antibodies for HIF1α or HIF2α (Figure 4.8B). In agreement with recent studies (Mole et al., 2009; Pescador et al., 2010), HIF1α knockdown prevented GYS1 induction in hypoxia in both U87 and MCF-7 cell lines, as measured by RT-qPCR and confirmed by Western blotting (Figure 4.8). However, unlike GYS1, hypoxic PYGL induction was not HIF1-dependent in U87 or MCF-7 cells (Figure 4.8). Rather, in MCF-7 cells, both RT-qPCR and Western blot analyses revealed a reduction in PYGL after HIF2α knockdown (Figure 4.8). However, this finding was not confirmed in U87 cells, and may therefore arise indirectly. Further experiments are therefore required to determine precisely how PYGL induction is regulated. It should be noted, however, that consistent with PYGL induction being HIF1-independent, chromatin immunoprecipitation analysis linked to high throughput sequencing performed on MCF-7 cells with HIF specific antibodies did not show any signal at the PYGL locus (Mole et al., 2009). Conversely, this analysis was able to identify a HIF-binding site in the promoter region of GYS1 (personal communication, Dr David Mole).

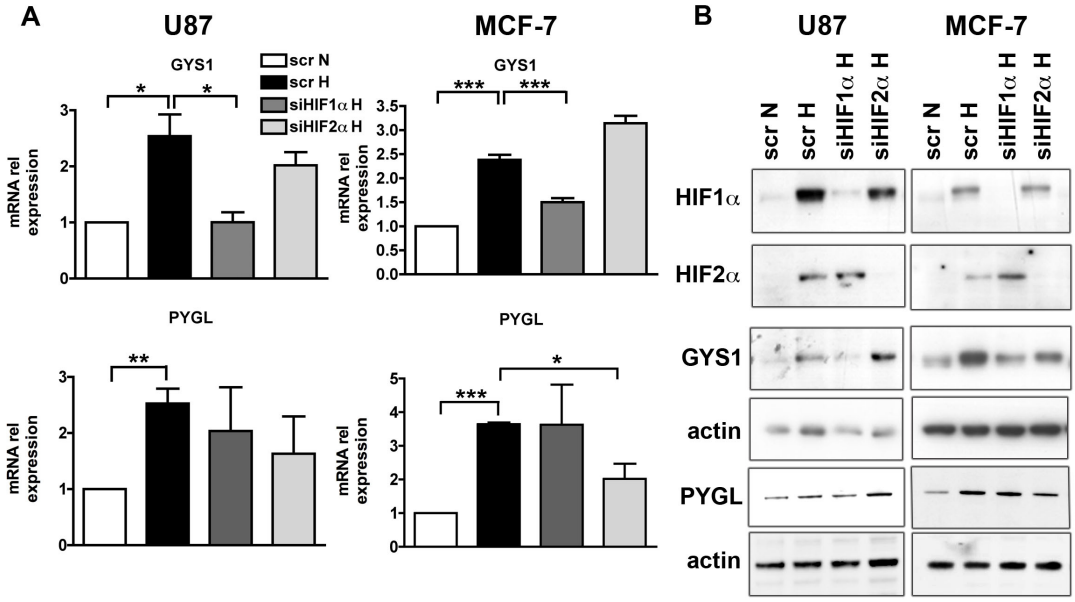


Figure 4.8 Role of HIF in the hypoxic regulation of GYS1 and PYGL.
U87 and MCF-7 cells were transiently transfected with scramble control (scr), siHIF1α, or siHIF2α and exposed to hypoxia for 48 hours (GYS1 expression) or 72 hours (PYGL expression). GYS1 and PYGL expression was analysed at the mRNA level by RT-qPCR (**A**) and protein levels by Western Blotting (**B**). mRNA under hypoxia are relative to scr in normoxia. Mean ± SEM of three independent experiments is shown (* $p<0.05$, ** $p<0.01$, *** $p<0.001$).

4.2.5 GYS1 sustains glycogen synthesis in hypoxia

Previous studies revealed that HIF1α-dependent induction of GYS1 in hypoxia promotes glycogen synthesis, and it is important for survival of mouse hepatoma cells under conditions of glucose and oxygen deprivation (Pescador et al., 2010). In agreement with these results, GYS1 knockdown in U87 cells was associated with a significant impairment of glycogen accumulation after 48 hours in hypoxia (Figures 4.9A and 4.9B). Since it was difficult to predict whether GYS knockdown was associated with changes in global protein expression, for a more reliable quantification, glycogen levels were normalised by cell number instead of protein

concentration. Reduced glycogen levels were also observed by PAS staining (Figure 4.9C).

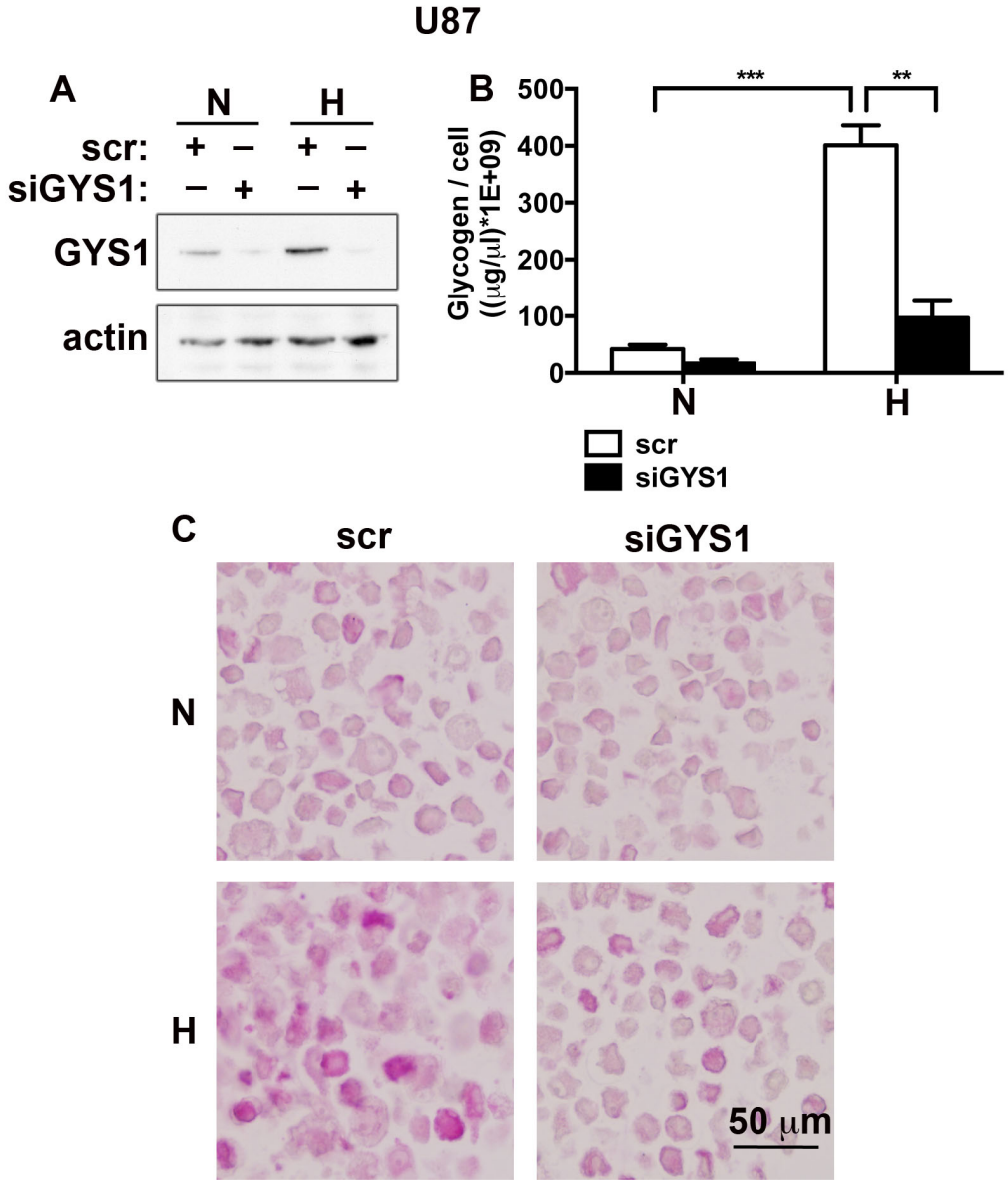


Figure 4.9 Glycogen synthesis in hypoxia is impaired after GYS1 depletion
A, U87 cells were transfected with siRNA against GYS1 or control siRNA (scr) and the efficiency of knockdown was determined by immunoblotting for GYS1 after 48 hours in normoxia (N) or hypoxia (H). Detection of actin levels was used as a loading control. **B**, glycogen levels were quantified under the same conditions as in A. Glycogen was normalized by cell number. Mean ± SEM of three independent experiments is shown (** $p<0.01$, *** $p<0.001$). **C**, representative images of PAS staining in sections of cell pellets treated as in A.

4.2.6 Effects of GYS1 depletion in human cancer cell lines.

To test if GYS1 was also important for cell survival, U87 and MCF-7 cells were transfected with a pool of 4 different siRNA sequences against GYS1 (siGYS1) or scr control, and cell viability was determined after 48 hours in normoxia or hypoxia. In addition to counting numbers of viable cells, the status of poly (ADP-ribose) polymerase (PARP), which is cleaved during the early steps of apoptosis, was observed by immunoblotting. PARP cleavage increased in MCF-7 cells exposed to hypoxia, suggesting that these cells undergo apoptosis when exposed to low oxygen concentrations. Contrasting results were obtained for the two cell lines following GYS1 depletion: U87 cells demonstrated no loss of viability after GYS1 knockdown, whilst MCF-7 cells exhibited reduced viability and increased PARP cleavage in normoxia, both of which were further exacerbated in hypoxia (Figure 4.10). Further studies will be required to explain these contrasting results. Amongst the possible interpretations is a different sensitivity of the two cell lines to siGYS1-dependent off-target effects. Moreover, a different basal level of glycogen between U87 and MCF-7 could also translate in distinct responses to GYS1 depletion.

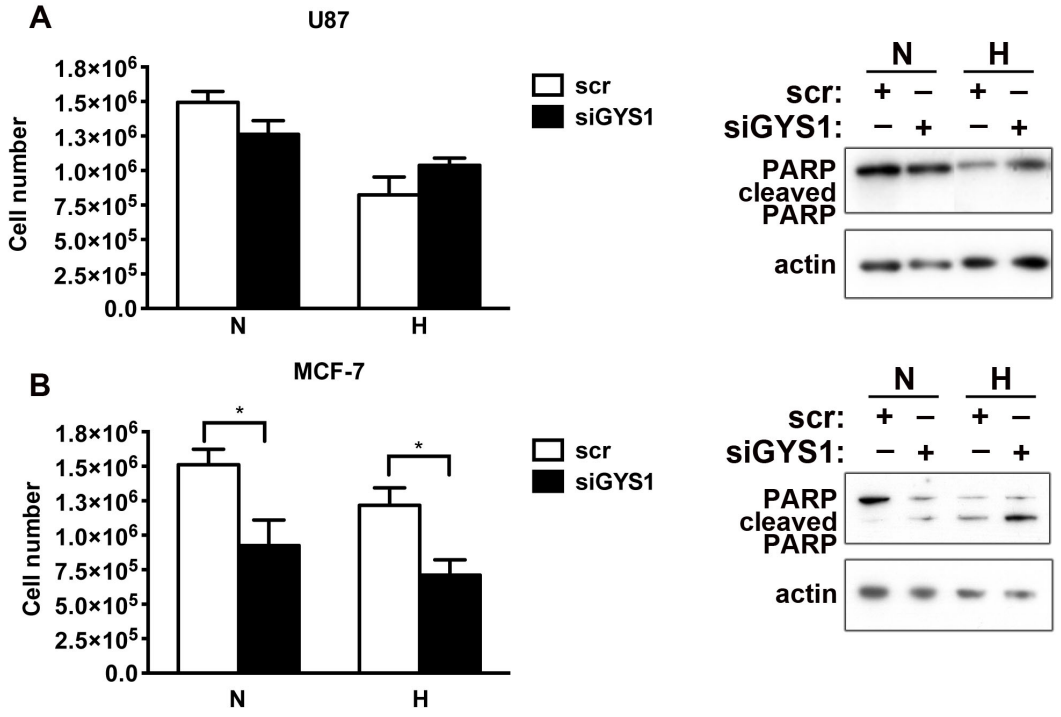


Figure 4.10 Effects of GYS1 knockdown on cell viability.
Cell viability was assessed in U87 (A) and MCF-7 (B) cells after 48 hours from transfection with siGYS1 or scr control. Cells were cultivated in normoxia (N) or hypoxia (H). Panels on the left show cell number quantification. Mean ± SEM of three independent experiments is shown (* $p<0.05$). Panels on the right show immunoblotting for cleaved PARP. Detection of actin was used as a loading control.

The effect of GYS1 depletion on survival was also analysed with a clonogenic assay. This assay was performed on cells seeded at a low density (1000 cells in a 6 cm dish), exposed to normoxia or hypoxia for 48 hours, and then grown in normoxia for 12 days. The number of colonies formed was counted after colouring with a solution containing methylene blue. This was only performed on MCF-7 cells, because U87 colonies were spread and difficult to count after colouring (data not shown). GYS1 depletion in MCF-7 cells was associated with a reduction of colony number formation, as compared to control cells, both in normoxia and hypoxia (Figure 4.11).

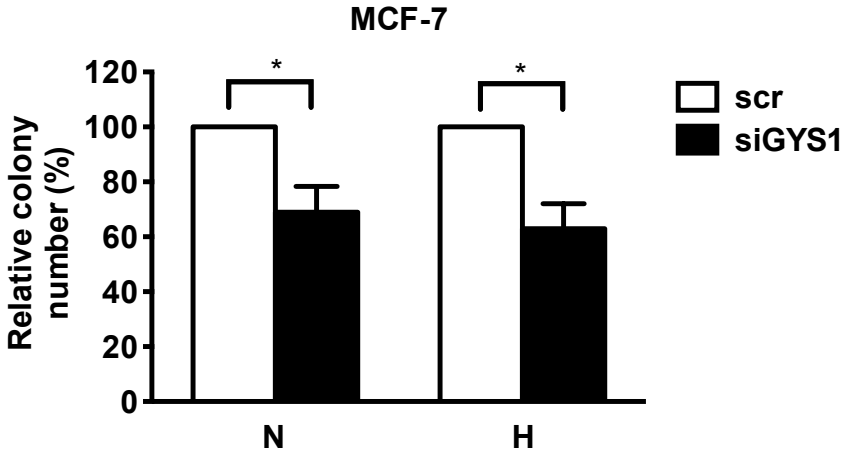


Figure 4.11 Effects of GYS1 knockdown on colony formation.
MCF-7 cells were transfected with siGYS1 or scr. 24 hours post-transfection, cells were reseeded at a density of 1000 cells per 6 cm dish and exposed to normoxia (N) or hypoxia (H) for 48 hours. Cells were then grown in normoxia for 12 days and fixed/stained with a methylene blue-containing solution. The number of colonies in each condition were counted and expressed as % of colonies relative to scr N (in normoxia) or H (in hypoxia). Mean ± SEM of three independent experiments is shown (* $p<0.05$).

Concordantly, GYS1 depletion reduced the growth of MCF-7-derived spheroids, which were approximately 50% smaller in volume, as compared to control spheroids. However, U87-derived spheroids did not show any significant reduction in growth following GYS1 depletion (Figure 4.12).

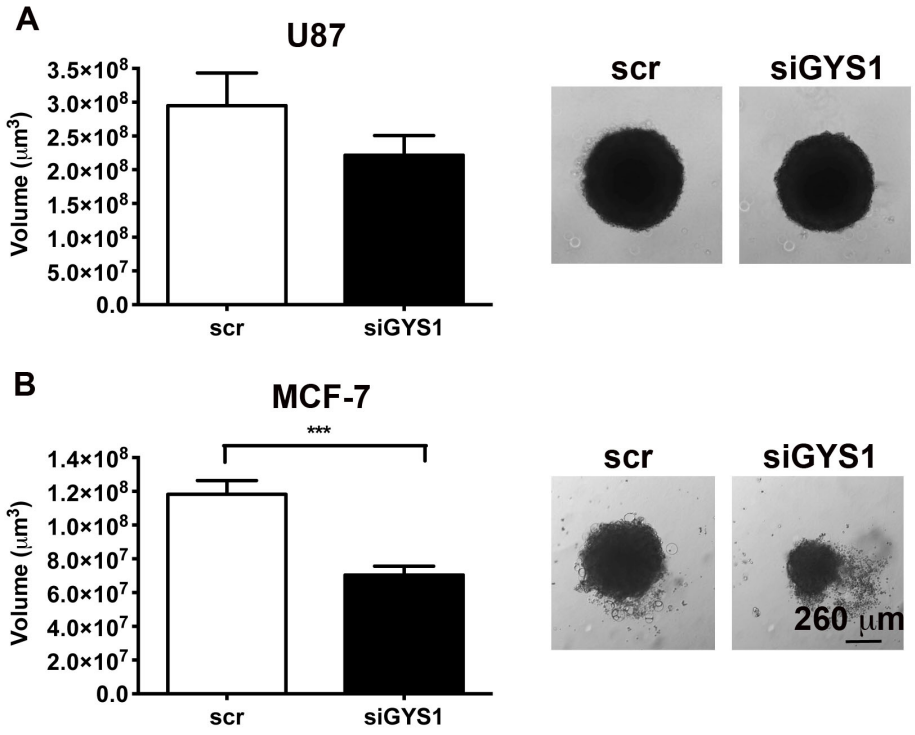


Figure 4.12 Consequences of GYS1 knockdown on spheroid growth.
Volumes of spheroids generated from GYS1 knockdown U87 (**A**) and MCF-7 (**B**) cells were measured after 7 days from plating. Panels on the left show mean ± SEM of three independent experiments (*** $p<0.001$), whereas panels on the right show representative images of spheroids collected at day 7.

4.2.7 Clinical significance of GYS1 and PYGL induction

To investigate the clinical relevance of GYS1 and PYGL induction, the Oncomine website (Oncomine.org) was queried for microarrays containing the genes *GYS1* and *PYGL*. When compared to normal tissue, both genes were found to be significantly upregulated in at least six tumour data sets (Figure 4.13).

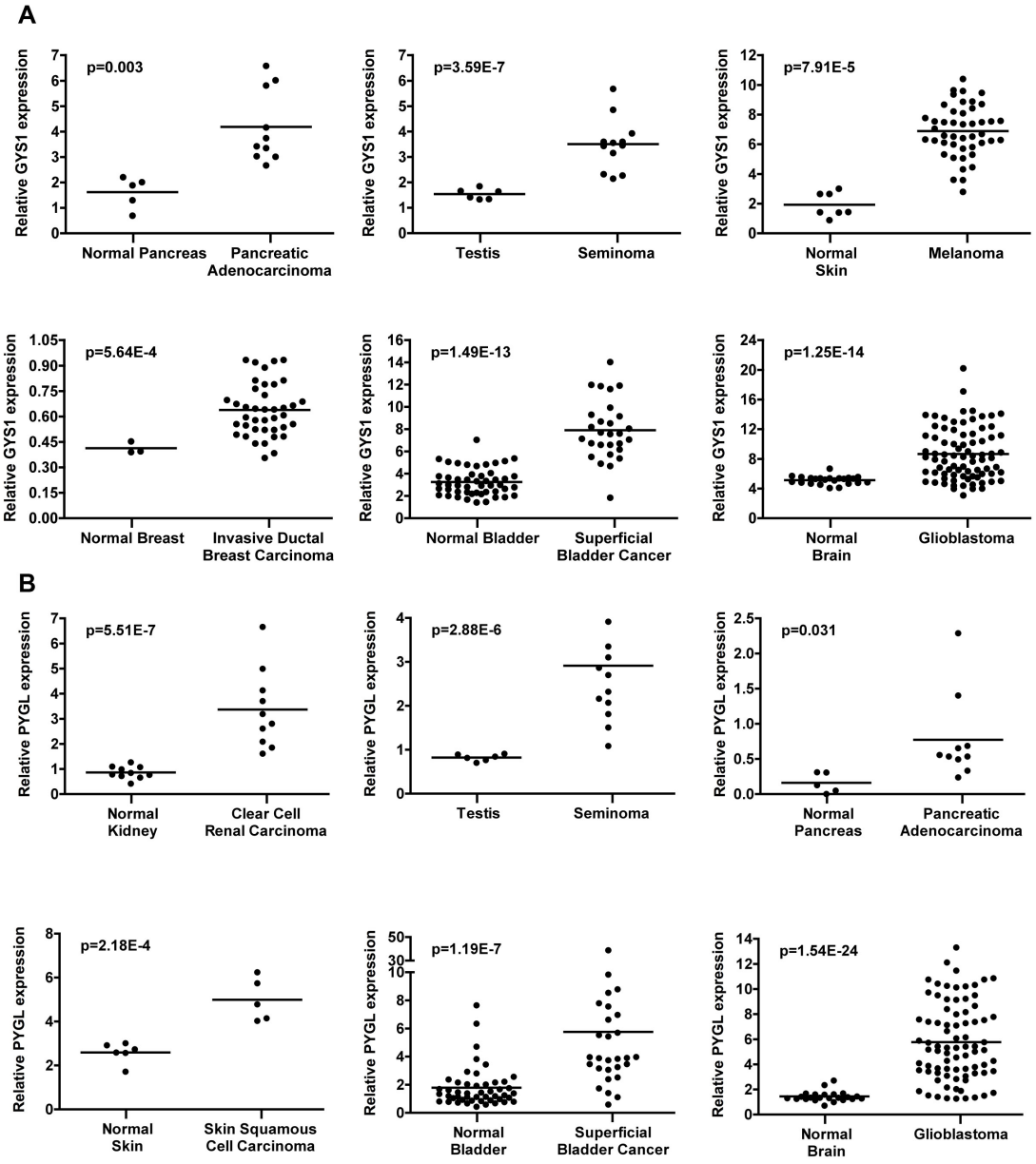


Figure 4.13 Expression of GYS1 and PYGL in tumours versus normal tissues. Oncomine website (Oncomine.org) was searched for gene expression studies containing the genes *GYS1* (**A**) and *PYGL* (**B**). Representative studies for 6 different tumour types are shown. Differential expression between normal and cancer tissues was set as a filter. Data for relative expression units, normalised to median z-score to enable comparison across multiple studies, were downloaded and graphed.

To determine the intracellular levels of GYS1 and PYGL at various stages of tumour development, a preliminary analysis was performed on a small tissue microarray (TMA) set with four different core biopsies from normal breast, ductal carcinoma *in*

situ, and invasive ductal breast carcinoma, respectively. Staining of sections revealed increased GYS1 and PYGL levels were associated with more advanced lesions, as compared to normal tissue, although significance was reached only for GYS1 in invasive carcinomas (Figures 4.14, 4.15, and 4.16). Collectively, these results suggest that increased glycogen turnover (as determined by increased GYS1 and PYGL expression) is associated with tumour progression.

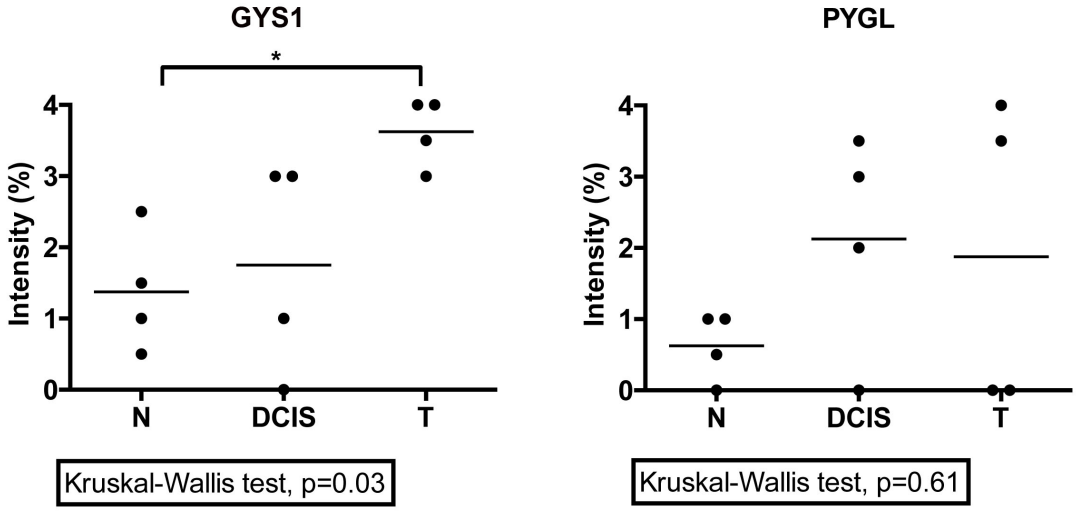


Figure 4.14 Expression of glycogen metabolising enzymes in TMA of breast origin.
Analysis of intensity of staining for GYS1 (left panel) and PYGL (right panel) in normal breast (N), ductal carcinoma *in sit*u (DCIS), and invasive breast carcinoma (T). 4 biopsies per group were analysed (* $p<0.05$).

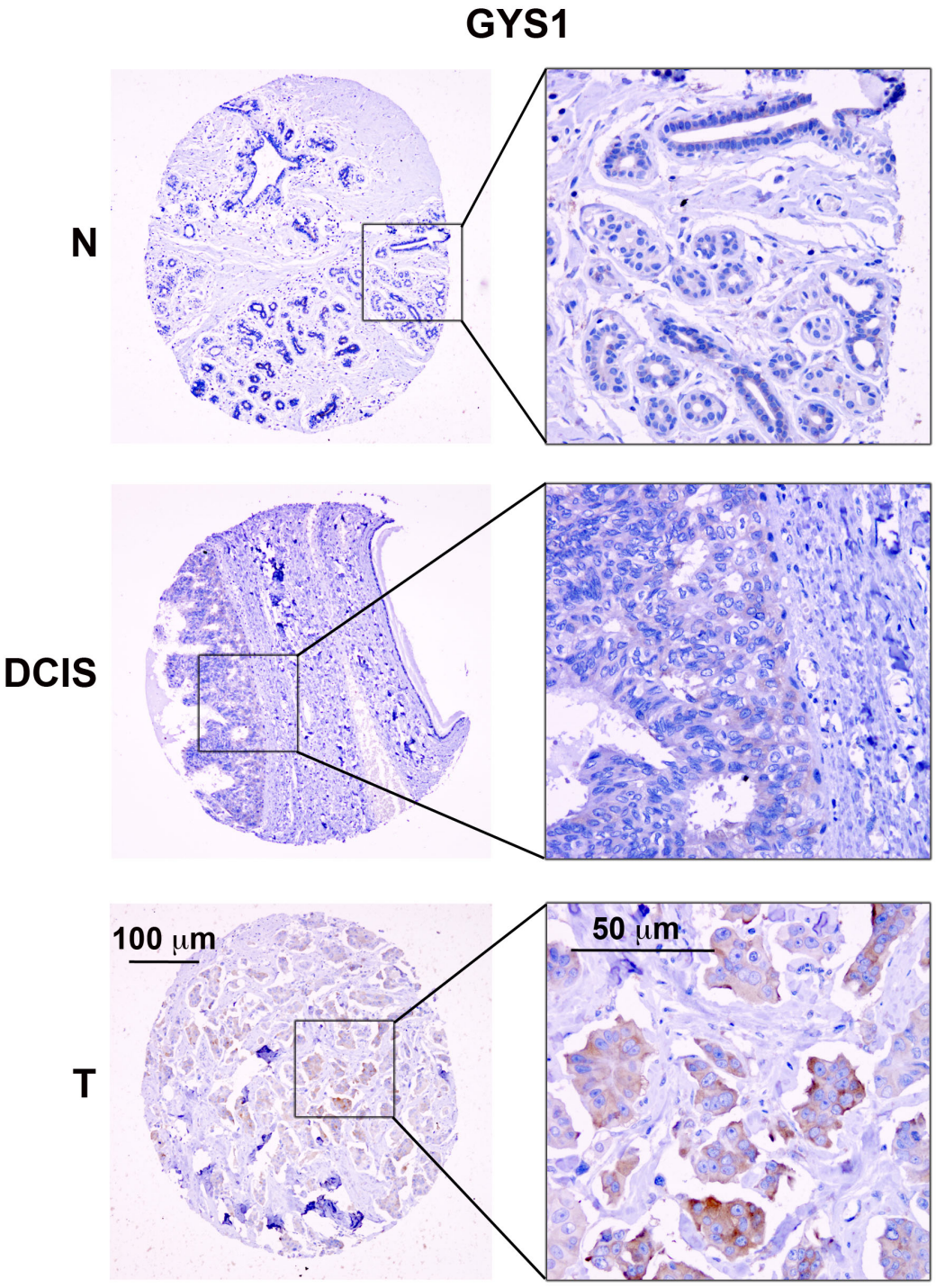


Figure 4.15 Staining of breast TMA for GYS1.
Representative pictures at 2 different magnifications of core biopsies stained for GYS1 from normal (N) breast tissue (top panels), ductal carcinoma *in situ* (DCIS) (middle panels), and invasive breast carcinoma (T) (bottom panels).

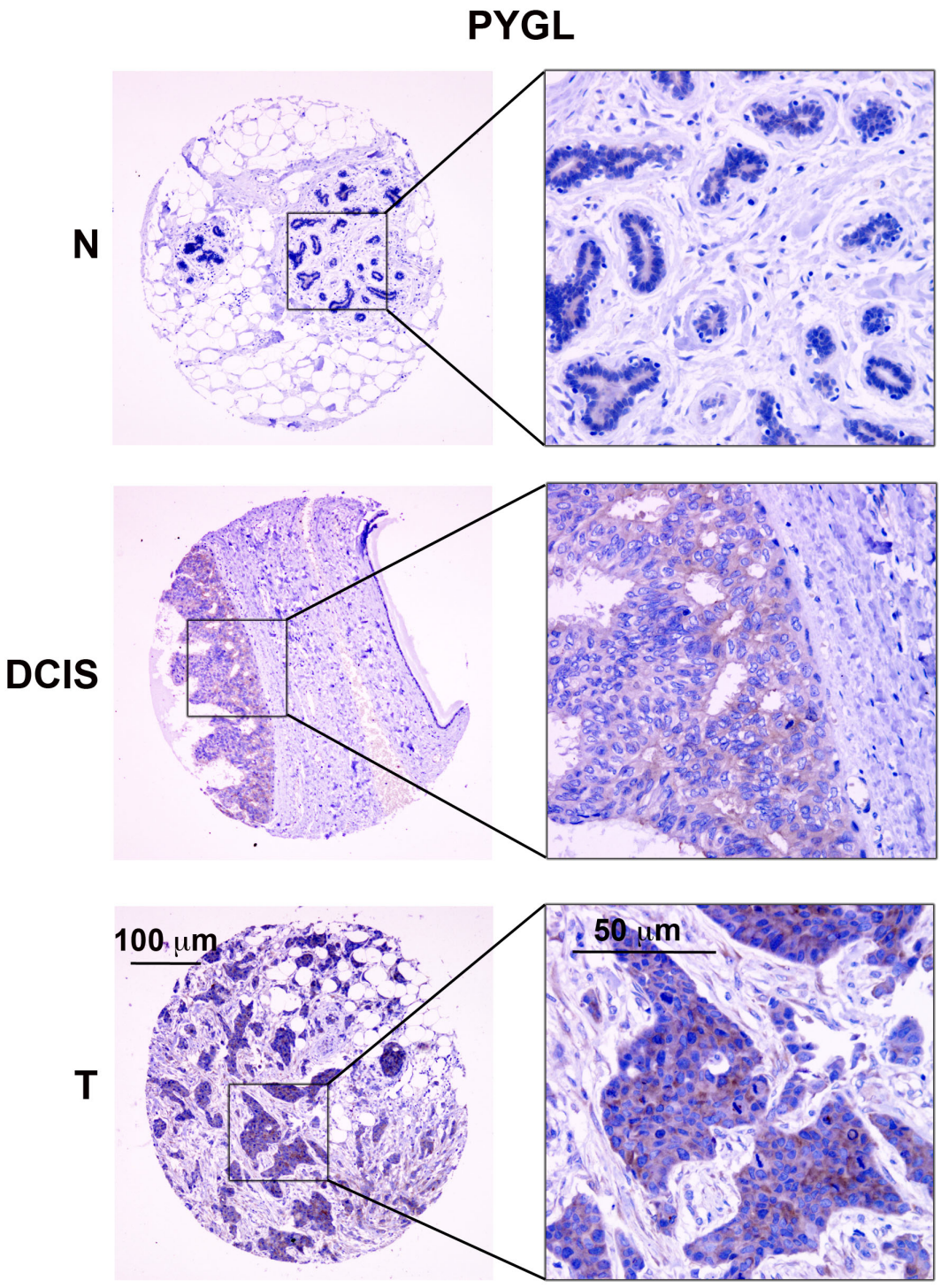


Figure 4.16 Staining of breast TMA for PYGL.
Representative pictures at 2 different magnifications of core biopsies stained for PYGL from normal (N) breast tissue (top panels), ductal carcinoma *in situ* (DCIS) (middle panels), and invasive breast carcinoma (T) (bottom panels).

4.3 DISCUSSION

Glycogen metabolism has recently been proposed as an important pathway of metabolic reprogramming in cancer cells (Brahimi-Horn et al., 2010; Pelletier et al., 2012; Pescador et al., 2010; Shen et al., 2010). Consistent with altered glycogen turnover being a feature of hypoxia, a number enzymes and regulatory proteins implicated in glycogen metabolism were observed to be upregulated following bevacizumab treatment *in vivo*. Among these, the key glycogen synthetic enzyme, GYS1, and glycogen catabolic enzyme, PYGL, were also upregulated. Previous reports have demonstrated the presence of HIF-binding sites in GYS1, PPP1R3C, and GBE1 (Mole et al., 2009; Pescador et al., 2010; Shen et al., 2010). Here, hypoxic induction of GYS1 was confirmed to be HIF1-dependent, whereas PYGL induction was not. A previous report on genome-wide analysis of HIF-DNA binding in MCF-7 cells did not reveal any PYGL promoter binding (Mole et al., 2009). Further studies will be required to understand the precise mechanism of PYGL induction in hypoxia. Some of the candidates that will be further investigated as potential PYGL regulators include the carbohydrate responsive element binding protein [ChREBP] and the nuclear factor κB (NF-kB). ChREBP has been shown to regulate numerous glycolytic and lipogenic genes by binding to a carbohydrate-responsive element in their promoter region. Although its role has been mainly characterised in hepatocytes and adipocytes, recent studies indicate its function also in cancer cells (Tong et al., 2009). NF-kB is a family of transcription factors involved in the regulation of different aspects of tumour biology, including cancer cell metabolism (Johnson and

Perkins, 2012). Moreover, its expression can be induced by a variety of cell stresses, including hypoxia (Perkins, 2007).

Characteristic signatures of GYS1 and PYGL induction, as well as glycogen accumulation, were observed in response to hypoxia in cancer cell lines cultivated *in vitro*. More specifically, GYS1 expression increased rapidly and then declined by 72 hours, whereas PYGL increased gradually and reached maximal level at 72 hours in hypoxia. Concomitantly, glycogen levels increased rapidly, peaked by 24 hours, and then started to decline by 72 hours. These data were consistent with an acute induction of glycogen synthesis catalysed by GYS1, followed by a subsequent PYGL-induced glycogen breakdown. These results provide a more comprehensive analysis of glycogen metabolism profile in hypoxia, as compared to previous studies where only the acute glycogen synthetic response was described (Pescador et al., 2010; Shen et al., 2010). Another study described a progressive increase of glycogen levels up to 96 hours at 1% O_2 in Chinese hamster lung fibroblasts CCL39 and in the human colon carcinoma cell line LS174 (Pelletier et al., 2012). A possible explanation of the difference in glycogen accumulation could be represented by the milder hypoxic conditions used, as compared to the ones used in this chapter (1% O_2 versus 0.1% O_2) and the different cell types analysed.

Analysis of the activity of GYS1 in hypoxia, as measured by analysis of phosphorylation status, suggested that GYS1 was most abundant/active at 24 hours in hypoxia. At the later time points, GYS1 levels declined, and this was also associated with a higher proportion of inactive (i.e. phosphorylated) enzyme. PYGL activity is also regulated by phosphorylation (Berg et al., 2002). However, the phosphorylation status of PYGL could not be evaluated in this study due to

unavailability of a commercial antibody. The anti-phospho-PYGL antibody described in Grempler et al. (Grempler et al., 2007) was tested, but this yielded poor quality Western blots (data not shown). However, the presence of active PYGL enzyme in hypoxia can be inferred from the observations that a) glycogen degradation onset correlates with PYGL maximal levels (48 and 72 hours), and b) glycogen degradation in hypoxia is significantly impaired when PYGL is depleted (as shown in chapter 5).

Consistent with the characteristic trend of glycogen accumulation observed in hypoxia, the synthetic enzyme GBE, and two phosphatases, PPP1R3B and PPP1R3C, were rapidly induced in hypoxia, similarly to GYS1, whereas the catabolic enzyme GAA was only induced at the later time points, similarly to PYGL. It will be of interest in future studies to examine the roles and contributions of these other glycogen metabolising enzymes to the adaptation of cancer cells to hypoxia. The early induction of glycogen synthesis in hypoxia is orchestrated by the increased expression of glycogen synthetic enzymes and regulatory proteins, all of which have been validated as HIF-targets or present a HIF-binding site in their promoter region (Mole et al., 2009; Ortiz-Barahona et al., 2010; Pelletier et al., 2012; Pescador et al., 2010; Shen et al., 2010). This suggests that a common, not yet identified, factor could also be responsible for the late induction of the two catalytic enzymes, PYGL and GAA.

Importantly, a similar pattern of GYS1 and PYGL induction, and glycogen accumulation occurred even in the presence of low extracellular glucose (5 mM), suggesting that this phenomenon is not an artefact caused by high glucose concentrations typically used in cell culture growth conditions (25 mM). The

physiological relevance of these findings was also supported by the *in vivo* observation that glycogen accumulation was induced by treatment of xenografts with bevacizumab.

Impairment of glycogen synthesis revealed contrasting results in U87 and MCF-7 cells. GYS1 depletion was detrimental to MCF-7 cells, suggesting that in this cell line, glycogen synthesis is required for survival. The fact that survival was also affected in normoxia would indicate the presence of a basal but indispensable level of glycogen metabolism in these conditions. Another study also demonstrated the requirement for glycogen synthesis through GYS1 for cell survival in the hepatoma cell line HepaC1 (Pescador et al., 2010). However, in this study, the survival advantage was assessed after hypoxic preconditioning (in order to allow for glycogen accumulation) and subsequent exposure to anoxia and glucose deprivation. Conversely, survival of U87 cells was apparently unaffected by GYS1 depletion. Different cell lines can therefore respond differently to glycogen synthesis inhibition, and it will be important to determine the factors that confer sensitivity to GYS1-depletion. For example, determination of basal levels of glycogen and the ability to accumulate it in hypoxia, which are considerably higher in U87 as compared to MCF-7 cells (basal level of glycogen is 52 ng/μg in U87 and 31 ng/μg in MCF-7 cells; glycogen fold induction after 24 hours in hypoxia is 11.5 and 3.5, in U87 and MCF-7 cells, respectively [Figure 4.4A]), and correlation with sensitivity to GYS1 depletion will be assessed in future studies. However, it cannot be excluded that the efficiency of GYS1 knockdown differs between the two cell lines analysed, and that the residual enzymatic activity enables the survival of one cell line, whilst is detrimentally low in the other cell line. Finally, it remains to be elucidated whether

MCF-7 cells present increased sensitivity to potential siGYS1-associated off-target effects, as compared to U87 cells.

The potential clinical significance of GYS1 and PYGL upregulation in cancer is supported by the results from both the analysis of Oncomine data and immunostaining of a TMA of tumours at different stages of development. These analyses will require further validation. More specifically, a more extensive analysis of all the studies available within tumour types in the Oncomine website should be performed. Moreover, analysis of TMA including higher number of cases and correlation with clinical parameters should be performed to confirm the putative correlation between GYS1 and PYGL levels and advanced tumour progression.

5 CHAPTER FIVE

PYGL sustains cancer cell proliferation

5.1 INTRODUCTION

In the previous chapter, the hypoxic regulation of glycogen turnover and glycogen-metabolising enzymes was characterised in xenografts, and in cancer cell lines. In this chapter, the role of PYGL and glycogen degradation in hypoxia was further investigated. The decision to primarily focus on PYGL was based on a number of observations. Firstly, PYGL is a key enzyme that is required for glycogen utilisation, and has a hitherto uncharacterised/undetermined function in cancer cells. Moreover, *PYGL* is one of the 99 genes included in the hypoxia 'metagene' that comprises a hypoxic signature with prognostic significance in HNSCC and breast cancer (Winter et al., 2007).

To characterize the function(s) of PYGL in hypoxia, stable or transient knockdown of PYGL was performed in cancer cell lines, and the phenotypic consequences characterised *in vitro*. The requirement for PYGL in promoting, and/or sustaining, tumour growth was also examined *in vivo* in U87-derived xenografts. The findings reported here suggest an important role for glycogen metabolism in the context of metabolic reprogramming of cancer cells.

5.2 RESULTS

5.2.1 PYGL depletion induces glycogen accumulation in hypoxia

To investigate the consequences of PYGL depletion, transient or stable PYGL knockdown cells were generated with RNA interference (RNAi). More specifically, transient knockdown of PYGL was performed using a pool of four different siRNA sequences (collectively labelled as 'siPYGL pool'), whereas stable knockdown of PYGL was performed using lentiviral particles encoding a short hairpin RNA sequence (labelled as 'shPYGL'). All RNAi sequences used in this study targeted a different site in the PYGL transcript (Chapter 2). To transiently deplete PYGL, U87 cells were transfected with 'siPYGL pool' and then transferred to hypoxia after 24 hours. PYGL protein levels were then determined by Western blotting for up to 7 days post-transfection. Whereas control cells exhibited a pronounced increase in PYGL levels in hypoxia (as described in Chapter 4, Figure 4.3), siPYGL cells revealed low levels of PYGL throughout the time-course analysed (Figure 5.1A). Similar findings were also observed in stably transduced shPYGL U87 cells (Figure 5.1B). PYGL knockdown was also verified in cell pellets by immunostaining (Figure 5.1C).

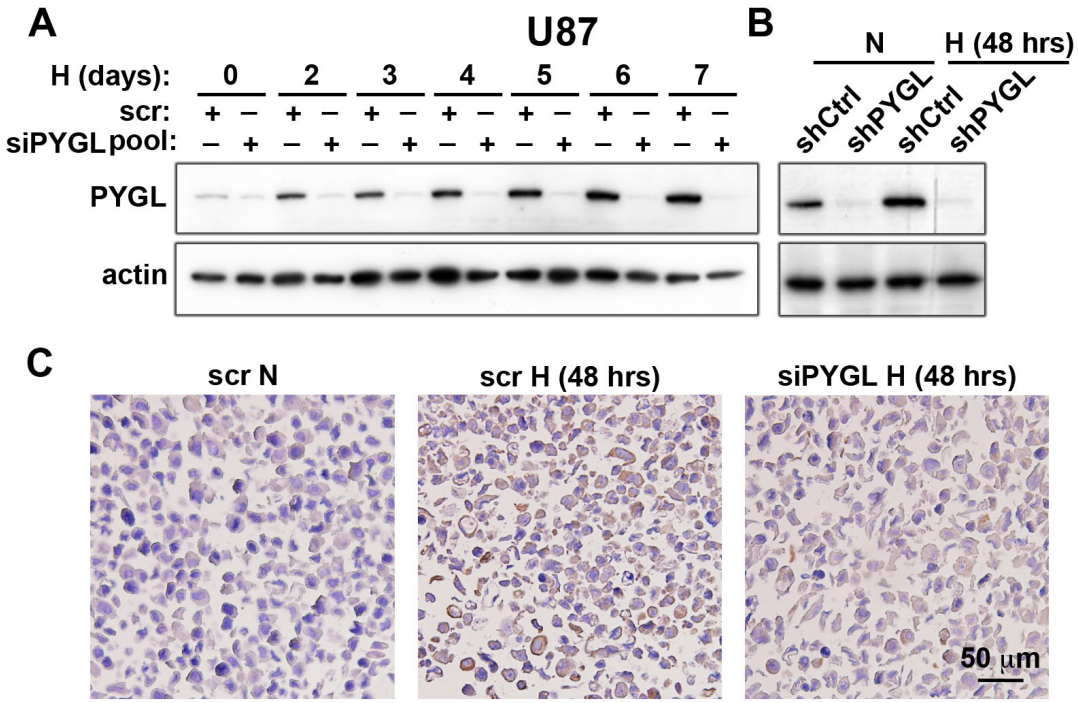


Figure 5.1 Efficiency of PYGL knockdown by RNAi.
A, U87 cells were transfected with 'siPYGL pool' and transferred to hypoxia 24 hours post-transfection. Protein extracts were analysed by Western blotting at the indicated time points. Actin levels are shown as a loading control. **B,** stably transduced shPYGL and shCtrl U87 cells were exposed to normoxia (N) or hypoxia (H) for 48 hours. Protein extracts were analysed as in A. **C,** immunostaining of U87 cell pellets showed attenuated PYGL expression in PYGL knockdown compared to scr control pellets in hypoxia. U87 cells were transfected with siPYGL pool or scr control and exposed to normoxia (N) or hypoxia (H) for 48 hours after transfection. Cells were formalin-fixed, harvested and cell pellets were paraffin-embedded. Sections were then stained for PYGL.

Next, the intracellular glycogen levels were measured in PYGL-depleted cells. As expected, depletion of PYGL was associated with elevated glycogen accumulation in hypoxia. Quantification of glycogen revealed increased glycogen levels after 24, 48, and 72 hours in hypoxia in siPYGL pool cells, and after 48 and 72 hours in shPYGL cells, as compared to control cells (Figure 5.2A and 5.2B). Accumulation of glycogen was also confirmed at 48 hours in U87 shPYGL cells using three other techniques (Figure 5.2C). Firstly, the incorporation of the fluorescent D-glucose

derivative, 2-NBDG, into glycogen was measured. This fluorescent probe enters cells via the same GLUT transporters used by D-glucose, is converted to another fluorescent metabolite by HKII, and is then incorporated into the non-reducing ends of glycogen molecules (Louzao et al., 2008). Imaging of the cells with fluorescence microscopy revealed the accumulation of fluorescence granules in the cytosol of U87 shPYGL cells, especially in hypoxia (Figure 5.2C). The second technique used was PAS staining for glycogen, which revealed increased staining intensity in hypoxic cells, as compared to normoxic cells, and a further increase after PYGL depletion (Figure 5.2C). The third one consisted in direct imaging of glycogen granules by TEM (performed by Prof David Ferguson at the Nuffield Department of Clinical Medicine, Oxford) (Figure 5.2C). This technique revealed the accumulation in hypoxia, and in particular in PYGL knockdown cells, of irregular-shaped cytoplasmic structures with electron-dense deposits both within and at the periphery. These structures correspond to areas of loosely packed glycogen particles that are condensed to the periphery during processing (courtesy of Prof David Ferguson) (Figure 5.2C). Taken together, these findings demonstrate a hyper-accumulation of glycogen in PYGL-depleted cells in hypoxia.

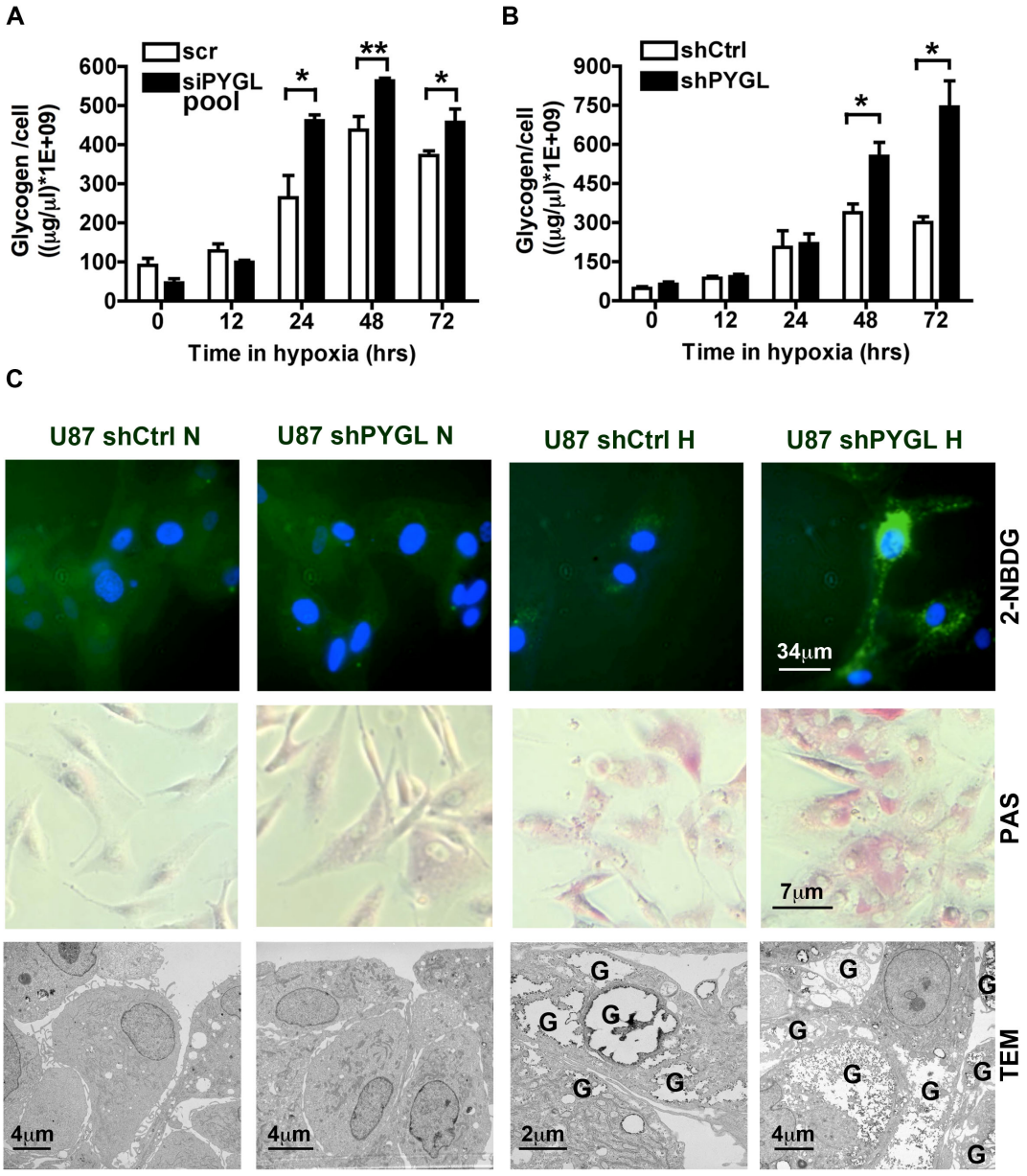


Figure 5.2 PYGL depletion results in increased glycogen accumulation.
U87 scr/siPYGL pool and shCtrl/shPYGL were exposed to hypoxia in a time course experiment. Knockdown of PYGL revealed increased accumulation of glycogen, as compared to control cells after 24, 48 and 72 hours in the transiently transfected cells (**A**), and after 48 and 72 hours in the stably transduced cells (**B**). The values are expressed as glycogen content normalized to cell numbers. Mean ± SEM of three independent experiments is shown (* $p<0.05$, ** $p<0.01$). **C**, glycogen accumulation in U87 shPYGL and control cells after 48 hours in hypoxia was detected with the green fluorescent D-glucose analogue 2-NBDG (top panels), by PAS staining (middle panels) and by TEM (bottom panels). G=glycogen.

Two possible scenarios exist to explain the hyper-accumulation of glycogen in PYGL-depleted cells in hypoxia. Furthermore, these are not mutually exclusive. In the first scenario, a failure to breakdown glycogen by PYGL results in its abnormally high accumulation. A second possible scenario is that PYGL depletion leads to increased synthesis of glycogen due to deregulation of GYS1. To test this possibility, GYS1 levels were analysed at 48 and 72 hours in hypoxic shPYGL cells. As described in Chapter 4 (Figure 4.3), GYS1 levels initially increase in hypoxia, and then decline at later time points. However, this characteristic pattern of GYS1 induction, followed by a decline in GYS1 levels, was indistinguishable in control versus shPYGL cells, suggesting that PYGL depletion does not noticeably affect GYS1 levels (Figure 5.3). However, it should be noted that any changes in the phosphorylation level/activity of GYS1 have not yet been examined, but will be determined in future analyses. These determinations will be of great importance, since the phosphorylated form of PYGL represents a potent allosteric inhibitor of PP1, which can dephosphorylate/activate glycogen synthase (Agius, 2010).

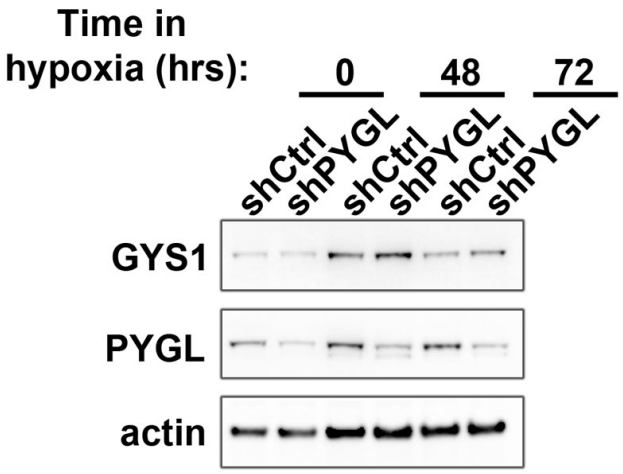


Figure 5.3 GYS1 levels are unaffected by PYGL depletion.

GYS1, PYGL and actin levels were measured in U87 shCtrl and shPYGL cells by Western blotting, at the indicated times. Actin levels were used as loading control.

5.2.2 PYGL sustains cancer cell proliferation

Next, the phenotypic consequences of PYGL depletion were determined. Interestingly, depletion of PYGL in hypoxia was associated with a reduction in cell numbers both in U87 shPYGL (at 48 and 72 hours in hypoxia) and siPYGL pool cells (at 24, 48, and 72 hours in hypoxia), as compared to control cells (Figure 5.4).

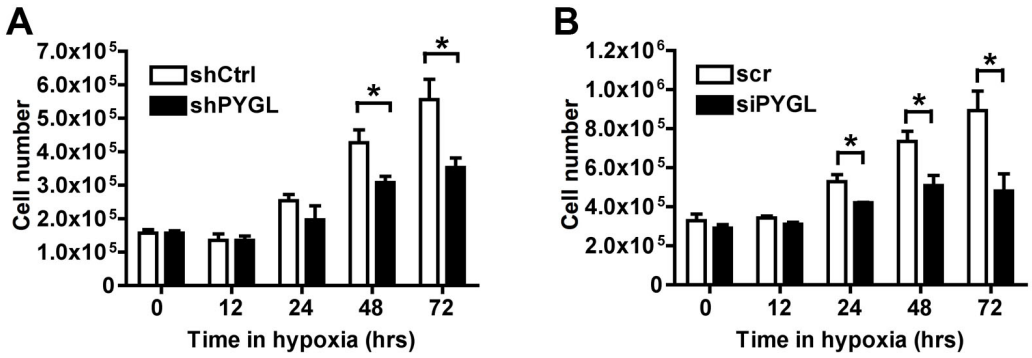


Figure 5.4 PYGL sustains proliferation in cancer cells.
PYGL depletion in U87 cells resulted in decreased proliferation both after stable knockdown (**A**), and transient transfection (**B**). Cells were exposed to hypoxia in a time course experiment. Transiently transfected cells were exposed to hypoxia 24 hours post- transfection. Mean ± SEM of three independent experiments is shown (* $p<0.05$).

The consequences of PYGL depletion were not restricted to cancer cells grown in hypoxia. Indeed, glycogen accumulation (35% increase) and inhibition of proliferation (25% decrease) were also observed in U87 PYGL knockdown cells in normoxia (Figure 5.5). However, these phenotypes were more pronounced in hypoxia, suggesting a more critical role for PYGL in hypoxia (Figure 5.5).

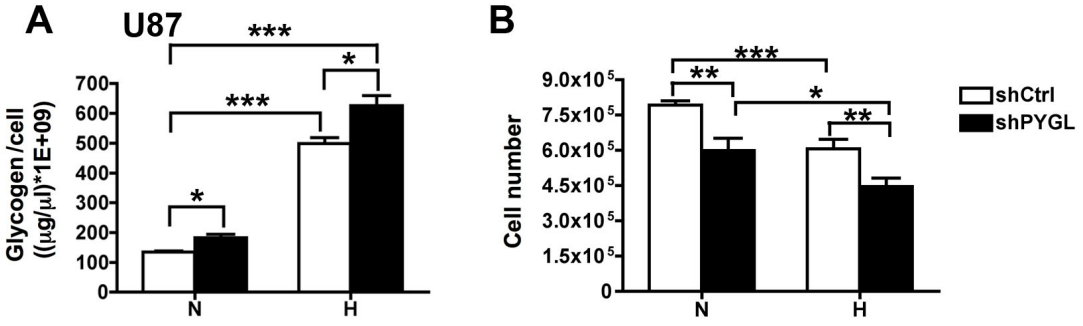


Figure 5.5 Consequences of PYGL knockdown in normoxic and hypoxic cells.
PYGL depletion induces glycogen accumulation (**A**) and reduced proliferation (**B**) in U87 cells. Cells were grown in normoxic or hypoxic conditions for 48 hours before analysis. Mean ± SEM of three independent experiments is shown (* $p<0.05$, ** $p<0.01$, *** $p<0.001$).

As discussed in Chapter 4, cell culture medium contains high amounts of glucose (25 mM). The effects of PYGL depletion were therefore compared in medium containing physiological glucose concentrations (5 mM). Glycogen accumulation and inhibition of cell growth were reproducibly observed in PYGL-depleted cells cultivated in the presence of 5 mM glucose, confirming the physiological relevance of these findings (Figure 5.6).

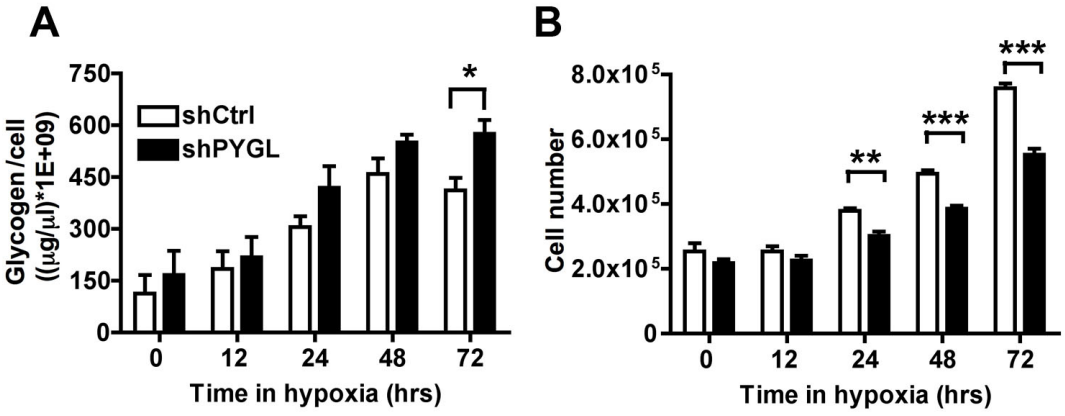


Figure 5.6 PYGL knockdown induces glycogen accumulation and cell growth inhibition at physiological glucose concentrations.
U87 cells expressing shCtrl or shPYGL were grown in the presence of 5mM glucose in a time course experiment in hypoxia. Glycogen content (**A**) and cell numbers (**B**)

were measured at the indicated times. Mean ± SEM of three independent experiments is shown (* $p<0.05$, ** $p<0.01$, *** $p<0.001$).

To further understand the mechanisms underlying this growth defect, the effect of PYGL knockdown on cell viability and cell cycle profile were investigated.

Analysis of Annexin V-positive cells and PARP cleavage, as indicators of apoptosis, revealed only a slight increase in apoptosis following PYGL depletion in U87, MCF-7, and HCT116 cell lines (Figure 5.7). This suggests that the decrease in cell numbers following PYGL depletion is not simply due to induction of apoptosis.

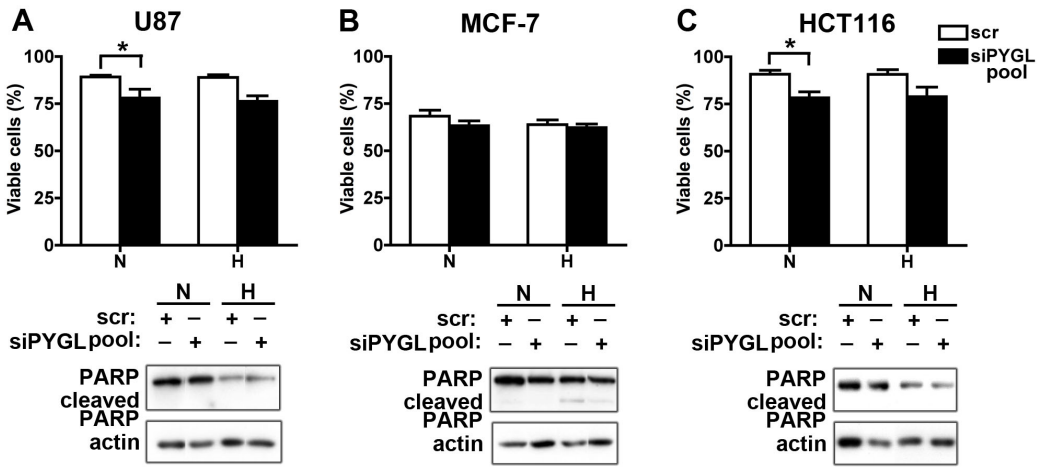


Figure 5.7 PYGL depletion does not induce apoptosis.
PYGL knockdown by siRNA was performed in U87 (**A**), MCF-7 (**B**), and HCT116 cells (**C**). The proportion of viable cells was measured by FACS analysis of Annexin V/Propidium Iodide positive cells (top panels), or by immunoblotting for PARP/cleaved PARP (bottom panels). Cells were exposed to normoxia (N) or hypoxia (H) for 48 hours. Mean ± SEM of three independent experiments is shown (* $p<0.05$).

Next, the cell cycle profile of PYGL-depleted cells was analysed. This revealed a higher proportion of cells in G1 phase, with a concomitant decrease of cells in both S and G2/M phases, as compared to control cells (Figure 5.8A). Because of the major

regulatory role of the p53-p21 axis in the G1 to S phase transition of the cell cycle (el-Deiry et al., 1993; Harper et al., 1993), the levels of p53 and p21 were examined in PYGL knockdown cells. All of the cell lines used in this study express functional p53 (Ahn et al., 2010; Liu and Bodmer, 2006). Interestingly, both p53 and its downstream target, p21, exhibited a marked increase in their levels in hypoxic PYGL-depleted U87 cells, as compared to control cells (Figure 5.8B). To investigate if increased p53 levels contributed to the inhibition of cell proliferation in these cells, a simultaneous knockdown of p53 and PYGL was performed. This resulted in efficient depletion of both targets, and a concomitant reduction in p21 levels (Figure 5.8B). Moreover, knockdown of p53 prevented the decreased growth rate phenotype normally associated with PYGL depletion in hypoxia (Figure 5.8C). This suggests that depletion of PYGL leads to a p53-dependent G1-arrest phenotype in hypoxia.

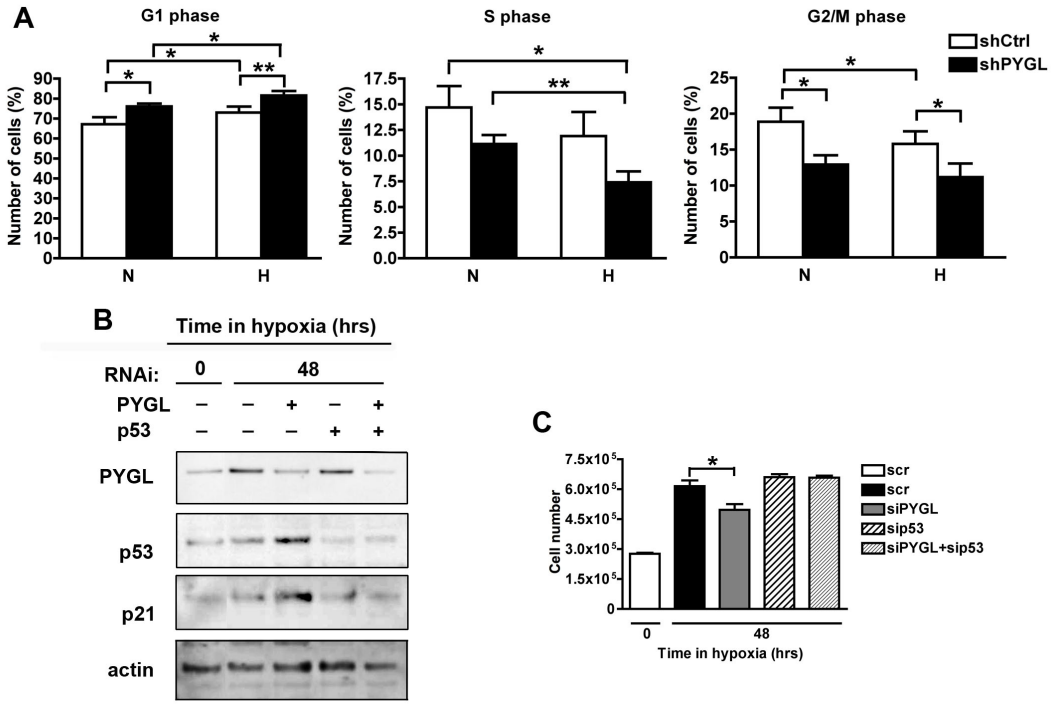


Figure 5.8 PYGL knockdown induces a p53-dependent cell cycle arrest in hypoxia.
A, U87 cells expressing shCtrl or shPYGL were grown in normoxia (N) or hypoxia (H) for 48 hours, and their cell cycle distribution analysed by FACS. Mean ± SEM of three independent experiments is shown (* $p<0.05$, ** $p<0.01$). **B & C**, U87 cells were co-transfected with two different siRNA sequences to deplete PYGL and p53, either alone, or in combination. Protein extracts were harvested and analysed at the indicated times by Western blotting. The levels of PYGL, p53, p21 and actin are shown (**B**). Cell numbers were also measured (**C**). Mean ± SEM of three independent experiments is shown (* $p<0.05$).

5.2.2 PYGL knockdown induces premature senescence

PYGL depletion in U87 and MCF-7 cells was associated with characteristic morphological changes (i.e. enlargement and flattening) that were indicative of increased cellular senescence (Figures 5.9A and 5.9B). To further test this possibility, in addition to a G1-cell cycle arrest, and increased levels of p53 and p21 (Figure 5.8), other markers of senescence were examined in PYGL-depleted cells (Collado et al., 2005; Schmitt, 2007). SA β-gal is a commonly used marker of cell

senescence, which measures the senescence-associated increased activity of the acid lysosomal β-galactosidase at a normally suboptimal pH 6 (Kurz et al., 2000; Schmitt, 2007). U87 and MCF-7 cells exhibited increased SA β-gal activity, when PYGL was depleted (Figures 5.9C-E). Furthermore, this phenotype was further increased in hypoxia (Figures 5.9C-E).

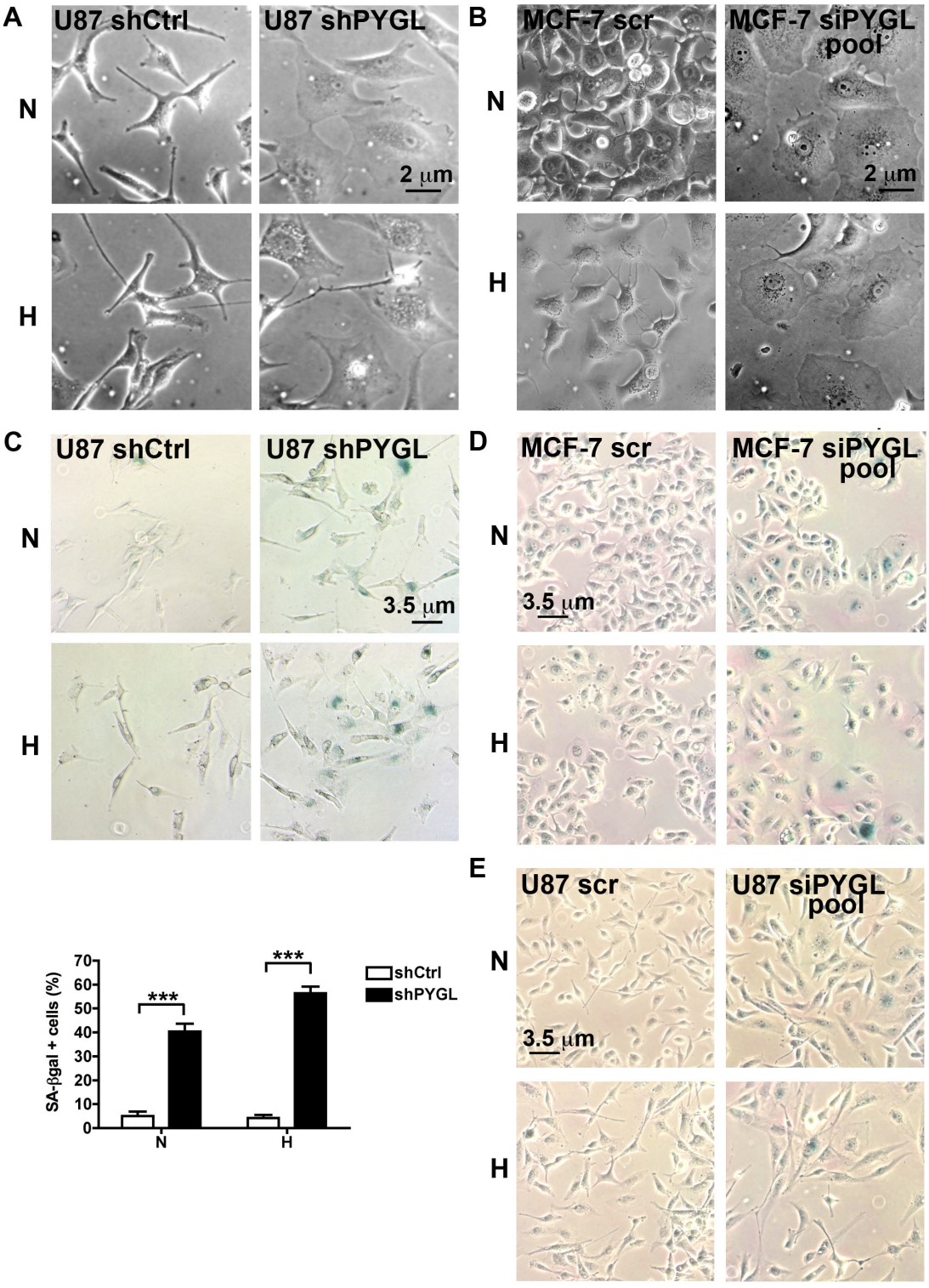


Figure 5.9 PYGL knockdown is associated with increased cell senescence. Representative images of control versus PYGL-depleted U87 (**A**) and MCF-7 (**B**) cells cultivated in normoxia (N) or hypoxia (H) for 48 hours. **C**, SA-βgal staining of U87 shCtrl and shPYGL cells treated as in (**A**). Senescent cells appear blue following X-gal staining. Senescence was quantified and expressed as the percentage

of SA-βgal positive cells in the total population (lower panel). SA-βgal staining of transiently transfected MCF-7 **(D)** and U87 (**E**) cells, treated as in **A**.

Increased SA-βgal activity correlates with an increase in lysosomal content (Collado et al., 2005; Kurz et al., 2000), and this represents another marker for cell senescence. Staining of cells with LysoTracker red, a dye that is selectively incorporated into lysosomes, revealed an increase in fluorescent vacuoles in U87 shPYGL cells, especially in hypoxia (Figure 5.10A). Lysosomes represent another site for glycogen degradation through the enzyme GAA. Since PYGL depletion was associated with glycogen accumulation and the induction of senescence, the expression of GAA was investigated. In agreement with the results found in Chapter 4 (Figure 4.6), GAA expression increased in U87 cells exposed to hypoxia for 48 hours, as compared to normoxia (Figure 5.10B). Moreover, GAA levels increased in PYGL-depleted cells, and this increase was most apparent in hypoxic PYGL-depleted cells (Figure 5.10B).

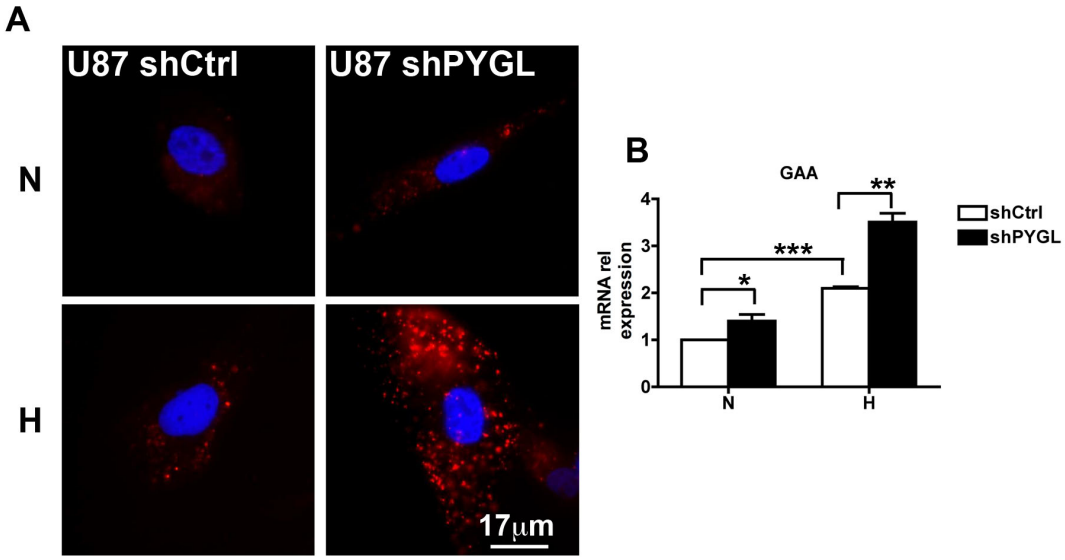


Figure 5.10 PYGL knockdown cells have increased lysosome content.
A, U87 cells expressing shCtrl or shPYGL were analysed for lysosome content using LysoTracker Red staining. Nuclei were stained with DAPI. Cells were either incubated in normoxia (N) or hypoxia (H) for 48 hours. **B**, under the same conditions, mRNA levels of lysosomal GAA were measured. Mean ± SEM of three independent experiments is shown (* $p<0.05$, ** $p<0.01$, *** $p<0.001$).

Finally, DEC1 level was also analysed because of its recognised role as a marker of senescence (Collado et al., 2005; Xu et al., 2012). Moreover, immunostaining for DEC1 was previously optimised in cells and tissues by Dr Helen Turley, using a in-house developed antibody (Turley et al., 2004). Consistent with the above observations, the levels of DEC1 were found to be increased in PYGL-depleted cells, as measured by immunostaining (Figure 5.11). Collectively, these findings indicate that PYGL depletion results in elevated glycogen accumulation in hypoxia, and reduced proliferation due to p53-induced premature senescence.

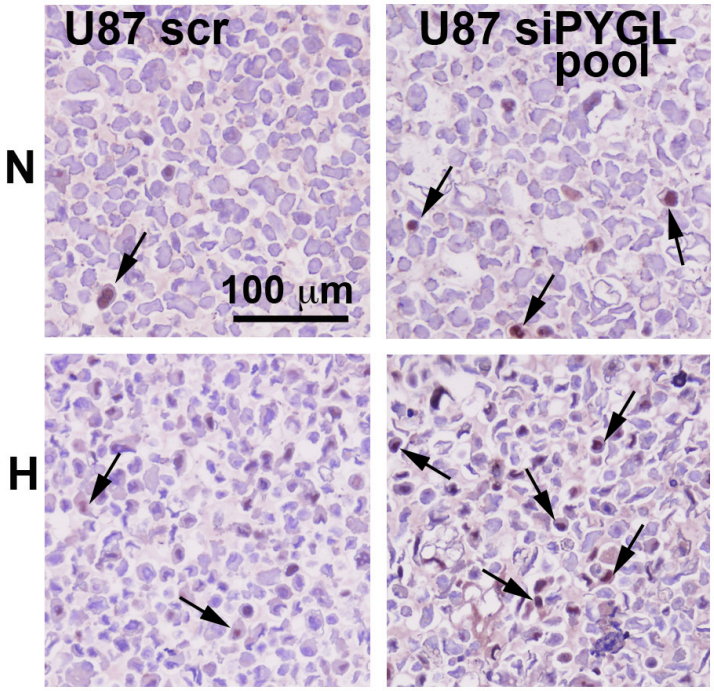


Figure 5.11 PYGL depletion is associated with increased DEC1 levels.
Immunihistochemical analysis of DEC1 in sections of U87 cells cultivated in normoxia (N) or hypoxia (H) for 48 hours after transfection. Arrows show representative DEC1-positive cells.

5.2.3 ROS contribute to cell growth arrest in PYGL-depleted cells

Further analyses were performed in order to understand the cause of premature senescence in PYGL knockdown cells. Because mitochondrial ROS are recognized contributors to premature senescence, and their effects are often mediated through activation of p53 (Kuilman et al., 2010; Lu and Finkel, 2008; Moiseeva et al., 2009), the level of mitochondrial superoxide was measured in PYGL-depleted U87 and MCF-7 cells. These determinations were conducted with the superoxide detector MitoSox in live cells grown in normoxia, where the senescent phenotype was evident, albeit less pronounced than in hypoxia. MitoSox levels were not evaluated in hypoxic cells, to avoid potential confounding factors due to re-oxygenation during

live cell imaging. Both U87 and MCF-7 cells demonstrated a marked increase in superoxide levels (as revealed by confocal microscopy, and measured by flow cytometry as % of cells exhibiting positive staining for MitoSox) following depletion of PYGL (50±6% vs. 33±1% in U87 and 33±4% vs. 17±0.5% in MCF-7, $p<0.05$ and $p<0.01$ respectively) (Figure 5.12A). To determine if increased levels of ROS contributed to the induction of senescence in PYGL-depleted cells, cell proliferation was evaluated after exposure to the cell-permeant ROS scavenger MnTMPyP. 25 μM MnTMPyP was added to the cells 24 hours post-transfection until the end of the experiment. As expected, MnTMPyP significantly reduced the levels of superoxide in both control and PYGL-depleted cells (Figure 5.12B). Interestingly, the reduced cell proliferation phenotype normally associated with PYGL depletion was also partially suppressed when cells were treated with MnTMPyP (Figure 5.12C). Future investigations will be undertaken to ascertain the efficiency of PYGL knockdown in the presence of MnTMPyP.

Taken together, this data suggests that elevated ROS contribute to increased senescence observed in PYGL-depleted cells.

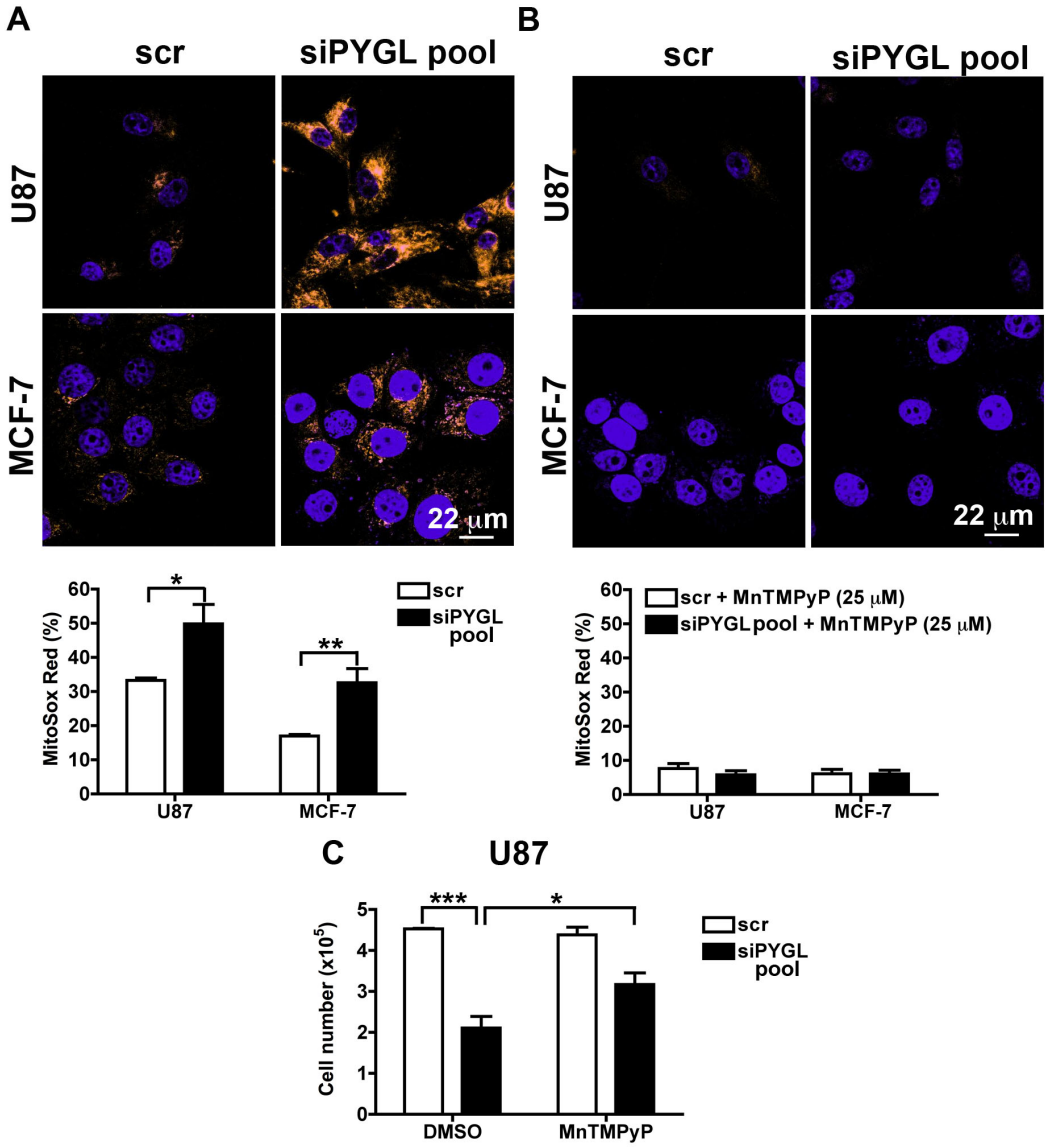


Figure 5.12 PYGL depletion is associated with elevated ROS.
U87 and MCF-7 cells were transfected with siCtrl or siPYGL, either in the absence (**A**), or the presence of 25 μM of MnTMPyP (**B**). Representative confocal images of cells stained with the mitochondrial superoxide detector, MitoSox are shown in the top panels, and quantification by flow cytometry is shown in the bottom panels. Cell numbers were also determined in each case (**C**). Mean ± SEM of three independent experiments is shown (* $p<0.05$, ** $p<0.01$).

5.2.4 Metabolic consequences of glycogen breakdown inhibition

The data described so far demonstrate that inhibition of glycogen degradation through PYGL is associated with glycogen accumulation, increased ROS and reduced proliferation due to p53-induced premature senescence. Although elevated ROS contribute to the onset of senescence in PYGL-depleted cells, it remains undetermined how and why these arise. The consequences of PYGL depletion were therefore examined in cells that were unable to accumulate glycogen in hypoxia. For this purpose, simultaneous GYS1 and PYGL co-depletion were performed in U87 cells, as this cell line was able to tolerate GYS1 depletion better than MCF-7 cells (Chapter 4, Figure 4.10). Transient transfection with siGYS1 and siPYGL, either alone, or in combination, effectively suppressed the hypoxic induction of the targeted mRNA sequences (Figure 5.13A). Furthermore, GYS1 knockdown was associated with reduced glycogen accumulation in hypoxia in both control and PYGL-depleted cells (Figure 5.13B). However, GYS1 depletion, either alone, or in conjunction with PYGL knockdown, did not affect cell proliferation, suggesting that glycogen accumulation is required for the induction of senescence normally caused by PYGL-depletion (Figure 5.13B).

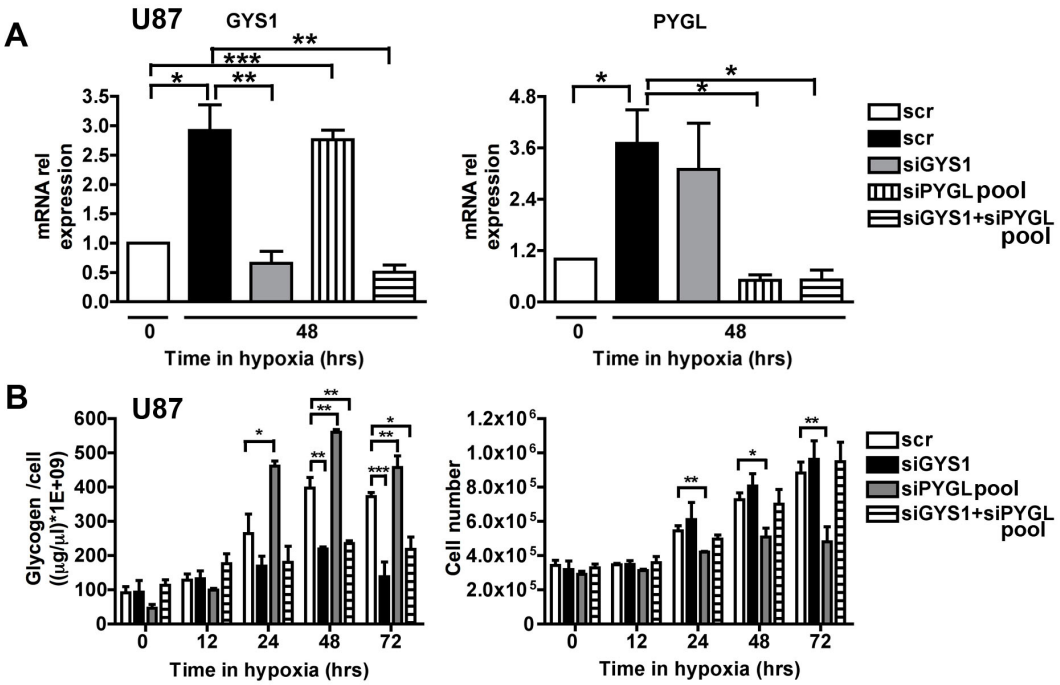


Figure 5.13 GYS1 knockdown prevents glycogen accumulation and premature senescence in PYGL-depleted cells.
A, U87 cells were simultaneously transfected with two siRNA pools: siGYS1 (or scr) and siPYGL pool (or scr). GYS1 mRNA levels and PYGL mRNA levels were measured after 48 hours in hypoxia. Values are relative to mRNA level in U87 scr cells at 0 hours in hypoxia. Mean ± SEM of three independent experiments is shown (* $p<0.05$, ** $p<0.01$, *** $p<0.001$). **B**, U87 scr, siGYS1, siPYGL pool, and U87 siGYS1 + siPYGL pool were exposed to hypoxia in a time course experiment. Glycogen levels and cell number were measured at the indicated times. Mean ± SEM of three independent experiments is shown (* $p<0.05$, ** $p<0.01$, *** $p<0.001$).

Glucose-1-P released from glycogen by PYGL is converted to glucose-6-P by the enzyme PGM. This can then either enter the glycolytic cascade and be metabolised to generate ATP, or enter the PPP. The PPP generates nucleotides required for sustained proliferation, as well as NADPH, which is an important reducing agent for nucleotide, amino acid and lipid synthesis, and also for ROS scavenging (Lunt and Vander Heiden, 2011; Roach et al., 2012). As expected, PYGL knockdown in MCF-7 and U87 cells was associated with a significant reduction of glucose-6-P levels

(Figure 5.14). Direct measurement of glucose-1-P was not undertaken because a glucose-1-P enzymatic assay was not available at this stage.

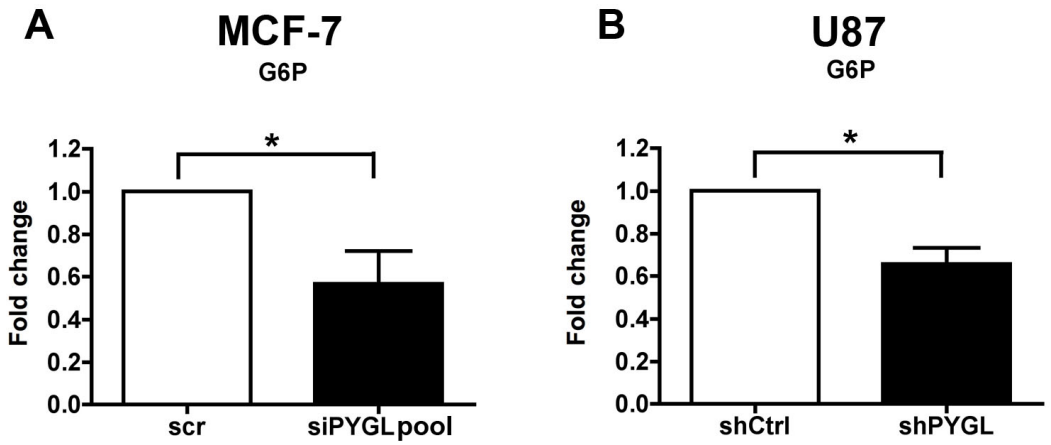


Figure 5.14 PYGL knockdown leads to decreased availability of glucose-6-P. **A,** MCF-7 cells were transfected with scr or siPYGL pool, and cultivated in normoxia for 48 hours. G6P levels were measured after 48 hours with the G6P enzymatic assay. G6P levels were normalised by cell number and expressed as fold change. **B**, U87 cells expressing shCtrl or shPYGL were cultivated in normoxia for 48 hours, and their G6P levels measured as described in (A). In both (A) and (B), Mean ± SEM of three independent experiments is shown (* $p<0.05$).

To obtain a more comprehensive overview of the metabolic changes induced by PYGL depletion, lysates from normoxic MCF-7 scr and siPYGL pool cells were processed for metabolic analysis by Metabolon Inc. Cells were harvested 24 hours post-transfection, in order to minimize changes in the metabolic profiles due to the activation of compensatory pathways. After 24 hours, PYGL mRNA was efficiently suppressed (93%) in PYGL knockdown cells, as compared to control cells (Figure 5.15B). Cell lysates were processed using gas chromatography/mass spectrometry (GC/MS) and liquid chromatography-tandem mass spectrometry (LC/MS/MS) to analyse their metabolic content (Griffin and Shockcor, 2004). From this data, a list of metabolites that were significantly altered following PYGL knockdown was

compiled (indicated as highlighted text in Figure 5.15A). Consistent with decreased flux of glucose-6-P through the PPP, PYGL knockdown cells exhibited lower levels of 6-phosphogluconate and nucleotides, whereas the levels of oxidized glutathione (GSSG) were significantly increased. Additionally, numerous amino acids were also reduced. Notably, NADPH is required for both the conversion of GSSG to reduced glutathione (GSH) and the synthesis of amino acids (Lunt and Vander Heiden, 2011; Roach et al., 2012). PYGL-depleted cells also contained lower levels of fumarate and malate, suggesting a decreased flux of glucose and glutamine through the Krebs cycle. Finally, extracellular glucose and lactate levels were not significantly altered following PYGL knockdown, suggesting that glucose uptake, and its metabolism through the glycolytic pathway, was unaffected by the depletion of PYGL (Figure 5.15B). It should be noted that although glucose-6-P levels were previously found to be reduced in PYGL-depleted cells (Figure 5.14), the ratio of glucose-6-P was not significantly altered in this analysis. Possible reasons for this discrepancy are a) the different time point at which the analyses were performed (24 hours post-transfection for the metabolic analysis by Metabolon Inc., and 48 hours post-transfection for the glucose-6-P enzymatic determination), and b) different sensitivity of the two assays.

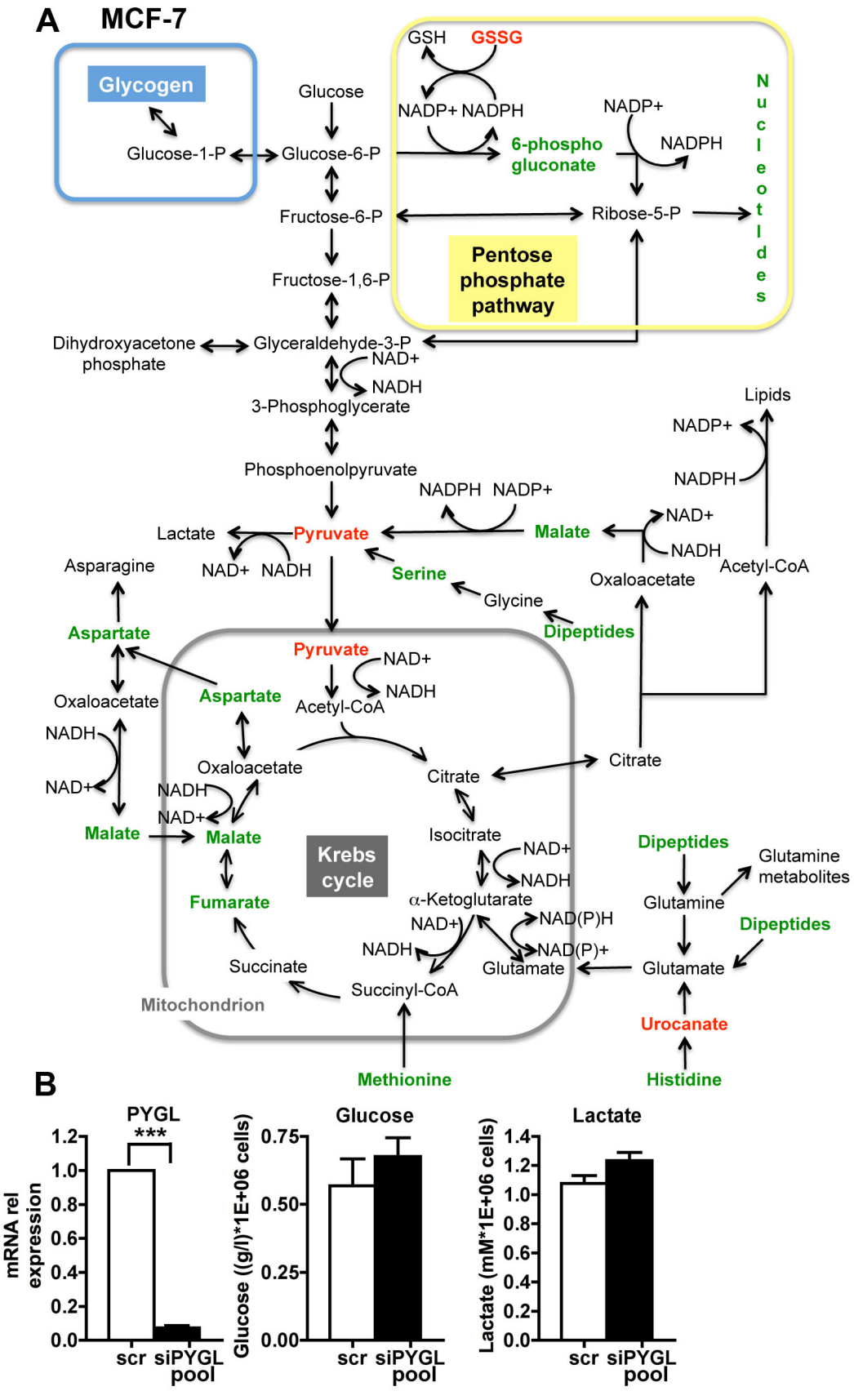

A
MCF-7
Glycogen
Glucose-1-P
Glucose
Glucose-6-P
Fructose-6-P
Fructose-1,6-P
Dihydroxyacetone phosphate
Glyceraldehyde-3-P
3-Phosphoglycerate
Phosphoenolpyruvate
GSH
GSSG
NADP+ NADPH
6-phospho gluconate
NADP+
NADPH
Ribose-5-P
Nucleotides
Pentose phosphate pathway
NAD+
NADH
Lipids
Lactate
Pyruvate
Malate
Asparagine
Serine
Glycine
Dipeptides
Aspartate
Oxaloacetate
Acetyl-CoA
Citrate
Isocitrate
Krebs cycle
α-Ketoglutarate
Fumarate
Succinate
Succinyl-CoA
Mitochondrion
Glutamine
Glutamine metabolites
Glutamate
NAD(P)H
NAD(P)+
Urocanate
Methionine
Histidine
B
PYGL
***
mRNA rel expression
scr siPYGL pool
Glucose
Glucose ((g/l)*1E+06 cells)
Lactate
Lactate (mM*1E+06 cells)

Figure 5.15 Metabolite alterations induced by PYGL knockdown in MCF-7 cells.
MCF-7 cells were transfected with scr or siPYGL pool, and then harvested for metabolic analysis 24 hours post-transfection. **A,** levels of metabolites were then measured by mass spectrometry. A schematic illustration of metabolic changes induced in PYGL-depleted cells is shown. Green text indicates metabolites that were significantly lower in PYGL-depleted cells (ratio < 1), whereas red text indicates metabolites that were significantly higher (ratio >1). Five replicates per group were analysed. Abbreviations used: NADH, nicotinamide adenine dinucleotide (reduced); NAD+, nicotinamide adenine dinucleotide; NADPH, nicotinamide adenine dinucleotide phosphate (reduced); NADP+, nicotinamide adenine dinucleotide phosphate; CoA, coenzyme A; GSH, glutathione (reduced); GSSG, glutathione (oxidized). **B**, PYGL mRNA levels (left), as well as extracellular glucose (middle) and lactate levels (right), were also measured under the same conditions. Mean ± SEM of five independent experiments is shown (*** $p<0.001$).

The results from the metabolic analysis suggested that several key metabolic pathways were altered in PYGL-depleted cells. Importantly, the glycolytic pathway was apparently unaffected, whereas the PPP activity was reduced in PYGL-depleted cells. Consistent with a reduction of the PPP activity, a significant increase in the $NADP^+$/NADPH ratio was detectable in MCF-7 following PYGL-depletion (Figure 5.16).

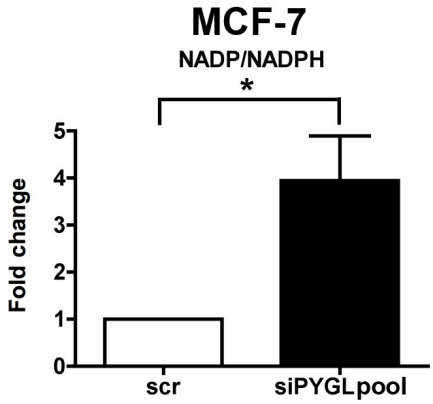


Figure 5.16 NADPH levels are reduced in PYGL-depleted cells.

MCF-7 cells were transfected with siCtrl or siPYGL and NADPH levels were measured at 48 hours post-transfection. Mean ± SEM of three independent experiments is shown (* $p<0.05$).

To further examine the utilisation of glucose in PYGL-depleted cells, a metabolic flux analysis with D-[1,2-^{13}C]glucose was conducted in U87 cells in collaboration with Drs Mei Chong and Daniel Tennant (University of Birmingham, UK). Nuclear magnetic resonance (NMR) spectroscopy was used to measure adenosine and guanosine nucleotides that contained a site-specific incorporation of glucose-derived ^{13}C into the ribose unit. This provides a measurement of glucose flux through the oxidative branch of the pentose phosphate pathway (Figure 5.17A). The analysis revealed a reduction of ^{13}C-labelled adenosine and guanosine nucleotides in PYGL depleted U87 cells, as compared to control cells (Figures 5.17B and 5.17C).

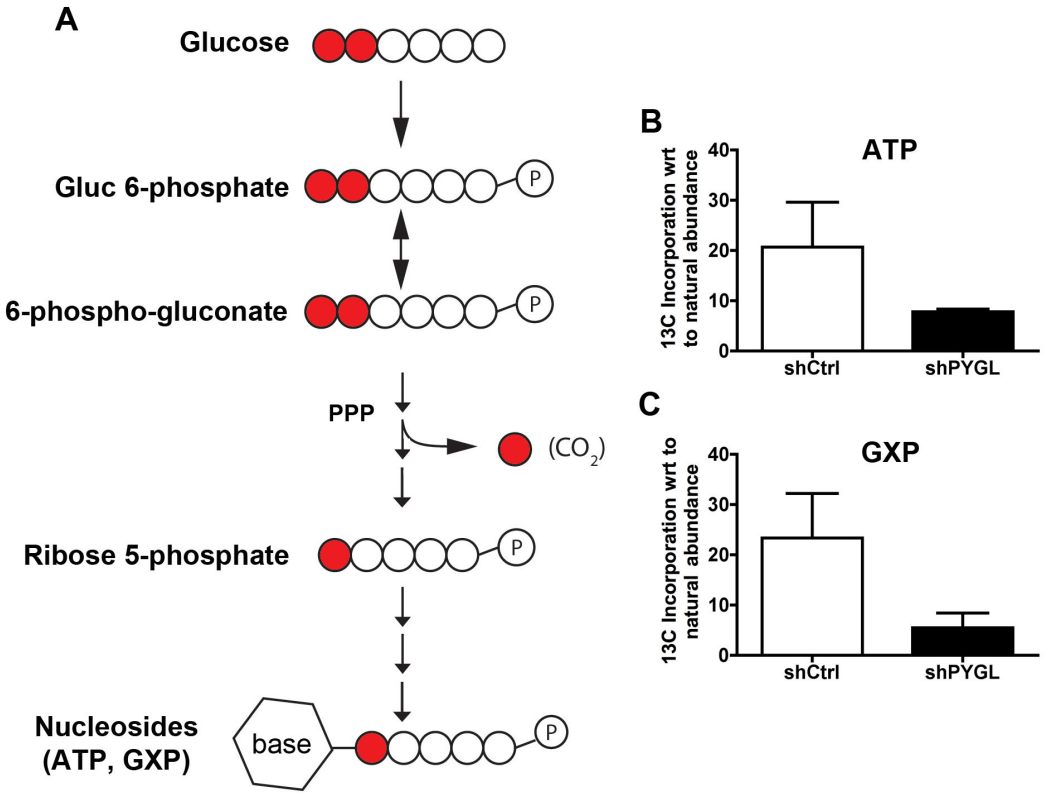


Figure 5.17 PYGL depletion reduces the activity of the oxidative pentose phosphate pathway.
A, schematic illustration of ^{13}C- incorporation from $^{13}C[1,2]$-glucose into nucleosides through PPP. **B,** U87 shCtrl and shPYGL cells were grown in media enriched for D-[1,2-^{13}C]glucose. Incorporation of ^{13}C from $^{13}C[1,2]$- glucose in a position in ribose into adenosine triphosphate (ATP) that is unique to oxidative PPP activity, is reduced in U87 shPYGL cells. Mean ± SEM of two independent experiments is shown. **C**, incorporation into the same ribose position into guanosine nucleotides (GXP) is also reduced in shPYGL cells, confirming the labelling phenotype observed in ATP (x is either M (mono-), D (di-) or T (tri-)). Mean ± SEM of two independent experiments is shown. Courtesy of Drs Mei Chong and Daniel Tennant.

Previous reports have proposed that inhibition of the pentose phosphate pathway is associated with the induction of senescence *in vitro* and *in vivo* (Shilkaitis et al., 2005; Sukhatme and Chan, 2012). This raises the possibility that the senescence phenotype in PYGL-depleted cells is primarily caused by a reduction in PPP activity. To further test this possibility, U87 cells were treated with two different inhibitors of

glucose-6-P dehydrogenase, which catalyses the first step of the oxidative branch of PPP (Polimeni et al., 2011). Consistent with a link between reduced PPP activity and senescence, treatment of U87 cells for 24 hours with 100 μM 6-aminonicotinamide (6-AN), or 100 μM dehydroepiandrosterone (DHEA), caused increased senescence in U87 cells (Figure 5.18). The drug concentration used was selected on the basis of a previous study that measured the PPP activity in cancer cells treated with different doses of DHEA or 6-AN (Polimeni et al., 2011).

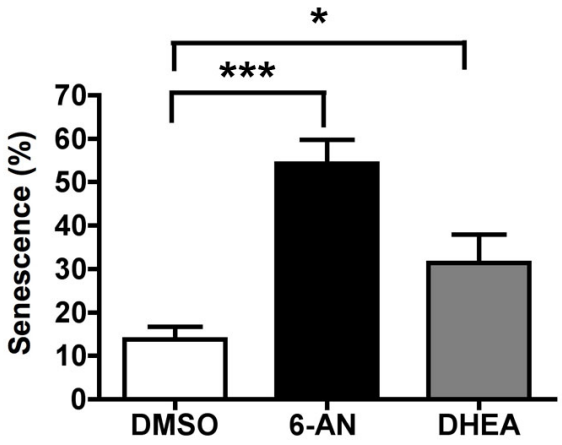


Figure 5.18 Induction of senescence after pharmacological inhibition of the PPP. U87 cells were treated for 24 hours with 100 μM 6-AN or DHEA, two specific PPP inhibitors. Cells were then stained for SA-βgal activity. Senescence was expressed as % of SA-βgal positive cells in each condition. Treatment with PPP inhibitors significantly increased the proportion of senescent cells. Mean ± SEM of three independent experiments is shown (* $p<0.05$, *** $p<0.001$).

5.2.5 PYGL depletion inhibits growth of spheroids

The consequences of PYGL knockdown on tumour cell growth were tested in spheroids, which more closely resemble the pattern of 3D tumour growth *in vivo*.

Both U87 and MCF-7 cells formed spheroids 1 day after plating, although MCF-7-derived spheroids grew slower than U87-derived spheroids, and started to disaggregate after 5-7 days from plating (Figure 5.19A, right panels). In both cell lines, spheroid volumes were markedly reduced in the PYGL-depleted groups, as compared to the control groups after 7 days (67% reduced in PYGL depleted cells for U87, and 41% reduced for MCF-7 cells) (Figure 5.19A, left panels). Growth of spheroids derived from U87 cells with stable PYGL knockdown was also significantly reduced (by 41%), and this was associated with increased glycogen levels, as measured by PAS staining (Figure 5.19B).

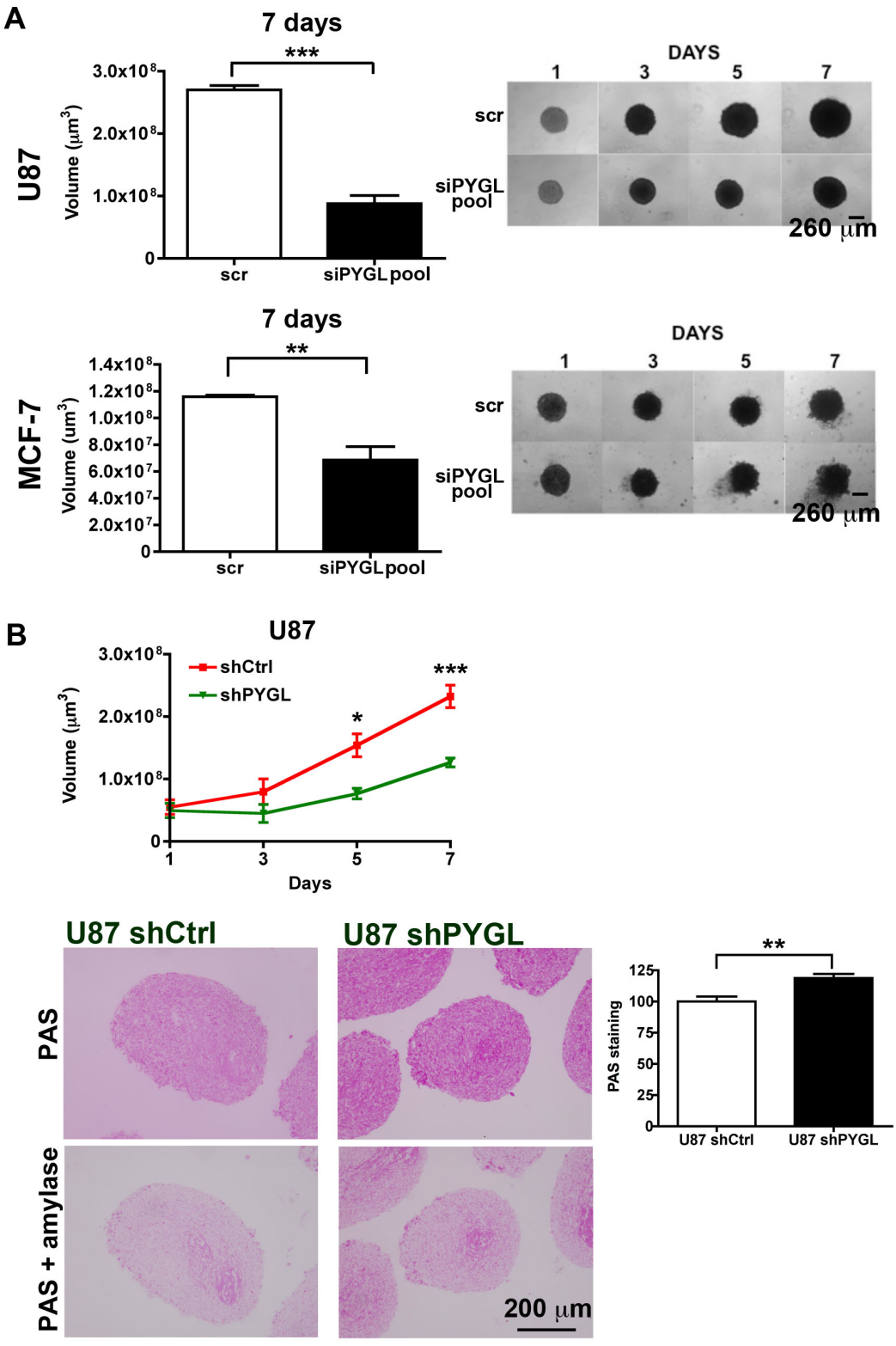


Figure 5.19 PYGL knockdown impairs spheroid growth.
A, U87 and MCF-7 cells were transfected with scr or siPYGL. At 24 hours post-transfections, cells were trypsinized and spheroids were generated (day 0). Panels on

the left show volume measurements after 7 days in culture. Representative images taken at day 1, 3, 5 and 7 are shown on the right. Mean ± SEM of three independent experiments is shown (** $p<0.01$, *** $p<0.001$). **B**, A growth curve of spheroids generated from U87 shCtrl and shPYGL cells is shown on the top panel. Mean ± SEM of three independent experiments is shown (* $p<0.05$, *** $p<0.001$). Bottom panels show representative images of spheroids harvested at day 7 and stained for glycogen with PAS staining. Specificity of PAS staining for glycogen was confirmed by the absence of staining after amylase pre-treatment. Quantification of PAS staining is displayed on the right panel. Mean ± SEM of three independent experiments is shown (** $p<0.01$).

5.2.6 PYGL depletion impairs tumour growth *in vivo*

To test the effect of PYGL depletion on tumour cell growth *in vivo*, U87 shPYGL or U87 shCtrl cells were injected subcutaneously into nude mice, and tumour growth monitored over time. Consistent with the *in vitro* data described above, PYGL depletion resulted in a marked impairment of tumour growth. At day 43 after injection, tumour volumes were 1095 ± 250 versus 130 ± 25 mm^3 in the control and the PYGL knockdown groups, respectively ($p<0.01$) (Figure 5.20A, left panel). As expected, the levels of PYGL were reduced in the PYGL knockdown tumours, although the extent of reduction was approximately 50% (Figures 5.20A, right panel, and 5.20B), which is considerably less than that obtained in the same cells when analysed *in vitro* (Figure 5.1A, right panel). A potential explanation for this discrepancy could be the selection for cells with reduced expression of the shPYGL construct. Consistent with the *in vitro* data, depletion of PYGL was associated with a significant increase in glycogen accumulation, as determined by PAS staining (Figure 5.20B). Increased glycogen accumulation was predominantly observed in perinecrotic/hypoxic areas (Figure 5.20B).

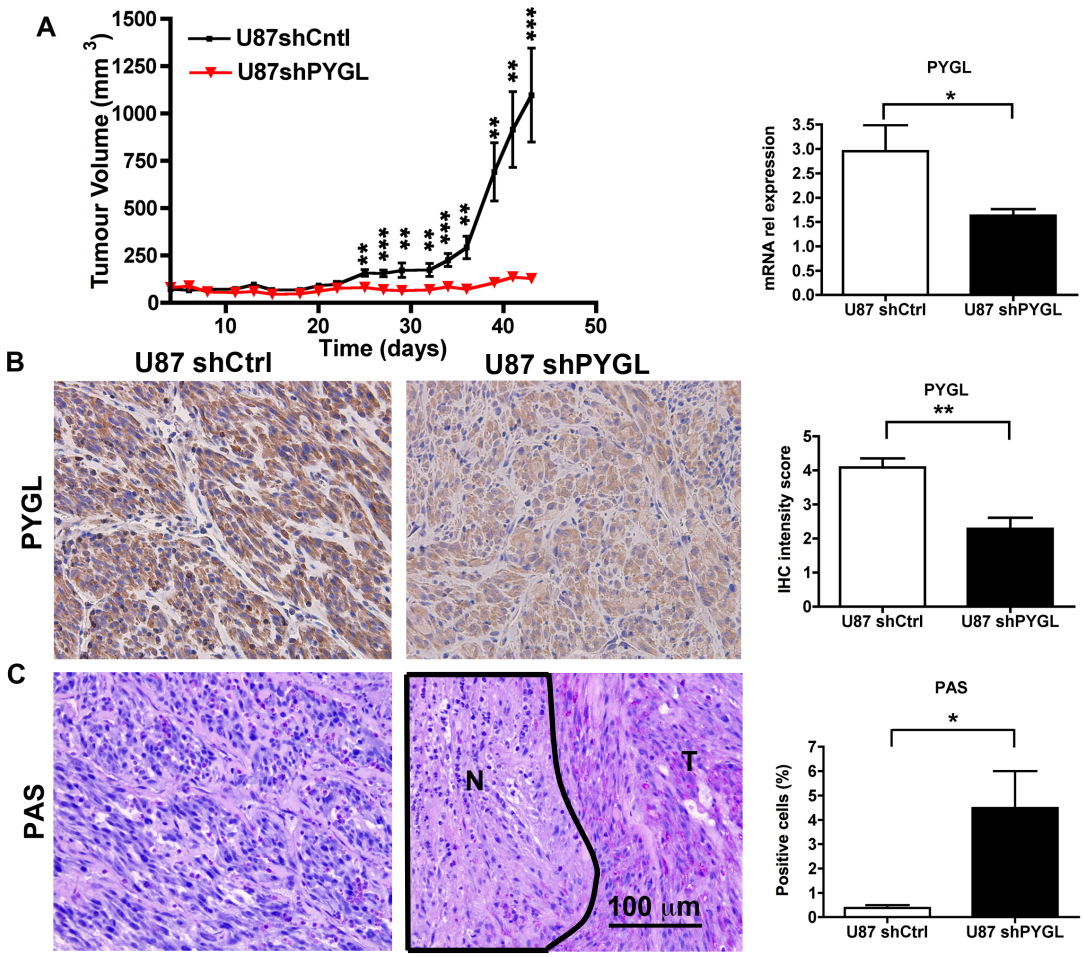


Figure 5.20 PYGL knockdown impairs tumour xenograft growth.
A, 10^7 PYGL knockdown or control U87 cells were injected subcutaneously into BALB/c nu/nu mice and tumour volumes were measured 3 times per week, up to day 43 (left panel). Data points represent the average size ± SEM of 5 to 7 tumours (** $p<0.01$, *** $p<0.001$). PYGL mRNA levels were analysed at the end of the experiment (right panel). Mean ± SEM of 5 to 7 tumours is shown (* $p<0.05$). Tumour sections were stained for PYGL (**B**), and glycogen levels (**C**). Representative pictures are shown on the left, and quantification of staining is shown on the right. For quantification, 3 to 6 fields of each tumour sample at x200 magnification were analyzed. Mean ± SEM of 5 to 7 tumours is shown (* $p<0.05$, ** $p<0.01$). N = necrotic area, T = viable tumour.

In vitro, PYGL depletion impaired cell proliferation via increased induction of senescence. To investigate whether a similar mechanism was responsible for growth inhibition in PYGL-depleted tumours *in vivo*, tumours collected at the end of the experiment were examined for the senescence-associated markers, DEC1 and p21.

PYGL reduction was associated with a significant 5-fold increase in the expression of both DEC1 (47.2 ± 3.8% versus 8.5 ± 1.1%) and p21 (17.2 ± 2.1% versus 3.4 ± 1.1%) (Figures 5.21B and 5.21C). Importantly, both PYGL knockdown and control tumours had similar levels of necrosis, excluding the possibility that this type of cell death was contributing to tumour growth suppression *in vivo* (Figure 5.21A).

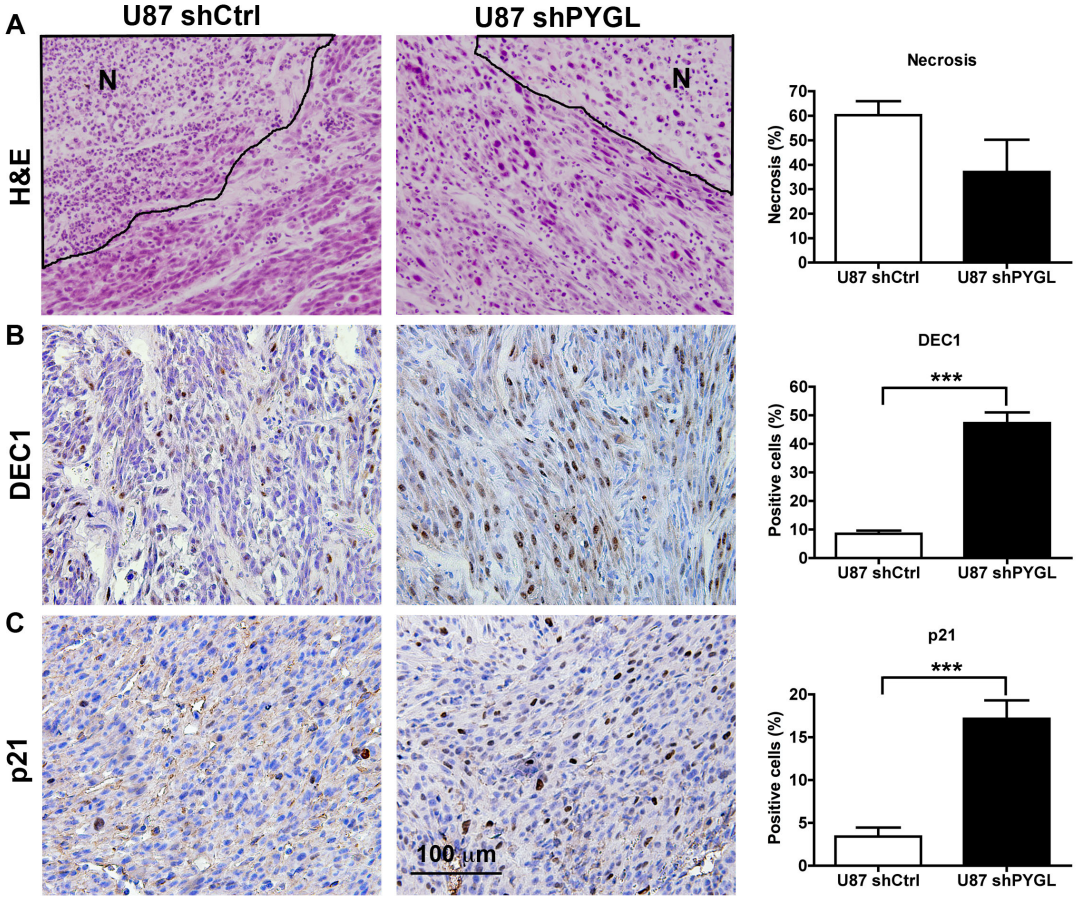


Figure 5.21 PYGL knockdown is associated with increased senescence *in vivo*. Tumour histology (hematoxylin and eosin staining [H&E]) of shCtrl versus shPYGL xenografts was analysed at day 43 after injection (**A**). Necrotic areas are indicated by N. Tumour cell senescence was measured by staining for DEC1 (**B**) and p21 (**C**). Representative images are shown on the left, and quantification is shown on the right. For quantification, 3 to 6 fields of each tumour sample at x200 magnification were analyzed. Mean ± SEM of 5 to 7 tumours is shown (** $p<0.01$, *** $p<0.001$).

5.3 Discussion

The results of this chapter further demonstrate the importance of glycogen metabolism in sustaining cancer cell proliferation in hypoxia. Indeed, knockdown of the key glycogen breakdown enzyme, PYGL, resulted in increased glycogen accumulation that was associated with reduced proliferation and increased induction of senescence. Induction of senescence in tumour cells as a mechanism to restrain cell proliferation has been previously proposed as a potential treatment strategy for cancer (Schmitt, 2007).

A number of observations suggest that the findings reported here have physiological relevance for the study of tumour growth *in vivo*. Firstly, as discussed in Chapter 4, evidence of PYGL upregulation, and glycogen accumulation, was observed *in vivo* following the treatment of xenografts with bevacizumab. In cancer cell lines cultivated *in vitro*, increased glycogen accumulation and induction of senescence were consistently observed when PYGL was depleted by either stable or transient knockdown. Importantly, the sequences used by the two RNAi methods were directed against different regions of the PYGL mRNA transcript, excluding the possibility that the phenotypes reported here were due to off-target effects (Echeverri et al., 2006). Furthermore, increased glycogen accumulation in PYGL-depleted cells occurred even in the presence of physiological concentrations of glucose, suggesting that this phenomenon is not simply an artifact caused by high glucose concentrations typically used in cell culture growth conditions. Finally, increased glycogen accumulation and senescence were detectable in tumour cell xenografts derived from

PYGL-depleted cell lines, suggesting that the phenotypes observed *in vitro* were also recapitulated *in vivo*.

The phenotypic consequences of disrupting glycogen breakdown were surprisingly profound, despite the abundant availability of extracellular glucose. This suggests that channeling of glucose through glycogen has important implications for tumour cell growth. Furthermore, this also suggests an additional physiological function of glycogen that goes beyond its role as an energy source in situations of increased glucose demand. A similar phenomenon, whereby glucose is incorporated into glycogen and subsequently released as glucose-1-P even in the presence of abundant extracellular glucose, has been described previously in the brain (predominantly in astrocytes) both *in vitro* and *in vivo*, and is referred to as the 'glycogen shunt' (Obel et al., 2012). The precise reasons for this physiological response remain unexplained, although some evidence indicates that it provides energy for the maintenance of an optimal glutamatergic neurotransmission (Schousboe et al., 2010; Sickmann et al., 2009; Walls et al., 2009).

Following depletion of PYGL, a contribution of both p53 and ROS to the induction of premature senescence was demonstrated by the amelioration of this phenotype when p53 was co-depleted, or when PYGL-depleted cells were grown in the presence of a ROS scavenger, MnTMPyP. It would be of particular interest to extend these analyses to p53-negative or mutant cancer cell lines, in order to further substantiate the role of p53 in the induction of senescence. Whether ROS-induced p53 activation is solely responsible for the onset of premature senescence in PYGL-depleted cells, or if high levels of glycogen can directly lead to p53 activation, remains to be elucidated and should represent the focus of future investigations. In

particular, it will be of interest to examine p53 (and glycogen) levels in PYGL depleted cells following exposure to MnTMPyP, to determine the contribution of ROS to p53 activation. Moreover, it cannot be excluded that ROS contribute to the onset of senescence also through the activation of signalling pathways such as the misshapen-like kinase (MINK)-p38 pathway (Kuilman et al., 2010). Finally, given the effect on ROS accumulation, it would be of interest to explore the consequences of PYGL inhibition on radiation sensitivity.

Following PYGL knockdown, increased expression of the lysosomal glycogen metabolising enzyme GAA was also observed. It remains undetermined if this induction of GAA reflects the increased lysosomal content/activity that is characteristic of senescent cells, or if this indicates the activation of a compensatory mechanism in response to excessive glycogen accumulation. Confirmation of either of these hypotheses could lead to further avenues of investigation. First, lysosome-rich PYGL-depleted cells may exhibit increased sensitivity to lysosome-targeting anti-cancer drugs (Kallunki et al., 2012). These drugs cause cell death through lysosomal membrane permeabilization, and consequent release of lysosomal contents into the cytosol (Groth-Pedersen and Jaattela, 2010). Alternatively, increased cell dependency on lysosomal activity could make PYGL-deficient cells more vulnerable to autophagy inhibitors (Rabinowitz and White, 2010). Finally, inhibition of GAA in PYGL-deficient cells could exacerbate the senescence phenotype reported here by further increasing intracellular glycogen levels.

The induction of premature senescence occurs, at least in part, due to reduced flux through the PPP, which is important for the generation of NADPH, nucleotides,

amino acids, and lipids required for continued cell proliferation. Both flux and metabolomic analyses were consistent with this hypothesis. The metabolic profile also revealed a reduction in intermediates of the Krebs cycle, as well as reduced amino acid levels. A ROS-dependent decrease in aconitase activity has been previously documented (Bulteau et al., 2003), and this could contribute to the observed effects on the Krebs cycle, as well as the accumulation of intracellular pyruvate, reported here. Notably, analysis of the metabolic profiles only provides information on the steady state levels of metabolites; therefore definitive conclusions on the activity of the glycolytic pathway and the Krebs cycle will require detailed metabolic flux analysis with ^{13}C-labelled substrates.

These findings suggest the existence of a preferential channelling of glucose derived from glycogen into the PPP, where it is used for the reduction of NADPH and the generation of nucleotides and other building blocks required by proliferating cells. Inhibition of glycogen breakdown and the consequent reduction of PPP activity, directly contributes to cellular senescence. Although this is the preferred hypothesis, another aspect to consider is that glycogen itself could also fulfil important intracellular signalling functions, at least when present at high levels. Indeed, when glycogen accumulation in hypoxia was attenuated (but not abolished) by GYS1 knockdown, the induction of senescence in PYGL-depleted cells was also prevented. This raises the possibility that glycogen accumulation above a critical threshold promotes the onset of senescence, particularly in cells with compromised pentose phosphate pathway / ROS clearance machinery. The putative signalling functions of glycogen may arise due to its ability to directly regulate the activity of the master regulator of intracellular energy homeostasis, AMPK (McBride et al., 2009), which

can lead to p53-dependent cellular senescence if persistently activated (Jones et al., 2005). Indeed, in patients affected by McArdle's disease, the inability to mobilize glycogen due to mutations in the muscle isoform of glycogen phosphorylase, PYGM, is associated with hyperactivation of AMPK during exercise (Nielsen et al., 2002).

A number of other studies have verified the importance of glycogen phosphorylase in sustaining continued cell proliferation. A previous study demonstrated that the yeast homologue of PYGL, Gph1p, is required to prevent ROS-dependent induction of premature aging when nutrients are limiting (Favre et al., 2008). Another study demonstrated that inhibition of glycogen phosphorylase using a small molecule inhibitor (CP-320626) promoted apoptosis by limiting glucose oxidation, nucleic acid and lipid synthesis in a human pancreatic cancer cell line (Lee et al., 2004a). A more recent proteomic analysis performed on these cells revealed the activation of various stress-induced pathways, as well as increased levels of the cell cycle regulators p21, p27 and p53 (Ma et al., 2012). A similar effect on cell viability was reported in human umbilical endothelial cells treated with escalating doses of CP-320626 (Vizan et al., 2009). However, the specificity of these results remains to be determined, in view of the considerably higher (more than 1000 fold) IC_{50} reported by the authors compared to that previously determined on purified enzyme (Oikonomakos et al., 2002). Moreover, glycogen accumulation after glycogen phosphorylase inhibition was not measured.

In the proposed working model (Figure 5.22), glycogen degradation by PYGL provides a source of glucose-6P, which can maintain the reduction of NADPH and glutathione, and the synthesis of nucleotides, through the pentose phosphate

pathway. Moreover, PYGL can limit the intracellular levels of glycogen (that can otherwise directly contribute to the induction of senescence). In hypoxic cells lacking PYGL, glycogen accumulation, decreased nucleotide synthesis and increased levels of ROS can all additively contribute to a p53-dependent growth arrest.

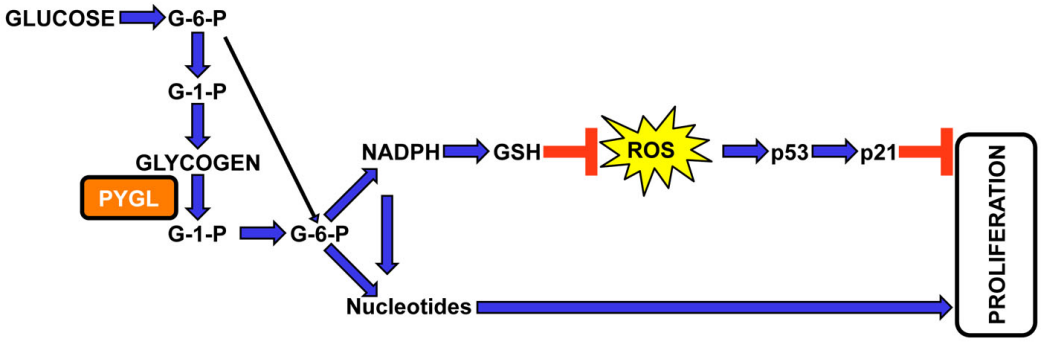


Figure 5.22 Working model.
Glycogen degradation through PYGL releases glucose-1-P units that are then converted into glucose-6-P. Glucose-6-P is required for nucleotide synthesis and the maintenance of NADPH and glutathione in their reduced state, through the PPP. Glutathione plays an important role in antioxidant defense. Therefore, inhibition of PYGL leads to decreased nucleotide synthesis and increased levels of ROS that result in p53-dependent growth arrest.

Importantly, targeting of PYGL for cancer therapy would likely present limited side effects, because patients affected by Hers' disease, an inherited glycogen storage disease caused by deficiency of PYGL, present only mild symptoms during childhood and most adults are asymptomatic (Dagli and Weinstein, 1993). Indeed, small molecules inhibitors of PYGL are currently under investigation for the treatment of diabetes (Praly and Vidal, 2010). The present findings suggest that these could also warrant consideration as possible novel anti-cancer therapies in future studies. In particular, given that PYGL expression is increased following bevacizumab treatment *in vivo*, targeting of this pathway is likely to be more effective in tumors that are markedly hypoxic. It will be of great interest to

investigate the combined effects of PYGL inhibition and bevacizumab and to determine if PYGL is required for resistance to antiangiogenic therapy.

6 CHAPTER SIX

Concluding remarks

6.1 Clinical perspectives on miR-210 regulation in cancer

In chapter 3, the HIF-miR-210 axis was characterised as an important regulator of cancer metabolic reprogramming through its downstream target ISCU, resulting in impaired mitochondrial function and a switch to glycolytic metabolism. This was also associated with an increase in ROS levels that could have important implications in cancer biology, by activating survival pathways and by increasing tumour genetic instability by damaging DNA. MiR-210 represents the most robustly and consistently hypoxia-upregulated miRNA both in tumours and normal tissues (Chan et al., 2012). A growing number of studies are confirming its association with the adaptation of cancer cells to hypoxia (Devlin et al., 2011). Potential novel ways of identifying and selectively targeting hypoxic tumours are of major significance because these tumour types are notoriously resistant to conventional cancer therapies. MiR-210 influence extends over all of the hallmarks of cancer, through the multiplicity of its validated targets, and their involvement in cell survival, proliferation, angiogenesis, DNA repair, and metabolism. However, a substantial number of predicted targets still need to be confirmed, and the physiological relevance of their altered regulation in hypoxia determined, for a more comprehensive understanding of the complex biological roles of miR-210. The data presented in this study, and independently validated by other groups, have demonstrated that miR-210 can indirectly disrupt the normal activity of two mitochondrial enzymes, aconitase and Complex I, by interfering with the synthesis of cognate Fe-S cluster cofactors (Chan et al., 2009; Favaro et al., 2010). Further investigation will be required to determine if the activity of other Fe-S-dependent

metabolic enzymes (e.g. Complexes II and III, SDH and FH) are similarly affected, and also contribute to mitochondrial dysfunction. Although several metabolic enzymes have already been validated as direct miR-210 targets, including SDHD and COX10, a substantial number of predicted targets with metabolic implications still await validation. This, combined with a comprehensive analysis of the metabolic and phenotypic changes associated with miR-210 expression, will provide a useful tool for the systematic characterisation of miR-210 impact on metabolism.

The potential of miR-210 as a diagnostic and prognostic tool is substantiated by several preclinical and clinical observations. Firstly, higher miR-210 expression levels have been observed in a variety of solid tumours, and this is inversely correlated with patient survival and response to treatment. Secondly, miR-210 and miRNAs in general, are extremely stable and resistant to degradation, as compared to mRNAs. This property enables their detection and quantification in formalin-fixed paraffin-embedded clinical specimens (Liu and Xu, 2011). Moreover, non-invasive methods for detection of mir-210 levels can be successfully undertaken in blood and other body fluids of cancer patients, where they serve as markers of various types of cancer and they retain prognostic significance (Chan et al., 2012; Hong et al., 2012).

Given the paucity and the inadequacy of the present biomarkers, miR-210 most interesting clinical application will be as a marker of tumour hypoxia. For examples, future trials will evaluate the predictive impact of miR-210 expression (as a marker of tumour hypoxia) on the response of head and neck cancer patients to radiosensitisers in combination with radiotherapy (personal communication to Prof Adrian Harris). The prediction is that the miR-210 expression could drive the identification of the most hypoxic tumours, which would benefit the most from this

combination therapy, as shown previously using a hypoxia gene expression signature (Toustrup et al., 2012).

Of note, the interest in mir210 as a reliable biomarker for tumour hypoxia has led to a recent patent of the methods of using miR-210 as a biomarker for hypoxia (http://www.uspto.gov, patent publication number = 2011-0166200 A1).

Given the ability of miR-210 to regulate several DNA repair enzymes, by either targeting them directly (e.g. RAD52 (Crosby et al., 2009)), or by lowering Fe-S clusters through the suppression of ISCU (and therefore disrupting Fe-S-dependent DNA repair enzymes such as XPD and FANCJ), miR-210 expression levels could be used as an indicator of response to cancer therapy. For example, chemotherapeutic agents that induce DNA crosslinks (e.g. mitomycin C and cisplatin), or double-strand DNA breaks (e.g. PARP inhibitors (Wilson and Hay, 2011)) could be particularly toxic to cells with high levels of mir210 (and low levels of RAD52, XPD and FANCJ). Furthermore, because glycolysis is upregulated in cells with high levels of miR-210, it will be interesting to test if these cells are also particularly sensitive to glycolysis inhibitors. Future experiments, including examining the effects of simultaneous combined therapeutic approaches, should test these hypotheses.

Because of its pleiotropic functions in tumour biology and putative role in the adaptation of cancer cells to hypoxia, miR-210 has also a strong potential as a candidate for therapeutic targeting. However, before considering this further, a number of important factors will need to be addressed:

1) As discussed above, a more complete characterisation of mir210 targets, and the phenotypic consequences of their altered regulation in hypoxia, is needed in order to fully understand the roles of mir210 in cancer biology. New methods have been

developed for the identification of miR-210-modulated genes; these consist in the direct analysis of the mRNA targets associated with the RISC or AGO proteins in miR-210 overexpressing cells (Devlin et al., 2011);

2) The impact of miR-210 modulation in other clinical conditions characterised by the development of hypoxia (i.e. cerebrovascular and cardiovascular diseases, wound healing) should be carefully defined, in order to estimate the risk of side-effects;

3) Tumours which will most benefit from miR-210 targeting will need to be carefully selected. Indeed, some tumours present downregulation or depletion of miR-210. For example, recent studies have indicated miR-210 as a tumour-suppressive miRNA in esophageal squamous cell carcinoma (where miR-210 is downregulated)(Tsuchiya et al., 2011), and in epithelial ovarian cancer (where miR-210 is frequently deleted) (Giannakakis et al., 2008). Moreover, ectopic miR-210 expression in head and neck and pancreatic cancer cells injected in mice repressed the initiation of tumour growth (Huang et al., 2009). Therefore, a clear understanding of the mechanisms favouring a tumour suppressor over a tumour promoting function have to be elucidated before moving to the clinical settings.

4) A major challenge will be the development of efficient anti-miRNA agents to use *in vivo*. These need to be selectively delivered to the tumour tissue, and provide sustained inhibition of the miRNA target. To date, only one miRNA-targeted drug has reached advanced clinical trials. This study examined the effects of administration of a LNA construct targeting miR-122 ('miravirsen') to patients with chronic HCV infection (Jopling et al., 2005). Phases I and II studies have shown promising results and low toxicity after subcutaneous administration of miravirsen, which persist for more than 4 weeks post-injection (http://www.santaris.com).

In conclusion, miR-210 is a major regulatory hub in the adaptation of cancer cells to hypoxia, and represents exciting possibilities as both a novel cancer biomarker, as well as a possible novel therapeutic target for cancer treatment.

6.2 Final considerations and open questions on glycogen metabolism in cancer

The data presented in Chapters 4 and 5 of this study highlight glycogen metabolism as an important pathway that is altered following cancer metabolic reprogramming. In hypoxic cells, depletion of PYGL caused enhanced glycogen accumulation and the induction of premature senescence. Moreover, depletion of PYGL was associated with markedly impaired tumor growth *in vivo.*

An important question that still needs to be addressed is why glycogen metabolism plays such an important role for cancer cells. For this, the following factors should be considered:

1) Glycogen acts as an energy source for the cells. This represents the most intuitive explanation, since the physiological role of glycogen in normal tissues is to provide glucose for ATP production under conditions of nutrient deprivation. This is also suggested by studies in hypoxia, where glycogen accumulation improves survival in response to low oxygen concentration and glucose deprivation (Mamedova et al., 2003; Pelletier et al., 2012; Pescador et al., 2010; Vigoda et al., 2003). However, the reasons for glycogen accumulation, and utilisation, even when extracellular glucose is abundant remain undetermined.

2) Glycogen acts as a source of precursors for biosynthetic pathways and antioxidant defences of the cell. The results presented in this study support this hypothesis,

because PYGL depletion reduces NADPH levels and the activity of the PPP. This is similar to glycolysis, whose main role is to provide a constant stream of precursors for biosynthetic pathways and preserve the antioxidant defences of the cell (through the reduction of NADPH). Furthermore, glycolytic reprogramming is upregulated in cancer and is further induced in hypoxia. Similarly, evidence is provided here and by others, that the expression of key glycogen-metabolising enzymes (i.e. GYS1 and PYGL) is increased in several cancer types, as compared to normal tissues, and can be induced in hypoxia (Mole et al., 2009; Pelletier et al., 2012; Pescador et al., 2010; Shen et al., 2010).

Whether the negative effects on tumour growth observed here directly arise due to limited NADPH and nucleotide production through the PPP, remains to be demonstrated. However, an indication that this might not be the full story is suggested by the evidence that patients with defective PPP activity due to glucose-6-P dehydrogenase deficiency, are not protected against cancer (Cocco, 1987). Notably, alternative pathways can contribute to the reduction of NADPH, including the oxidative decarboxylation of malate to pyruvate by malic enzyme, and the conversion of citrate into α-ketoglutarate by IDH1 (Schulze and Harris, 2012). Moreover, it is possible that glycogen degradation through PYGL provides precursors for the Krebs cycle or other biosynthetic pathways.

3) Finally, it is also possible that glycogen performs additional structural and/or signalling roles within cells, and cells normally regulate their glycogen levels very carefully. PYGL may simply act as an intracellular ‘glycogen sculptor’ in this respect. Future analyses will be required to address these open questions.

Of wider significance, the results presented here, together with a number of clinical observations, highlight glycogen metabolism, and PYGL in particular, as a promising target for cancer treatment. PYGL inhibitors are already being developed for the treatment of type 2 diabetes following effective trials in animal models (Agius, 2007). Although little is known about their clinical effects in humans, impairment of PYGL activity is predicted to be largely asymptomatic, based on the phenotypes of patients affected by Hers disease.

A major challenge of targeting cancer cell metabolism is the plasticity of the metabolic network that can easily adapt and overcome pitfalls occurring in one pathway. A small number of drugs targeting metabolic enzymes are currently in clinical trials, including 2-deoxyglucose (2-DG, targeting HKII), dichloroacetic acid (DCA, targeting PDK), Metformin (targeting mitochondrial complex I), and nicotinamide phosphoribosyltransferase (NAMPT) inhibitors (Vander Heiden, 2011). Consistent with redundancy being a feature of cancer metabolic pathways, early indications suggest that 2-DG does not seem to have a significant impact on tumour growth as monotherapy (Tennant et al., 2010). A similar scenario is likely to apply to the inhibition of PYGL; therefore, a comprehensive understanding of the metabolic perturbations associated with PYGL inhibition should reveal which other cellular processes are essential for viability. Additionally, because of the enrichment of lysosomes in PYGL-depleted cells, a potentially lethal drug combination could be predicted with PYGL inhibitors combined with lysosome permeabilizing drugs (Groth-Pedersen and Jaattela, 2010). Finally, given the increased reliance of cancer

cells on glycogen metabolism in hypoxia, the combination of PYGL inhibition with antiangiogenic drugs (bevacizumab) should be investigated.

7 LIST OF PUBLICATIONS

Favaro E., Bensaad K., Chong M.G., Tennant D.A., Ferguson D.J.P., Snell C., Steers G., Turley H., Li J.L., Günther U.L., Buffa F.M., McIntyre A., Harris A.L. Glucose utilisation via glycogen phosphorylase sustains proliferation and prevents premature senescence in cancer cells. *Cell Metabolism* 2012, 16(6).

Favaro E., Lord S., Harris A.L., Buffa F.M. Gene expression and hypoxia in breast cancer. *Genome Med,* 2011, 3(8):55.

Lord S., Favaro E., Harris A.L. Cancer metabolism as a target for therapy. *MIMS Oncology,* 2011, 5(1).

Favaro E., Ramachandran A., McCormick R., Gee H., Blancher C., Crosby M., Devlin C., Blick C., Buffa F., Li JL., Vojnovic B., Pires das Neves R., Glazer P., Iborra F., Ivan M., Ragoussis J., Harris AL. MicroRNA-210 regulates mitochondrial free radical response to hypoxia and krebs cycle in cancer cells by targeting iron sulfur cluster protein ISCU. *PLoS One*, 2010, 5(4).

8 REFERENCES

Adam, J., Hatipoglu, E., O'Flaherty, L., Ternette, N., Sahgal, N., Lockstone, H., Baban, D., Nye, E., Stamp, G.W., Wolhuter, K., Stevens, M., Fischer, R., Carmeliet, P., Maxwell, P.H., Pugh, C.W., Frizzell, N., Soga, T., Kessler, B.M., El-Bahrawy, M., Ratcliffe, P.J., and Pollard, P.J. (2011). Renal cyst formation in Fh1-deficient mice is independent of the Hif/Phd pathway: roles for fumarate in KEAP1 succination and Nrf2 signaling. Cancer Cell 20, 524-537.

Agius, L. (2007). New hepatic targets for glycaemic control in diabetes. Best practice & research. Clinical endocrinology & metabolism 21, 587-605.

Agius, L. (2010). Physiological control of liver glycogen metabolism: lessons from novel glycogen phosphorylase inhibitors. Mini Rev Med Chem 10, 1175-1187.

Ahn, B.Y., Trinh, D.L., Zajchowski, L.D., Lee, B., Elwi, A.N., and Kim, S.W. (2010). Tid1 is a new regulator of p53 mitochondrial translocation and apoptosis in cancer. Oncogene 29, 1155-1166.

Altenberg, B., and Greulich, K.O. (2004). Genes of glycolysis are ubiquitously overexpressed in 24 cancer classes. Genomics 84, 1014-1020.

Amary, M.F., Bacsi, K., Maggiani, F., Damato, S., Halai, D., Berisha, F., Pollock, R., O'Donnell, P., Grigoriadis, A., Diss, T., Eskandarpour, M., Presneau, N., Hogendoorn, P.C., Futreal, A., Tirabosco, R., and Flanagan, A.M. (2011). IDH1 and IDH2 mutations are frequent events in central chondrosarcoma and central and periosteal chondromas but not in other mesenchymal tumours. The Journal of pathology 224, 334-343.

Ambros, V. (2004). The functions of animal microRNAs. Nature 431, 350-355.

Astuti, D., Latif, F., Dallol, A., Dahia, P.L., Douglas, F., George, E., Skoldberg, F., Husebye, E.S., Eng, C., and Maher, E.R. (2001). Gene mutations in the succinate dehydrogenase subunit SDHB cause susceptibility to familial pheochromocytoma and to familial paraganglioma. American journal of human genetics 69, 49-54.
Bartel, D.P. (2009). MicroRNAs: target recognition and regulatory functions. Cell 136, 215-233.

Baysal, B.E., Ferrell, R.E., Willett-Brozick, J.E., Lawrence, E.C., Myssiorek, D., Bosch, A., van der Mey, A., Taschner, P.E., Rubinstein, W.S., Myers, E.N., Richard, C.W., 3rd, Cornelisse, C.J., Devilee, P., and Devlin, B. (2000). Mutations in SDHD, a mitochondrial complex II gene, in hereditary paraganglioma. Science 287, 848-851.

Bell, E.L., Klimova, T.A., Eisenbart, J., Schumacker, P.T., and Chandel, N.S. (2007). Mitochondrial reactive oxygen species trigger hypoxia-inducible factor-dependent extension of the replicative life span during hypoxia. Mol Cell Biol 27, 5737-5745.

Bensaad, K., Tsuruta, A., Selak, M.A., Vidal, M.N., Nakano, K., Bartrons, R., Gottlieb, E., and Vousden, K.H. (2006). TIGAR, a p53-inducible regulator of glycolysis and apoptosis. Cell 126, 107-120.

Berg, J.M., Tymoczko, J.L., and Stryer, L. (2002). Biochemistry. (New York: WH Freeman).

Bertout, J.A., Patel, S.A., and Simon, M.C. (2008). The impact of O2 availability on human cancer. Nat Rev Cancer 8, 967-975.

Brahimi-Horn, M.C., Bellot, G., and Pouyssegur, J. (2010). Hypoxia and energetic tumour metabolism. Curr Opin Genet Dev 21, 67-72.

Brown, A.M. (2004). Brain glycogen re-awakened. J Neurochem 89, 537-552.

Bruning, U., Cerone, L., Neufeld, Z., Fitzpatrick, S.F., Cheong, A., Scholz, C.C., Simpson, D.A., Leonard, M.O., Tambuwala, M.M., Cummins, E.P., and Taylor, C.T. (2011). MicroRNA-155 promotes resolution of hypoxia-inducible factor 1alpha activity during prolonged hypoxia. Mol Cell Biol 31, 4087-4096.

Bulteau, A.L., Ikeda-Saito, M., and Szweda, L.I. (2003). Redox-dependent modulation of aconitase activity in intact mitochondria. Biochemistry 42, 14846-14855.

Calin, G.A., Dumitru, C.D., Shimizu, M., Bichi, R., Zupo, S., Noch, E., Aldler, H., Rattan, S., Keating, M., Rai, K., Rassenti, L., Kipps, T., Negrini, M., Bullrich, F., and Croce, C.M. (2002). Frequent deletions and down-regulation of micro- RNA genes miR15 and miR16 at 13q14 in chronic lymphocytic leukemia. Proc Natl Acad Sci U S A 99, 15524-15529.

Calin, G.A., Ferracin, M., Cimmino, A., Di Leva, G., Shimizu, M., Wojcik, S.E., Iorio, M.V., Visone, R., Sever, N.I., Fabbri, M., Iuliano, R., Palumbo, T., Pichiorri, F., Roldo, C., Garzon, R., Sevignani, C., Rassenti, L., Alder, H., Volinia, S., Liu, C.G., Kipps, T.J., Negrini, M., and Croce, C.M. (2005). A MicroRNA signature associated with prognosis and progression in chronic lymphocytic leukemia. The New England journal of medicine 353, 1793-1801.

Camps, C., Buffa, F.M., Colella, S., Moore, J., Sotiriou, C., Sheldon, H., Harris, A.L., Gleadle, J.M., and Ragoussis, J. (2008). hsa-miR-210 Is induced by hypoxia and is an independent prognostic factor in breast cancer. Clin Cancer Res 14, 1340-1348.

Cantor, J.R., and Sabatini, D.M. (2012). Cancer cell metabolism: one hallmark, many faces. Cancer discovery 2, 881-898.

Cascio, S., D'Andrea, A., Ferla, R., Surmacz, E., Gulotta, E., Amodeo, V., Bazan, V., Gebbia, N., and Russo, A. (2010). miR-20b modulates VEGF expression by targeting HIF-1 alpha and STAT3 in MCF-7 breast cancer cells. Journal of cellular physiology 224, 242-249.

Cervera, A.M., Bayley, J.P., Devilee, P., and McCreath, K.J. (2009). Inhibition of succinate dehydrogenase dysregulates histone modification in mammalian cells. Molecular cancer 8, 89.

Chan, S.Y., Zhang, Y.Y., Hemann, C., Mahoney, C.E., Zweier, J.L., and Loscalzo, J. (2009). MicroRNA-210 controls mitochondrial metabolism during hypoxia by repressing the iron-sulfur cluster assembly proteins ISCU1/2. Cell Metab 10, 273-284.

Chan, Y.C., Banerjee, J., Choi, S.Y., and Sen, C.K. (2012). miR-210: the master hypoxamir. Microcirculation 19, 215-223.

Chang, T.C., Yu, D., Lee, Y.S., Wentzel, E.A., Arking, D.E., West, K.M., Dang, C.V., Thomas-Tikhonenko, A., and Mendell, J.T. (2008). Widespread microRNA repression by Myc contributes to tumorigenesis. Nature genetics 40, 43-50.

Chen, C., Ridzon, D.A., Broomer, A.J., Zhou, Z., Lee, D.H., Nguyen, J.T., Barbisin, M., Xu, N.L., Mahuvakar, V.R., Andersen, M.R., Lao, K.Q., Livak, K.J., and Guegler, K.J. (2005). Real-time quantification of microRNAs by stem-loop RT-PCR. Nucleic acids research 33, e179.

Chen, Z., Li, Y., Zhang, H., Huang, P., and Luthra, R. (2010). Hypoxia-regulated microRNA-210 modulates mitochondrial function and decreases ISCU and COX10 expression. Oncogene 29, 4362-4368.

Chio, C.C., Lin, J.W., Cheng, H.A., Chiu, W.T., Wang, Y.H., Wang, J.J., Hsing, C.H., and Chen, R.M. (2012). MicroRNA-210 targets antiapoptotic Bcl-2 expression and mediates hypoxia-induced apoptosis of neuroblastoma cells. Archives of toxicology.

Chitneni, S.K., Palmer, G.M., Zalutsky, M.R., and Dewhirst, M.W. (2011). Molecular imaging of hypoxia. J Nucl Med 52, 165-168.

Clerkin, J.S., Naughton, R., Quiney, C., and Cotter, T.G. (2008). Mechanisms of ROS modulated cell survival during carcinogenesis. Cancer Lett 266, 30-36.

Cocco, P. (1987). Does G6PD deficiency protect against cancer? A critical review. Journal of epidemiology and community health 41, 89-93.

Collado, M., Gil, J., Efeyan, A., Guerra, C., Schuhmacher, A.J., Barradas, M., Benguria, A., Zaballos, A., Flores, J.M., Barbacid, M., Beach, D., and Serrano, M. (2005). Tumour biology: senescence in premalignant tumours. Nature 436, 642.

Crosby, M.E., Kulshreshtha, R., Ivan, M., and Glazer, P.M. (2009). MicroRNA regulation of DNA repair gene expression in hypoxic stress. Cancer Res 69, 1221-1229.

Cunningham, J.T., Rodgers, J.T., Arlow, D.H., Vazquez, F., Mootha, V.K., and Puigserver, P. (2007). mTOR controls mitochondrial oxidative function through a YY1-PGC-1alpha transcriptional complex. Nature 450, 736-740.

Dagli, A.I., and Weinstein, D.A. (1993). Glycogen Storage Disease Type VI.

Dang, C.V. (2012). MYC on the path to cancer. Cell 149, 22-35.

Dang, C.V., Le, A., and Gao, P. (2009a). MYC-induced cancer cell energy metabolism and therapeutic opportunities. Clin Cancer Res 15, 6479-6483.

Dang, L., White, D.W., Gross, S., Bennett, B.D., Bittinger, M.A., Driggers, E.M., Fantin, V.R., Jang, H.G., Jin, S., Keenan, M.C., Marks, K.M., Prins, R.M., Ward, P.S., Yen, K.E., Liau, L.M., Rabinowitz, J.D., Cantley, L.C., Thompson, C.B., Vander Heiden, M.G., and Su, S.M. (2009b). Cancer-associated IDH1 mutations produce 2-hydroxyglutarate. Nature 462, 739-744.

DeBerardinis, R.J. (2008). Is cancer a disease of abnormal cellular metabolism? New angles on an old idea. Genetics in medicine : official journal of the American College of Medical Genetics 10, 767-777.

DeBerardinis, R.J., and Cheng, T. (2010). Q's next: the diverse functions of glutamine in metabolism, cell biology and cancer. Oncogene 29, 313-324.

Denko, N.C. (2008). Hypoxia, HIF1 and glucose metabolism in the solid tumour. Nat Rev Cancer 8, 705-713.

Denko, N.C., Fontana, L.A., Hudson, K.M., Sutphin, P.D., Raychaudhuri, S., Altman, R., and Giaccia, A.J. (2003). Investigating hypoxic tumor physiology through gene expression patterns. Oncogene 22, 5907-5914.

Devlin, C., Greco, S., Martelli, F., and Ivan, M. (2011). miR-210: More than a silent player in hypoxia. IUBMB Life 63, 94-100.

Echeverri, C.J., Beachy, P.A., Baum, B., Boutros, M., Buchholz, F., Chanda, S.K., Downward, J., Ellenberg, J., Fraser, A.G., Hacohen, N., Hahn, W.C., Jackson, A.L., Kiger, A., Linsley, P.S., Lum, L., Ma, Y., Mathey-Prevot, B., Root, D.E., Sabatini, D.M., Taipale, J., Perrimon, N., and Bernards, R. (2006). Minimizing the risk of reporting false positives in large-scale RNAi screens. Nature methods 3, 777-779.

el-Deiry, W.S., Tokino, T., Velculescu, V.E., Levy, D.B., Parsons, R., Trent, J.M., Lin, D., Mercer, W.E., Kinzler, K.W., and Vogelstein, B. (1993). WAF1, a potential mediator of p53 tumor suppression. Cell 75, 817-825.

Fabian, M.R., and Sonenberg, N. (2012). The mechanics of miRNA-mediated gene silencing: a look under the hood of miRISC. Nature structural & molecular biology 19, 586-593.

Fang, R., Xiao, T., Fang, Z., Sun, Y., Li, F., Gao, Y., Feng, Y., Li, L., Wang, Y., Liu, X., Chen, H., Liu, X.Y., and Ji, H. (2012). MicroRNA-143 (miR-143) regulates cancer glycolysis via targeting hexokinase 2 gene. J Biol Chem 287, 23227-23235.

Fasanaro, P., D'Alessandra, Y., Di Stefano, V., Melchionna, R., Romani, S., Pompilio, G., Capogrossi, M.C., and Martelli, F. (2008). MicroRNA-210 modulates endothelial cell response to hypoxia and inhibits the receptor tyrosine kinase ligand Ephrin-A3. J Biol Chem 283, 15878-15883.

Fasanaro, P., Greco, S., Lorenzi, M., Pescatori, M., Brioschi, M., Kulshreshtha, R., Banfi, C., Stubbs, A., Calin, G.A., Ivan, M., Capogrossi, M.C., and Martelli, F. (2009). An integrated approach for experimental target identification of hypoxia-induced miR-210. J Biol Chem 284, 35134-35143.

Fassone, E., and Rahman, S. (2012). Complex I deficiency: clinical features, biochemistry and molecular genetics. Journal of medical genetics 49, 578-590.

Favaro, E., Lord, S., Harris, A.L., and Buffa, F.M. (2011). Gene expression and hypoxia in breast cancer. Genome medicine 3, 55.

Favaro, E., Ramachandran, A., McCormick, R., Gee, H., Blancher, C., Crosby, M., Devlin, C., Blick, C., Buffa, F., Li, J.L., Vojnovic, B., Pires das Neves, R., Glazer, P., Iborra, F., Ivan, M., Ragoussis, J., and Harris, A.L. (2010). MicroRNA-210 regulates mitochondrial free radical response to hypoxia and krebs cycle in cancer cells by targeting iron sulfur cluster protein ISCU. PLoS One 5, e10345.

Favre, C., Aguilar, P.S., and Carrillo, M.C. (2008). Oxidative stress and chronological aging in glycogen-phosphorylase-deleted yeast. Free Radic Biol Med 45, 1446-1456.

Fei, X., Qi, M., Wu, B., Song, Y., Wang, Y., and Li, T. (2012). MicroRNA-195-5p suppresses glucose uptake and proliferation of human bladder cancer T24 cells by regulating GLUT3 expression. FEBS Lett 586, 392-397.

Ferrer, J.C., Favre, C., Gomis, R.R., Fernandez-Novell, J.M., Garcia-Rocha, M., de la Iglesia, N., Cid, E., and Guinovart, J.J. (2003). Control of glycogen deposition. FEBS Lett 546, 127-132.

Filipowicz, W., Bhattacharyya, S.N., and Sonenberg, N. (2008). Mechanisms of post-transcriptional regulation by microRNAs: are the answers in sight? Nat Rev Genet 9, 102-114.

Frezza, C., Zheng, L., Folger, O., Rajagopalan, K.N., MacKenzie, E.D., Jerby, L., Micaroni, M., Chaneton, B., Adam, J., Hedley, A., Kalna, G., Tomlinson, I.P., Pollard, P.J., Watson, D.G., Deberardinis, R.J., Shlomi, T., Ruppin, E., and Gottlieb, E. (2011). Haem oxygenase is synthetically lethal with the tumour suppressor fumarate hydratase. Nature 477, 225-228.

Fuchs, B.C., and Bode, B.P. (2005). Amino acid transporters ASCT2 and LAT1 in cancer: partners in crime? Seminars in cancer biology 15, 254-266.

Fyles, A., Milosevic, M., Hedley, D., Pintilie, M., Levin, W., Manchul, L., and Hill, R.P. (2002). Tumor hypoxia has independent predictor impact only in patients with node-negative cervix cancer. J Clin Oncol 20, 680-687.

Gao, P., Tchernyshyov, I., Chang, T.C., Lee, Y.S., Kita, K., Ochi, T., Zeller, K.I., De Marzo, A.M., Van Eyk, J.E., Mendell, J.T., and Dang, C.V. (2009). c-Myc suppression of miR-23a/b enhances mitochondrial glutaminase expression and glutamine metabolism. Nature 458, 762-765.

Gao, P., Zhang, H., Dinavahi, R., Li, F., Xiang, Y., Raman, V., Bhujwalla, Z.M., Felsher, D.W., Cheng, L., Pevsner, J., Lee, L.A., Semenza, G.L., and Dang, C.V. (2007). HIF-dependent antitumorigenic effect of antioxidants in vivo. Cancer Cell 12, 230-238.

Garzon, R., Marcucci, G., and Croce, C.M. (2010). Targeting microRNAs in cancer: rationale, strategies and challenges. Nat Rev Drug Discov 9, 775-789.

Gee, H.E., Camps, C., Buffa, F.M., Patiar, S., Winter, S.C., Betts, G., Homer, J., Corbridge, R., Cox, G., West, C.M., Ragoussis, J., and Harris, A.L. (2010). hsa-mir-210 is a marker of tumor hypoxia and a prognostic factor in head and neck cancer. Cancer 116, 2148-2158.

Giannakakis, A., Sandaltzopoulos, R., Greshock, J., Liang, S., Huang, J., Hasegawa, K., Li, C., O'Brien-Jenkins, A., Katsaros, D., Weber, B.L., Simon, C., Coukos, G., and Zhang, L. (2008). miR-210 links hypoxia with cell cycle regulation and is deleted in human epithelial ovarian cancer. Cancer Biol Ther 7, 255-264.

Graeber, T.G., Osmanian, C., Jacks, T., Housman, D.E., Koch, C.J., Lowe, S.W., and Giaccia, A.J. (1996). Hypoxia-mediated selection of cells with diminished apoptotic potential in solid tumours. Nature 379, 88-91.

Green, A., and Beer, P. (2010). Somatic mutations of IDH1 and IDH2 in the leukemic transformation of myeloproliferative neoplasms. The New England journal of medicine 362, 369-370.

Gregersen, L.H., Jacobsen, A., Frankel, L.B., Wen, J., Krogh, A., and Lund, A.H. (2012). MicroRNA-143 down-regulates Hexokinase 2 in colon cancer cells. BMC Cancer 12, 232.

Grempler, R., Zibrova, D., Schoelch, C., van Marle, A., Rippmann, J.F., and Redemann, N. (2007). Normalization of prandial blood glucose and improvement of glucose tolerance by liver-specific inhibition of SH2 domain containing inositol phosphatase 2 (SHIP2) in diabetic KKAy mice: SHIP2 inhibition causes insulin-mimetic effects on glycogen metabolism, gluconeogenesis, and glycolysis. Diabetes 56, 2235-2241.

Griffin, J.L., and Shockcor, J.P. (2004). Metabolic profiles of cancer cells. Nat Rev Cancer 4, 551-561.

Groth-Pedersen, L., and Jaattela, M. (2010). Combating apoptosis and multidrug resistant cancers by targeting lysosomes. Cancer Lett.
Groves, A.M., Win, T., Haim, S.B., and Ell, P.J. (2007). Non-[18F]FDG PET in clinical oncology. Lancet Oncol 8, 822-830.

Guimbellot, J.S., Erickson, S.W., Mehta, T., Wen, H., Page, G.P., Sorscher, E.J., and Hong, J.S. (2009). Correlation of microRNA levels during hypoxia with predicted target mRNAs through genome-wide microarray analysis. BMC medical genomics 2, 15.

Guo, H., Ingolia, N.T., Weissman, J.S., and Bartel, D.P. (2010). Mammalian microRNAs predominantly act to decrease target mRNA levels. Nature 466, 835-840.

Guzy, R.D., Hoyos, B., Robin, E., Chen, H., Liu, L., Mansfield, K.D., Simon, M.C., Hammerling, U., and Schumacker, P.T. (2005). Mitochondrial complex III is required for hypoxia-induced ROS production and cellular oxygen sensing. Cell Metab 1, 401-408.

Han, Y., Chen, J., Zhao, X., Liang, C., Wang, Y., Sun, L., Jiang, Z., Zhang, Z., Yang, R., Chen, J., Li, Z., Tang, A., Li, X., Ye, J., Guan, Z., Gui, Y., and Cai, Z. (2011). MicroRNA expression signatures of bladder cancer revealed by deep sequencing. PLoS One 6, e18286.

Hanahan, D., and Weinberg, R.A. (2000). The hallmarks of cancer. Cell 100, 57-70.
Hanahan, D., and Weinberg, R.A. (2011). Hallmarks of cancer: the next generation. Cell 144, 646-674.

Harper, J.W., Adami, G.R., Wei, N., Keyomarsi, K., and Elledge, S.J. (1993). The p21 Cdk-interacting protein Cip1 is a potent inhibitor of G1 cyclin-dependent kinases. Cell 75, 805-816.

Hebert, C., Norris, K., Scheper, M.A., Nikitakis, N., and Sauk, J.J. (2007). High mobility group A2 is a target for miRNA-98 in head and neck squamous cell carcinoma. Molecular cancer 6, 5.

Ho, A.S., Huang, X., Cao, H., Christman-Skieller, C., Bennewith, K., Le, Q.T., and Koong, A.C. (2010). Circulating miR-210 as a Novel Hypoxia Marker in Pancreatic Cancer. Translational oncology 3, 109-113.

Hockel, M., Schlenger, K., Aral, B., Mitze, M., Schaffer, U., and Vaupel, P. (1996). Association between tumor hypoxia and malignant progression in advanced cancer of the uterine cervix. Cancer Res 56, 4509-4515.

Hong, L., Yang, J., Han, Y., Lu, Q., Cao, J., and Syed, L. (2012). High expression of miR-210 predicts poor survival in patients with breast cancer: a meta-analysis. Gene 507, 135-138.

Hsu, S.H., Wang, B., Kota, J., Yu, J., Costinean, S., Kutay, H., Yu, L., Bai, S., La Perle, K., Chivukula, R.R., Mao, H., Wei, M., Clark, K.R., Mendell, J.R., Caligiuri, M.A., Jacob, S.T., Mendell, J.T., and Ghoshal, K. (2012). Essential metabolic, anti-inflammatory, and anti-tumorigenic functions of miR-122 in liver. The Journal of clinical investigation 122, 2871-2883.

Hu, J., Xu, Y., Hao, J., Wang, S., Li, C., and Meng, S. (2012). MiR-122 in hepatic function and liver diseases. Protein & cell 3, 364-371.

Hu, W., Chan, C.S., Wu, R., Zhang, C., Sun, Y., Song, J.S., Tang, L.H., Levine, A.J., and Feng, Z. (2010). Negative regulation of tumor suppressor p53 by microRNA miR-504. Mol Cell 38, 689-699.

Huang, X., Ding, L., Bennewith, K.L., Tong, R.T., Welford, S.M., Ang, K.K., Story, M., Le, Q.T., and Giaccia, A.J. (2009). Hypoxia-inducible mir-210 regulates normoxic gene expression involved in tumor initiation. Mol Cell 35, 856-867.
Huang, X., Le, Q.T., and Giaccia, A.J. (2010). MiR-210--micromanager of the hypoxia pathway. Trends in molecular medicine 16, 230-237.

Hwang-Verslues, W.W., Chang, P.H., Wei, P.C., Yang, C.Y., Huang, C.K., Kuo, W.H., Shew, J.Y., Chang, K.J., Lee, E.Y., and Lee, W.H. (2011). miR-495 is upregulated by E12/E47 in breast cancer stem cells, and promotes oncogenesis and hypoxia resistance via downregulation of E-cadherin and REDD1. Oncogene 30, 2463-2474.

Isaacs, J.S., Jung, Y.J., Mole, D.R., Lee, S., Torres-Cabala, C., Chung, Y.L., Merino, M., Trepel, J., Zbar, B., Toro, J., Ratcliffe, P.J., Linehan, W.M., and Neckers, L. (2005). HIF overexpression correlates with biallelic loss of fumarate hydratase in renal cancer: novel role of fumarate in regulation of HIF stability. Cancer Cell 8, 143-153.

Ivan, M., Kondo, K., Yang, H., Kim, W., Valiando, J., Ohh, M., Salic, A., Asara, J.M., Lane, W.S., and Kaelin, W.G., Jr. (2001). HIFalpha targeted for VHL-mediated destruction by proline hydroxylation: implications for O2 sensing. Science 292, 464-468.

Ivascu, A., and Kubbies, M. (2007). Diversity of cell-mediated adhesions in breast cancer spheroids. Int J Oncol 31, 1403-1413.

Jiang, S., Heller, B., Tagliabracci, V.S., Zhai, L., Irimia, J.M., DePaoli-Roach, A.A., Wells, C.D., Skurat, A.V., and Roach, P.J. (2010). Starch binding domain-containing protein 1/genethonin 1 is a novel participant in glycogen metabolism. J Biol Chem 285, 34960-34971.

Johnson, L.N. (1992). Glycogen phosphorylase: control by phosphorylation and allosteric effectors. FASEB J 6, 2274-2282.

Johnson, R.F., and Perkins, N.D. (2012). Nuclear factor-kappaB, p53, and mitochondria: regulation of cellular metabolism and the Warburg effect. Trends in biochemical sciences 37, 317-324.

Jones, R.G., Plas, D.R., Kubek, S., Buzzai, M., Mu, J., Xu, Y., Birnbaum, M.J., and Thompson, C.B. (2005). AMP-activated protein kinase induces a p53-dependent metabolic checkpoint. Mol Cell 18, 283-293.

Jopling, C.L., Yi, M., Lancaster, A.M., Lemon, S.M., and Sarnow, P. (2005). Modulation of hepatitis C virus RNA abundance by a liver-specific MicroRNA. Science 309, 1577-1581.

Jubb, A.M., Buffa, F.M., and Harris, A.L. (2010). Assessment of tumour hypoxia for prediction of response to therapy and cancer prognosis. J Cell Mol Med 14, 18-29.

Jung, E.J., Santarpia, L., Kim, J., Esteva, F.J., Moretti, E., Buzdar, A.U., Di Leo, A., Le, X.F., Bast, R.C., Jr., Park, S.T., Pusztai, L., and Calin, G.A. (2012). Plasma microRNA 210 levels correlate with sensitivity to trastuzumab and tumor presence in breast cancer patients. Cancer 118, 2603-2614.

Kaelin, W.G., Jr. (2002). Molecular basis of the VHL hereditary cancer syndrome. Nat Rev Cancer 2, 673-682.

Kallunki, T., Olsen, O.D., and Jaattela, M. (2012). Cancer-associated lysosomal changes: friends or foes? Oncogene.

Kim, H.W., Haider, H.K., Jiang, S., and Ashraf, M. (2009). Ischemic preconditioning augments survival of stem cells via miR-210 expression by targeting caspase-8-associated protein 2. J Biol Chem 284, 33161-33168.

Kim, J.W., Tchernyshyov, I., Semenza, G.L., and Dang, C.V. (2006). HIF-1-mediated expression of pyruvate dehydrogenase kinase: a metabolic switch required for cellular adaptation to hypoxia. Cell Metab 3, 177-185.

Kroemer, G., and Pouyssegur, J. (2008). Tumor cell metabolism: cancer's Achilles' heel. Cancer Cell 13, 472-482.

Kuilman, T., Michaloglou, C., Mooi, W.J., and Peeper, D.S. (2010). The essence of senescence. Genes Dev 24, 2463-2479.

Kulshreshtha, R., Ferracin, M., Wojcik, S.E., Garzon, R., Alder, H., Agosto-Perez, F.J., Davuluri, R., Liu, C.G., Croce, C.M., Negrini, M., Calin, G.A., and Ivan, M. (2007). A microRNA signature of hypoxia. Mol Cell Biol 27, 1859-1867.

Kumar, M.S., Lu, J., Mercer, K.L., Golub, T.R., and Jacks, T. (2007). Impaired microRNA processing enhances cellular transformation and tumorigenesis. Nature genetics 39, 673-677.

Kurz, D.J., Decary, S., Hong, Y., and Erusalimsky, J.D. (2000). Senescence-associated (beta)-galactosidase reflects an increase in lysosomal mass during replicative ageing of human endothelial cells. J Cell Sci 113 (Pt 20), 3613-3622.

Launonen, V., Vierimaa, O., Kiuru, M., Isola, J., Roth, S., Pukkala, E., Sistonen, P., Herva, R., and Aaltonen, L.A. (2001). Inherited susceptibility to uterine leiomyomas and renal cell cancer. Proc Natl Acad Sci U S A 98, 3387-3392.

Lawrie, C.H., Gal, S., Dunlop, H.M., Pushkaran, B., Liggins, A.P., Pulford, K., Banham, A.H., Pezzella, F., Boultwood, J., Wainscoat, J.S., Hatton, C.S., and Harris, A.L. (2008). Detection of elevated levels of tumour-associated microRNAs in serum of patients with diffuse large B-cell lymphoma. Br J Haematol 141, 672-675.

Le, M.T., Teh, C., Shyh-Chang, N., Xie, H., Zhou, B., Korzh, V., Lodish, H.F., and Lim, B. (2009). MicroRNA-125b is a novel negative regulator of p53. Genes Dev 23, 862-876.

Lee, D.W., Futami, M., Carroll, M., Feng, Y., Wang, Z., Fernandez, M., Whichard, Z., Chen, Y., Kornblau, S., Shpall, E.J., Bueso-Ramos, C.E., and Corey, S.J. (2012). Loss of SHIP-1 protein expression in high-risk myelodysplastic syndromes is associated with miR-210 and miR-155. Oncogene 31, 4085-4094.

Lee, W.N., Guo, P., Lim, S., Bassilian, S., Lee, S.T., Boren, J., Cascante, M., Go, V.L., and Boros, L.G. (2004a). Metabolic sensitivity of pancreatic tumour cell apoptosis to glycogen phosphorylase inhibitor treatment. Br J Cancer 91, 2094-2100.

Lee, Y., Kim, M., Han, J., Yeom, K.H., Lee, S., Baek, S.H., and Kim, V.N. (2004b). MicroRNA genes are transcribed by RNA polymerase II. The EMBO journal 23, 4051-4060.

Lei, Z., Li, B., Yang, Z., Fang, H., Zhang, G.M., Feng, Z.H., and Huang, B. (2009). Regulation of HIF-1alpha and VEGF by miR-20b tunes tumor cells to adapt to the alteration of oxygen concentration. PLoS One 4, e7629.

Li, J., Donath, S., Li, Y., Qin, D., Prabhakar, B.S., and Li, P. (2010). miR-30 regulates mitochondrial fission through targeting p53 and the dynamin-related protein-1 pathway. PLoS Genet 6, e1000795.

Li, J.L., Sainson, R.C., Shi, W., Leek, R., Harrington, L.S., Preusser, M., Biswas, S., Turley, H., Heikamp, E., Hainfellner, J.A., and Harris, A.L. (2007). Delta-like 4 Notch ligand regulates tumor angiogenesis, improves tumor vascular function, and promotes tumor growth in vivo. Cancer Res 67, 11244-11253.

Liu, A., and Xu, X. (2011). MicroRNA isolation from formalin-fixed, paraffin-embedded tissues. Methods Mol Biol 724, 259-267.

Liu, Y., and Bodmer, W.F. (2006). Analysis of P53 mutations and their expression in 56 colorectal cancer cell lines. Proc Natl Acad Sci U S A 103, 976-981.

Locasale, J.W., Grassian, A.R., Melman, T., Lyssiotis, C.A., Mattaini, K.R., Bass, A.J., Heffron, G., Metallo, C.M., Muranen, T., Sharfi, H., Sasaki, A.T., Anastasiou, D., Mullarky, E., Vokes, N.I., Sasaki, M., Beroukhim, R., Stephanopoulos, G., Ligon, A.H., Meyerson, M., Richardson, A.L., Chin, L., Wagner, G., Asara, J.M., Brugge, J.S., Cantley, L.C., and Vander Heiden, M.G. (2011). Phosphoglycerate dehydrogenase diverts glycolytic flux and contributes to oncogenesis. Nature genetics 43, 869-874.

Louzao, M.C., Espina, B., Vieytes, M.R., Vega, F.V., Rubiolo, J.A., Baba, O., Terashima, T., and Botana, L.M. (2008). "Fluorescent glycogen" formation with sensibility for in vivo and in vitro detection. Glycoconjugate journal 25, 503-510.

Lu, J., Getz, G., Miska, E.A., Alvarez-Saavedra, E., Lamb, J., Peck, D., Sweet-Cordero, A., Ebert, B.L., Mak, R.H., Ferrando, A.A., Downing, J.R., Jacks, T., Horvitz, H.R., and Golub, T.R. (2005). MicroRNA expression profiles classify human cancers. Nature 435, 834-838.

Lu, T., and Finkel, T. (2008). Free radicals and senescence. Exp Cell Res 314, 1918-1922.

Lujambio, A., and Lowe, S.W. (2012). The microcosmos of cancer. Nature 482, 347-355.

Lunt, S.Y., and Vander Heiden, M.G. (2011). Aerobic glycolysis: meeting the metabolic requirements of cell proliferation. Annu Rev Cell Dev Biol 27, 441-464.

Ma, D., Wang, J., Zhao, Y., Lee, W.N., Xiao, J., Go, V.L., Wang, Q., Recker, R.R., and Xiao, G.G. (2012). Inhibition of glycogen phosphorylation induces changes in cellular proteome and signaling pathways in MIA pancreatic cancer cells. Pancreas 41, 397-408.

Mamedova, L.K., Shneyvays, V., Katz, A., and Shainberg, A. (2003). Mechanism of glycogen supercompensation in rat skeletal muscle cultures. Mol Cell Biochem 250, 11-19.

Matoba, S., Kang, J.G., Patino, W.D., Wragg, A., Boehm, M., Gavrilova, O., Hurley, P.J., Bunz, F., and Hwang, P.M. (2006). p53 regulates mitochondrial respiration. Science 312, 1650-1653.

Mazurek, S. (2011). Pyruvate kinase type M2: a key regulator of the metabolic budget system in tumor cells. The international journal of biochemistry & cell biology 43, 969-980.

McBride, A., Ghilagaber, S., Nikolaev, A., and Hardie, D.G. (2009). The glycogen-binding domain on the AMPK beta subunit allows the kinase to act as a glycogen sensor. Cell Metab 9, 23-34.

Mizuno, Y., Tokuzawa, Y., Ninomiya, Y., Yagi, K., Yatsuka-Kanesaki, Y., Suda, T., Fukuda, T., Katagiri, T., Kondoh, Y., Amemiya, T., Tashiro, H., and Okazaki, Y. (2009). miR-210 promotes osteoblastic differentiation through inhibition of AcvR1b. FEBS Lett 583, 2263-2268.

Mochel, F., Knight, M.A., Tong, W.H., Hernandez, D., Ayyad, K., Taivassalo, T., Andersen, P.M., Singleton, A., Rouault, T.A., Fischbeck, K.H., and Haller, R.G. (2008). Splice mutation in the iron-sulfur cluster scaffold protein ISCU causes myopathy with exercise intolerance. American journal of human genetics 82, 652-660.

Moiseeva, O., Bourdeau, V., Roux, A., Deschenes-Simard, X., and Ferbeyre, G. (2009). Mitochondrial dysfunction contributes to oncogene-induced senescence. Mol Cell Biol 29, 4495-4507.

Mole, D.R., Blancher, C., Copley, R.R., Pollard, P.J., Gleadle, J.M., Ragoussis, J., and Ratcliffe, P.J. (2009). Genome-wide association of hypoxia-inducible factor (HIF)-1alpha and HIF-2alpha DNA binding with expression profiling of hypoxia-inducible transcripts. J Biol Chem 284, 16767-16775.

Mracek, T., Drahota, Z., and Houstek, J. (2012). The function and the role of the mitochondrial glycerol-3-phosphate dehydrogenase in mammalian tissues. Biochim Biophys Acta.

Muhlenhoff, U., and Lill, R. (2000). Biogenesis of iron-sulfur proteins in eukaryotes: a novel task of mitochondria that is inherited from bacteria. Biochim Biophys Acta 1459, 370-382.

Mullen, A.R., Wheaton, W.W., Jin, E.S., Chen, P.H., Sullivan, L.B., Cheng, T., Yang, Y., Linehan, W.M., Chandel, N.S., and DeBerardinis, R.J. (2012). Reductive carboxylation supports growth in tumour cells with defective mitochondria. Nature 481, 385-388.

Murphy, M.P. (2009). How mitochondria produce reactive oxygen species. Biochem J 417, 1-13.

Neal, C.S., Michael, M.Z., Rawlings, L.H., Van der Hoek, M.B., and Gleadle, J.M. (2010). The VHL-dependent regulation of microRNAs in renal cancer. BMC medicine 8, 64.

Newgard, C.B., Hwang, P.K., and Fletterick, R.J. (1989). The family of glycogen phosphorylases: structure and function. Crit Rev Biochem Mol Biol 24, 69-99.

Nielsen, J.N., Wojtaszewski, J.F., Haller, R.G., Hardie, D.G., Kemp, B.E., Richter, E.A., and Vissing, J. (2002). Role of 5'AMP-activated protein kinase in glycogen synthase activity and glucose utilization: insights from patients with McArdle's disease. J Physiol 541, 979-989.

Niemann, S., and Muller, U. (2000). Mutations in SDHC cause autosomal dominant paraganglioma, type 3. Nature genetics 26, 268-270.

Nordsmark, M., Bentzen, S.M., Rudat, V., Brizel, D., Lartigau, E., Stadler, P., Becker, A., Adam, M., Molls, M., Dunst, J., Terris, D.J., and Overgaard, J. (2005). Prognostic value of tumor oxygenation in 397 head and neck tumors after primary radiation therapy. An international multi-center study. Radiother Oncol 77, 18-24.

Oikonomakos, N.G., Zographos, S.E., Skamnaki, V.T., and Archontis, G. (2002). The 1.76 A resolution crystal structure of glycogen phosphorylase B complexed with glucose, and CP320626, a potential antidiabetic drug. Bioorg Med Chem 10, 1313-1319.

Olsson, A., Lind, L., Thornell, L.E., and Holmberg, M. (2008). Myopathy with lactic acidosis is linked to chromosome 12q23.3-24.11 and caused by an intron mutation in the ISCU gene resulting in a splicing defect. Human molecular genetics 17, 1666-1672.

Ortiz-Barahona, A., Villar, D., Pescador, N., Amigo, J., and del Peso, L. (2010). Genome-wide identification of hypoxia-inducible factor binding sites and target genes by a probabilistic model integrating transcription-profiling data and in silico binding site prediction. Nucleic acids research 38, 2332-2345.

Paez-Ribes, M., Allen, E., Hudock, J., Takeda, T., Okuyama, H., Vinals, F., Inoue, M., Bergers, G., Hanahan, D., and Casanovas, O. (2009). Antiangiogenic therapy elicits malignant progression of tumors to increased local invasion and distant metastasis. Cancer Cell 15, 220-231.

Parsons, D.W., Jones, S., Zhang, X., Lin, J.C., Leary, R.J., Angenendt, P., Mankoo, P., Carter, H., Siu, I.M., Gallia, G.L., Olivi, A., McLendon, R., Rasheed, B.A., Keir, S., Nikolskaya, T., Nikolsky, Y., Busam, D.A., Tekleab, H., Diaz, L.A., Jr., Hartigan, J., Smith, D.R., Strausberg, R.L., Marie, S.K., Shinjo, S.M., Yan, H., Riggins, G.J., Bigner, D.D., Karchin, R., Papadopoulos, N., Parmigiani, G., Vogelstein, B., Velculescu, V.E., and Kinzler, K.W. (2008). An integrated genomic analysis of human glioblastoma multiforme. Science 321, 1807-1812.

Pelletier, J., Bellot, G., Gounon, P., Lacas-Gervais, S., Pouyssegur, J., and Mazure, N.M. (2012). Glycogen Synthesis is Induced in Hypoxia by the Hypoxia-Inducible Factor and Promotes Cancer Cell Survival. Front Oncol 2, 18.

Perkins, N.D. (2007). Integrating cell-signalling pathways with NF-kappaB and IKK function. Nature reviews. Molecular cell biology 8, 49-62.

Pescador, N., Villar, D., Cifuentes, D., Garcia-Rocha, M., Ortiz-Barahona, A., Vazquez, S., Ordonez, A., Cuevas, Y., Saez-Morales, D., Garcia-Bermejo, M.L., Landazuri, M.O., Guinovart, J., and del Peso, L. (2010). Hypoxia promotes glycogen accumulation through hypoxia inducible factor (HIF)-mediated induction of glycogen synthase 1. PLoS One 5, e9644.

Peschiaroli, A., Giacobbe, A., Formosa, A., Markert, E.K., Bongiorno-Borbone, L., Levine, A.J., Candi, E., D'Alessandro, A., Zolla, L., Finazzi Agro, A., and Melino, G. (2012). miR-143 regulates hexokinase 2 expression in cancer cells. Oncogene.

Polimeni, M., Voena, C., Kopecka, J., Riganti, C., Pescarmona, G., Bosia, A., and Ghigo, D. (2011). Modulation of doxorubicin resistance by the glucose-6-phosphate dehydrogenase activity. Biochem J 439, 141-149.

Possemato, R., Marks, K.M., Shaul, Y.D., Pacold, M.E., Kim, D., Birsoy, K., Sethumadhavan, S., Woo, H.K., Jang, H.G., Jha, A.K., Chen, W.W., Barrett, F.G., Stransky, N., Tsun, Z.Y., Cowley, G.S., Barretina, J., Kalaany, N.Y., Hsu, P.P., Ottina, K., Chan, A.M., Yuan, B., Garraway, L.A., Root, D.E., Mino-Kenudson, M., Brachtel, E.F., Driggers, E.M., and Sabatini, D.M. (2011). Functional genomics reveal that the serine synthesis pathway is essential in breast cancer. Nature 476, 346-350.

Postema, E.J., McEwan, A.J., Riauka, T.A., Kumar, P., Richmond, D.A., Abrams, D.N., and Wiebe, L.I. (2009). Initial results of hypoxia imaging using 1-alpha-D: -(5-deoxy-5-[18F]-fluoroarabinofuranosyl)-2-nitroimidazole (18F-FAZA). Eur J Nucl Med Mol Imaging 36, 1565-1573.

Poyton, R.O., Ball, K.A., and Castello, P.R. (2009). Mitochondrial generation of free radicals and hypoxic signaling. Trends in endocrinology and metabolism: TEM 20, 332-340.

Praly, J.P., and Vidal, S. (2010). Inhibition of glycogen phosphorylase in the context of type 2 diabetes, with focus on recent inhibitors bound at the active site. Mini Rev Med Chem 10, 1102-1126.

Pugh, C.W., and Ratcliffe, P.J. (2003). Regulation of angiogenesis by hypoxia: role of the HIF system. Nat Med 9, 677-684.

Puissegur, M.P., Mazure, N.M., Bertero, T., Pradelli, L., Grosso, S., Robbe-Sermesant, K., Maurin, T., Lebrigand, K., Cardinaud, B., Hofman, V., Fourre, S., Magnone, V., Ricci, J.E., Pouyssegur, J., Gounon, P., Hofman, P., Barbry, P., and

Mari, B. (2011). miR-210 is overexpressed in late stages of lung cancer and mediates mitochondrial alterations associated with modulation of HIF-1 activity. Cell Death Differ 18, 465-478.

Pulkkinen, K., Malm, T., Turunen, M., Koistinaho, J., and Yla-Herttuala, S. (2008). Hypoxia induces microRNA miR-210 in vitro and in vivo ephrin-A3 and neuronal pentraxin 1 are potentially regulated by miR-210. FEBS Lett 582, 2397-2401.

Qin, L., Chen, Y., Niu, Y., Chen, W., Wang, Q., Xiao, S., Li, A., Xie, Y., Li, J., Zhao, X., He, Z., and Mo, D. (2010). A deep investigation into the adipogenesis mechanism: profile of microRNAs regulating adipogenesis by modulating the canonical Wnt/beta-catenin signaling pathway. BMC genomics 11, 320.

Quinlan, C.L., Orr, A.L., Perevoshchikova, I.V., Treberg, J.R., Ackrell, B.A., and Brand, M.D. (2012). Mitochondrial complex II can generate reactive oxygen species at high rates in both the forward and reverse reactions. J Biol Chem 287, 27255-27264.

Rabinowitz, J.D., and White, E. (2010). Autophagy and metabolism. Science 330, 1344-1348.

Ramanathan, A., and Schreiber, S.L. (2009). Direct control of mitochondrial function by mTOR. Proc Natl Acad Sci U S A 106, 22229-22232.

Ratcliffe, P.J., O'Rourke, J.F., Maxwell, P.H., and Pugh, C.W. (1998). Oxygen sensing, hypoxia-inducible factor-1 and the regulation of mammalian gene expression. J Exp Biol 201, 1153-1162.

Redova, M., Poprach, A., Besse, A., Iliev, R., Nekvindova, J., Lakomy, R., Radova, L., Svoboda, M., Dolezel, J., Vyzula, R., and Slaby, O. (2012). MiR-210 expression in tumor tissue and in vitro effects of its silencing in renal cell carcinoma. Tumour biology : the journal of the International Society for Oncodevelopmental Biology and Medicine.

Ren, Y., Gao, J., Liu, J.Q., Wang, X.W., Gu, J.J., Huang, H.J., Gong, Y.F., and Li, Z.S. (2012). Differential signature of fecal microRNAs in patients with pancreatic cancer. Molecular medicine reports 6, 201-209.

Roach, P.J., Depaoli-Roach, A.A., Hurley, T.D., and Tagliabracci, V.S. (2012). Glycogen and its metabolism: some new developments and old themes. Biochem J 441, 763-787.

Rodriguez, A., Griffiths-Jones, S., Ashurst, J.L., and Bradley, A. (2004). Identification of mammalian microRNA host genes and transcription units. Genome research 14, 1902-1910.

Rouault, T.A., and Tong, W.H. (2008). Iron-sulfur cluster biogenesis and human disease. Trends in genetics : TIG 24, 398-407.

Rousset, M., Paris, H., Chevalier, G., Terrain, B., Murat, J.C., and Zweibaum, A. (1984). Growth-related enzymatic control of glycogen metabolism in cultured human tumor cells. Cancer Res 44, 154-160.

Rousset, M., Zweibaum, A., and Fogh, J. (1981). Presence of glycogen and growth-related variations in 58 cultured human tumor cell lines of various tissue origins. Cancer Res 41, 1165-1170.

Rudolf, J., Makrantoni, V., Ingledew, W.J., Stark, M.J., and White, M.F. (2006). The DNA repair helicases XPD and FancJ have essential iron-sulfur domains. Mol Cell 23, 801-808.

Ruifrok, A.C., and Johnston, D.A. (2001). Quantification of histochemical staining by color deconvolution. Anal Quant Cytol Histol 23, 291-299.

Saito, Y., Liang, G., Egger, G., Friedman, J.M., Chuang, J.C., Coetzee, G.A., and Jones, P.A. (2006). Specific activation of microRNA-127 with downregulation of the proto-oncogene BCL6 by chromatin-modifying drugs in human cancer cells. Cancer Cell 9, 435-443.

Schieke, S.M., Phillips, D., McCoy, J.P., Jr., Aponte, A.M., Shen, R.F., Balaban, R.S., and Finkel, T. (2006). The mammalian target of rapamycin (mTOR) pathway regulates mitochondrial oxygen consumption and oxidative capacity. J Biol Chem 281, 27643-27652.

Schmitt, C.A. (2007). Cellular senescence and cancer treatment. Biochim Biophys Acta 1775, 5-20.

Schulze, A., and Harris, A.L. (2012). How cancer metabolism is tuned for proliferation and vulnerable to disruption. Nature 491, 364-373.

Selak, M.A., Armour, S.M., MacKenzie, E.D., Boulahbel, H., Watson, D.G., Mansfield, K.D., Pan, Y., Simon, M.C., Thompson, C.B., and Gottlieb, E. (2005). Succinate links TCA cycle dysfunction to oncogenesis by inhibiting HIF-alpha prolyl hydroxylase. Cancer Cell 7, 77-85.

Semenza, G.L. (1998). Hypoxia-inducible factor 1: master regulator of O2 homeostasis. Curr Opin Genet Dev 8, 588-594.

Semenza, G.L. (2002). Involvement of hypoxia-inducible factor 1 in human cancer. Intern Med 41, 79-83.

Semenza, G.L. (2007). Oxygen-dependent regulation of mitochondrial respiration by hypoxia-inducible factor 1. Biochem J 405, 1-9.

Semenza, G.L. (2010). Defining the role of hypoxia-inducible factor 1 in cancer biology and therapeutics. Oncogene 29, 625-634.

Semenza, G.L., Jiang, B.H., Leung, S.W., Passantino, R., Concordet, J.P., Maire, P., and Giallongo, A. (1996). Hypoxia response elements in the aldolase A, enolase 1, and lactate dehydrogenase A gene promoters contain essential binding sites for hypoxia-inducible factor 1. J Biol Chem 271, 32529-32537.

Shen, G.M., Zhang, F.L., Liu, X.L., and Zhang, J.W. (2010). Hypoxia-inducible factor 1-mediated regulation of PPP1R3C promotes glycogen accumulation in human MCF-7 cells under hypoxia. FEBS Lett 584, 4366-4372.

Shen, J., Liu, Z., Todd, N.W., Zhang, H., Liao, J., Yu, L., Guarnera, M.A., Li, R., Cai, L., Zhan, M., and Jiang, F. (2011). Diagnosis of lung cancer in individuals with solitary pulmonary nodules by plasma microRNA biomarkers. BMC Cancer 11, 374.

Shen, J., Stass, S.A., and Jiang, F. (2012). MicroRNAs as potential biomarkers in human solid tumors. Cancer Lett.

Shilkaitis, A., Green, A., Punj, V., Steele, V., Lubet, R., and Christov, K. (2005). Dehydroepiandrosterone inhibits the progression phase of mammary carcinogenesis by inducing cellular senescence via a p16-dependent but p53-independent mechanism. Breast Cancer Res 7, R1132-1140.

Singh, R., and Cuervo, A.M. (2011). Autophagy in the cellular energetic balance. Cell Metab 13, 495-504.

Soengas, M.S., Alarcon, R.M., Yoshida, H., Giaccia, A.J., Hakem, R., Mak, T.W., and Lowe, S.W. (1999). Apaf-1 and caspase-9 in p53-dependent apoptosis and tumor inhibition. Science 284, 156-159.

Srinivasan, C., Liba, A., Imlay, J.A., Valentine, J.S., and Gralla, E.B. (2000). Yeast lacking superoxide dismutase(s) show elevated levels of "free iron" as measured by whole cell electron paramagnetic resonance. J Biol Chem 275, 29187-29192.

Stehling, O., Vashisht, A.A., Mascarenhas, J., Jonsson, Z.O., Sharma, T., Netz, D.J., Pierik, A.J., Wohlschlegel, J.A., and Lill, R. (2012). MMS19 assembles iron-sulfur proteins required for DNA metabolism and genomic integrity. Science 337, 195-199.

Sukhatme, V.P., and Chan, B. (2012). Glycolytic cancer cells lacking 6-phosphogluconate dehydrogenase metabolize glucose to induce senescence. FEBS Lett 586, 2389-2395.

Swietach, P., Hulikova, A., Vaughan-Jones, R.D., and Harris, A.L. (2010). New insights into the physiological role of carbonic anhydrase IX in tumour pH regulation. Oncogene 29, 6509-6521.

Taguchi, A., Yanagisawa, K., Tanaka, M., Cao, K., Matsuyama, Y., Goto, H., and Takahashi, T. (2008). Identification of hypoxia-inducible factor-1 alpha as a novel target for miR-17-92 microRNA cluster. Cancer Res 68, 5540-5545.

Takahashi, S., Satomi, A., Yano, K., Kawase, H., Tanimizu, T., Tuji, Y., Murakami, S., and Hirayama, R. (1999). Estimation of glycogen levels in human colorectal cancer tissue: relationship with cell cycle and tumor outgrowth. Journal of gastroenterology 34, 474-480.

Tatum, J.L., Kelloff, G.J., Gillies, R.J., Arbeit, J.M., Brown, J.M., Chao, K.S., Chapman, J.D., Eckelman, W.C., Fyles, A.W., Giaccia, A.J., Hill, R.P., Koch, C.J., Krishna, M.C., Krohn, K.A., Lewis, J.S., Mason, R.P., Melillo, G., Padhani, A.R., Powis, G., Rajendran, J.G., Reba, R., Robinson, S.P., Semenza, G.L., Swartz, H.M., Vaupel, P., Yang, D., Croft, B., Hoffman, J., Liu, G., Stone, H., and Sullivan, D. (2006). Hypoxia: importance in tumor biology, noninvasive measurement by imaging, and value of its measurement in the management of cancer therapy. Int J Radiat Biol 82, 699-757.

Tennant, D.A., Duran, R.V., and Gottlieb, E. (2010). Targeting metabolic transformation for cancer therapy. Nat Rev Cancer 10, 267-277.

Thomson, D.W., Bracken, C.P., and Goodall, G.J. (2011). Experimental strategies for microRNA target identification. Nucleic acids research 39, 6845-6853.

Tomlinson, I.P., Alam, N.A., Rowan, A.J., Barclay, E., Jaeger, E.E., Kelsell, D., Leigh, I., Gorman, P., Lamlum, H., Rahman, S., Roylance, R.R., Olpin, S., Bevan, S., Barker, K., Hearle, N., Houlston, R.S., Kiuru, M., Lehtonen, R., Karhu, A., Vilkki, S., Laiho, P., Eklund, C., Vierimaa, O., Aittomaki, K., Hietala, M., Sistonen, P., Paetau, A., Salovaara, R., Herva, R., Launonen, V., and Aaltonen, L.A. (2002). Germline mutations in FH predispose to dominantly inherited uterine fibroids, skin leiomyomata and papillary renal cell cancer. Nature genetics 30, 406-410.

Tong, W.H., and Rouault, T. (2000). Distinct iron-sulfur cluster assembly complexes exist in the cytosol and mitochondria of human cells. The EMBO journal 19, 5692-5700.

Tong, W.H., and Rouault, T.A. (2007). Metabolic regulation of citrate and iron by aconitases: role of iron-sulfur cluster biogenesis. Biometals : an international journal on the role of metal ions in biology, biochemistry, and medicine 20, 549-564.

Tong, X., Zhao, F., Mancuso, A., Gruber, J.J., and Thompson, C.B. (2009). The glucose-responsive transcription factor ChREBP contributes to glucose-dependent anabolic synthesis and cell proliferation. Proc Natl Acad Sci U S A 106, 21660-21665.

Toustrup, K., Sorensen, B.S., Alsner, J., and Overgaard, J. (2012). Hypoxia gene expression signatures as prognostic and predictive markers in head and neck radiotherapy. Seminars in radiation oncology 22, 119-127.

Toyama, T., Kondo, N., Endo, Y., Sugiura, H., Yoshimoto, N., Iwasa, M., Takahashi, S., Fujii, Y., and Yamashita, H. (2012). High expression of microRNA-

210 is an independent factor indicating a poor prognosis in Japanese triple-negative breast cancer patients. Japanese journal of clinical oncology 42, 256-263.

Tsai, W.C., Hsu, P.W., Lai, T.C., Chau, G.Y., Lin, C.W., Chen, C.M., Lin, C.D., Liao, Y.L., Wang, J.L., Chau, Y.P., Hsu, M.T., Hsiao, M., Huang, H.D., and Tsou, A.P. (2009). MicroRNA-122, a tumor suppressor microRNA that regulates intrahepatic metastasis of hepatocellular carcinoma. Hepatology 49, 1571-1582.

Tsuchiya, S., Fujiwara, T., Sato, F., Shimada, Y., Tanaka, E., Sakai, Y., Shimizu, K., and Tsujimoto, G. (2011). MicroRNA-210 regulates cancer cell proliferation through targeting fibroblast growth factor receptor-like 1 (FGFRL1). J Biol Chem 286, 420-428.

Turley, H., Wykoff, C.C., Troup, S., Watson, P.H., Gatter, K.C., and Harris, A.L. (2004). The hypoxia-regulated transcription factor DEC1 (Stra13, SHARP-2) and its expression in human tissues and tumours. The Journal of pathology 203, 808-813.

Ullah, M.S., Davies, A.J., and Halestrap, A.P. (2006). The plasma membrane lactate transporter MCT4, but not MCT1, is up-regulated by hypoxia through a HIF-1alpha-dependent mechanism. J Biol Chem 281, 9030-9037.

van Engeland, M., Nieland, L.J., Ramaekers, F.C., Schutte, B., and Reutelingsperger, C.P. (1998). Annexin V-affinity assay: a review on an apoptosis detection system based on phosphatidylserine exposure. Cytometry 31, 1-9.

van Loon, J., Janssen, M.H., Ollers, M., Aerts, H.J., Dubois, L., Hochstenbag, M., Dingemans, A.M., Lalisang, R., Brans, B., Windhorst, B., van Dongen, G.A., Kolb, H., Zhang, J., De Ruysscher, D., and Lambin, P. (2010). PET imaging of hypoxia using [18F]HX4: a phase I trial. Eur J Nucl Med Mol Imaging 37, 1663-1668.

van Nederveen, F.H., Korpershoek, E., Lenders, J.W., de Krijger, R.R., and Dinjens, W.N. (2007). Somatic SDHB mutation in an extraadrenal pheochromocytoma. The New England journal of medicine 357, 306-308.

Vander Heiden, M.G. (2011). Targeting cancer metabolism: a therapeutic window opens. Nat Rev Drug Discov 10, 671-684.

Vandesompele, J., De Preter, K., Pattyn, F., Poppe, B., Van Roy, N., De Paepe, A., and Speleman, F. (2002). Accurate normalization of real-time quantitative RT-PCR data by geometric averaging of multiple internal control genes. Genome Biol 3, RESEARCH0034.

Vaupel, P., Hockel, M., and Mayer, A. (2007). Detection and characterization of tumor hypoxia using pO2 histography. Antioxidants & redox signaling 9, 1221-1235.
Vaupel, P., and Mayer, A. (2007). Hypoxia in cancer: significance and impact on clinical outcome. Cancer Metastasis Rev 26, 225-239.

Ventura, A., and Jacks, T. (2009). MicroRNAs and cancer: short RNAs go a long way. Cell 136, 586-591.

Vigoda, A., Mamedova, L.K., Shneyvays, V., Katz, A., and Shainberg, A. (2003). Glycogen metabolism in rat heart muscle cultures after hypoxia. Mol Cell Biochem 254, 311-318.

Vizan, P., Sanchez-Tena, S., Alcarraz-Vizan, G., Soler, M., Messeguer, R., Pujol, M.D., Lee, W.N., and Cascante, M. (2009). Characterization of the metabolic changes underlying growth factor angiogenic activation: identification of new potential therapeutic targets. Carcinogenesis 30, 946-952.

Volinia, S., Galasso, M., Sana, M.E., Wise, T.F., Palatini, J., Huebner, K., and Croce, C.M. (2012). Breast cancer signatures for invasiveness and prognosis defined by deep sequencing of microRNA. Proc Natl Acad Sci U S A 109, 3024-3029.

Vousden, K.H., and Ryan, K.M. (2009). p53 and metabolism. Nat Rev Cancer 9, 691-700.

Wang, J., Chen, J., Chang, P., LeBlanc, A., Li, D., Abbruzzesse, J.L., Frazier, M.L., Killary, A.M., and Sen, S. (2009). MicroRNAs in plasma of pancreatic ductal adenocarcinoma patients as novel blood-based biomarkers of disease. Cancer Prev Res (Phila) 2, 807-813.

Warburg, O. (1956). On the origin of cancer cells. Science 123, 309-314.

Ward, P.S., and Thompson, C.B. (2012). Metabolic reprogramming: a cancer hallmark even warburg did not anticipate. Cancer Cell 21, 297-308.

Wilson, W.R., and Hay, M.P. (2011). Targeting hypoxia in cancer therapy. Nat Rev Cancer 11, 393-410.

Winter, S.C., Buffa, F.M., Silva, P., Miller, C., Valentine, H.R., Turley, H., Shah, K.A., Cox, G.J., Corbridge, R.J., Homer, J.J., Musgrove, B., Slevin, N., Sloan, P., Price, P., West, C.M., and Harris, A.L. (2007). Relation of a hypoxia metagene derived from head and neck cancer to prognosis of multiple cancers. Cancer Res 67, 3441-3449.

Wise, D.R., DeBerardinis, R.J., Mancuso, A., Sayed, N., Zhang, X.Y., Pfeiffer, H.K., Nissim, I., Daikhin, E., Yudkoff, M., McMahon, S.B., and Thompson, C.B. (2008). Myc regulates a transcriptional program that stimulates mitochondrial glutaminolysis and leads to glutamine addiction. Proc Natl Acad Sci U S A 105, 18782-18787.

Wouters, B.G., and Koritzinsky, M. (2008). Hypoxia signalling through mTOR and the unfolded protein response in cancer. Nat Rev Cancer 8, 851-864.

Wykoff, C.C., Beasley, N.J., Watson, P.H., Turner, K.J., Pastorek, J., Sibtain, A., Wilson, G.D., Turley, H., Talks, K.L., Maxwell, P.H., Pugh, C.W., Ratcliffe, P.J.,

and Harris, A.L. (2000). Hypoxia-inducible expression of tumor-associated carbonic anhydrases. Cancer Res 60, 7075-7083.

Xu, Q., Ma, P., Hu, C., Chen, L., Xue, L., Wang, Z., Liu, M., Zhu, H., Xu, N., and Lu, N. (2012). Overexpression of the DEC1 protein induces senescence in vitro and is related to better survival in esophageal squamous cell carcinoma. PLoS One 7, e41862.

Xu, W., Yang, H., Liu, Y., Yang, Y., Wang, P., Kim, S.H., Ito, S., Yang, C., Wang, P., Xiao, M.T., Liu, L.X., Jiang, W.Q., Liu, J., Zhang, J.Y., Wang, B., Frye, S., Zhang, Y., Xu, Y.H., Lei, Q.Y., Guan, K.L., Zhao, S.M., and Xiong, Y. (2011). Oncometabolite 2-hydroxyglutarate is a competitive inhibitor of alpha-ketoglutarate-dependent dioxygenases. Cancer Cell 19, 17-30.

Yamakuchi, M., Lotterman, C.D., Bao, C., Hruban, R.H., Karim, B., Mendell, J.T., Huso, D., and Lowenstein, C.J. (2010). P53-induced microRNA-107 inhibits HIF-1 and tumor angiogenesis. Proc Natl Acad Sci U S A 107, 6334-6339.

Yan, H., Parsons, D.W., Jin, G., McLendon, R., Rasheed, B.A., Yuan, W., Kos, I., Batinic-Haberle, I., Jones, S., Riggins, G.J., Friedman, H., Friedman, A., Reardon, D., Herndon, J., Kinzler, K.W., Velculescu, V.E., Vogelstein, B., and Bigner, D.D. (2009). IDH1 and IDH2 mutations in gliomas. The New England journal of medicine 360, 765-773.

Yanaihara, N., Caplen, N., Bowman, E., Seike, M., Kumamoto, K., Yi, M., Stephens, R.M., Okamoto, A., Yokota, J., Tanaka, T., Calin, G.A., Liu, C.G., Croce, C.M., and Harris, C.C. (2006). Unique microRNA molecular profiles in lung cancer diagnosis and prognosis. Cancer Cell 9, 189-198.

Yang, W., Sun, T., Cao, J., Liu, F., Tian, Y., and Zhu, W. (2012). Downregulation of miR-210 expression inhibits proliferation, induces apoptosis and enhances radiosensitivity in hypoxic human hepatoma cells in vitro. Exp Cell Res 318, 944-954.

Ying, Q., Liang, L., Guo, W., Zha, R., Tian, Q., Huang, S., Yao, J., Ding, J., Bao, M., Ge, C., Yao, M., Li, J., and He, X. (2011). Hypoxia-inducible microRNA-210 augments the metastatic potential of tumor cells by targeting vacuole membrane protein 1 in hepatocellular carcinoma. Hepatology 54, 2064-2075.

Yoshioka, Y., Kosaka, N., Ochiya, T., and Kato, T. (2012). Micromanaging Iron Homeostasis: hypoxia-inducible micro-RNA-210 suppresses iron homeostasis-related proteins. J Biol Chem 287, 34110-34119.

Yuneva, M., Zamboni, N., Oefner, P., Sachidanandam, R., and Lazebnik, Y. (2007). Deficiency in glutamine but not glucose induces MYC-dependent apoptosis in human cells. The Journal of cell biology 178, 93-105.

Zhang, Z., Sun, H., Dai, H., Walsh, R.M., Imakura, M., Schelter, J., Burchard, J., Dai, X., Chang, A.N., Diaz, R.L., Marszalek, J.R., Bartz, S.R., Carleton, M., Cleary, M.A., Linsley, P.S., and Grandori, C. (2009). MicroRNA miR-210 modulates cellular response to hypoxia through the MYC antagonist MNT. Cell Cycle 8, 2756-2768.

Zhao, A., Li, G., Peoc'h, M., Genin, C., and Gigante, M. (2012). Serum miR-210 as a novel biomarker for molecular diagnosis of clear cell renal cell carcinoma. Experimental and molecular pathology.

Zu, X.L., and Guppy, M. (2004). Cancer metabolism: facts, fantasy, and fiction. Biochem Biophys Res Commun 313, 459-465.